DISSERTATION

MECHANISTIC STUDIES OF NANOCLUSTER NUCLEATION, GROWTH, AND AGGLOMERATION

Submitted by

Eric E. Finney

Department of Chemistry

In partial fulfillment of the requirements

For the Degree of Doctor of Philosophy

Colorado State University

Fort Collins, Colorado

Summer 2009

ProQuest LLC
789 East Eisenhower Parkway
P.O. Box 1346
Ann Arbor, MI 48106-1346

COLORADO STATE UNIVERSITY

May 18, 2009

WE HEREBY RECOMMEND THAT THE DISSERTATION PREPARED UNDER OUR SUPERVISION BY ERIC E. FINNEY ENTITLED MECHANISTIC STUDIES OF NANOCLUSTER NUCLEATION, GROWTH, AND AGGLOMERATION BE ACCEPTED AS FULFILLING IN PART REQUIREMENTS FOR THE DEGREE OF DOCTOR OF PHILOSOPHY.

Committee on Graduate Work

Anthony K. Rappé

Bruce A. Parkinson

Gary E. Maciel

David S. Dandy

Advisor Richard G. Finke

Department Head Anthony K. Rappé

ABSTRACT OF DISSERTATION

MECHANISTIC STUDIES OF NANOCLUSTER NUCLEATION, GROWTH, AND AGGLOMERATION

Following a critical review of the relevant literature, the research presented herein focuses on the mechanisms by which transition-metal nanoclusters nucleate, grow, and agglomerate. The studies include: (i) the generality of the recently uncovered, 4-step mechanism for nanocluster formation and agglomeration; (ii) a study addressing the question of whether the hydrogenation of olefins using (1,5-COD)Pt^{II} complexes proceeds via homogeneous or heterogeneous catalysis; and (iii) a comparison of the kinetics of transition-metal nanocluster formation and the kinetics of solid-state reactions.

Recently, a new, 4-step mechanism was discovered for the nucleation, growth, and agglomeration of transition-metal nanoclusters, using a single Pt complex in the system under study. Herein, the mechanism is shown to be general to the formation of nanoclusters of at least four other metals. In addition, the effects of ligands, concentration, temperature, solvent, and stirring on the mechanism are examined. Several alternative mechanisms are ruled out, leaving the 4-step mechanism as the only one to date that can account for the observed kinetics.

The question of "is it homogeneous or heterogeneous catalysis?" is addressed with respect to the hydrogenation of olefins using (1,5-COD)Pt^{II} complexes. The data presented herein provide compelling evidence that these complexes are first reduced to Pt^0 nanoclusters and/or bulk metal, which are the true hydrogenation catalysts. Included herein is a brief overview of the literature of Pt-catalyzed hydrosilylation reaction, with respect to the "is it homogeneous or heterogeneous catalysis?" question.

The literature is replete with mechanisms describing solid-state phase transitions, the kinetics of which appear similar to the kinetics of transition-metal nanocluster formation. It is found that the solid-state equation can fit nanocluster formation kinetic data, and vice versa. This finding leads into a comparison of solid-state reaction mechanisms and the Finke-Watzky mechanism, with a focus on the strengths and limitations of each.

Eric E. Finney
Department of Chemistry
Colorado State University
Fort Collins, CO 80523
Summer 2009

TABLE OF CONTENTS

CHAPTER I

INTRODUCTION

The broad theme of this dissertation is the mechanism of transition-metal nanocluster formation. This dissertation is written in the "journals-format" style (see Appendix A for a discussion of this type of dissertation), and is based on three separate publications and a published literature report written in a format set by the American Chemical Society. Continuity of this dissertation as a single document is achieved by (i) this introduction, (ii) the use of bridging paragraphs at the beginning of each chapter, and (iii) a final summary chapter. A concise overview of each chapter's contents is presented below.

Chapter II is a published review of the literature of nanocluster nucleation, growth, and agglomeration (Finney, E. E., Finke, R. G. *J. Coll. Interface Sci.* **2007,** *317*, 351). A general overview of nucleation theory is given, along with specific literature examples of mechanistic studies of nanocluster formation. Also given is a brief discussion of the literature of mechanistic studies of semiconductor

nanocrystals, solid-state transformations, and protein agglomeration. The second of these topics will be relevant to Chapter V.

Chapter III is a publication (Finney, E. E.; Finke, R. G. *Chem. Mater.* **2008**, *20*, 1956) describing the 4-step, double-autocatalytic mechanism for transition-metal nanocluster nucleation, growth, and agglomeration. This work is an extension of two earlier papers that first described the 4-step mechanism,[1,2] and examines several factors that determine the mechanism by which nanoclusters nucleate, grow, and agglomerate.

Chapter IV presents a publication (Finney, E. E.; Finke, R. G. *Inorg. Chim. Acta* **2006**, *359*, 2879) investigating of the question of "Is it homogeneous or heterogeneous catalysis?" for the use of Pt(1,5-COD)X_2 (X = halogen, alkyl) in the hydrogenation of olefins. The work described in this chapter provides compelling evidence for heterogeneous Pt^0 catalysis, and includes a brief survey of the homogeneous versus heterogeneous catalysis question regarding hydrosilylation using platinum.

Chapter V is a submitted paper describing an investigation of solid-state transformation mechanisms. This work reveals similarities and differences between the kinetic data of solid-state transformations and kinetic data of solution-phase transition-metal nanocluster formation. This paper also presents a mathematical basis for the similarity between the transition-metal nanocluster formation kinetics and the Avrami-Erofe'ev equation, the basis for solid-state phase transition kinetic studies.

Chapter VI is a concise summary of the material presented in this dissertation. There are also three additional publications[1,2,3] (for a total of seven papers) resulting

from my time at Colorado State University (the three publications cited above not being formally part of this dissertation, as they included significant work by Claire Besson[1,2] and Murielle Watzky[3]).

References

[1] Besson, C.; Finney, E. E.; Finke, R. G. *J. Am. Chem. Soc.* **2005**, *127*, 8179.

[2] Besson, C.; Finney, E. E.; Finke, R. G. *Chem. Mater.* **2005**, *17*, 4925.

[3] Watzky, M. A.; Finney, E. E.; Finke, R. G. *J. Am. Chem. Soc.* **2008**, *130*, 11959.

CHAPTER II

NANOCLUSTER NUCLEATION AND GROWTH KINETIC AND MECHANISTIC STUDIES: A REVIEW EMPHASIZING TRANSITION-METAL NANOCLUSTERS

This dissertation chapter contains the manuscript adapted from a review published in *Journal of Colloid and Interface Science* (Finney, E. E., Finke, R. G. *J. Coll. Interface Sci.* **2007,** *317*, 351). This chapter contains a brief overview of nucleation theory, followed by a critical review of the literature of transition-metal nanocluster formation kinetic and mechanistic studies. Concluding this chapter are three Appendices that briefly summarize the literature of the mechanisms of semiconductor nanocrystal formation, solid-state phase transitions, and protein agglomeration.

This chapter was prepared by Eric E. Finney (E.E.F.), with assistance and editing from Richard G. Finke (R.G.F.)

Abstract

A review of the literature of kinetic and mechanistic studies of transition-metal nanocluster nucleation and growth is presented; the focus is on nucleation processes. A brief survey of nucleation theory is given first, with an emphasis on classical nucleation theory, as this is the logical starting point of transition-metal nanocluster nucleation and growth studies. The main experimental methods for following nanocluster formation are examined next—dynamic light scattering, UV–visible spectroscopy, electron microscopy, and X-ray spectroscopies—with special attention paid to their strengths and weaknesses. Several specific examples of transition-metal nanocluster formation are then given, beginning with LaMer's classic sulfur sol system and including the Finke–Watzky mechanism of slow continuous nucleation, A→B, followed by fast autocatalytic surface growth, A+B→2B. Finally, brief overviews of semiconductor nanoparticle preparations, solid-state nucleation studies—emanating from Avrami's work—and protein agglomeration mechanistic studies are also provided, as these processes are relevant, conceptually and in a general sense, to the field of transition-metal nanocluster nucleation and growth mechanisms.

Introduction

Nucleation and growth—the appearance of a new phase out of an old phase—is a ubiquitous phenomenon in nature.[1] The process occurs in everything from cloud formation to volcano eruptions to nanocluster formation reactions. In fact, it has been suggested that "it should not be a surprise if it proves that even the Big Bang was a nucleation phenomenon".[1] The majority of the theoretical work with nucleation theory (i.e., the development and modification of classical nucleation theory, *vide infra*) has been done for the condensation of liquid from the vapor phase.[2] This work has been extended to the nucleation of solid from the melt (i.e., freezing),[3] as well as precipitation and crystallization of solids from solution.[4] Nucleation and growth has received a great deal of study in the areas of semiconductor particles, solid-state nucleation (most notably Avrami's work and the subsequent work that it inspired), and protein aggregation, topics which are examined briefly in Appendices A, B, and C. An experimental-based understanding of nucleation in these processes is limited, the reason being illustrated by the statement that "the understanding of crystallization, especially the nucleation process, has been very much limited mainly due to a lack of quantitative experimental data."[5] The nucleation, and subsequent growth, of soluble nanoclusters in solution has received relatively little prior attention, this contribution being the first review of the subject.

Recently, however, the nucleation and growth of metal nanoclusters in solution has been the subject of increasing study. It is well known that at the nanometer scale, the optical, electronic, and catalytic properties of transition-metal nanoclusters are highly sensitive to their size and shape.[6] Therefore, one of the main

goals of nanocluster science is the ability to prepare nanoclusters that have very narrow size distributions (so-called "near-monodisperse" nanoclusters of $\leq \pm 15\%$[7]), thereby allowing for greater uniformity of nanocluster properties. A fundamental understanding of the mechanism of nanocluster formation should allow greater control over nano-cluster size, shape, and composition (e.g., of multimetallic "nano-onions"[8]), resulting in the ability to tune the above-mentioned properties simply by varying the reaction conditions.

This review will focus on the nucleation of soluble nanoclusters in solution, but brief mention of the vapor and precipitation systems will be given first, as they provide the basis for the nucleation theory applied to other areas of science, including transition-metal nanoclusters. Reviews of nucleation, especially of classical nucleation theory and its derivatives, are plentiful,[9,10] and excellent texts giving detailed descriptions of general nucleation theory exist.[1,11] Therefore, this review will only briefly summarize the dominant theories currently in practice, with appropriate references for the interested reader; the focus of this review is the application of nucleation to transition-metal nanoparticles in solution.

Although nucleation in general has been extensively studied, the high levels of accuracy and precision that are enjoyed by other fields of science remain elusive in the study of nucleation. A general shortcoming of nucleation theory is that much of the theory comes from fitting experimental data and adjusting theoretical parameters accordingly. As a result the theory in general has little predictive power.[12] Therefore, a main goal of nucleation theory is to improve the accuracy of the theory to better match, and then accurately predict, experimental observations.[13] The large gap

between a theoretical (mathematical) understanding of nucleation and an experimental (physical) understanding is a gap that is only recently being bridged by physicists and physical chemists. As Oxtoby has observed, "nucleation theory is one of the few areas of science in which agreement of predicted and measured rates to within several orders of magnitude is considered a major success."[9] Zukoski notes that errors of tens of orders of magnitude are not unprecedented![14] Closer agreement between theory and experiment is, therefore, a goal of nucleation science.

Classical nucleation theory

What is now known as classical nucleation theory (CNT) was pioneered by Volmer[15,16] and Becker and Döring.[17] CNT uses the Gibbs capillary approximation, which treats the nucleus as if it were a bulk phase—which, rigorously, it is not. The free energy of nucleus formation is expressed in different ways, but every expression contains two competing terms: one negative, for the favorable formation of bonds in the nucleus, and one positive, for the unfavorable creation of an interface between the nucleus in its new phase and the medium of the old phase. In its simplest form and in terms of the cluster radius, the expression for the cluster free energy is that given in eq 2.1.[9]

$$\Delta G = -\frac{4}{3}\pi r^3 \left|\Delta G_V\right| + 4\pi r^2 \gamma \qquad (2.1)$$

This equation assumes a spherical nucleus, as this shape minimizes the surface area of the nucleus. Here, r is the radius of the cluster, ΔG_V is the difference in bulk free energy per volume between the old and new phases, and γ is the surface free energy per unit area. The cluster free energy can also be expressed in terms of the number of atoms in the cluster; one such general expression is given in eq 2.2,[11]

$$\Delta G = -nk_B T \ln\left(\frac{x}{x_{sat}}\right) + \sigma b n^{\frac{2}{3}} \qquad (2.2)$$

where n is the number of atoms in the cluster, k_B is the Boltzmann constant, T is the temperature, σ is the surface tension of the cluster, b is a geometric factor, and the quantity x/x_{sat} is called the supersaturation of the solution, where x is the mole fraction of the species present in solution, and x_{sat} is the mole fraction of the species in a saturated solution. Alternatively, the supersaturation can be expressed in terms of concentration, and becomes C/C_{eq}, where C_{eq} is the solubility (the equilibrium concentration) of the species. When the expression is used for the nucleation of droplets from vapor, the supersaturation is expressed in terms of pressure, p/p_{eq}. The free energy of formation of nuclei is at the heart of CNT, it being noted that "the exact determination of ΔG (for the critical nucleus) seems to be the real problem of nucleation theory."[18]

When comparisons are made to experimental work, the nucleation rate (denoted as either I or J) is generally the parameter that is measured. This parameter is also expressed in different ways; one of these is given in eq 2.3,[19]

$$I = \Gamma \exp\left[-\frac{16\pi}{3k_B T}\frac{\gamma^3}{\left(\rho_s|\Delta\mu|\right)^2}\right] \qquad (2.3)$$

where ρ_s is the number density of the solid, γ is again the solid–liquid interface free energy density, $\Delta\mu$ is the change in chemical potential between the solid and the liquid phases, and $\Gamma = \sum Z\rho_l f_c^+$. In this last expression, Z is the Zeldovich factor,

$\left(|\Delta\mu| / 6\pi k_B T n_c\right)^{1/2}$, where n_c is the number of particles in the critical nucleus, and f_c^+ is the attachment rate of particles to the cluster, which is given by $f_c^+ = \frac{24 D_S n_c^{2/3}}{\lambda^2}$; here, D_S is a self-diffusion coefficient and λ is a diffusion distance. An expression for the nucleation rate is given as eqs 2.4 and 2.5. In eq 2.4, B is pre-exponential factor which is a collection of the terms described above, and ΔG^* is the activation energy for nucleation.

$$J = B \exp\left(-\frac{\Delta G^*}{RT}\right) \tag{2.4}$$

$$\Delta G^* = \frac{16\pi r^2 V_m^2}{3|\Delta\mu|^2} \tag{2.5}$$

The dependence of the free energy of a cluster as a function of the radius of the cluster, based on classical nucleation theory, is shown qualitatively in Figure 2.1.[11] Because the cluster free energy has negative (bond making) and positive (surface energy) terms, the free energy has a maximum at some radius, called the critical radius, r^*. Differentiating eq 2.1 with respect to r and substituting back into eq 2.1 gives an expression for the maximum free energy, ΔG^*, eq 2.6, where $\Delta G_V = -(RT/V_m) \ln S$, where V_m is the molar volume of the relevant species and S is the degree of supersaturation. Note that eq 2.6 has the same general form as eq 2.5.

$$\Delta G^* = \frac{16\pi r^3}{3|\Delta G_V|^2} \tag{2.6}$$

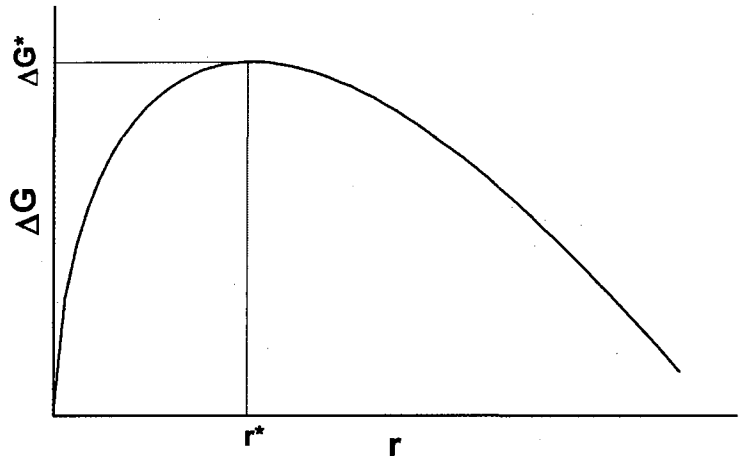

Figure 2.1. Dependence of the free energy, ΔG, of a cluster on the radius of the cluster, r. The curve has a maximum free energy ΔG^* at the critical nucleus, which has a radius of r^*.

This maximum of the curve, where $d\Delta G/dr = 0$, gives the radius of the critical nucleus of the cluster. For clusters smaller than r^*, growth is unfavorable and the cluster dissolves. For clusters larger than r^*, growth is favored. Alternatively, the critical nucleus can be expressed in terms of the number of atoms contained within it, n^*, by differentiating eq 2.2 and finding the maximum. For clusters containing less than n^* atoms, growth is unfavorable and the cluster dissolves. For clusters containing more than n^* atoms, growth is favored. The *critical nucleus* is therefore the activated complex along the reaction coordinate of nucleation.[9]

The greatest flaw of CNT is that it treats nuclei as bulk material having macroscopic properties. The key assumptions involved here are that (i) the nucleus behaves as the bulk, and (ii) the surface free energy of the cluster is the same as that of an infinite planar surface.[9–11] Both of these assumptions become unreasonable when considering a nucleus of only several (or even several hundred) atoms or molecules; the center of the cluster is far from the thermodynamic limit, and the sharp

curvature of the cluster significantly increases the free energy of its surface. In the context of eq 2.3 above, accurate definitions and values of the constants λ and γ are unavailable for small nuclei versus bulk material. As stated by Martínez et al. in the case of liquid–vapor nucleation, "clearly the use of bulk liquid properties to describe a process involving small metallic states is problematic."[20] Obviously, the same can be said for solid particles.

In 1986, Hale reported a scaled nucleation theory (SNT),[21] which introduced critical temperature and pressure, T_c and p_c, as well as a new parameter Ω for the excess surface entropy. This new parameter effectively corrects for the supersaturation and therefore for the nucleation rate and nucleation free energy. The value of Ω is dependent on density, which must be approximated for non-bulk systems. Unfortunately, a consistent method of approximating Ω is not available. Different researchers have obtained values of Ω using different methods.[20] The fitting of experimental data to SNT shows that no one method for approximating Ω is universal—some of the experimental data are fit better when the surface tension is approximated using the critical temperature, while other data are fit better when actual experimental $d\gamma/dT$ data are used.[20]

Computationally, Gránàsy developed diffuse interface theory to predict nucleation rates of nonane from the vapor, and then compared his calculated values to experiment along with calculations using CNT.[22] Diffuse interface theory contains two assumptions that are somewhat relaxed compared to CNT: (i) that only the very center of the nucleus, but not the entire nucleus, has the properties of the bulk, and (ii) that the thickness of the liquid–vapor interface is independent of the nucleus size.

These modifications gave results that were closer to experiment than CNT, further showing how the very basic assumptions of CNT fail to account for experimental observations. The diffuse interface theory was also compared to CNT in a computational study of the temperature dependence of the nucleation rate of gold particles during freezing, using clusters composed of various numbers of gold atoms.[23] In this case, similar results were obtained—CNT overestimated the nucleation rate at high temperatures, while diffuse interface theory fit the observed nucleation rate.

The validity of CNT has been examined experimentally, mostly in systems of liquid droplet formation from the vapor. For example, El-Shall et al. used vapor-phase nucleation of dodecane, hexadecane, and octadecane to check the accuracy of CNT.[24,25] They found that the theory breaks down at low temperatures ($T \leq$ ~300 K). At these temperatures, CNT predicts a higher level of supersaturation needed for nucleation than was found experimentally, and it underestimates the number of atoms in the critical nucleus, n^*, for their system.[24] In accordance with this data, the authors used the scaling model of Hale[21] and added extra terms to the theory to compensate for the temperature dependence of the nucleation rate.[24] By adding a term for the increased surface entropy of the cluster, the theory became much better at predicting the nucleation rate over the temperature range studied, 280–350 K. The classic work of Strey et al. in 1994[26] also tested the validity of CNT in the condensation of 1-butanol from the vapor using a "nucleation pulse chamber" to measure nucleation rates. These authors obtained a result similar to that of El-Shall et al., specifically that

CNT accurately describes nucleation of liquid droplets at high temperature, but is less accurate at lower temperatures (≤240 K).

One of the difficulties of using many of the various nucleation theories is that they contain the γ term for the interfacial energy of the cluster. The value of this parameter is not known for small nuclei.[19] An attempt to solve this problem has been made by Sugimoto et al., who formulated an expression for the solid–liquid interfacial energy,[27,28] and then used their formulation to calculate the value of γ for silver halide particles.[29] A brief review of studies attempting to obtain the interfacial energy is given in reference 29. Their result is shown in eq 2.7,

$$\gamma = -N^{\sigma} \lambda k_B T \ln x_{(\infty)} \tag{2.7}$$

where N^{σ} is the surface density of surface monomers (a "monomer" in the case of AgX clusters studied here is defined as a single AgX unit, where X = Cl, Br, or I), λ is the ratio of open sites on a surface monomer to that of a free monomer, k_B is the usual Boltzmann constant, T is the temperature, and $x_{(\infty)}$ is the solubility of the bulk material given by the mole fraction of monomers in the liquid phase. The authors were able to use textbook values for the AgX crystals, such as the lattice parameter and molar volume, to calculate γ for the clusters. They also showed theoretically that γ is independent of the size of the cluster, and then verified this experimentally.[29]

In a separate report, the surface tension of poly(methyl methacrylate) spheres was estimated using laser scanning confocal microscopy.[30] The results were in "reasonable agreement"[30] with computational results. In addition, the shapes of the nuclei were observed to be roughly elliptical, rather than spherical.

Nucleus shape considerations

It has been found using computational studies that underneath a face-centered cubic (fcc) crystal nucleus is a layer with body-centered cubic (bcc) symmetry.[31] This finding has been investigated as an extension of Ostwald's "step rule"[32] of solid-state chemistry, which states that the structure of the nucleus that is first formed does not have to be the most thermodynamically stable, but is the one that most resembles the parent solid phase. Density functional theory (DFT) calculations performed by Oxtoby[33] corroborated this finding, with the conclusion that metastable states are crucial in the formation of nuclei. This result is perhaps not surprising given that the critical nucleus itself is a metastable state.[9,11] A "Bain transformation" is one where a bcc critical nucleus yields a fcc crystal (or, also, the reverse process).[33]

A similar result was found by Frenkel et al. in the formation of bimetallic Pt–Ru particles.[34] Fits to EXAFS data gave evidence of an fcc structure for the particles, while bulk Pt–Ru alloys have a hexagonal close packed (hcp) structure. The final nanocluster structure was determined to also have an fcc structure. Yet another example is given in the diffuse interface theory study of freezing gold particles mentioned above,[23] in which the nuclei assume an hcp structure as opposed to the more stable fcc structure. Some transformation from hcp to fcc was observed for some of the gold nuclei, but the calculated barrier for the transformation was large.

Cacciuto and Frenkel have noted that the principle of Ostwald's step rule is not taken into account by CNT.[35] They found that CNT cannot account for stress that exists within crystal nuclei arising from the formation of a surface; CNT assumes that the nuclei are incompressible, and this assumption, the authors claim, is

unnecessary.[35] The stress experienced by the nuclei can influence the structure of the nuclei; therefore, understanding the stress that nuclei experience can enable predictions about the structure of the nuclei in conjunction with the step rule. Using theoretical studies, the authors found that under certain conditions small crystal nuclei are less dense (i.e., experience less stress) than large ones. This fact, which likely has an effect on nucleation rates and the critical nucleus, is not taken into account by CNT.

Nanocluster formation in solution

Methods used to study nanocluster formation

Early measurements of the formation of nanoclusters were visual. In the work of Nielson in the 1960s, solutions were mixed and the time it took for a precipitate to be observed was measured.[36,37] Since that time, a handful of spectroscopic techniques have become common for measuring the kinetics of nanocluster formation. Some of those methods are mentioned briefly here. A main problem with nearly all methods is that they tend to measure larger clusters—that is, growth—and not the desired nucleation.

Dynamic light scattering (DLS)

Dynamic light scattering is used to obtain information about particle sizes in solution, as well as interactions between macromolecules such as proteins.[38] In chemistry, DLS is a common technique for measuring the sizes of polymer clusters,[39] but is less common for the measurement of nanoclusters, the dominant technique being *ex situ* transmission electron microscopy (*vide infra*). Measurement of particle size from fitting DLS data requires knowledge of the diffusion coefficient of the

clusters and viscosity of the solvent. DLS is advantageous in that it is noninvasive and is performed on a solution sample, so that the cluster solution requires little manipulation and can be recovered after analysis. In the nanocluster literature, DLS measurements are often compared to measurements from other techniques, most commonly transmission electron microscopy; the agreement is generally close,[40] at least in cases where no sample damage has occurred from electron microscopy.

UV–visible spectroscopy

A popular method that is used to study the kinetics of nanocluster formation in solution as well as the sizes of nanoclusters is UV–visible spectroscopy. Although this is a useful method for some systems, it requires that the nanoclusters under investigation absorb in the UV–visible region, and this tends to restrict such studies to the metals with distinct plasmon absorbances in the visible region, namely Ag, Au, and Cu.[41] This tends to exclude nanoclusters of many interesting metals, including Co, Ni, Re, Ir, and Pt, that primarily tail off into the UV region.[41] Therefore, other methods are necessary to study the kinetics of nanocluster nucleation and growth. Alternatively, UV–visible spectroscopy can be used to follow the *loss* of the nanocluster *precursor*, provided that the precursor absorbs in the UV–visible region. An example of such use is the study of Pt_n^0 nanoclusters from the reduction of $[Pt^{II}Cl_4]^{2-}$ by Henglein et al. (*vide infra*).[42]

One major problem with studying nanocluster formation using UV–visible spectroscopy is that unless the formation can be studied *in situ* (i.e., without significant manipulation of the sample), there is no way to be certain that the *observed* behavior of the nanoclusters is the same as their *actual* behavior under the

specific reaction conditions. There have been attempts to obtain UV–visible spectra of nanoclusters *in situ*; one of these methods, used in the formation of CdSe nanocrystals, is given in Appendix 2A.

Once an *in situ* UV–visible method for measuring nucleation kinetics is achieved, another issue arises—namely, that there are often numerous other species in the reaction medium that may absorb in the UV–visible region and interfere with the nanocluster spectra. Among these are metal ions, solvent, reductant, and added stabilizers. This problem has also been addressed;[43,44] the results are presented later in this review.

Electron microscopy

Another common method used in nanocluster formation studies is *ex situ* electron microscopy. The most popular microscopy used in the nanocluster literature is transmission electron microscopy (TEM). TEM is often used to characterize the *growth* of nanoclusters, as nuclei are typically too small to be seen, non-high resolution, "routine" TEM typically being limited to $\geq$1 nm despite stated resolution limits typically of $\pm\geq$0.2 nm. Recently, however, the method of high-angle annular dark-field (HAADF) imaging with scanning TEM (STEM) has become available,[45] so-called "Z-contrast" microscopy. This method, which has increased contrast in heavier atom samples, has been shown to achieve atomic resolution—for example, in one study, germanium and erbium atoms were visualized on a SiC support.[45] In general, TEM offers several advantages, including powerful visual images and direct measurement of nanocluster size. However, because TEM is a solid-state (i.e., *ex situ*) technique, the nanoclusters must be taken out of solution and dried before they can be

analyzed, during which further growth and agglomeration of the nanoclusters in the increasingly concentrated solution (i.e., before achieving dryness) can take place. In addition, some monometallic and other, especially first- or second-row transition-metal nanocluster precursor complexes yield nanoclusters in the TEM beam.[46,47] Hence, TEM alone cannot tell if nanoclusters are nucleating in solution or *being produced in the TEM beam*. The TEM beam may also change the nanoparticles under observation, another major disadvantage, and one that has been studied in detail.[48] A TEM textbook notes that "in the end, you can damage virtually anything you put into the TEM". [49] For these reasons, TEM alone is not a reliable method to study the nucleation of nanoclusters.

Another notable method for visualizing nanoclusters is scanning tunneling microscopy (STM).[50–52] Again, however, STM studies are confined to nanoclusters examined under ultrahigh vacuum conditions on a support.[53]

X-ray spectroscopies

Two potentially powerful methods for directly observing the nucleation process utilize X-ray spectroscopy—X-ray absorption near-edge spectroscopy (XANES) and extended X-ray absorption fine structure spectroscopy (EXAFS).[54] These methods are valuable because they give information about the identity of atoms in the nanoclusters, as well as information about the nearest neighbors of the atoms, allowing atomic-level characterization. The recent, major advances in X-ray optics as well as the analysis of multiple-shell scattering currently make these techniques among the most attractive for studying nanoclusters.[55] Frenkel and coworkers have pioneered the use of these X-ray spectroscopies to study the formation of transition-

metal nanoclusters.[34,55–57] Using advanced modeling techniques, they were able to study the shape of bimetallic Pt–Ru nanoclusters described above.[34] In addition, they found that early in the formation of the Pt–Ru nanoclusters, Pt is found preferentially at the core of the nuclei; as the nanoclusters grow, a core–shell inversion takes place, after which Pt is found mainly on the surface of the clusters.[56] Along with determining the structure of the nuclei versus the structure of the final nanocluster, the shapes of carbon-supported clusters were determined to be hemispherical; this was found to be the case for both Pt–Ru bimetallic nanoclusters and carbon-supported Pt nanoclusters.[55] The wealth of structural information that is possible from X-ray spectroscopies makes this technique very promising in the characterization of transition-metal nanocluster nucleation if it can be done *in situ*. Appropriate EXAFS, XANES, and other studies of Ir_n^0 and other transition-metal nanocluster formation are being pursued collaboratively between the Nuzzo, Frenkel, and Finke laboratories.[58]

To summarize, the best characterization techniques for studying the nucleation and growth of transition-metal nanoclusters are those that can be performed *in situ*/operando, allowing for direct observation of the nucleation and growth processes. Electron microscopy fails at this, despite its relative ease and the visually striking images that it provides. UV–visible and X-ray spectroscopies, however, require less sample manipulation and may be performed *in situ*. Using these techniques in combination, while keeping in mind the advantages and limitations of each, is necessary to gain a better picture of what is happening during nanocluster nucleation and growth.

LaMer's experimental cluster nucleation studies

The most famous and widely cited example of the application of nucleation theory to cluster formation is the work done by LaMer in the 1950s.[59,60] LaMer used CNT to describe the formation of sulfur sols from the decomposition of sodium thiosulfate in hydrochloric acid, Scheme 2.1. The model he presented, Figure 2.2, shows the concentration of nucleating species (sulfur in this case) versus time. The essence of the mechanism, as illustrated by Figure 2.2, is as follows: the concentration of elemental sulfur builds up slowly until some critical concentration is reached, or more specifically a critical supersaturation level, C/C_{eq} where C_{eq} is the solubility of sulfur in the solution (*vide supra*), stage I in Figure 2.2. At this point, "self-nucleation" (i.e., homogeneous nucleation) occurs at a rate that has been called "effectively infinite",[59] stage II; this is the origin of the idea of "burst" nucleation. The burst of nucleation immediately lowers the supersaturation level of monomers in the solution; as a result, nucleation essentially stops at this time. Growth then occurs by diffusion of sulfur atoms throughout the solution, stage III.

Scheme 2.1. The system studied by LaMer.

$$2HS_2O_3^- \rightleftharpoons 2HSO_3^- + S_2$$

$$nS_2 \rightleftharpoons S_{2n}$$

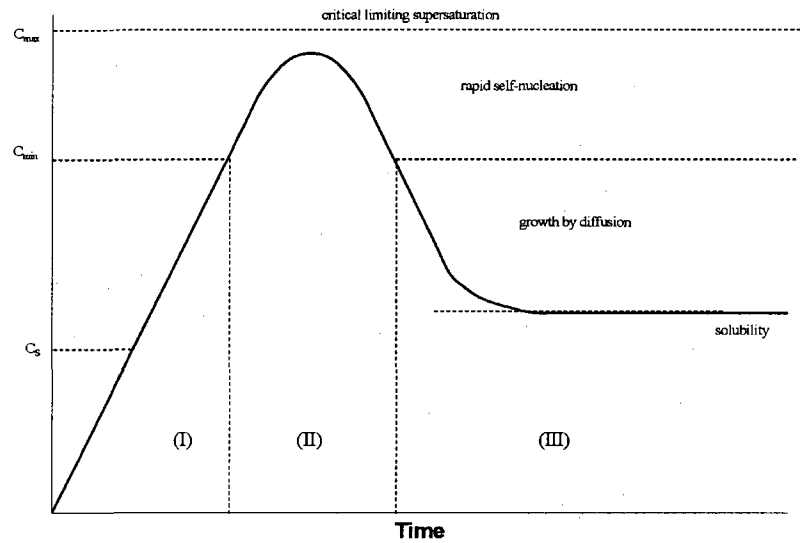

Figure 2.2. The LaMer mechanism of nucleation of sulfur. The (theoretical) curve shows sulfur concentration as a function of time. Adapted from reference 59 with permission.

LaMer's mechanism has been cited many times in the studies of nucleation of various clusters; for example, a Web of Science search reveals that LaMer's 1950 paper has been cited >380 times. While it may be a viable mechanism for the specific system of *sulfur sol formation* (and others, *vide infra*), it is not expected to be the mechanism by which transition-metal nanoclusters nucleate and grow from dilute solutions. Despite this, LaMer's pioneering mechanistic work described above (Scheme 2.1) has been applied to nanocluster preparations.[61] This has led the opinion that LaMer's work has been "overcited";[61] Finke and Watzky have pointed out that this statement is unfair to LaMer and coworkers, given that LaMer's mechanism was the only one available for almost 50 years![62]

Studies of AgX clusters by Sugimoto et al. building off both his previous work[27,28] (*vide supra*) and LaMer's mechanism were directed at predicting the number density of the AgX clusters and the time at which nucleation ends and growth

begins.[63] Using the LaMer mechanism and the condition of continuously added monomers, Sugimoto et al. developed a quantitative theory of nucleation, and then verified it experimentally via the formation of AgCl[63] and AgBr[64] clusters. Essentially, these authors showed that the LaMer mechanism can be applied to the formation of AgX clusters from a supersaturated solution. It is interesting to note that the authors suggest a "sort of Ostwald ripening"[63] during the nucleation process, in which larger nuclei grow at the expense of smaller nuclei. This is effectively another way of saying that the nucleation process is an equilibrium one until the critical nucleus is attained, with nuclei dissolving and their monomers going to other nuclei.

Experimental studies of transition-metal nanocluster nucleation and growth

Turkevich's organizer theory of nucleation

Shortly after LaMer's work, in 1951, Turkevich and coworkers put forth what they called the "organizer" model for nucleation.[65] In their study, they reduced chloroauric acid in the presence of citrate ion, $C_6H_5O_7^{3-}$, as a stabilizer at different temperatures and different Au and citrate concentrations. They measured nucleation rates using electron microscopy (a newly developed technique at that time). They found that particle formation followed kinetics consisting of an induction period, followed by a fast increase in the number of particles, followed by a linear increase, followed by a rapid decrease in the rate, Figure 2.3. In their "organizer theory," various species in the reaction solution bind to the gold ions to form "copolymers" of gold ion and the "organizer". The "organizer" in this case was proposed to be the citrate ion, which would become oxidized to acetonedicarboxylic acid upon reduction of the gold ions, Scheme 2.2.

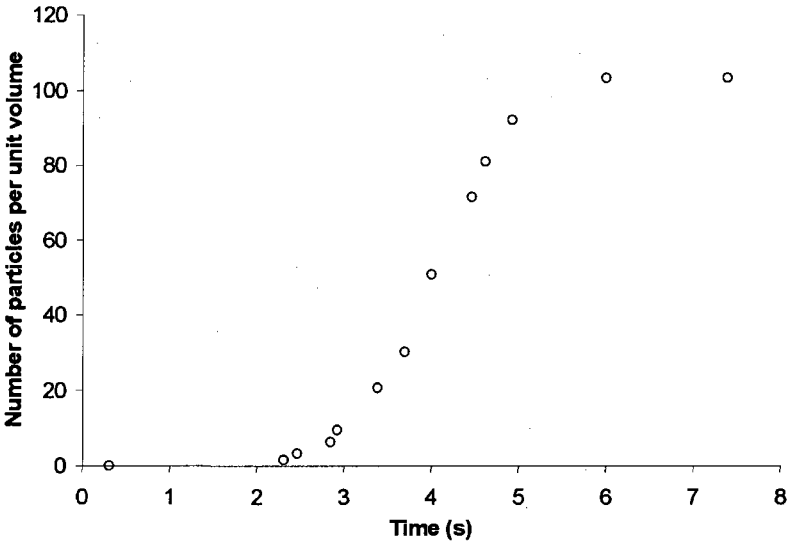

Figure 2.3. Nucleation curve for the reduction of $HAuCl_4$. Adapted from reference 65 by permission of The Royal Society of Chemistry.

Scheme 2.2. Oxidation of citric acid to acetonedicarboxylic acid.

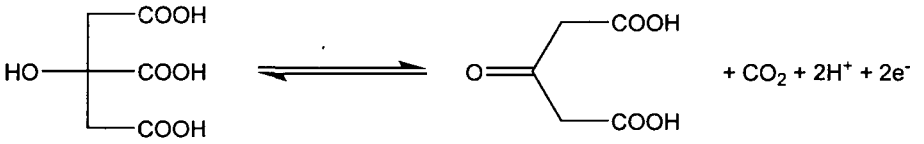

Further evidence presented for this process was that when acetonedicarboxylic acid was added to chloroauric acid instead of citrate, the nucleation curve did not show an induction period. Therefore, the induction period was proposed to be the time that is necessary for the citrate ion to become oxidized to acetonedicarboxylic acid, which rapidly reduces the gold ions to Au^0. Considering the Finke–Watzky mechanism discussed in a moment, it seems likely that the induction period is actually due to the formation of critical Au_n nuclei.

The "organizer" model, while obscure in its chemical details in comparison to LaMer's straightforward, 2-step mechanism, is experimentally well-supported and was a step toward a more relevant mechanism for the formation of transition-metal

nanoclusters. However, Turkevich's mechanism uses only words to describe the nanocluster nucleation and growth process. Restated, the "organizer" model lacks precise chemical equations that sum to the observed stoichiometry and which define the rate constants of the nucleation and growth steps, keys to a more detailed mechanistic understanding of the nanocluster formation process.

The Finke–Watzky 2-step, slow, continuous nucleation and then fast autocatalytic growth, mechanism

The next step in the study of transition-metal nanocluster formation did not come until 1997, when Finke and Watzky described a mechanism for the reduction of transition-metal salts under H_2 that consists of slow, continuous (not burst) nucleation followed by fast, autocatalytic (not diffusion-controlled) surface growth, Scheme 2.3.[62]

Scheme 2.3. The Finke–Watzky 2-step mechanism for transition-metal nanocluster nucleation (rate constant k_1) and growth (rate constant k_2). A represents the nanocluster precursor, and B represents the surface of the growing cluster.

$$A \xrightarrow{k_1} B$$

$$A + B \xrightarrow{k_2} 2B$$

Scheme 2.4. The cyclohexene hydrogenation reporter reaction used to measure the kinetics of nanocluster formation.

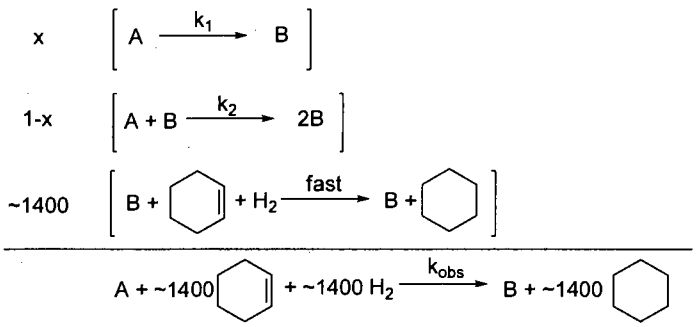

In the initial studies, A represents the nanocluster precursor complex $[Bu_4N]_5Na_3[(1,5\text{-COD})Ir{\cdot}P_2W_{15}Nb_3O_{62}]$, and B represents the growing surface of the Ir_n^0 nanocluster.* The kinetics of nanocluster nucleation and growth are measured using the reporter reaction of cyclohexene hydrogenation, Scheme 2.4; what is actually measured is the loss of hydrogen. In this way, *in situ*/operando kinetic measurement of the nanocluster nucleation and growth is achieved, yielding well-defined rate constants k_1 and k_2 for nucleation and growth, respectively. The rate constants are determined by fitting the hydrogen loss data (converted for convenience as shown in Figure 2.4 to the equivalent cyclohexene loss by the known 1:1 stoichiometry) to the analytic rate equation, eq 2.8, derived from the 2-step mechanism in Scheme 2.3.

$$[A]_t = \frac{\frac{k_1}{k_2} + [A]_0}{1 + \frac{k_1}{k_2[A]_0}\exp(k_1 + k_2[A]_0)t} \qquad (2.8)$$

It should be noted that although the rate constants are determined using the indirect cyclohexene hydrogenation reporter reaction, control experiments using the more direct (but less precise) gas–liquid chromatography (GLC) measurement of cyclooctane evolution from reduction under H_2 of the 1,5-cyclooctadiene present in the nanocluster precursor, $[Bu_4N]_5Na_3[(1,5\text{-COD})Ir{\cdot}P_2W_{15}Nb_3O_{62}]$, demonstrates that the rate constants calculated from both methods *are the same within experimental*

* It must be remembered that the steps in Scheme 2.3 are *composite*, pseudoelementary steps,[62] and therefore there are kinetically hidden mechanistic steps in the overall, multistep nanocluster formation mechanism for example as shown in Scheme 2.5.

error.[8] Following the reduction by ^{1}H NMR has also shown that the cyclohexene reporter reaction method provides accurate rate constants.[66]

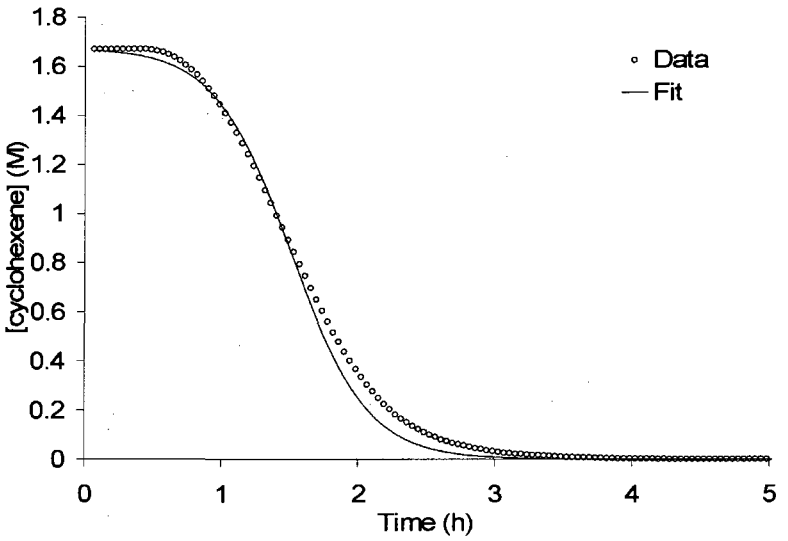

Figure 2.4. Typical cyclohexene loss versus time curve and curve-fit for the reduction of $[Bu_4N]_5Na_3[(1,5\text{-COD})Ir{\cdot}P_2W_{15}Nb_3O_{62}]$ under H_2. The fit is obtained using non-linear least-squares methods to the analytic equation, eq 2.8, for A→B, A+B→2B autocatalytic mechanism, Scheme 2.3. Of the >700 kinetic experiments done to date, the fits are generally good to excellent. When some deviations versus the experimental data are seen, as in the above, deliberately chosen example of one of the *poorer* fits, these can often be quantitatively accounted for by a 3- or 4-step mechanism, *vide infra*.

It is important to point out at this stage that the composite, pseudo-elementary steps,[62] A→B and A+B→2B, are really something more like the following, Scheme 2.5.

The problem of integral calculus[†] of such steps is treated in a simplest (Ockham's Razor), average way to start (as good mechanism must) via the A→B, A+B→2B 2-step mechanism. The rate constants k_1 and k_2 are, therefore and necessarily, averages. An average "x_{growth}" factor has been introduced[62] to account for

[†] Population balance kinetic modeling such as those done by Zukoski[14] is another way to describe the more explicit treatment of all the steps given in Scheme 2.5 herein, and Scheme 2 and Figure 7 in a 2001 paper.[69]

the changing surface area of the nanocluster, and a more continuous way to treat that change is forthcoming;[67] see also reference 68. Importantly, numerical integration simulations done elsewhere[69] of the first ca. 50 of the above steps show that (i) a sigmoidal curve just like that in Figure 2.4 is obtained, *and* (ii) that resultant curve is fit extremely well by the Finke–Watzky, 2-step kinetic model (see Figure 7 presented elsewhere[69]).

Scheme 2.5. As discussed in the main text, other intermediates besides Ir^0, in particular Ir–H (iridium hydrides), are possible if not probable. The individual steps shown are postulated, and have not been directly detected.

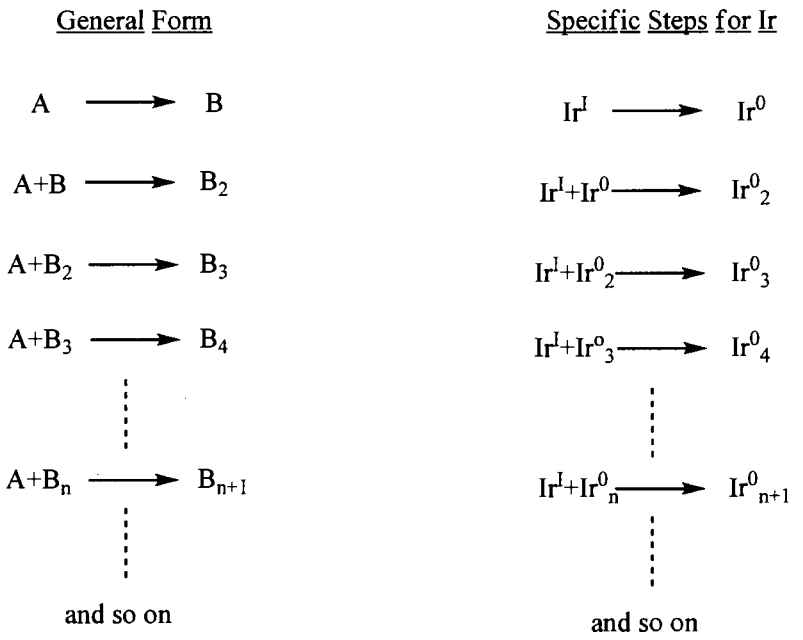

The separation of nucleation and growth in time, necessary for narrow size distributions, is achieved in this system as seen visually by the induction period followed by fast cyclohexene loss in the overall sigmoidal curve in Figure 2.4. The ratio of growth and nucleation rates, R (eq 2.9), can be used to determine the level of kinetic control over nanocluster formation.[8]

$$R = \frac{\text{growth rate}}{\text{nucleation rate}} = \frac{k_2[A][B]}{k_1[A]} = \frac{k_2[B]}{k_1} \qquad (2.9)$$

Faster growth compared to nucleation, giving a higher value of R, ensures that growth of existing nuclei dominates over the formation of new nuclei, thereby achieving near-monodisperse (defined as $\pm \leq 15\%$ size distribution[7]) nanoclusters. The $k_2[B]/k_1$ ratio is also a predictor of nanocluster size, smaller values correlating with smaller nanoclusters and larger values with larger nanoclusters.[8]

Interesting to note here is that the mechanism in Scheme 2.3 *can be used to give an excellent fit to the data obtained by Turkevich*, Figure 2.5.[70] This is excellent, kinetic-based evidence that the nanoclusters studied by Turkevich are formed via an analogous autocatalytic mechanism. This fact and Figure 2.5 have not been previously published.

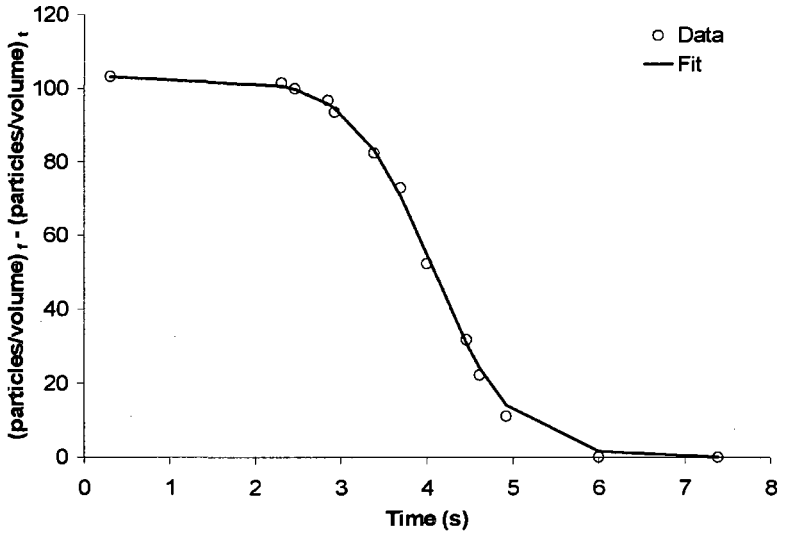

Figure 2.5. The kinetic data from Turkevich's system of reduction of $HAuCl_4$, fit to the 2-step mechanism in Scheme 2.3.[62] The data was converted to give a curve that represents the loss of $HAuCl_4$, and then was fit to the analytic eq 2.8 using Microcal Origin: $k_1 = 3(1) \times 10^{-4}\ h^{-1}$; $k_2 = 30(2)\ M^{-1}\ h^{-1}$.

An important synthetic insight gained from the autocatalytic mechanism in Scheme 2.4 is the need to avoid *heterogeneous* nucleation when forming nanoclusters.[71] Heterogeneous nucleation of metal on solid surfaces is often energetically more favorable (lower $\Delta G^{\ddagger}$) than homogeneous nucleation.[26] In addition, since heterogeneous nucleation is often highly variable, reproducible nanocluster formation is not possible in the presence of heterogeneous nucleation. It has been found that the nucleation rate constant k_1 varies by $\geq 10^3$ when heterogeneous nucleation occurs whereas k_1 varies by $\leq 10^{1.2}$ when homogeneous nucleation occurs.[71] Heterogeneous nucleation can lead to the formation of thin metal films, which also have been shown to form by the autocatalytic A→B, A+B→2B mechanism.[71] One can question whether or not nucleation is ever truly homogeneous in such systems, as typically the amount of dust particles is not controlled (ca. 106 particles per cubic foot in a typical laboratory[72]). A control experiment was done, however, showing that increasing the amount of glass surface area (by adding glass beads) had no measurable effect on k_1 or k_2.[73]

Since the initial reports of the 2-step, autocatalytic mechanism for nanocluster formation, Scheme 2.3, *vide supra*, a more general mechanism for transition-metal nanocluster formation has been described which includes nanocluster agglomeration, adding a third, B+B→C bimolecular agglomeration step[74] and then, very recently, adding a fourth, *autocatalytic agglomeration* step, B+C→1.5C.[66,75] In these new steps, C represents larger, approaching-like metal particles, Scheme 2.6. While each of these modifications adds growth and agglomeration steps to the overall mechanism, the nucleation step A→B remains the same. The 4-step mechanism has a

distinctive kinetic curve, Figure 2.6, in comparison to the 2-step mechanism in Figures 2.4 and 2.5. An example of the almost step-function like kinetic curve is shown in Figure 2.6; note the exceedingly good fit to this unusually shaped kinetic curve.

Scheme 2.6. Illustration of the 4-step mechanism for transition-metal nanocluster nucleation, growth, and then bimolecular plus autocatalytic agglomeration, using the reduction of Pt^{II} as an example.[66,75]

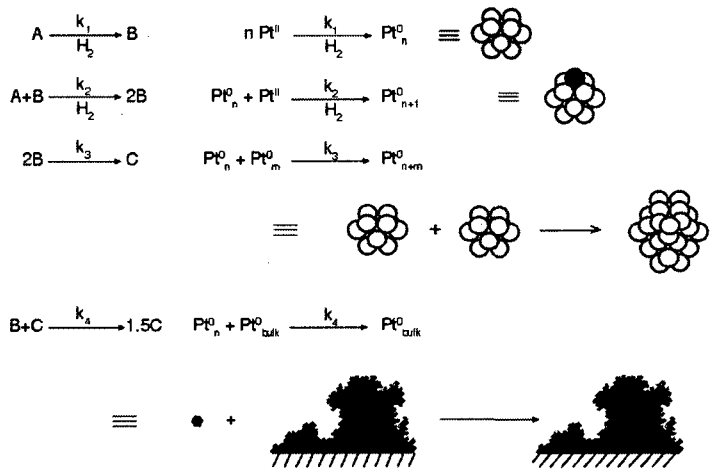

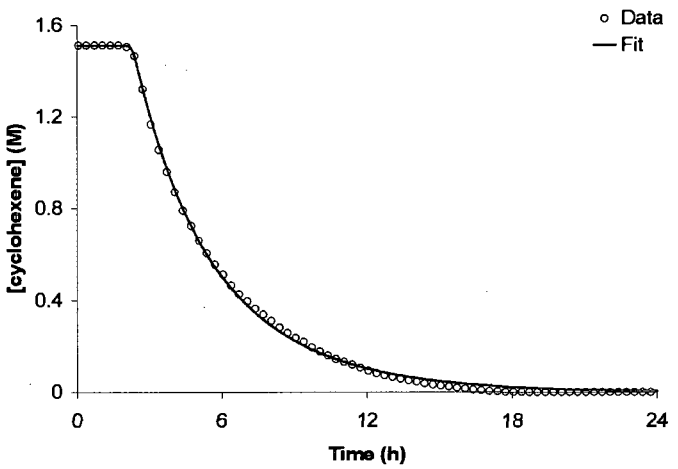

Figure 2.6. Kinetic curve for the reduction of Pt(1,5-COD)Cl_2 under H_2 in acetone and concomitant cyclohexene hydrogenation. The curve is distinctive in that no cyclohexene loss is observed for 0.5–3 h, and then suddenly begins in an approaching step-function like manner. The excellent fit is to the 4-step mechanism in Scheme 2.6: $k_1 \approx 1\times10^{-7}$ h^{-1}, $k_2 \approx 1.6\times10^{3}$ M^{-1} h^{-1}, $k_3 \approx 1.7\times10^{2}$ M^{-1} h^{-1}, $k_4 \approx 9.1\times10^{2}$ M^{-1} h^{-1}; residual = 0.012.

In the four-step, double autocatalytic mechanism, the rate constants are determined using numerical integration, which involves finding the (ideally) global minimum in a five-dimensional space (i.e., four rate constants plus the residual).[66] As a result, the nucleation rate constant k_1 carries with it an experimental uncertainty of $10^{\pm 4}$ in the one well-studied case to date,[66,75] despite there being ~500 to 1000 data points for the calculation of four parameters (rate constants), which gives ~125 to 250 data points per parameter of high precision data (±0.01 psig H_2; ±0.025% out of 40 psig H_2 initially) in that case.[66,75] (Recall that for the 2-step mechanism, variability in k_1 for the synthesis of Ir_n^0 nanoclusters was limited[71] to $\pm \leq 10^{1.2}$ that seems to be mostly experimental in origin.) This $10^{\pm 4}$ variability in the nucleation rate constant k_1 for the 4-step mechanism has been addressed, and is at least in part expected (as has been argued elsewhere[66,75]), given that large-molecule materials are involved, in which less precision is a physical fact of Nature versus small-molecule chemistry.[66]

In addition, sources of experimental error in the k_1 and k_2 and overall synthesis of $Ir_{\sim 300}^0$ nanoclusters have been examined and include trace water, an unidentified impurity in the acetone solvent, and any source of heterogeneous nucleation.[26,71,73] The effects of always imperfect stirring have also been shown to be a factor in the irreproducibility of any reaction that involves autocatalysis.[76] All of these contribute to what Epstein has described as "kinetic indeterminacy",[77] and shows why Oxtoby's observation mentioned previously holds true (i.e., his remark that "nucleation theory is one of the few areas of science in which agreement of predicted and measured rates to within several orders of magnitude is considered a major success"[9]). In short, the

relatively large indeterminacy in k_1, for the 4-step mechanism of nanocluster nucleation, growth, plus two kinds of agglomeration, appears to be a fact of Nature.

In the Finke–Watzky mechanism of slow nucleation and autocatalytic growth, the induction period is the time during which nucleation events are occurring—the formation of the critical nucleus, according to classical nucleation theory,[9,11] as well as according to recent experimental results.[78] The rate constant k_1 is the nucleation rate constant, and the critical nucleus is the size of the cluster at the end of the induction period, when the clusters begin to grow and hence survive long enough to become catalytically active. Measurement of the size of the clusters at this point in the reaction should provide some idea about the number of atoms in the critical nucleus, which can then be compared to the number of atoms in the critical nucleus predicted by theory. Based on the GLC data for the hydrogenation of cyclooctadiene, for the $Ir^0_{\sim 300}$ nanocluster system an upper limit of the critical nucleus was *estimated* as $Ir^0_{\sim 15}$.[8] Recent results suggest that for the nucleation reaction is actually $n\text{A}\rightarrow\text{B}_n$ and not $1\text{A}\rightarrow 1\text{B}$.[67]

Interestingly, small values of the critical nucleus have been found in other areas of science, for example in the protein agglomeration literature (see Appendix B), in which plotting log(rate) versus log(concentration) suggests a critical nucleus size of a *single* misfolded monomer.[79] This is a telling—if not frightening—insight, that a *single* misfolded protein is apparently involved in neurological disease.[79]

The nanocluster composition studies establish the final oxidation state of the nanoclusters as zero, specifically $Ir^0_{\sim 300}$.[80] While these studies have provided a phenomenological nucleation step of "A→B" (really "nA→B$_n$") with a nucleation

rate constant $k_{1,obs}$, the finer details by which the resultant metal^0 nanoclusters are nucleated is not yet clear and is under further study. One unanswered question is: what steps does the metal undergo in going from an ion in a salt to a zero-valent atom in a nanocluster? A number of hypotheses can be put forward, including:

- Under H_2 reduction conditions, metal hydrides are a key to the nucleation process, $M_xH_n^{+/-y}$;
- The reduction of metal ions and removal of ligands is followed by nucleation of neutral, but highly energetic, M^0 atoms, presumably highly ligated ones so as to be meta-stable (see footnote 43a[62] and footnote 4c elsewhere[69]);
- The nucleation of metal ions, with some of their associated ligands, is followed by reduction of the overall cationic cluster, $M_xL_n^{+y}$;
- Some combination of the previous hypotheses; the nucleus consists of a core of M^0 atoms surrounded by metal ions, $\left[M_a^0M_b^{+n}L_c\right]^{y+}$, possibly with hydrides, $\left[M_a^0M_b^{+n}L_cH_d\right]^{y+/0/-}$.

Experimentally supporting or disproving these hypotheses is a major challenge in understanding the nucleation of transition-metal nanoclusters. There is currently disagreement in the literature as to whether metal reduction to M^0, or critical nucleus formation to different species, occurs first.[42,69] While the nucleation mechanism likely depends on reaction conditions, a more complete, more general

picture of what happens during the nanocluster nucleation and growth processes does not exist at this time.‡

The process of how nucleation occurs was considered in some detail in the work of Finke et al.[62,69] The high energy of free Ir^0 atoms is apparent when one considers that the $\Delta H_{vaporization}$ of Ir is 159 kcal/mol, which shows that free Ir^0 atoms are very unstable thermodynamically in comparison to bulk Ir_n^0; see footnote 44 elsewhere.[62] As first noted elsewhere,[62,69] this suggests one of two possibilities: first, that *if* single Ir^0 atoms are formed during the nucleation process to make Ir^0–Ir^0 bonds, then they must be stabilized by coordination by solvent, anionic ligands ($P_2W_{15}Nb_3O_{62}^{9-}$ in that system[62]), or other ligands present,[62] such as olefins. Alternatively, Ir–Ir bond formation may occur with at least one Ir atom still in a higher oxidation state (i.e., Ir^I–Ir^I or Ir^I–Ir^0), followed by reduction to all Ir_n^0. Restated, given that the formation of free (i.e., unsolvated or unligated) M^0 atoms in the nucleation process is thermodynamically *disfavored*, the remaining issues are: (i) when reduction takes place (as the final oxidation state of the metal in the nanocluster is[80] M^0), and (ii) what are the roles of hydrides and other ligands in the nucleation process. Overall, it seems likely that nucleation has more of an "inner-sphere" nature

‡ As has been described previously,[62] as well as back in Scheme 2.5, the A+B→2B step in the Finke–Watzky mechanism is in reality not $Ir^0 + Ir^I \rightarrow Ir_2^0$, but the more general $Ir_n^0 + Ir^I \rightarrow Ir_{n+1}^0$, with n increasing as the nanocluster grows. The change in n is accounted for kinetically by a growth factor, x_{growth}, in the rate equation associated with the growth rate constant k_2. Therefore, the key assumption made in this model is that the rate constant k_2 for each of the growth steps is the same, although it almost surely changes with the size of the nanocluster. In other words, the value obtained for $k_{2,obs}$ is an average value.

than is represented, for example, in purely "outer-sphere," hard-sphere Monte Carlo simulation in a 2004 Nature paper.[81]

Henglein's Pt, Pd, and Ag nanocluster formation studies

Henglein and coworkers have used thermodynamic arguments and absorption spectroscopy to propose the formation of Pt^{I} intermediates in the aqueous reduction of $[Pt^{II}Cl_4]^{2-}$ by hydrogen in a 2000 paper.[42] They reported that aging the solutions of $[Pt^{II}Cl_4]^{2-}$ speeds the reduction when placed under H_2. This is presumably due to the displacement of two Cl^- ligands by H_2O, forming the more reactive complex $Pt^{II}Cl_2(H_2O)_2$; the diaqua complex has been found computationally to be a viable intermediate (*vide infra*). Four separate mechanisms were considered for the reduction of Pt^{II} and formation of Pt nanoclusters based on the possible intermediates in the reduction: (i) formation of Pt^0 by complete reduction by H_2, eq 2.10a, (ii) formation of Pt^{I} by partial reduction, eq 2.10b, (iii) Pt–H hydride formation, eq 2.10c, and (iv) formation of Pt_2^0 by the reaction of two $PtCl_2(H_2O)_2$ molecules with H_2, eq 2.10d.

$$PtCl_2(H_2O)_2 + H_2 \rightarrow Pt^0 + 2H^+Cl^- + 2H_2O \qquad (2.10a)$$

$$2PtCl_2(H_2O)_2 + H_2 \rightarrow 2Pt^{I} + 2H^+ + 4Cl^- + 4H_2O \qquad (2.10b)$$

$$PtCl_2(H_2O)_2 + 1.5H_2 \rightarrow Pt\text{–}H + 2H^+Cl^- + 2H_2O \qquad (2.10c)$$

$$2PtCl_2(H_2O)_2 + H_2 \rightarrow 2\,Pt_2^0 + 4H^+Cl^- + 4H_2O \qquad (2.10d)$$

The Pt^0, Pt–H, and Pt_2^0 intermediates were dismissed on the grounds of high ΔG of reaction (70.3, 42.0, and 64.1 kcal/mol, respectively). These arguments appear to be

flawed, however, as they assume completely bare Pt atoms or ions without ligation from any of the other species present. It had already been pointed out in 1997 that bare M_n^0 atoms are prohibited on energetic grounds.[62] In other words, water molecules or chloride ions can (and likely do) bond to Pt ions and atoms, for example, thereby stabilizing them and lowering the ΔG of the reaction. Indeed, well-known molecular, M^0 compounds with ligands are stable and isolable, including Ru^0(1,5-COD)(1,3,5-COT) (COT = cyclooctatriene),[82] Pt^0(1,5-COD)$_2$,[83] $Pt_2^0(dba)_3$,[84] and $Pd_2^0(dba)_3$ [84] (dba = dibenzylideneacetone).

The authors were left with the Pt^I mechanism, which they proposed as the true mechanism of Pt_n^0 nanocluster formation. They admitted that this mechanism is "plausible, although not proven by direct experiment".[42] (Of course no mechanism is ever *proven*; instead, alternative mechanisms are *disproven*.[85]) What we believe the authors meant is that they were being careful to point out the lack of direct spectroscopic evidence for Pt^I. Therefore, a Pt^I intermediate is a feasible, but not unequivocally supported, hypothesis in this case. Also meriting further reinvestigation is a $Pt_2^{n+/0}$ hypothesis.

Prior to the above experiments, Henglein et al. reached a similar conclusion for the formation of Pd^0 colloids by radiolysis of $Pd^{II}(NH_3)_4Cl_2$.[86] (A 2006 review is available on "Nucleation, Growth, and Properties of Nanoclusters Studied by Radiation Chemistry".[87]) In this system, they used radiolysis to form a hydrated electron that reduced Pd^{II} to Pd^I. They then imagined two different scenarios for the formation of Pd "clusters" (e.g., Pd–Pd dimers, where the Pd atoms are coordinated by NH_3, Cl^-, and/or H_2O ligands). In one scenario, they imagined two ligated Pd^I ions

coming together to form Pd_2^{2+} complexes. In the other scenario, two Pd^{I} complexes disproportionated to Pd^0 and Pd^{II}, and the complexed Pd^0 atoms came together to form Pd_n^0. Although, as they stated, "a clear distinction between these two cases cannot be made",[86] they favored the Pd_2^{2+} mechanism based on differences in reactivity between the Pd "cluster" and fully reduced Pd colloids. Specifically, the Pd_2^{2+} cluster and Pd_n^0 colloids were each reacted with H_2S and CN^-. In the reactions with H_2S, the Pd_2^{2+} reaction is $(Pd_2)^{2+} + 2H_2S \rightarrow 2PdS + H_2 + H^+$, while the Pd_n^0 colloid reaction is $Pd_n^0 + nH_2S \rightarrow (PdS)_n + nH_2$. In the reactions with CN^-, the cluster formed $Pd(CN)_4^{2-}$, while the colloid formed a different product, which was assigned as $(PdCN)_2$. Again, these results are not solid evidence for or against either intermediate, but they do demonstrate the feasibility of the Pd_2^{2+} species as a participant in the nanocluster formation process. Problematic in this work is that kinetic evidence for the proposed nucleation steps is lacking. Nevertheless, the evidence for $M_2^{+n/0}$—and/or $M_2H_x^0$ we hypothesize—as a key species in nanocluster nucleation is slowly accumulating.

Although Ag is not strictly a transition metal (having no partially filled d or f orbitals), Henglein's studies of Ag cluster formation are relevant to the present review because of the mechanistic insights gained from those studies. The pulse radiolysis method[87] was used to reduce Ag^+ to Ag^0.[88] UV–visible spectroscopy was used to detect and follow the formation of small silver dimers and tetramers, Ag_2^+ and Ag_4^{2+}. A mechanism for colloid formation was presented in which small Ag_x clusters form via coalescence of even smaller clusters. These small clusters were designated "Type-

I" nuclei;[89] though Henglein did not use this term, they can be thought of as sub-critical nuclei. It was then assumed that at a critical size, the cluster grows by addition of a single Ag^+ ion to the cluster surface. These critical nuclei were called "Type-II" nuclei. It was predicted that the critical size of Ag_m clusters "is possibly reached in the range of *m* from 10 to 20",[89] although no direct evidence for this was given. The mechanism described by Henglein closely resembles the 1997 Finke–Watzky mechanism in Scheme 2.3, in which nucleation of metal atoms up to the critical size is followed by growth via surface reduction of more metal ions. Unfortunately, the kinetic data necessary to unequivocally support this was not published.[89]

The effects of added citrate ligand were examined in the formation of Ag clusters as well.[89] It was found that as the citrate concentration was increased, the particle size decreased exponentially. The ability of the citrate to stabilize the size of the critical nucleus, Ag_m, was proposed to change with the citrate concentration so that the size of the critical nucleus was proposed to depend on the citrate concentration and its cluster-capping action.

Bönnemann's Pt nanocluster intermediate studies

The work of Bönnemann et al. on the preparation of Pt nanoclusters offers another idea of what *might* happen during nucleation.[90–93] In the reaction of $Pt(acac)_2$ (acac = acetoacetanoate) with $Al(CH_3)_3$, an intermediate was proposed consisting of two tetramethylplatinum species bridged by two methylaluminum species, Scheme 2.7.[94] This putative intermediate complex was characterized by ^1H NMR, ^{13}C NMR, mass spectroscopy, EXAFS, XANES, and anomalous small-angle X-ray scattering (ASAXS) spectroscopy, along with modeling using DFT.

Scheme 2.7. Reaction of $Pt(acac)_2$ and $Al(CH_3)_3$ to form the stable intermediate, which is presumed to go on to form Pt^0 nanoclusters.

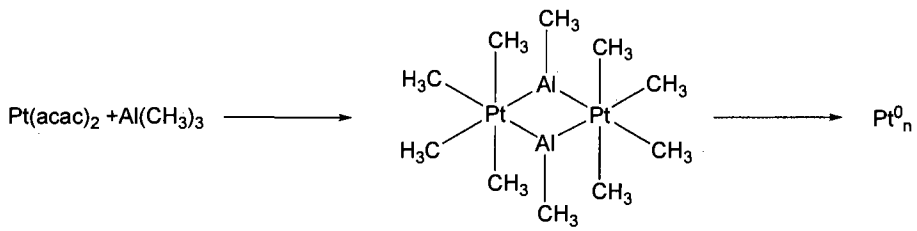

Although the proposed nanocluster intermediate was extensively characterized, the formation mechanism of the Pt nanoclusters themselves from this putative intermediate was never investigated. Restated, lacking are the crucial kinetic studies necessary to demonstrate that this *isolable* (stable) complex is a true intermediate along the reaction pathway, as opposed to a dead-end species as "Halpern's Rules" for catalysis predict (since it is stable and isolable).[95] In addition, the authors assumed that nanocluster nucleation takes place via the association of individual Pt^0 atoms; that is, reduction of Pt^{II} to Pt^0 occurs before nucleation. The authors did not give any evidence for this; instead, they stated that "the rate controlling step for the nucleation is the decomposition of the thermally unstable binuclear precursor molecules and is not the subsequent diffusion-controlled agglomeration of the *single zero-valent Pt atoms into particles*" (italics have been added).[94] Therefore, they assumed, without providing experimental evidence, that the intermediate is reduced to give single Pt^0 atoms, which then quickly nucleate and grow into Pt_n^0 nanoclusters. This assumption contradicts the thermodynamic considerations already described, that bare M^0 atoms are prohibited energetically.[42,62]

An interesting finding, in the work of Bönnemann et al., is that if excess 1,5-cyclooctadiene is added to the reaction, Pt_n^0 nanoclusters are *not* formed. Instead, the dimethylplatinum complex $Pt(1,5\text{-COD})(CH_3)_2$ is formed, supposedly reforming $Al(CH_3)_3$ (a balanced stoichiometry was not provided by the original authors; hence, a *possible* reaction stoichiometry is given herein as Scheme 2.8).[96] The 1,5-COD ligand apparently has a preventative effect on nucleation, breaking apart the Al-bridged intermediate to form an organometallic complex. The details of this not well-defined transformation, including kinetic and mechanistic studies, or even a proven stoichiometry, have not been reported.

Scheme 2.8. Balanced chemical reaction showing the formation of $Pt(1,5\text{-COD})(CH_3)_2$ from the stable Pt–Al complex and 1,5-COD.

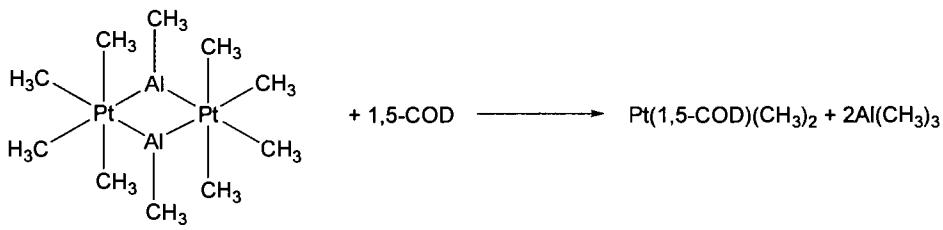

Co nanoclusters from the Co^0 complex $Co_2(CO)_8$

The formation of cobalt oxide nanoclusters has been studied in detail by Tannenbaum and coworkers.[97] The precursor complex used in their studies was $Co_2(CO)_8$. The use of a precursor in which the metal is already zero-valent nicely removes the issue of whether *reduction* occurs before or after cluster formation. However, the final product is the oxidized Co_xO_y, so that an equivalent issue, of whether Co^0 or *oxidized* Co_n^{m+} clusters nucleate, is introduced into that work. The

decomposition of $Co_2(CO)_8$ was assumed to take place via the well-known process of removal of CO ligands before clustering occurs.[98] In their work, Tannenbaum et al. proposed three steps to nanocluster formation and stabilization in the presence of polymers such as poly(methyl methacrylate) (PMMA):[97] (i) the formation of "metallomers" (small clusters—presumably the critical nuclei) by heating a solution of $Co_2(CO)_8$ to 90 °C, (ii) the aggregation of metallomers to larger particles, and (iii) the adsorption of PMMA to the metal particle surface. The idea that the polymer does not interact with the metal throughout the nanocluster formation process, but instead waits in the background until a nucleus has formed and then grown to a cluster—even when it is present in the reaction solution from the beginning of the reaction—is highly questionable and unsupported by firm evidence. In this system, the main method of characterizing the nanoclusters is infrared spectroscopy (IR), which was used to follow the CO stretches of the precursor to measure the kinetics of its decomposition. The IR data shows that no change in the PMMA spectral features occurs until the onset of nanocluster formation. This is contradictory to intuition, which predicts that the polymer would interact with the metal from the beginning of nanocluster formation. It also contradicts recent experimental evidence—albeit in a different, Ir system[99]—which shows that *especially lower* MW_{ave} ~3500 *poly(vinyl pyrrolidone) appears to have a dramatic effect on the nucleation of* Ir_n^0 *nanoclusters*.[99] (A significant issue in this second system is the broad molecular weight distributions of the polymers, so that one does not know which MW component of the polymer gives the observed effect.[99]) The putative lack of PMMA interaction with the growing nucleus further stands in contrast to an earlier report

studying Co nanocluster formation in the presence of polystyrene in which the authors concluded that the polymer was interacting with the "*forming* cobalt clusters" (italics added).[100] Because the PMMA is present with the precursor complex, it is much more likely that the polymer interacts with the metal throughout the nanocluster formation reaction. Consistent with these points, it has recently been recognized that "it is unlikely that these ligands only begin to function after nucleation is complete."[101]

Infrared data were also used to address the question of the sequence of oxidation and clustering of Co atoms.[100] The characteristic CO absorption band at 1858 cm^{-1} and Co–O band for the oxidized $(Co_2O_3)_n$ clusters at 883 cm^{-1} were both followed during the reaction. The appearance of the Co–O band did not correlate with the decrease in intensity of the CO band. The decrease of the CO band, corresponding to the decomposition of $Co_2(CO)_8$, began immediately, while the appearance of the Co–O band, corresponding to the formation of Co_2O_3 clusters, showed a ~2 h induction period. This led the authors to conclude that decomposition of $Co_2(CO)_8$ occurs to form Co_n nuclei, which are then oxidized to yield $(Co_2O_3)_n$ clusters. A major problem with these otherwise valuable studies is that *CO loss from $Co_2(CO)_8$ is a significant part of, if not the, rate-determining step*. This, unfortunately, hides kinetically the nanocluster nucleation and growth steps of interest. The $Co_2(CO)_8$ thermolysis system, therefore, is probably not the ideal one in which to learn the intimate details of the nucleation and growth of $(Co_2O_3)_n$ nanoclusters.

The size of the critical nucleus was estimated for the $Co_2(CO)_8$ system using TEM and dynamic light scattering (DLS) experiments. In these experiments, samples

from the reaction solution were analyzed during the induction period for the formation of Co_n nuclei, as well as at the end of the $(Co_2O_3)_n$ nanocluster forming reaction. No clusters were observed during the induction period above the DLS detection limit of 3 nm; therefore, an upper limit to the critical nucleus size of $\leq$3 nm was assigned to the Co_n nuclei which in turn can be used to calculate a $\leq Co_{1285}$ cluster in the limit of a hypothetical, unligated 3 nm Co particle. This study illustrates the disadvantage of TEM (and DLS) mentioned earlier, that relatively high detection limits are only able to set an upper limit to nucleus sizes, but cannot accurately measure them. More measurements taken after the induction period, but before the end of the reaction, should provide more information about the formation of the nanoclusters, but such results have not been reported.

The formation of bimetallic "$CoPt_3$" nanoclusters was recently studied in detail by Weller et al. using the same $Co_2(CO)_8$ precursor along with $Pt(acac)_2$.[102] Because of the lack of compositional studies, the nanoclusters should be written formally as "$[Co_aPt_{3a}(CO)_b(acac)_c]^{n+/-}$" to take into account all species that may be involved in the (unknown) nanocluster composition. This study focused on the dependence of nucleation and growth rates on temperature and precursor concentrations. Using CNT arguments, specifically eq 2.4, they explained why higher reaction temperatures give smaller nanoclusters by relating the final nanocluster size to the rate of nucleation, Scheme 2.9, stating without evidence that the nucleation rate is more sensitive to temperature than the growth rate. These authors also observed that with an increase in the concentration of their nanocluster stabilizer, 1-adamantanecarboxylic acid (ADA), the final nanocluster size *increased*, a result

opposite to Turkevich's finding with Au/citrate described earlier.[65] The stabilizer was hypothesized to interact strongly with the monomers, slowing nucleation and leading ultimately to larger nanoclusters, as shown in Scheme 2.9.[102]

Scheme 2.9. Reprinted with permission from reference 102.

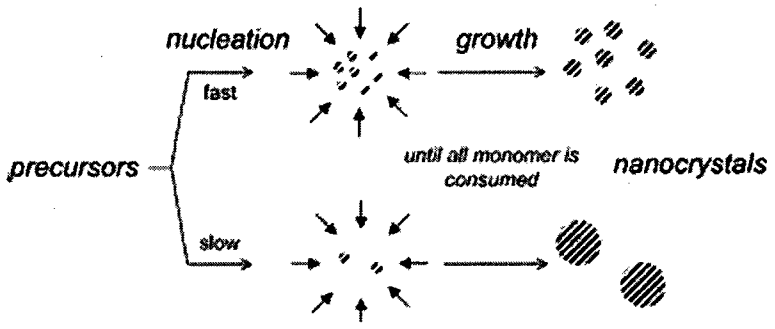

The nucleation mechanism put forth by Weller et al. is as follows, although the kinetic data necessary to put the following mechanistic speculation on firm ground are lacking.[102] The critical nucleus for formation of the Co/Pt nanocluster is proposed to consist of only Co atoms (i.e., and no Pt) based on the observation that an increase in Pt led to an increase in the final size of the $CoPt_3$ particles. One can suppose that the nuclei are composed of $Co_n(CO)_m$ units, where n and m are small integers; experimental evidence for or against this hypothesis is lacking, however. The Co clusters are then hypothesized to catalyze the reduction of Pt^{II} from $Pt(acac)_2$ to Pt^{I}, which is incorporated into the Co/Pt cluster. The proposition of this Pt^{II} to Pt^{I} reduction step is based on computational studies of Pt cluster formation (*vide infra*). The cluster is then thought by the authors to be reduced by either CO or 1,2-hexadecandiol, which is present in the reaction solution. Finally, the authors

hypothesize that the process of $Pt^{II} \rightarrow Pt^{I}$ reduction and addition, followed by cluster reduction, is iterated to form fully reduced $CoPt_3$ alloy nanoclusters.

The mechanism put forth above was formulated based on CNT and the sizes of the nanoclusters, the latter with respect to the dependence of nanocluster size on the nucleation and growth rates. However, without the support of the necessary kinetic data, the conclusions in the study can be, strictly speaking, only considered hypotheses based on nucleation theory (which has been shown to be inaccurate in many cases, *vide supra*). The lack of an established composition for the resultant $[Co_aPt_{3a}(CO)_b(acac)_c]^{n+/-}$, as well as a balanced reaction stoichiometry that is the first step to reliable mechanistic work, are other, fundamental problems with this work.

Rothenberg's UV–visible study of Pd, Au, and Ag nanocluster formation

As mentioned earlier, a problem with *in situ* UV–visible measurements of nanoclusters is that many other species are present which could interfere with the spectrum of the nanocluster. To deal with this problem, Rothenberg et al. devised a system, called the "net analyte signal/principle component analysis" (NAS/PCA), in which the spectra of the interfering species are essentially subtracted out of the spectrum, leaving a difference spectrum that they assume is only the spectrum of the nanoclusters.[43] These authors used the NAS/PCA method to study the formation of Pd, Au, and Ag nanoclusters, as well as to study the possibility of forming bimetallic nanoclusters using combinations of those metals. Following the corrected nanocluster spectrum and the metal salt spectrum with time, they were able to measure the kinetics of salt reduction and nanocluster formation, Figure 2.7. From their data, they concluded that reduction of the metal salt occurs *before* the formation of clusters.

Also, for the formation of Au^0 nanoclusters from $HAu^{III}Cl_4$, a Au^I intermediate was inferred based on the NAS/PCA data and the reduction potentials of Au^{III} and Au^I. The authors noticed distinct induction periods in which no detectable clustering took place (see Figure 2.7). Although they do not mention the implications of this, there is a possibility of using this data—in particular the first induction period—to gain information about the critical nucleus of the clusters. The second and third clusterings are presumably periods of nanocluster growth, although this is not certain. The necessary rigorous kinetic analysis of this UV–visible data is missing. Again, the balanced reaction stoichiometry required for reliable mechanistic studies is also missing.

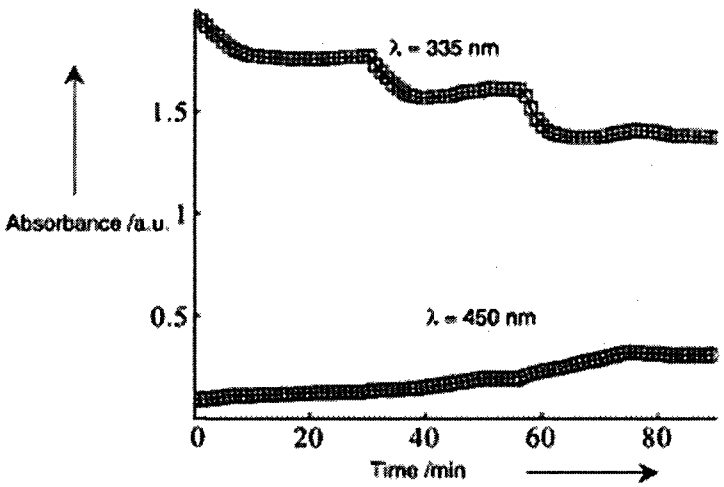

Figure 2.7. Absorbance profiles of Pd^{2+} ions (top) and Pd^0 clusters (bottom). Three distinct periods can be seen. During the flat parts of the Pd^{2+} profile, reduction of Pd^{2+} stops, but cluster growth is believed to be still occurring at these times. Reprinted with permission from reference 43.

Observation of Rh_{4-6} clusters in dehydrogenation reactions by XAFS

In 2005, Chen, Fulton, Linehan and Autrey at Pacific Northwest National Labs (PNNL) reported an EXAFS and XANES study on the rhodium-catalyzed

dehydrogenation of dimethylamine borane beginning with a $[Rh(1,5\text{-}COD)Cl]_2$ catalyst precursor.[103] This reaction, which shows promise for applications of hydrogen fuel storage and release,[104] had been previously studied by Manners' group[46,105] with the goal of determining the true catalyst. Manners' studies indicated that a heterogeneous Rh species, likely a Rh^0 colloid, catalyzes the dehydrogenation. Using XAFS, the PNNL team studied the dehydrogenation of dimethylamine borane starting with $[Rh(1,5\text{-}COD)Cl]_2$. Taking advantage of the strong Rh backscattering in the EXAFS, they were able to show that small Rh_x^{n+} clusters are formed in the reaction—suggesting, but not kinetically verifying or disproving—that these small, sub-nanometer (ca. 0.3 nm) clusters and not larger Rh^0 nanoclusters, are the true catalysts. These sub-nanometer clusters were initially assigned to be Rh_6 based on comparisons with the carbonyl complex $Rh_6(CO)_6$; since this report, further studies have suggested that the clusters are actually Rh_{4-6},[106] results which emphasize the ≥20–30% or more error in determination of the coordination number (i.e., and thus the number of metal–metal bonds) by EXAFS, a point emphasized by Gates.[107]

Examination of previous literature reveals at least two reports that support the idea of a M_4, and we hypothesize more likely a M_4H_4, sub-nanometer cluster, as an important catalytically active species. In 1987 it was hypothesized by Duff et al. that nucleation occurs by addition of metal atoms to a tetrahedral nucleus, since the tetrahedron is the simplest metastable unit.[108] TEM visualization of silver clusters provided evidence for this hypothesis in that a structure reflecting the symmetry of an underlying Td species is seen; computer-image simulations corroborated this evidence. However, as described above, this evidence must be considered equivocal

as TEM is capable of affecting the observed structure of especially non-third-row transition-metals.[46,47]

In 2001, the hypothesis of polytetrahedral organization of particles was put forth by Chaudret et al. for the formation of Rh nanoclusters from reduction of $[Rh(C_2H_2)_2Cl]_2$ by Cp_2V.[109] In this case, both high-resolution TEM and wide angle X-ray scattering (WAXS) were used to support the tetrahedral cluster hypothesis, but lack of a defined stoichiometry or any kinetic evidence makes the conclusions equivocal.

These data support the hypothesis that the critical nucleus is *not* composed of neutral metal atoms, but decorated with ligands—again, we suspect that hydrides are likely more common ligands. Further evidence of the possibility of $Rh^{n+}H_n$ sub-nanometer clusters comes from the literature of Rh-hydride cluster complexes, for example $[Rh(1,5\text{-COD})H]_4$ [110] and $\left[Cp^*RhH\right]_4^{2+}$.[111] Computational evidence also supports the idea of non-zero-valent metals as crucial intermediates en route to nanoclusters (*vide infra*). In light of the PNNL group's EXAFS results, the idea of M_4 (or M_4H_4 as we prefer at present) sub-nanometer catalysts deserves immediate attention and may in fact open up a new area of *active, sub-nanometer catalysts*. Tantalizingly consistent with the idea of a M_4 sub-nanometer catalyst is the observation of Finke, Finney, and Starkey-Ott[67] showing that the kinetic critical nucleus of the well-studied Ir_n^0 nanocluster system is $n \geq 2$. Of course, $2 \times 2 = 4$, so that dimerization (aggregation) to a more stable Ir_4 nucleus is one intriguing idea requiring EXAFS, XANES, and other, in-progress studies.[112]

Other factors affecting nanocluster preparation

Control over nanocluster nucleation is expected to lead to control over nanocluster size, shape, and other properties. In this section, control over nanocluster nucleation is examined in two ways: the first looks at the inherent effect of the transition metal itself on the size of the critical nucleus, and the second examines the technique of seeding nucleation by adding preformed clusters.

Effect of metal–metal bonds on the critical nucleus

As described earlier and shown in Figure 2.1, the critical nucleus has a specific size, r^*, associated with it. The hypothesis can be put forth that for transition-metal nanoclusters, the size of the critical nucleus is dependent on the strength of the M–M (metal–metal) bonds (see Figures 2.8, 2.9, and 2.10 herein, *vide infra*, for initial data supporting this hypothesis). Precedent for this hypothesis can be found in Stranski's 1935 paper, where he uses a $\Delta H_{\text{vaporization(sublimation)}}$ versus a $\Delta H_{\text{surface}}$ energy term as part of his theoretical treatment.[113] Since a metal's heat of vaporization, ΔH_{vap}, can be used as a measure of the M–M bond strength, and since the critical nucleus strongly influences the final size of the nanocluster, there should therefore be a correlation between a metal's ΔH_{vap} and the size of the metal nanocluster. More specifically, a metal with higher M–M bond strength, as reflected by a higher value of ΔH_{vap}, should favor nucleation over growth and result in smaller nanoclusters. Conversely, a metal with lower M–M bond strength and therefore lower ΔH_{vap} should favor growth over nucleation, resulting in larger nanoclusters. All of this, of course, assumes that nanoclusters of all metals are formed *under the same mechanism*—a necessary hypothesis for the plots which follow, but not one expected to be

completely correct. Restated, this hypothesis can only be supported or disproven using identical reaction conditions for all metals (temperature, concentration, solvent, and ligands).

An examination of literature preparations of transition-metal nanoclusters using many different metals seems to support the hypothesis: *that the size of the nanoclusters in general decreases with increasing heat of vaporization, ΔH_{vap}.* A well-known relationship that must be mentioned here is the Gibbs–Thompson relation, stating that the partial molar free energy of a metal atom in a particle of radius R, $\mu(R)$, differs from that in the bulk, $\mu(\infty)$, as a function of the surface free energy of that same metal, γ, and the volume per metal atom of the bulk metal, Ω, eq 2.11. An excellent recent paper which discusses the Gibbs–Thompson relation, and shows nanocluster size effects even more dramatic than those predicted by eq 2.11, is a 2002 paper by Campbell and coworkers.[114]

$$\mu(R) - \mu(\infty) = \frac{2\gamma\Omega}{R} \tag{2.11}$$

The most illustrative data consistent with the preceding hypothesis is Hirai's classic preparation of nanoclusters from transition-metal chlorides ($RuCl_3 \cdot 3H_2O$, $RhCl_3 \cdot 3H_2O$, $PdCl_2$, $H_2PtCl_6 \cdot 6H_2O$, and $HAuCl_4 \cdot 4H_2O$), one oxide (OsO_4), and one nitrate ($AgNO_3$).[115] A plot of nanocluster size versus the metal ΔH_{vap} is shown in Figure 2.8, and gives a roughly linear plot with an R^2 value of 0.915.[115] The nanoclusters were prepared by refluxing solutions of the precursor complexes and polyvinyl alcohol (PVA) in a methanol/water mixture in air. The sizes of the nanoclusters were measured by TEM; unfortunately, this was the only characterization method used so the true composition of the nanoclusters is unknown

(and, for example, since the nanoclusters were formed in air, the formation of surface oxides is highly likely[116]). Also, the methanol used as a solvent can form formaldehyde and formic acid, both of which may interact with the metal surface. This gives a possible total composition of the nanoclusters of $[M^0_n(Cl^-)_m(PVP)_p(O)_q(OH^-)_r(OH_2)_s(CH_3O^-)_t(CH_2O)_u(HCO_2^-)_v]^{x+/-}$, with unknown of values of m–v.

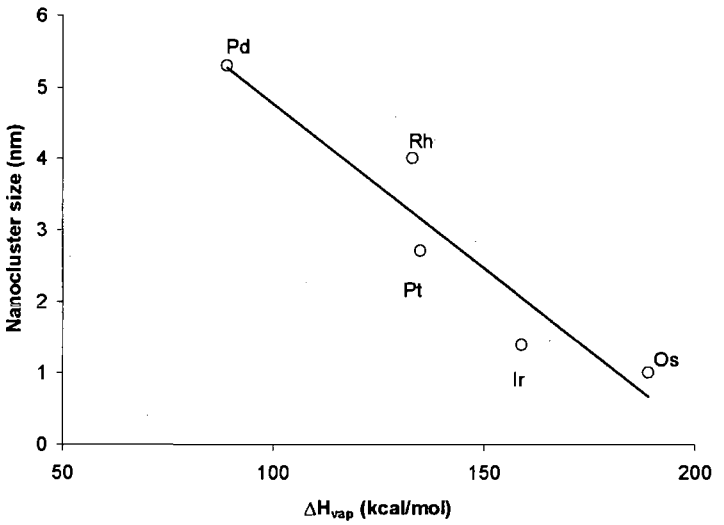

Figure 2.8. Analysis of Hirai's[115] transition-metal nanocluster data showing a correlation between ΔH_{vap} and nanocluster size for six different metals.

Another example showing a correlation between nanocluster size and ΔH_{vap} comes from our analysis, Figures 2.9a and 2.9b, of Bönnemann's 1996 report of "nanoscale colloidal metals stabilized by solvents and surfactants."[117] In this preparation, halide salts of Ir, Pd, Fe, Rh, Ru, and Co were reduced in THF, and salts of Cu, Ag, Au, and Cr were reduced in toluene. Since the metals were prepared in different solvents, two different plots are shown in Figure 2.9, one for each solvent used. The correlations are at least suggestive—for THF, the R^2 value is 0.856 and for

toluene the R^2 value is 0.759.[117] The difference in slopes between the two curves is very interesting (in curve A the slope is −0.021 nm/kcal mol^{-1}, and in curve B the slope is −0.334 nm/kcal mol^{-1}) and could be due to the different solvents used, the different metals, both of these, or other factors. A simple experiment to determine if the solvent is the (major) factor that determines the slope of the line would be to reduce the same set of metal precursors in different solvents. The physical meaning of the slopes of the lines could provide key insight into the nature of these two domains of nanocluster size dependence on M–M bond strength.

The previously unpublished results in Figures 2.8 and 2.9 are quite interesting. However, what is needed to determine if such a correlation between nanocluster size and a given metal is in fact real and perhaps more general are studies in a system in which the nanocluster formation mechanism is known and where all the other conditions besides the metal are kept constant. The nanocluster system in which the autocatalytic A→B, A+B→2B mechanism has been extensively studied is in principle the best system at present in which to perform the needed studies.[62] The separation of nucleation and growth k_1 and k_2 steps should allow each of those steps to be correlated with nanocluster size and M–M bond strength.

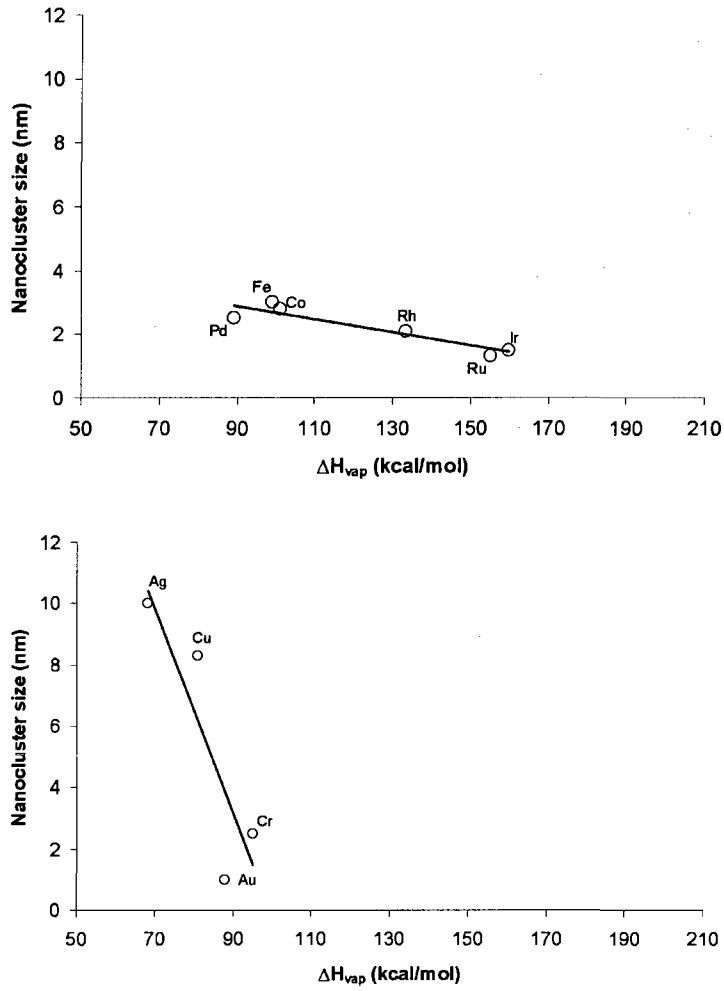

Figure 2.9. Analysis of Bönnemann's[117] transition-metal nanocluster data for the preparation of nanoclusters in THF (top) and in toluene (bottom). The slope of the line in toluene is an order of magnitude greater than that in THF. This could be due to the different metals studied, the different solvent, or some other factor(s).

The needed studies were attempted for the polyoxoanion-stabilized transition-metal nanoclusters, $[(1,5\text{-COD})M{\cdot}P_2W_{15}Nb_3O_{62}]^{n+}$. Unfortunately, only the Ir[62] and Rh[118] precursor complexes have been successfully synthesized; the nanocluster size versus ΔH_{vap} "2-point plot" for these metals is shown in Figure 2.10. At least its trend is as expected, but, of course, the "2-point line" is unconvincing. This in turn led to the idea of using the commercially available metal salts $[M^I(1,5\text{-COD})Cl]_2$ (M = Ir,

Rh) or $[M^{II}(1,5\text{-COD})Cl_2]$ (M = Pt, Pd, Ru) under H_2 in propylene carbonate as the solvent (as propylene carbonate, with its relatively high dielectric constant of 69, can allow even weak nanocluster stabilizers such as Cl^- to give stable, soluble nanoclusters[118,119]). Optimization of the experimental conditions to allow this direct comparison of nanocluster size versus metal is currently in progress. Also fascinating here is the idea of trying to see the critical nucleus, and other nanocluster size versus time data, by EXAFS and XANES plus the required kinetic studies, efforts that are in progress.[120]

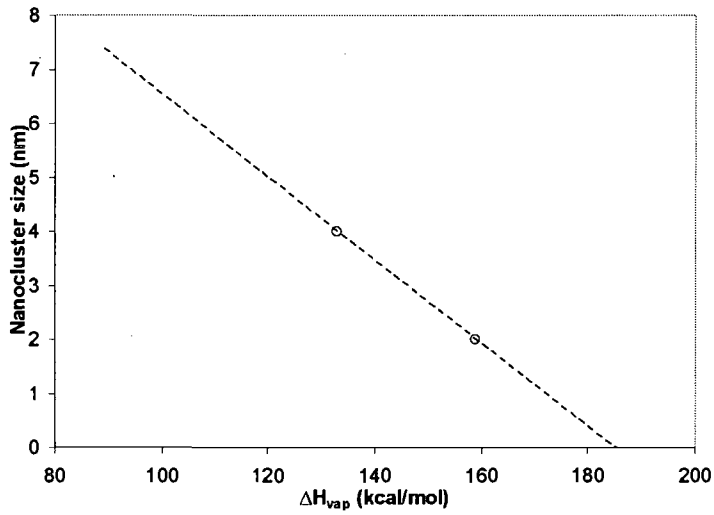

Figure 2.10. "Two-point plot" for the reduction of $[(1,5\text{-COD})Ir{\cdot}P_2W_{15}Nb_3O_{62}]^{8+}$ and $[(1,5\text{-COD})Rh{\cdot}P_2W_{15}Nb_3O_{62}]^{8+}$. The Ir and Rh complexes are the only ones that have been successfully synthesized and reduced to obtain nanocluster sizes, but suggest that a correlation *may* be present between metal $\Delta H_{vaporization}$ and nanocluster size in this system as well.

Seeded nucleation

Growth of nanoclusters using seeds as nuclei has been performed since 1906.[121] In an important study by Buhro et al., seeds of $Au_{101}(PPh_3)_{21}Cl_5$ were used to nucleate nanoparticles of Bi, In, and Sn.[122] It was found that using a small

concentration of Bi, In, or Sn gave quite narrow size distributions (from 5.6% to 13.2%). The experimental average nanoparticle size matched calculated sizes with ratios of observed to theoretical sizes at or near 1.0.[122] In the absence of the Au seeds, "extremely broad size distributions" were observed (no quantitative data were provided, however[122]). If the concentration of Bi, In, or Sn was too large, self-nucleation became competitive with the seeded nucleation and broader size distributions resulted which, in turn, did not match the theoretical sizes. The advantage of the seeding method is the obvious control over nucleation and the resultant size and size dispersion. Disadvantages of this method include that the resulting Bi, In, and Sn nanoclusters are contaminated with Au, although the Au is at least initially at the center of the nanocluster and its amount is small (a few percent), depending on the size of the nanoclusters. Still, if 100% pure metal nanoclusters are required, this heteroelement-seeding procedure would need to be avoided.

Self-nucleation has been reported as a problem to be avoided in the work of Murphy et al.[123] They found that reducing $AuCl_4^-$ in the presence of preformed 12 ± 2 nm Au nanoclusters gave varying sizes and size distributions of Au nanoclusters depending on the ratio of seed to Au salt and on the rate of addition of reducing agent (ascorbic acid in that study). Specifically, when the concentration of $AuCl_4^-$ is much larger than the concentration of Au nanocluster seeds, self-nucleation of the $AuCl_4^-$ dominates over seeded growth (just as Buhro et al. found for the preparation of Bi, In, and Sn nanoclusters[122]). Self-nucleation was also observed by Murphy et al. when the reducing agent was added quickly.[123] Slow addition of ascorbic acid prevented self-nucleation, but resulted in deviations in nanocluster shapes from spheres. The authors

presented size-separation and X-ray powder diffraction data to disprove the hypothesis that very small nanoclusters (i.e., too small to be observed in the TEM) were formed and acted as (hidden) seeds for the nanocluster formation.[123]

Seeded nucleation has been found to be necessary for the reduction of some complexes. Whitesides found that the platinum complex $Pt(1,5\text{-}COD)(CH_3)_2$ cannot be reduced by H_2 unless Pt^0 is present as a catalyst.[124] More recently, Finney and Finke found that the presence of $Ir^0_{\sim 300}$ nanoclusters as seeds catalyzed the reduction of $Pt(1,5\text{-}COD)(CH_3)_2$ under H_2.[125] In this case, the formation of putatively Ir^0(core)/Pt^0(shell) nanoclusters quickly agglomerated to bulk metal. As with Buhro's system, this technique results in bimetallic nanoclusters and is, therefore, not desirable if very pure nanoclusters are needed—or very desirable if Ir^0(core)/Pt^0(shell) bimetallic nano-onions[8] are one's goal.

The use of nanoclusters as seeds for organic structures has also been reported.[126] Specifically, rods of arachidic acid ($CH_3(CH_2)_{18}COOH$) have been nucleated onto CdSe nanocrystals by spin coating. The rods are of uniform height (0.95 ± 0.09 nm) and width (5.39 ± 0.05 nm) and lengths that vary from 50 to 250 nm. These results suggest that the use of nanoclusters as seeds will be useful not only for the formation of other nanoclusters, but also for the preparation of organic–inorganic hybrid materials.[127] The ability to tune the properties of the nanocluster seeds will in turn allow for the ability to change the properties of the hybrid materials.

Computational studies of nanocluster nucleation

The vast majority of computational work on the nucleation of clusters has been done for gas-phase nucleation of liquid droplets or solid nanoparticles formed by

chemical vapor deposition, since computations for gas phase systems are, of course, much simpler than for, say, solution nanocluster systems. This is illustrated by the extensive computational studies by Zachariah et al. of the nucleation, growth, and agglomeration of Si[128–130] and SiO_2 nanoparticles[131–133] by CVD. Simulations of the nucleation of SiO_2 particles focused on the effects of pressure and temperature on nucleation rate and particle concentration. In contrast, relatively few computational studies exist for the formation of transition-metal nanoparticles in solution.

Recently, Ciacchi et al. published computational studies using first principles molecular dynamics simulations of the nucleation of Pt clusters from $[Pt^{II}Cl_4]^{2-}$ in aqueous solution,[134] and their growth by addition of Pt^{II} complexes.[135] In their simulations, they observed the formation of Pt^{I}–Pt^{II} and Pt^{I}–Pt^{I} dimers, which could then react with another Pt^{II} species to form Pt^{I}–Pt^{II}–Pt^{I} or Pt^{I}–Pt^{II}–Pt^{II} trimers.[136] Based on their observations, the authors proposed that at least in the case of platinum, cluster formation occurs via bonding of metal ions before reduction to Pt^0, as opposed to full reduction to Pt^0 followed by nucleation of the Pt^0 atoms. Their proposed nucleation mechanism does away with the classical idea of the critical nucleus; instead they state that "each Pt^{II} complex that reacts with a reducing electron can be thought of as a 'critical nucleus' for the growth of metallic platinum clusters".[136] The discarding of the well-entrenched idea of the critical nucleus, based on this one computational study—and its lack of analysis or discussion of the extensive literature cited herein on the critical nucleus concept—is at best unjustified. In fact, these computational observations are in line with experimental considerations concluding that partially oxidized metal clusters are formed before the critical nucleus is attained.

It would be of interest to return to these studies and see if Pt_2^0, $Pt_4^{n+/0}$ or $Pt_4H_4^{n+/0}$ satisfy the criteria of being either critical nuclei or special (metastable) intermediates.

In their calculations, the authors *assumed* a Pt^I intermediate, and accordingly ran their simulations with the $[Pt^{II}Cl_4]^{2-}$ ion and one reducing electron; that is, they simulated their specific mechanistic hypothesis and found it acceptable energetically. Therefore, while their calculations are evidence for the plausibility of a mechanism involving Pt^I species, they do not provide the necessary disproof of other mechanisms[85] (e.g., including complete reduction to Pt^0 as a significant step on the process, or the $Pt_n^{2+/0}$, $Pt_n^{4+/0}$, or $Pt_4H_n^{4+/0}$ alternative hypotheses put forward above). These computational studies are, in general, based on assumptions about what happens during nucleation; more solid experimental evidence of what occurs in the nucleation events is needed to guide further computational studies, to add hydrides or other appropriate ligands to them, and overall to make such calculations more realistic and, therefore, even more valuable.

Conclusions

The main conclusions of this review are:

- There is currently no clear, experimentally quantitative description of what happens during the nucleation of transition-metal nanoclusters in solution. Indeed, the nucleation of clusters in general is poorly quantitated in general, due mainly to a lack of good quantitative experimental kinetic and other data. The kinetics of reactions of known stoichiometry are especially lacking in all but a few cases.

• Although nucleation and growth of clusters has been studied exhaustively in the theoretical sense, experimental results are far less common and in many cases contradict theory, often by many orders of magnitude.

• A number of issues remain to be investigated with regard to the nucleation of nanoclusters, including:

  ◦ If the formation of the nuclei occurs before, during, or after the reduction (or oxidation) of the metal in the metal precursor complex.

  ◦ If ligands—and especially hydrides to start—are a key part of nucleation, or are they merely spectators until the nanoclusters are fully formed, as has been suggested, albeit without evidence.[97] Or, are ligands involved in every step of nanocluster formation, including nucleation, as Finke and coworkers,[8] as well as van Embden and Mulvaney[101] have suggested, as the influence of PVP over nucleation, for example, show,[99] and as one's intuition expects?

  ◦ If ligands are crucial to the nucleation step, how does the strength of the metal–metal bond (or metal–hydride bond) affect the critical nucleus and, therefore, the final size of the nanoclusters, and how do the size and shape of the critical nucleus relate to those of the fully formed nanoclusters? Much of the experimental evidence supports the hypothesis that nuclei consist of at least partially oxidized metal clusters which are reduced after reaching some critical size, although the details of this mechanism have yet to be worked out.

• The Finke–Watzky 2-step mechanism fits nanocluster formation, as well as solution agglomeration of proteins in at least some cases (see Appendix C). As such, evidence is accumulating that the 2-step mechanism may be the more general, simplest Ockham's Razor) mechanism of at least some 1st order phase transitions in solution, a hypothesis under further investigation.[137]

• Promising are the studies indicating a higher order kinetic critical nucleation step, $n\mathrm{A} \rightarrow \mathrm{B}_n$ [67] and the EXAFS and XANES studies implying a Rh_4 (or Rh_4H_4) metastable (sub-) nanocluster.[58,112] Further efforts on the M_4/M_4H_4 critical nucleus hypothesis, detailed herein for the first time, are being actively pursued.[58,112]

The ultimate goal of nucleation studies, as well as studies of growth and agglomeration, of transition-metal nanoclusters is a general, complete mechanistic understanding of what occurs during nanocluster formation. The information gained from such an understanding should shed considerable light on the process of nanocluster formation, therefore leading to enhanced control over nanocluster size, shape and other desired properties. It is hoped that the present review will assist in achieving these goals.

Appendix 2A. Nucleation studies of semiconductor nanocrystals

Of the nanoparticle systems formed in solution, one of the most thoroughly studied systems is the formation of quantum dots of the form CdE (E = Se, S, Te), with the most attention given to CdSe. Although these are not transition-metal nanoclusters, they have been the subject of significant study with regard to the mechanism of their formation and, therefore, warrant at least brief mention here. The CdE nanocrystals are prepared using the hot-injection method described by Bawendi et al.,[138] in which a chalcogen compound, often in a solution of phosphine, is injected into a hot (≥300 °C) solution of a Cd^{2+} species (usually $Cd(CH_3)_2$ or CdO) in a phosphine solution. After the injection, the solution is allowed to cool to <100 °C. This change in temperature from the hot injection to the cooling immediately afterward accomplishes the separation of nucleation and growth that results in narrow size distributions of the nanocrystals, impressively as low as 5–6% as measured by TEM.[138] Nucleation occurs over a ~20 s timescale and growth is slower, occurring over the next ~60 min. It is interesting to note that the relative rates of (fast) nucleation and (slow) growth for this system is opposite that of the Finke–Watzky mechanism,[62] in which slow nucleation is followed by fast, autocatalytic nanocluster growth. It should be remembered that the CdE nanocrystal preparations are performed at high temperatures, as opposed to the room-temperature syntheses of transition-metal nanoclusters; this could be one source of the apparently different mechanisms (the systems are completely different as well, of course).

The kinetics and mechanism of CdSe growth were first studied by Alivisatos et al. in 1998.[139] These authors focused their study on nanocrystal growth and avoided

studying nucleation, noting that "the kinetics of nucleation are difficult to study."[139] Photoluminescence spectroscopy was used to probe the growth of the nanocrystals.

Qu et al. presented a possible *in situ* method for characterizing CdSe nanocrystals by UV–visible spectroscopy to probe the nucleation and growth of the nanocrystals.[5] In this way, the samples can be characterized at the actual reaction temperature instead of taking aliquots of reaction solution, cooling them to room temperature, and then characterizing them.[139] This avoids problems of changing the reaction solution by removing significant amounts for characterization, as well as changing the nanocrystals themselves by cooling them before characterization. The *in situ* UV–visible spectra of the solutions at 250 °C were indeed different from those taken at 25 °C; specifically, absorbances were shifted to higher wavelength and broadened in the spectra taken at higher temperatures. Unfortunately, the *in situ* UV–visible method was abandoned in favor of photoluminescence spectroscopy[139] along with computer simulations to measure the sizes of the nanocrystals. Therefore, while the method of *in situ* UV–visible spectroscopy was shown to be easily employed, the only conclusion based on the UV–visible method given in this study was that the spectra are different at higher temperatures. No information about the nucleation of the nanocrystals was obtained using UV–visible spectroscopy.

It is notable that Qu et al. found that classical nucleation theory does *not* accurately describe CdSe nanocrystal nucleation, at least the "semiquantitative" data collected by the authors.[5] Specifically, these authors found that the concentration of the CdSe nanocrystals depends on the concentration of monomers in solution, while CNT predicts that there should be no dependence. (Note that in the recently observed

nucleation step $n\text{A} \rightarrow \text{B}_n$ for transition-metal salts, the concentration of nanoclusters is also dependent on the concentration of "monomer," [*A*]—this dependence is manifested as $k_{1,\text{obs}} = nk_{1,\text{true}}[A]^{n-1}$.[67]) The various uncertainties in the CdSe nanocrystal formation data, however, led the authors to treat with caution their conclusion of a nanocluster dependence on monomer concentration. In particular, as noted by the authors,[5] the uncertainty and inherent irreproducibility in the accuracy of the injection rate of Se into the Cd solution reduces the accuracy of, and thus the confidence in, the measured nucleation data.

The nucleation of CdSe nanocrystals was recently studied in detail by van Embden and Mulvaney.[101] Like Qu et al.,[5] they found that *CNT is unable to explain the nucleation of CdSe*; the slow nucleation they observed also did not agree with LaMer's "burst" colloid nucleation mechanism.[59,60] These authors formulated the hypothesis of "ligand controlled nucleation," in which certain ligands, referred by the authors as "nucleation agents," will have an affect on the size of the critical nucleus, as well as the concentration of nuclei formed and their probability of surviving. To test this hypothesis, they added the ligand bis(2,2,4-trimethylpentyl) phosphinic acid (TMPPA) to a reaction solution containing a modification of the general preparation of CdSe nanocrystals.[138] The TMPPA ligand was chosen with the idea that it would preferentially bind to the CdSe nanocrystal surface over the monomers, preventing redissolution of the nuclei. Using UV–visible spectroscopy, the authors found that when TMPPA was added to the reaction, smaller CdSe nuclei resulted, increasing the concentration of nuclei versus the control reaction without added TMPPA, and slowing the nanocrystal growth process. It was inferred that the binding of the ligand

to the nucleus lowered the free energy of the critical nucleus and the surface free energy, γ; the result is a lowering of the barrier to nucleation. The relevant equations used (eqs 2A.1 and 2A.2) are similar to those given above by Auer and Frenkel[19] (eq 2.6):

$$k_{\text{nucleation}} = aT \exp\left(-\frac{\Delta G_{\max}}{RT}\right) \tag{2A.1}$$

$$\Delta G_{\max} = \frac{16\pi\gamma^3}{3\Delta G_V} \tag{2A.2}$$

Equation 2A.1 has the general form of an "Eyring-type" equation. In eq 2A.2, ΔGv is the free energy per unit volume for the condensation of the monomer, ΔGv = $-(RT/V_m)\ln S$, where V_m is the molar volume of CdSe (in this case) and S is the degree of supersaturation; that is, the product [Cd][Se] in solution divided by the solubility product $[Cd]_{eq}[Se]_{eq}$. The ultimate utility of the addition of "nucleating agents," according to the authors, is in the ability to tune the nucleation and growth of the nanocrystals (in conjunction with the addition of "growth agents"), leading to a control of nanocrystal sizes.

The kinetics of nucleation (and growth) of the CdSe nanocrystals are measured with UV–visible spectroscopy. The nanocrystals absorb between ~500 and 700 nm depending on their size; the growth of the nanocrystals is monitored by the shift in the absorbance to higher wavelength. The sizes of the nanocrystals are determined by the absorbance, and the concentration of particles is determined by the absorbance. Accurate determinations of the sizes and concentrations of the particles depend on good calibration curves; this has been done by at least two researchers[140,141] and results have been found to agree with both determinations.[142]

Appendix 2B. Solid-state nucleation studies

The solid-state chemical literature has a history of nucleation and growth studies dating back to the 1930s, and the kinetics of solid-state reactions have been reviewed.[143,144] The reason for including these studies here, as well as those on protein agglomeration in Appendix 2C, is that it is probable that nucleation and growth phenomena throughout nature are closely interconnected, so that insights from one area can fuel advances in other areas.

A brief summary of the solid-state decomposition mechanism literature is given in Table 2B.1. Solid-state nucleation theory has its roots in CNT, eq 2B.1,

$$\Delta G = m\Delta G_B + \sigma\gamma \qquad (2B.1)$$

in which the free energy change depends on the shape of the nucleus, as expressed by the shape factor σ ($4\pi r^2$ for a spherical interface) and the strain energy per unit area of the interface, γ.[143] In this equation, m is a function of the nucleation area ($4/3\pi r^3$ for a spherical nucleation region) and ΔG_B is the free energy difference between the phases.

The basic starting equation for solid-state nucleation and growth is the Avrami–Erofe'ev equation, $[-\ln(1-\alpha)] = (kt)^n$, where, according to Erofe'ev's derivation,[148] α is the fraction of starting material that has reacted to form product, n is a parameter that can range from 2 to 4 in so-called "acceleratory" kinetics or can be 1, ½, ⅓, and so on in "deceleratory" kinetics, and k is the rate constant. A problem appears immediately for chemical systems with regard to the meaning of the parameters n and k. First, the notion of "acceleratory" versus "deceleratory" kinetics

Table 2B.1. Kinetic models for solid-state reactions

Date	Author(s)	Reaction system	Rate equation(s)	Comments	Ref.
1939	Johnson and Mehl	None, but use model to fit various existing experimental data	$f(t) = 1 - e^{-\frac{\pi}{3} N_v G^3 t^4}$; $f(t)$=fraction of reactant transformed to product, N_v=nucleation rate, G=growth rate, t=time	Kinetic models for solid-state reactions Equation becomes more complex when nucleation and growth rates are allowed to change during the reaction; Good fits to experimental data	145
1940	Avrami	None; uses general nucleation theory	$N' = N\left(1 - e^{-nt}\right)$; N'=number of growth nuclei, N=number of germ nuclei, n=probability of growth nucleus formation	Lack of chemical equations causes confusion about what the rate equation really describes physically	146
1944	Prout and Tompkins	$2KMnO_4 \rightarrow MnO_2 + KMnO_4 + O_2$	$\frac{p}{p_f - p} = e^{k(t - t_{max})}$; p=pressure, p_f=final pressure, k=rate constant (different for acceleratory vs deceleratory periods), t_{max}=time of maximum rate	Induction period is removed in order to get a good fit; Does not fit data for $AgMnO_4$ decomposition; Two different equations needed for acceleratory and deceleratory parts of the reaction	147

1946	Erofe'ev	None; uses generalized theory	$\alpha = 1 - e^{-kt^n}$; α=fraction of reactant transformed to product, n="dimensionality" of reaction	Uses empirically determined rate laws, Mott's nucleation theory for irreversible vs steady-state reaction	148
1971	Šestàk and Berggren	None	General equation: $\frac{d\alpha}{dt} = k\alpha^m(1-\alpha)^n(-\ln(1-\alpha))^p$; m, n, and p are exponents that depend on the type of nucleation and growth	Begins to resemble autocatalysis (rate increases with amount of product); Used to describe various modes of nucleation and growth, with changing exponents; the exponents are not given clear physical definitions. Later (in 1991) [149] found to not be general (i.e., does not agree with other, higher-order rate equations)	150

1975	Ng	None	General equation: $\frac{d\alpha}{dt} = k\alpha^{1-p}\left(1-\alpha^{1-q}\right)$; p and q are exponents between 0 and 1, not clearly defined	Gives analysis of the given equation in relation to Avrami, Prout–Tompkins, Erofe'ev, and Roginskii–Shulz equations; assert that these equations differ only in their values of p and q	151
1984	Cardew et al.	None, but use their model to fit NH_4NO_3 decomposition data	$\alpha = \frac{t^4}{\left(\tau_N \tau_G^3\right)/2}$; τ_N = nucleation time, τ_G = growth time	A more general model that reduces to Avrami equation at early times; Introduces many complicating factors, reduced variables that lose chemical meaning; Shows a dependence of size on ratio of growth to nucleation rates	152
1996	Burnham et al.	Coal and kerogen pyrolysis and maturation	$\frac{d\alpha}{dt} = k\alpha(1-0.99\alpha)^m$	Similar to Avrami equation except for the introduction of the 0.99 term to account for non-zero initial rate	153

1997	Jacobs	None, but uses model to fit Prout and Tompkins' $AgMnO_4$ data	$\ln\left[\frac{a}{1-\frac{a}{2a_i}}\right]-\ln\left[\frac{a_0}{1-\frac{a_0}{2a_i}}\right]=k(t-t_0)$; α = fraction of reactant transformed to product, α_i = value of α at the inflection point, α_0 = value of α at the end of the induction period, t_0 = induction period	Called the "generalized Prout–Tompkins equation"; Fits the $AgMnO_4$ data better than Prout–Tompkins reaction, in which the kinetic curve is not symmetric about the inflection point; Claims that the induction period is due to slow nucleus growth	154
2004	Skrdla	None, but uses model to fit Prout and Tompkins' $AgMnO_4$ data	$\frac{d\alpha}{dt}=k(1-\alpha)+k'(1-\alpha)\left(\frac{k}{k'}+\alpha\right)$; k = nucleation rate constant, k'= growth ("nucleus branching") rate constant	Used to fit data from Prout and Tompkins; Still does not fit the induction period well	155
2005	Skrdla and Robertson	None, but uses model to fit Prout and Tompkins' $AgMnO_4$ data	$\frac{dx}{dt}=e^{-\frac{\alpha}{t}e^{\beta t^2-1}}\left(-\frac{2\alpha\beta}{t}e^{\beta t^2-1}+\frac{\alpha}{t^2}e^{\beta t^2-1}\right)$ for "acceleratory kinetics"; $\frac{dx}{dt}=e^{\alpha' te^{-\beta' t^2-1}}\left(-2\alpha'\beta' te^{-\beta' t^2-1}+\alpha' e^{\beta' t^2-1}\right)$ for "deceleratory kinetics"; α,β,α', and β' are constants containing rate constant terms and various physical constants	Starts from ideal monatomic gas assumption, Maxwell–Boltzmann distribution of energies	156

is not well defined, and in some cases the parameter n is allowed to change *during the course of a single experiment*. Therefore, this parameter seems to be little more than a fitting factor, included to ensure a good fit without adding any physical meaning. Second, the rate constant k appears to be a conglomerate of nucleation and growth rate constants, convoluted into a single constant.[157]

As can be seen in Table 2B.1, the Avrami–Erofe'ev equation has been generalized several times since its initial derivation, that is, all of the subsequent models simplify to the Avrami–Erofe'ev equation under certain conditions. Basically, fitting solid-state kinetic data involves choosing a general expression from one of those in Table 2B.1 (or deriving a more complex one), and then changing parameters until a sufficiently good fit is attained. In the majority of reports, the values of the relevant parameters are given, *but their chemical meaning is generally not discussed.* In fact, worth noting is that most of the models in the solid-state literature *lack the chemical reactions and rate definitions that are necessary to clearly define kinetically and mechanistically the system under study*. Instead, theories are developed and then either left as is or modified to fit prior literature data.

The most significant problem with the theories described above is that they do not fit *all* of the experimental data. In fact, some of the models only do well from approximately ¼ to at most ¾ of the total reaction when only one model is used.[155,156] *The reason for this is that most of the models do not account for the induction period seen in the decomposition data.* To deal with the induction period, the models either shift the data so that the initial time is at the end of the induction period (by adding a $(t - t_0)$ term where t_0 is the induction time), or the models use different equations for

different parts of the experimental data. Even the more complete model put forth by Skrdla in 2004 (entry 9 in Table 2B.1) cannot fit well the induction period of the classic Prout–Tompkins data for $AgMnO_4$ decomposition, Figure 2B.1.[155] A modification of the model was developed the following year (entry 10 in Table 2B.1), and could fit the induction period much better.[156] However, this model relies on even more added parameters that lack significant chemical meaning. Adding to the confusion of this model is that it employs kinetic energy distributions based on a *monatomic ideal gas* in order to model the kinetics of *solid-state reactions.*

Recently, the simpler, more chemically precise and thus intuitive Finke–Watzky 2-step model, A→B, A+B→2B, has been used to fit solid-state kinetic data.[157] Note that a single equation is used for the entire reaction—that is, *the induction period is treated explicitly and simply.* In addition, the Finke–Watzky model uses separate rate constants for nucleation and growth, and all of the parameters therein (see eq 2.8) have clear physical meanings—rate constants and initial complex concentrations are the only variables needed to describe the system.

Close examination of the solid-state kinetics literature and related equations (Table 2B.1) suggests the hypothesis that the Finke–Watzky mechanism is a simpler, more chemical version of the more complex solid-state kinetic models. For example, the classic Prout–Tompkins system of decomposing $AgMnO_4$[147] can be expressed as two steps, eq 2B.2—a nucleation and then autocatalytic growth mechanism. This is the Finke–Watzky mechanism: A→B, A +B→2B.

$$AgMnO_4 \rightarrow AgMnO_3 + 1/2O_2 \quad (2B.2a)$$

$$AgMnO_4 + AgMnO_3 \rightarrow 2AgMnO_3 + 1/2O_2 \quad (2B.2b)$$

$$2AgMnO_4 \rightarrow 2AgMnO_3 + O_2 \quad (2B.2c)$$

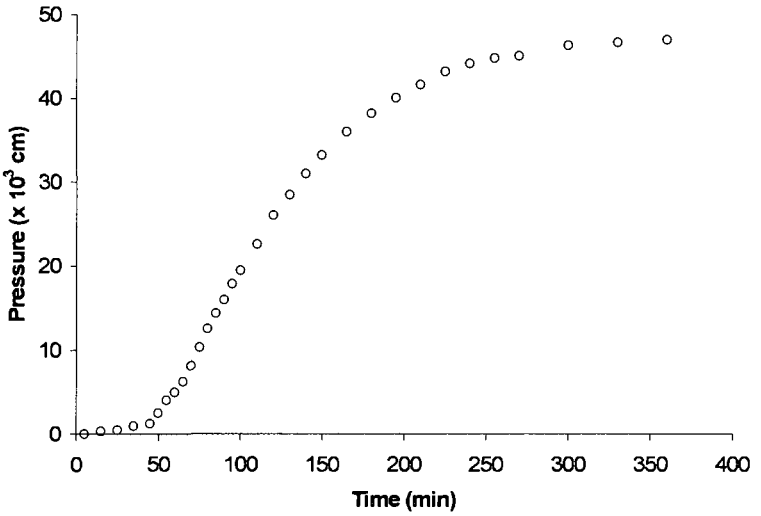

Figure 2B.1. Prout and Tompkins' data for the decomposition of $AgMnO_4$. Adapted from reference 147b.

This autocatalysis is also seen in the rate equations; for example, the Šestàk–Berggren equation (entry 4 in Table 2B.1) with $p = 0$ has the rate equation $d\alpha/dt = k\alpha^m(1-\alpha)^n$, which, assuming an elementary reaction, represents the reaction $n\mathrm{A}+m\mathrm{B}\rightarrow(n+m)\mathrm{B}$, with $[A] = (1-\alpha)$ and $[B] = \alpha$. Studies are currently in progress to determine if the Finke–Watzky 2-step nanocluster formation mechanism is indeed related to the solid-state kinetics described above.[157]

Appendix 2C. Protein agglomeration

Mechanistic studies (theoretical and experimental) of the agglomeration of proteins have been underway since the early 1960s.[158] Nucleation theory has been used to describe the agglomeration (or polymerization) of proteins. The

agglomeration of proteins has been implicated in diseases such as Alzheimer's disease,[159] Huntington's disease,[79,160] Parkinson's disease[161] and transmissible spongiform encephalopathies,[162] the most infamous of the latter being bovine spongiform encephalopathy (mad-cow disease). Analyses of several different protein agglomeration mechanisms have suggested that the process is autocatalytic, albeit typically without quantitative kinetic fits *demonstrating* autocatalysis, A+B→2B.[162]

As early as the 1980s it was observed that "homogeneous nucleation is an essential part of the kinetic mechanism for sickle hemoglobin polymerization."[163] For this system of hemoglobin polymerization, a "double nucleation" mechanism was put forward, which is described in the following way. Homogeneous nucleation occurs until a critical nucleus is attained. This critical nucleus then grows to a long polymer chain. A new polymer chain can form either by the same homogeneous nucleation mechanism or by heterogeneous nucleation, in which monomers attach to an existing polymer chain and then grow into a new chain from there. The double nucleation mechanism was found to fit experimental data very well, as long as the nucleus size was allowed to change with respect to monomer concentration.[162]

In 2002, Ferrone et al. reported a study of the kinetics of polyglutamine aggregation and its effect of the onset age of Huntington's disease.[79] The critical nucleus in this system was found to be *one monomer*; this suggests that the folding of a single monomer is the rate-limiting step, after which growth of the misfolded protein oligomer is autocatalytic and fast. Perhaps the most significant and interesting finding from this kinetic study is that the energy difference between benign and pathological polyglutamine is less than 1 kcal/mol; that is, the implication is that

processes differing by less than 1 kcal/mol might conceivably be involved in Huntington's disease! The knowledge of the nucleation and autocatalytic growth mechanism of protein agglomeration is obviously extremely important for finding ways to stop the onset of this serious disease. It was noted in a 2001 Nature Hypothesis that for Huntington's and related diseases, "therapy should be aimed at preventing or reversing aggregation".[160] We would say that the identification of the nucleation process of the aggregates needs to be one focus of disease prevention.

The aggregation of polyglutamine in Ferrone's study was monitored by circular dichroism (CD), HPLC, light scattering, and thioflavin T methods.[79] The results are shown in Figure 2C.1. The data are fit by the empirical eq 2C.1, where Δ is the concentration of monomer that has gone to polymer, k_+ is the forward elongation rate constant, K_{n^*} is the equilibrium constant for the nucleation of monomers, c is the bulk concentration of monomer, and t is time. One of the more interesting findings of this paper is that plotting log(agglomeration rate) versus log(protein concentration) gives a linear plot with a slope equal to n^*+2; that is, such a plot can give the (kinetic) critical nucleus size.[79]

$$\Delta = \frac{1}{2} k_+^2 K_{n^*} c^3 t^2 \qquad (2C.1)$$

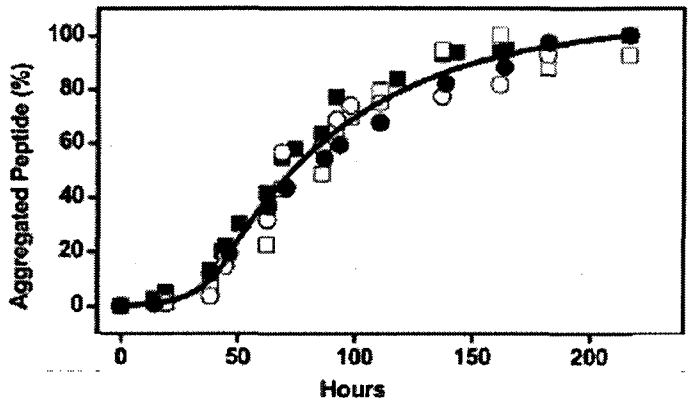

Figure 2C.1. Concentration profile of the aggregated polyglutamine as monitored by circular dichroism (dark squares), high-performance liquid chromatography (dark circles), light scattering (open squares), and thioflavin T (open circles). The fit to the data (line) is to eq 2C.1. Reprinted with permission from reference 79.

The data in Figure 2C.1 bears a striking resemblance to the 1997 transition-metal nanocluster formation mechanism in Scheme 2.4 in the main text.[62] In fact, the data are reasonably well fit by the 2-step Finke–Watzky mechanism, Figure 2C.2, an insight not previously published. In addition, the pictorial mechanism proposed by Ferrone et al. for the agglomeration of polyglutamine, Figure 2C.3 resembles that of the formation of transition-metal nanoclusters shown in Scheme 2.4 in the main text. Fitting the polyglutamine agglomeration data to the Finke–Watzky 2-step mechanism, with A as the monomer and B as the polymer (and possibly C as larger, aggregated polymers) has the potential to simplify, and perhaps at the same time provide additional insights into, the mechanistic studies of protein agglomeration.[137] Overall, it appears that nucleation and growth mechanisms in Nature share key features in common between at least nanocluster formation, solid-state transitions, and protein agglomeration, to cite examples presented in this review.

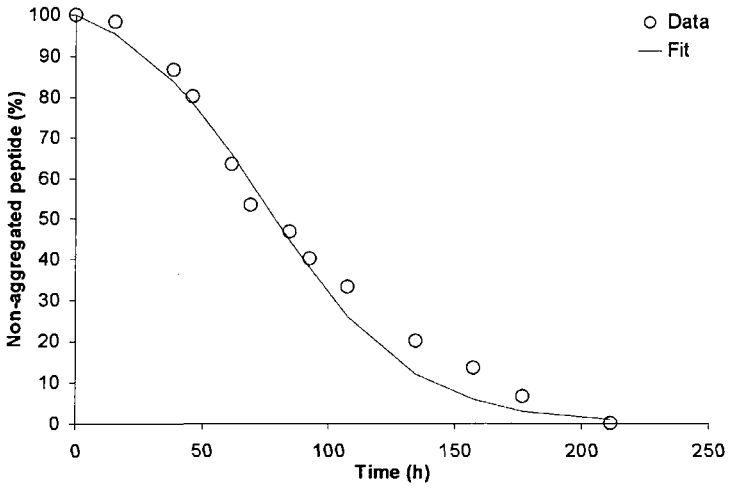

Figure 2C.2. Fit of the data for peptide aggregation shown in Figure 2C.1 to the 2-step Finke–Watzky mechanism in Scheme 2.4 of the main text. The data was converted to % non-aggregated protein and was fit with the analytic eq 2.8 with resultant rate constants: $k_1 = 2.2(6) \times 10^{-3}\ h^{-1}$, $k_2 = 3.6(6) \times 10^{-4}\ M^{-1}\ h^{-1}$.

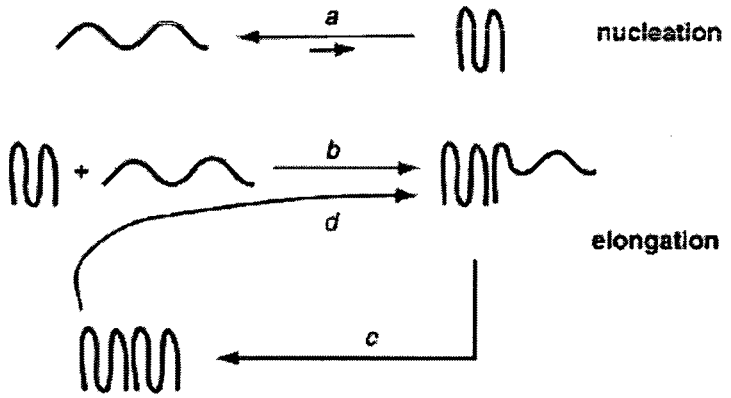

Figure 2C.3. Proposed mechanism for polyglutamine aggregation consisting of (a) compacting of a chain (which is the formation of a critical nucleus), (b) addition of another chain to the compacted structure, (c) compacting of the added chain, and (d) repeat of the process. Reprinted with permission from reference 79.

References

[1] Kashchiev, D. *Nucleation: Basic Theory with Applications*; Butterworth Heinmann: Oxford, 2000.

[2] (a) McGraw, R. *J. Chem. Phys.* **1981**, *75*, 5514. (b) Ruth, V.; Hirth, J. P.; Pound, G. M. *J. Chem. Phys.* **1988**, *88*, 7079. (c) Girshick, S. L.; Chiu, C.-P. *J. Chem. Phys.* **1993**, *93*, 1273. (d) Dillmann, A.; Meier, G. E. A. *J. Chem. Phys.* **1991**, *94*, 3872. (e) Zeng, X. C.; Oxtoby, D. W. *J. Chem. Phys.* **1991**, *94*, 4472. (f) Viisanen, Y.; Strey, R.; Reiss, H. *J. Phys. Chem.* **1993**, *99*, 4680. (g) Fenelonov, V. B.; Kodenyov, G. G.; Kostrovsky, V. G. *J. Phys. Chem. B* **2001**, *105*, 1050.

[3] (a) Huang, J.; Bartell, L. S. *J. Phys. Chem.* **1995**, *99*, 3924. (b) Ford, I. J. *J. Phys. Chem. B* **2001**, *105*, 11649. (c) Dickens, D. B.; Sloan, J. J. *J. Phys. Chem. A* **2002**, *106*, 10543. (d) Turner, G. W.; Bartell, L. S. *J. Phys. Chem. A* **2005**, *109*, 6877.

[4] (a) Watson, J. N.; Iton, L. E.; Keir, R. I.; Thomas, J. C.; Dowling, T. L.; White, J. W. *J. Phys. Chem. B* **1997**, *101*, 10094. (b) Liang, K.; White, G.; Wilkinson, D.; Ford, L. J.; Roberts, K. J.; Wood, W. M. L. *Cryst. Growth Des.* **2004**, *4*, 1039. (c) Lyall, E.; Mougin, P.; Wilkinson, D.; Roberts, K. J. *Ind. Eng. Chem. Res.* **2004**, *43*, 4947.

[5] Qu, L.; Yu, W.; Peng, X. *Nano Lett.* **2004**, *4*, 465.

[6] *Clusters and Colloids: From Theory to Applications*; Schmid G., Ed.; VHC: New York, 1994.

[7] Finke, R. G. In *Metal Nanoparticles: Synthesis, Characterization, and Applications*; Feldheim, D. L.; Foss, C. A., Jr., Eds.; Marcel Dekker: New York, 2001, Chapter 2.

[8] Watzky, M. A.; Finke, R. G. *Chem. Mater.* **1997**, *9*, 3083.

[9] Oxtoby, D. W. *Acc. Chem. Res.* **1998**, *31*, 91.

[10] (a) Kashchiev, D. *J. Phys. Chem.* **1992**, *76*, 5098. (b) Oxtoby, D. W. *J. Phys. Condens. Matter* **1992**, *4*, 7627. (c) Laaksonen, A.; Talanquer, V.; Oxtoby, D. W. *Annu. Rev. Phys. Chem.* **1995**, *46*, 489.

[11] Everett, D. H. *Basic Principles of Colloid Science*; Royal Society of Chemistry: London, 1988.

[12] Lubetkin, S. D. *Langmuir* **2003**, *19*, 2575.

[13] Ferrone, F. *Methods Enzymol.* **1999**, *309*, 256.

[14] Dixit, N. M.; Zukoski, C. F. *Phys. Rev. E* **2002**, *66*, 051602.

[15] Volmer, M.; Weber, A. *Z. Phys. Chem. (Leipzig)* **1926**, *119*, 227.

[16] Volmer, M. *Kinetik der Phasenbildung, Steinfopff*; Leipzig, 1939.

[17] Becker, R.; Döring, W. *Ann. Phys.* **1935**, *24*, 719.

[18] Dillmann, A.; Meier, G. E. A. *Chem. Phys. Lett.* **1989**, *160*, 71.

[19] Auer, S.; Frenkel, D. *Ann. Rev. Phys. Chem.* **2004**, *55*, 333.

[20] Martínez, D. M.; Ferguson, F. T.; Heist, R. H.; Nuth, J. A., III *J. Chem. Phys.* **2001**, *115*, 310.

[21] Hale, B. N. *Phys. Rev. A* **1986**, *33*, 4156.

[22] Gránàsy, L. *J. Phys. Chem.* **1996**, *100*, 10768.

[23] Chushak, Y. G.; Bartell, L. S. *J. Phys. Chem. B* **2001**, *105*, 11605.

[24] Rusyniak, M.; Abdelsayed, V.; Campbell, J.; El-Shall, M. S. *J. Phys. Chem. B* **2001**, *105*, 11866.

[25] Rusyniak, M.; El-Shall, M. S. *J. Phys. Chem. B* **2001**, *105*, 11873.

[26] Strey, R.; Wagner, P. E.; Viisanen, Y. *J. Phys. Chem.* **1994**, *98*, 7748.

[27] Sugimoto, T. *J. Colloid Interface Sci.* **1996**, *181*, 259.

[28] Sugimoto, T. *J. Colloid Interface Sci.* **1996**, *183*, 299.

[29] Sugimoto, T.; Shiba, F. *J. Phys. Chem. B* **1999**, *103*, 3607.

[30] Gasser, U.; Weeks, E. R.; Schofield, A.; Pusey, P. N.; Weitz, D. A. *Science* **2001**, *292*, 258.

[31] ten Wolde, P. R.; Ruiz-Montero, M. J.; Frenkel, D. *Phys. Rev. Lett.* **1995**, *75*, 2714.

[32] Ostwald, W. *Z. Phys. Chem.* **1897**, *22*, 289.

[33] Shen, Y. C.; Oxtoby, D. W. *Phys. Rev. Lett.* **1996**, *77*, 3585.

[34] Nashner, M. S.; Frenkel, A. I.; Adler, D. L.; Shapley, J. R.; Nuzzo, R. G. *J. Am. Chem. Soc.* **1997**, *119*, 760.

[35] Cacciuto, A.; Frenkel, D. *J. Phys. Chem. B* **2005**, *109*, 6587.

[36] Nielson, A. E. *Kinetics of Precipitation;* Pergamon Press: Oxford, 1964.

[37] Nielson, A. E. *Kristal Tech.* **1969**, *4*, 17.

[38] Berne, B. J.; Pecora, R. *Dynamic Light Scattering with Applications to Chemistry, Biology, and Physics*; Dover Publications: New York, 2000.

[39] Brown W., Ed. *Dynamic Light Scattering: The Method and Some Applications*; Oxford Univ. Press: Oxford, 1993.

[40] (a) Sangregorio, C.; Galeotti, M.; Bardi, U.; Baglioni, P. *Langmuir* **1996**, *12*, 5800. (b) Graf, C.; van Blaaderen, A. *Langmuir* **2002**, *18*, 524. (c) Raula, J.; Shan, J.; Nuopponen, M.; Niskanen, A.; Jiang, H.; Kauppinen, E. I.; Tenhu, H. *Langmuir* **2003**, *19*, 3499. (d) Thoma, S. G.; Sanchez, A.; Provencio, P. P.; Abrams, B. L.; Wilcoxon, J. P. *J. Am. Chem. Soc.* **2005**, *127*, 7611.

[41] Creighton, J. A.; Eadon, D. G. *J. Chem. Soc. Faraday Trans.* **1991**, *87*, 3881.

[42] Henglein, A.; Giersig, M. *J. Phys. Chem. B* **2000**, *104*, 6767.

[43] Wang, J.; Boelens, H. F. M.; Thathagar, M. B.; Rothenberg, G. *Phys. Chem. Chem. Phys.* **2004**, *5*, 93.

[44] Gaikwad, A. V.; Rothenberg, G. *Phys. Chem. Chem. Phys.* **2006**, *8*, 1.

[45] Kaiser, U.; Muller, D. A.; Grazul, J. L.; Chuvilin, A.; Kawasaki, M. *Nat. Mater.* **2002**, *1*, 102.

[46] Jaska, C. A.; Manners, I. *J. Am. Chem. Soc.* **2004**, *126*, 9776.

[47] Hagen, C. M.; Widegren, J. A.; Maitlis, P. M.; Finke, R. G. *J. Am. Chem. Soc.* **2005**, *127*, 4423.

[48] Schmid, G. *Chem. Rev.* **1992**, *92*, 1709.

[49] Williams, D. B.; Carter, C. B. *Transmission Electron Microscopy*; Plenum Press: New York, 1996, Chapter 4.

[50] Wu, Q.; Chen, W.; Madey, T. E. *J. Phys. Chem. B* **2002**, *106*, 6419.

[51] Wu, Q.; Madey, T. E. *Surf. Sci.* **2004**, *555*, 167.

[52] Min, B. K.; Wallace, W. T.; Santra, A. K.; Goodman, D. W. *J. Phys. Chem. B* **2004**, *108*, 16339.

[53] *In situ* (so-called "environmental") STM measurements of metal surfaces are more common; for example: Maurice, V.; Strehblow, H.-H.; Marcus, P. *Surf. Sci.* **2000**, *458*, 185.

[54] Margaritondo, G. *Elements of Synchrotron Light: For Biology, Chemistry, and Medical Research*; Oxford Univ. Press: Oxford, 2002.

[55] Frenkel, A. I.; Hills, C. W.; Nuzzo, R. G. *J. Phys. Chem. B* **2001**, *105*, 12689.

[56] Nashner, M. S.; Frenkel, A. I.; Somerville, D.; Hills, C. W.; Shapley, J. R.; Nuzzo, R. G. *J. Am. Chem. Soc.* **1998**, *120*, 8093.

[57] Frenkel, A. I. *J. Synchrotron Rad.* **1999**, *6*, 293.

[58] Menard, L.; Frenkel, A. I.; Nuzzo, R. G.; Finney, E. E.; Graham, C.; Alley, W. M.; Finke, R. G. Experiments in progress.

[59] LaMer, V. K.; Dinegar, R. H. *J. Am. Chem. Soc.* **1950**, *72*, 4847.

[60] LaMer, V. K. *Ind. Eng. Chem.* **1952**, *44*, 1270.

[61] Matijevic, E. *Chem. Mater.* **1993**, *5*, 412.

[62] Watzky, M. A.; Finke, R. G. *J. Am. Chem. Soc.* **1997**, *118*, 10382.

[63] Sugimoto, T.; Shiba, F.; Sekiguchi, T.; Itoh, H. *Colloids Surf. A* **2000**, *164*, 183.

[64] Sugimoto, T.; Shiba, F. *Colloids Surf. A* **2000**, *164*, 205.

[65] Turkevich, J.; Stevenson, P. C.; Hillier, J. *Faraday Discuss. Chem. Soc.* **1951**, *11*, 55.

[66] Besson, C.; Finney, E. E.; Finke, R. G. *Chem. Mater.* **2005**, *17*, 4925.

[67] Finney, E. E.; Ott, L. S.; Watzky, M. A.; Finke, R. G. Manuscript in preparation.

[68] Schmidt, A. F.; Smirnov, V. V. *Top. Catal.* **2005**, *32*, 71.

[69] Widegren, J. A.; Aiken, J. D., III; Özkar, S.; Finke, R. G. *Chem. Mater.* **2001**, *13*, 312.

[70] Finney, E. E.; Finke, R. G. Unpublished result.

[71] Widegren, J. A.; Bennett, M. A.; Finke, R. G. *J. Am. Chem. Soc.* **2003**, *125*, 10301.

[72] de Vos, V. *Science* **1998**, *279*, 1710.

[73] Lin, Y.; Finke, R. G. *Inorg. Chem.* **1994**, *33*, 4891.

[74] Hornstein, B. J.; Finke, R. G. *Chem. Mater.* **2004**, *16*, 139.

[75] Besson, C.; Finney, E. E.; Finke, R. G. *J. Am. Chem. Soc.* **2005**, *127*, 8179.

[76] Epstein, I. R. *Nature* **1995**, *374*, 321.

[77] Nagypál, I.; Epstein, I. R. *J. Phys. Chem.* **1986**, *90*, 6285.

[78] Finney, E. E.; Finke, R. G. Manuscript in preparation.

[79] Chen, S.; Ferrone, F. A.; Wetzel, R. *Proc. Natl. Acad. Sci.* **2002**, *99*, 11884.

[80] Lin, Y.; Finke, R. G. *J. Am. Chem. Soc.* **1994**, *116*, 8335.

[81] Cacciuto, A.; Auer, S.; Frenkel, D. *Nature* **2004**, *428*, 404.

[82] Pertuci, P.; Vituli, G. *Inorg. Synth.* **1983**, *22*, 178.

[83] Crascall, L. E.; Spencer, J. L. *Inorg. Synth.* **1990**, *28*, 126.

[84] Moseley, K.; Maitlis, P. M. *Chem. Commun.* **1971**, 982.

[85] Platt, J. R. *Science* **1964**, *146*, 347.

[86] Michaelis, M.; Henglein, A. *J. Phys. Chem.* **1992**, *96*, 4719.

[87] Belloni, J. *Catal. Today* **2006**, *113*, 141.

[88] Henglein, A.; Tausch-Treml, R. *J. Colloid Interface Sci.* **1981**, *80*, 84.

[89] Henglein, A.; Giersig, M. *J. Phys. Chem. B* **1999**, *103*, 9533.

[90] Angermund, K.; Bühl, M.; Dinjus, E.; Endruschat, U.; Gassner, F.; Haubold, H.-G.; Hormes, J.; Köhl, G.; Mauschick, F. T.; Modrow, H.; Mörtel, R.; Mynott, R.; Tesche, B.; Vad, T.; Waldöfner, N.; Bönnemann, H. *J. Phys. Chem. B* **2002**, *41*, 4041.

[91] Bönnemann, H.; Waldöfner, N.; Haubold, H.-G.; Vad, T. *Chem. Mater.* **2002**, *14*, 1115.

[92] Haubold, H.-G.; Vad, T.; Waldöfner, N.; Bönnemann, H. *J. Appl. Cryst.* **2003**, *36*, 617.

[93] Beuermann, L.; Maus-Friedrichs, W.; Krischok, S.; Kempter, V.; Bucher, S.; Modrow, H.; Hormes, J.; Waldöfner, N.; Bönnemann, H. *Appl. Organomet. Chem.* **2003**, *17*, 268.

[94] Angermund, K.; Bühl, M.; Endruschat, U.; Mauschick, F.T.; Mörtel, R.; Mynott, R.; Tesche, B.; Waldöfner, N.; Bönnemann, H.; Köhl, G.; Modrow, H.; Hormes, J.; Dinjus, E.; Gassner, F.; Haubold, H.-G.; Vad, T.; Kaupp, M. *J. Phys. Chem. B* **2003**, *107*, 7507.

[95] Hagen, C. M.; Vieille-Petit, L.; Laurenczy, G.; Süss-Fink, G.; Finke, R. G. *Organometallics* **2005**, *24*, 1819.

[96] Wen, F.; Bönnemann, H. *Appl. Organomet. Chem.* **2005**, *19*, 94.

[97] King, S.; Hyunh, K.; Tannenbaum, R. *J. Phys. Chem. B* **2003**, *107*, 12097.

[98] Ungváry, F.; Markó, L. *J. Organomet. Chem.* **1974**, *71*, 283.

[99] Ott, L. S.; Hornstein, B. J.; Finke, R. G. *Langmuir* **2006**, *22*, 9357.

[100] Tannenbaum, R. *Langmuir* **1997**, *13*, 5056.

[101] van Embden, J.; Mulvaney, P. *Langmuir* **2005**, *21*, 10226.

[102] Shevchenko, E. V.; Talapin, D. V.; Schnablegger, H.; Kornowski, A.; Festin, Ö.; Svedlindh, P.; Haase, M.; Weller, H. *J. Am. Chem. Soc.* **2003**, *125*, 9090.

[103] Chen, Y.; Fulton, J. L.; Linehan, J. C.; Autrey, T. *J. Am. Chem. Soc.* **2005**, *127*, 3254.

[104] *The Hydrogen Economy: NRC and NAE*; The National Academies Press: Washington, DC, 2004.

[105] Jaska, C.A.; Temple, K.; Lough, A. J.; Manners, I. *J. Am. Chem. Soc.* **2003**, *125*, 9424.

[106] Linehan, J. C. Personal communication.

[107] Alexeev, O.; Gates, B. C. *Top. Catal.* **2000**, *10*, 273.

[108] Duff, D. G.; Curtis, A. C.; Edwards, P. P.; Jefferson, D. A.; Johnson, B. F. G.; Logan, D. E. *J. Chem. Soc. Chem. Commun.* **1987**, 1264.

[109] Choukroun, R.; de Caro, D.; Chaudret, B.; Lecante, P.; Snoeck, E. *New J. Chem.* **2001**, *25*, 525.

[110] (a) Kulzick, M.; Price, R. T.; Muetterties, E. L.; Day, V. W. *Organometallics* **1982**, *1*, 1256. (b) Duan, Z.; Hampden-Smith, M. J.; Sylwester, A. P. *Chem. Mater.* **1992**, *4*, 1146.

[111] (a) Espinet, P.; Bailey, P. M.; Piraino, P.; Maitlis, P. M. *Inorg. Chem.* **1979**, *18*, 2706. (b) Ricci, J. S.; Koetzle, T. F.; Goodfellow, R. J.; Espinet, P.; Maitlis, P. M. *Inorg. Chem.* **1984**, *23*, 1823.

[112] Autrey, T.; Linehan, J. C.; Fulton, J. L.; Özkar, S.; Finke, R. G. Experiments in progress.

[113] Stranski, I. N. *Phys. Ztsch.* **1935**, *36*, 393.

[114] Campbell, C. T.; Parker, S. C.; Starr, D. E. *Science* **2002**, *298*, 811.

[115] Hirai, H.; Nakao, Y.; Toshima, N. *J. Macromol. Sci. Chem. A* **1979**, *13*, 727.

[116] (a) Kolb, U.; Quaiser, S. A.; Winter, M.; Reetz, M. T. *Chem. Mater.* **1996**, *8*, 1889. (b) Reetz, M. T.; Quaiser, S. A.; Winter, M.; Becker, J. A.; Schafer, R.; Stimming, U.; Marmann, A.; Vogel, R.; Konno, T. *Angew. Chem. Int. Ed. Engl.* **1996**, *35*, 2092. (c) Harada, M.; Asakura, K.; Ueki, Y.; Toshima, N. *J. Phys. Chem.* **1992**, *96*, 9730. (d) Logan, A. D.; Sharoudi, K.; Datye, A. K. *J. Phys. Chem.* **1991**, *95*, 5568.

[117] Bönnemann, H.; Braun, G.; Brijoux, W.; Brinkmann, R.; Tilling, A. S.; Seevogel, K.; Siepen, K. *J. Organomet. Chem.* **1996**, *520*, 143.

[118] Aiken, J.D., III; Finke, R. G. *J. Am. Chem. Soc.* **1999**, *121*, 8803.

[119] Ott, L. S.; Finke, R. G. *Coord. Chem. Rev.* **2007**, *251*, 1075.

[120] Finney, E. E.; Frenkel, A. I.; Finke, R. G. Experiments in progress.

[121] Michel, J. B.; Schwartz, J. T. In *Preparation of Catalysts: Scientific Bases for the Preparation of Heterogeneous Catalysts*; Delmon, B.; Grange, P.; Jacobs, P. A.; Poncelet, G., Eds.; vol. IV; Elsevier: New York, 1987, pp. 669–687.

[122] Yu, H.; Gibbons, P. C.; Kelton, K. F.; Buhro, W. E. *J. Am. Chem. Soc.* **2001**, *123*, 9198.

[123] Jana, N. R.; Gearheart, L.; Murphy, C. J. *Chem. Mater.* **2001**, *13*, 2313.

[124] (a) Lee, T. R.; Whitesides, G. M. *Acc. Chem. Res.* **1992**, *25*, 266. (b) Miller, T. M.; Izumi, A. N.; Shih, Y.-S.; Whitesides, G. M. *J. Am. Chem. Soc.* **1988**, *110*, 3146.

[125] Finney, E. E.; Finke, R. G. *Inorg. Chim. Acta* **2006**, *359*, 2879.

[126] Chen, D.; Wang, R.; Arachchige, I.; Mao, G.; Brock, S. L. *J. Am. Chem. Soc.* **2004**, *126*, 16290.

[127] (a) Hagrman, P. J.; Hagrman, D.; Zubieta, J. *Angew. Chem. Int. Ed.* **1998**, *38*, 2638. (b) Yamamoto, K.; Sakata, Y.; Nohara, Y.; Takahashi, Y.; Tatsumi, T. *Science* **2003**, *300*, 470. (c) Davis, T. M.; Drews, T. O.; Ramanan, H.; He, C.; Dong, J.; Schnablegger, H.; Katsoulakis, M. A.; Kokkoli, E.; McCormick, A. V.; Penn, R. L.; Tsapatsis, M. *Nat. Mater.* **2006**, *5*, 400.

[128] Zachariah, M. R.; Carrier, M. J. *J. Aerosol Sci.* **1999**, *30*, 1139.

[129] Zachariah, M. R.; Carrier, M. J.; Blaisten-Bajoras, E. *J. Phys. Chem.* **1996**, *100*, 14856.

[130] Hawa, T.; Zachariah, M. R. *Phys. Rev. B* **2004**, *69*, 035417-1.

[131] Ehrman, S. H.; Friedlander, S. K.; Zachariah, M. R. *J. Mater. Res.* **1999**, *14*, 4551.

[132] Suh, S.-H.; Zachariah, M. R.; Girshick, S. L. *J. Vac. Sci. Technol. A* **2001**, *19*, 940.

[133] Suh, S.-H.; Zachariah, M. R.; Girshick, S. L. *Aerosol Sci.* **2002**, *33*, 943.

[134] Ciacchi, L. C.; Pompe, W.; De Vita, A. *J. Am. Chem. Soc.* **2001**, *123*, 7371.

[135] Ciacchi, L. C.; Pompe, W.; De Vita, A. *J. Phys. Chem. B* **2003**, *107*, 1755.

[136] Ciacchi, L. C.; Mertig, M.; Pompe, W.; Meriani, S.; De Vita, A. *Platinum Met. Rev.* **2003**, *47*, 98.

[137] Morris, A. M.; Watzky, M. A.; Agar, J. N.; Finke, R. G. *Biochemistry* **2007**, *47*, 2413.

[138] Murray, C. B.; Norris, D. J.; Bawendi, M. G. *J. Am. Chem. Soc.* **1993**, *115*, 8706.

[139] Peng, X.; Wickham, J.; Alivisatos, A. P. *J. Am. Chem. Soc.* **1998**, *120*, 5343.

[140] Yu, W. W.; Qu, L.; Guo, W.; Peng, X. *Chem. Mater.* **2003**, *15*, 2854.

[141] Soloviev, V. N.; Eichhofer, A.; Fenske, D.; Banin, U. *J. Am. Chem. Soc.* **2000**, *122*, 2673.

[142] Bullen, C. R.; Mulvaney, P. *Nano Lett.* **2004**, *4*, 2303.

[143] *Reactions in the Solid State*; Bamford, C. H.; Tipper C. F. H., Eds.; vol. 22, Elsevier Scientific: Amsterdam, 1980, pp. 41–113.

[144] Burnham, A. K.; Braun, R. L. *Energy Fuels* **1999**, *13*, 1.

[145] Johnson, W. A.; Mehl, R. F. *Trans. AIME* **1939**, *135*, 416.

[146] (a) Avrami, M. *J. Chem. Phys.* **1939**, *7* 1103. (b) Avrami, M. *J. Chem. Phys.* **1940**, *8*, 212.

[147] (a) Prout, E. G.; Tompkins, F. C. *Trans. Faraday Soc.* **1944**, *40*, 488. (b) Prout, E. G.; Tompkins, F. C. *Trans. Faraday Soc.* **1946**, *44*, 468.

[148] Erofe'ev, B. V. *Dokl. Akad. Nauk SSSR* **1946**, *52*, 511.

[149] Màlek, J.; Criado, J. M. *Thermochim. Acta* **1991**, *175*, 305.

[150] Šestàk, J.; Berggren, G. *Thermochim. Acta* **1971**, *3*, 1.

[151] Ng, W.-L. *Aust. J. Chem.* **1975**, *28*, 1169.

[152] Cardew, P. T.; Davey, R. J.; Ruddick, A. J. *J. Chem. Soc. Faraday Trans.* **1984**, *80*, 659.

[153] Burnham, A. K.; Braun, R. L.; Coburn, T. T.; Sandvik, E. I.; Curry, D. J.; Schmidt, B. J.; Noble, R. A. *Energy Fuels* **1996**, *10*, 49.

[154] Jacobs, P. W. M. *J. Phys. Chem. B* **1997**, *101*, 10086.

[155] Skrdla, P. J. *J. Phys. Chem. A* **2004**, *108*, 6709.

[156] Skrdla, P. J.; Robertson, R. T. *J. Phys. Chem. B* **2005**, *109*, 10611.

[157] Martin, J. D.; Finney, E. E.; Finke, R. G. Manuscript in preparation.

[158] Oosawa, F.; Kasai, M. *J. Mol. Biol.* **1964**, *4*, 10.

[159] Harper, J. D.; Lansbury P. T., Jr. *Annu. Rev. Biochem.* **1997**, *66*, 385.

[160] Perutz, M. F.; Windle, A. H. *Nature* **2001**, *412*, 143.

[161] (a) Trojanowski, J. Q.; Goedert, M.; Iwatsubo, T.; Lee, V. M.-Y. *Cell Death Differentiation* **1998**, *5*, 832. (b) Narhi, L.; Wood, S. J.; Steavenson, S.; Jiang, Y.; Wu, G. M.; Anafi, D.; Kaufman, S. A.; Martin, F.; Sitney, K.; Denis, P.; Louis, J.-C.; Wypych, J.; Biere, A. L.; Citron, M. *J. Biol. Chem.* **1999**, *274*, 9843. (c) Dawson, T. M.; Dawson, V. L. *Science* **2003**, *302*, 819.

[162] (a) Masel, J.; Jansen, V. A. A.; Nowak, M. A. *Biophys. Chem.* **1999**, *77*, 139. (b) Eigen, M. *Biophys. Chem.* **1996**, *63*, A1.

[163] Ferrone, F. A.; Hofrichter, J.; Eaton, W. A. *J. Mol. Biol.* **1985**, *183*. 611.

CHAPTER III

THE FOUR-STEP, DOUBLE-AUTOCATALYTIC MECHANISM FOR TRANSITION-METAL NANOCLUSTER NUCLEATION, GROWTH, AND THEN AGGLOMERATION: METAL, LIGAND, CONCENTRATION, TEMPERATURE, AND SOLVENT DEPENDENCY STUDIES

This dissertation chapter contains the manuscript of a paper published in *Chemistry of Materials* (Finney, E. E.; Finke, R. G. *Chem. Mater.* **2008**, *20*, 1956). This chapter describes studies of the four-step, double-autocatalytic mechanism for transition-metal nanocluster formation and agglomeration. Examined in this work are the effects of metal, ligand, concentration, temperature, and solvent on the mechanism of formation, and in particular whether nanocluster agglomeration is observed. It was found that the four-step mechanism is general to at least five metals studied in this work. In addition, alternative mechanisms are tested and disproven, leaving the four-step mechanism as the only one to date that is able to fit the observed kinetics out of 18 total mechanisms examined.

The experiments in this chapter were performed by E.E.F. The manuscript was prepared by E.E.F. with assistance and editing by R.G.F.

Abstract

The four-step, double-autocatalytic mechanism for transition-metal nanocluster nucleation, growth, and agglomeration described previously has been found to be more general; specifically, the four-step mechanism is shown to apply to the reduction of five transition metals that were examined—Pt, Ru, Ir, Rh, and Pd—under conditions where a high enough concentration of a strongly coordinating ligand is also present. Reaction temperature, metal concentration, solvent, and stirring rate do not change the reduction mechanism within experimental error and within the range of conditions studied herein. Changing the solvent from acetone to the higher dielectric constant solvent propylene carbonate does, however, change the product of metal reduction from solid bulk metal to soluble metal particles. Three alternative mechanisms (in addition to the 15 tested already) are ruled out, leaving the four-step double autocatalytic mechanism as the only mechanism to date that is able to fit the observed kinetic data. Additional support for the generality of the four-step mechanism is given by the identification of three additional literature systems for which the four-step mechanism is observed. Multiple other experiments and results are also described and then summarized in a Conclusions section.

Introduction

Two recent reports[1,2] provided reaction product and stoichiometry, transmission electron microscopy (TEM), X-ray photoelectron spectroscopy (XPS), nuclear magnetic resonance (NMR) spectroscopy, gas–liquid chromatography (GLC), and extensive experimental kinetic and numerical integration curve-fitting data for a four-step mechanism for transition-metal nanocluster formation and agglomeration from metal salts under reductive conditions such as H_2 (Scheme 3.1). The proposed minimalistic ("Ockham's Razor") kinetic scheme and associated mechanism (Scheme 3.1) consists of[1,2] slow continuous nucleation, A→B (rate constant k_1), fast *autocatalytic* surface growth, A+B→2B (rate constant k_2), bimolecular agglomeration, B+B→2B (rate constant k_3), and a new, unprecedented *autocatalytic agglomeration step* between smaller particles (B) and what appear to be larger, more bulk-metal-like (C) particles, B+C→1.5C (rate constant k_4)—although the exact nature of B and C remain to be elucidated via in-progress studies using extended X-ray absorption fine structure (EXAFS), X-ray absorption near-edge spectroscopy (XANES), small-angle X-ray scattering (SAXS), and other physical methods.[3] A novel feature of the mechanism is that two autocatalytic steps (steps 2 and 4 in Scheme 3.1) are present, that is, two steps in which a product is also a reactant. Reaction mechanisms including two autocatalytic steps are rare in the literature, prior examples being limited to the reactions of nitriles in high-temperature water,[4] the action of ATPase pumps,[5] oscillating reactions,[6a] and amplification of chirality.[6b] The four-step mechanism in Scheme 3.1 is a culmination of studies since 1994

investigating the mechanism of transition-metal nanocluster formation under reductive conditions.[7,8]

Scheme 3.1. Schematic pictorial view detailing the four-step, double-autocatalytic mechanism for transition-metal nanocluster formation from metal salts under reducing conditions such as H_2. The precise size and exact nature of the critical nucleus, Pt_n^0, as well as of B and C versus time remain to be elucidated.

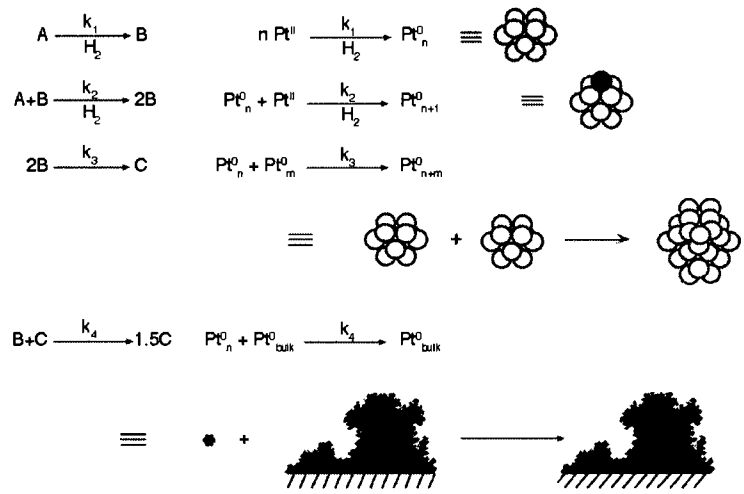

The primary system examined in our most recent kinetic and mechanistic work[1,2] is $Pt(1,5\text{-COD})Cl_2$ under the specific conditions of 1.34 mM $Pt(1,5\text{-COD})Cl_2$, 2.66 mM Bu_3N, 2.69 mM Proton Sponge (1,8-bis(dimethylamino)naphthalene, a strong, non-coordinating preferred base[9] used to scavenge the protons formed by H_2 reduction of Pt^{II}, Scheme 3.1), 1.65 M cyclohexene, and acetone as solvent, all initially under 40 psig of hydrogen. A typical, diagnostic—albeit unprecedented until recently[1,2]—kinetic curve is shown in Figure 3.1 in which a variable, ca. 0.4–3.0 h induction period is followed by the reaction "taking off" very suddenly after that in an almost step-function-like manner. The initially clear, colorless reaction solution changes to cloudy black just after the end of the induction period. TEM of a drop of

the solution harvested 5 min after the end of the induction period reveals the presence of 4.0 ± 1.0 nm nanoclusters.[1,2] At the end of the reaction, agglomerated black bulk Pt^0 metal (verified by XPS) is visible in the solution, on the stir bar, and on the walls of the reaction tube—that is, a phase transition to bulk Pt^0 begins near the end of the induction period when hydrogenation begins suddenly.

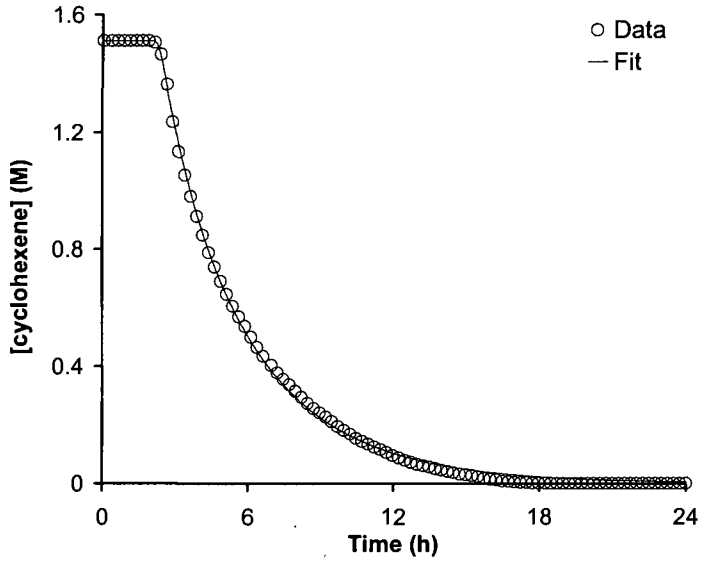

Figure 3.1. Typical kinetic curve for the reduction of Pt(1,5-COD)Cl_2, in the presence of 2 equivalents of Proton Sponge and 2 equivalents of Bu_3N, plus cyclohexene hydrogenation as a concomitant reporter reaction.[8] For clarity, only every fourth datum point is shown. The data are fit to the four-step mechanism shown in Scheme 3.1; note the excellent fit that results to this unusually shaped kinetic curve (residual = 0.012).

A key result from the prior reports is that the larger, apparently bulk-metal-like particles, C, are the superior hydrogenation catalyst over the normally more active nanoclusters, B, due to a postulated particle-size-dependent fractional surface-coverage effect including an apparent particle-size-dependent metal–ligand bond dissociation energy (BDE).[1,2] Independent experimental evidence for a size-dependent surface coverage exists; for example, Leff et al. found that for Au clusters

ligated with thiols the extent of surface coverage decreases with increasing cluster size,[10] as one might expect since smaller, highly curved nanoclusters are more readily covered by ligands than bulk metal, which has a relatively flat surface. Calculations of CO adsorbed on small Co clusters (containing 13–55 atoms) gave a similar trend of decreasing binding energy with increasing cluster size.[11,12] The existence of a greater number of more coordinatively unsaturated edge and terrace sites on nanoclusters versus bulk metal may be a factor in the increased ligand binding energy in nanoclusters. In 1992, Schmid reported differential scanning calorimetry (DSC) and extended X-ray absorption fine structure (EXAFS) studies that showed that Au-Au bond strengths in Au_{55} clusters are 15 kcal/mol greater than those in bulk Au metal.[13] In addition, N_2 bound to bulk Ni metal has a bond dissociation energy ~½ at of Ni_n(nanocluster)-N_2 bonds.[14] In short, the phenomenon of stronger metal–ligand bonds with decreasing particle size has precedent but was little appreciated in nanocluster chemistry until its effects in catalysis by B versus C (Scheme 3.1) were discovered in 2005.[1,2]

The prior studies of the reduction of Pt(1,5-COD)Cl_2[1,2] provided preliminary evidence that important variables in the four-step, double-autocatalytic mechanism in Scheme 3.1 include the initial metal precursor concentration, $[A]_0$ (e.g., Pt(1,5-COD)Cl_2 in the prior work[1,2]), the temperature, and added nanocluster ligands/poisons such as tributylamine or pyridine.[1,2] However, none of these variables were explored in any detail. Key questions left unanswered by the prior work[1,2] include the following: (i) How general is the four-step, double-autocatalytic mechanism in Scheme 3.1? (ii) Does the addition of ligands affect the reduction

mechanism, that is, can a reduction that follows the two-step mechanism (the first two steps of Scheme 3.1) be "forced" into the four-step mechanism by the addition of ligands, as our preliminary studies suggested might be the more general case?[1,2] (iii) How is the mechanism influenced by precursor concentration? (iv) How is the mechanism influenced by reaction temperature? Also, (v) are there major effects[15] of (always imperfect[15]) stirring on a reaction involving *two* autocatalytic steps? Reactions with even one autocatalytic step can be highly sensitive to such stirring effects.[15]

Herein we report studies showing the following: (i) The four-step mechanism is quite general to at least the five metals studied under selected conditions (*vide infra*): platinum, ruthenium, iridium, rhodium, and palladium. (ii) The concentration and type of ligands present have a large effect on the reduction mechanism (higher concentrations of strongly coordinating ligands favor the four-step mechanism). (iii) The reduction of Pd(1,5-COD)Cl_2 follows the four-step mechanism, but only when excess 1,5-COD is present; in the absence of excess 1,5-COD, the reduction occurs without an induction period. (iv) The number of steps of the reduction mechanism is independent of reaction temperature, metal concentration, and stirring rate. In addition, (v) the products of the metal reduction can be changed from bulk metal to nanoclusters by choice of solvent, rather than temperature and concentration as tentatively concluded previously, and (vi) changes in *nucleation* (rate constant k_1) are shown to have controlling effects on whether agglomerated/bulk-metal product is observed.[1,2] Also included is a section discussing additional literature systems found by us that exhibit the four-step, double-autocatalytic mechanism. The results are

significant in establishing the broader generality, and defining the key variables, of the four-step, double-autocatalytic mechanism of transition-metal nanocluster formation under the common conditions of H_2 reduction of metal salts. At least at present, there is no alternative, kinetically verified mechanism for transition-metal nanocluster nucleation, growth, and agglomeration.

Experimental

General considerations

All manipulations were carried out under air-free conditions using a Vacuum Atmospheres N_2 drybox maintained at $\leq$5 ppm O_2 as monitored by a Vacuum Atmospheres O_2 level monitor. Unless indicated otherwise, all commercially available solvents, compounds, and materials were used as received. Acetone (Burdick and Jackson, water content <0.2%) was purged with argon for 20 min and stored in the drybox. Propylene carbonate (Aldrich) was evacuated for 4 h before being stored in the drybox over activated 4 Å molecular sieves. Cyclohexene (Aldrich, 99%) and tributylamine (J.T. Baker Chemicals) were both purified by their separate distillation over sodium under argon followed by storage in the drybox. Hydrogen gas (General Air, 99.5%) was purified bypassing through a moisture trap, an O_2 cartridge, and an indicating O_2 trap (Trigon Technologies, Rancho Cordova, CA). The complexes $[Ir(1,5\text{-COD})Cl]_2$ (99%), $[Rh(1,5\text{-COD})Cl]_2$ (98%), $Pt(1,5\text{-COD})Cl_2$ (99%), $Pd(1,5\text{-COD})Cl_2$ (99%), and $Ru(1,5\text{- COD})Cl_2$ (99%) were obtained from Strem Chemicals and used as received. Proton Sponge (1,8-bis(dimethylamino)naphthalene) (99%), silver tetrafluoroborate (99.9%), 4-(dimethylamino)pyridine (99.9%), and tetrabutylammonium chloride ($\geq$97%) were

obtained from Aldrich and stored in the drybox. Octanethiol (Aldrich, 98%) was taken into the drybox only when needed and then removed immediately after its use, as thiols are known poisons for the drybox catalyst. Pyridine (Aldrich, 99%) was distilled under vacuum and stored in the drybox over activated 4 Å molecular sieves. Stock solutions of tributylamine and pyridine were prepared and stored in the drybox; the tributylamine solution (42 mM) was prepared by mixing 0.1 mL (0.42 mmol) of tributylamine and 9.9 mL of acetone; the pyridine solution (18 mM) was prepared by diluting 73 μL (0.91 mmol) of pyridine to 50 mL with acetone.

Hydrogenations: Standard Conditions

Hydrogenation reactions were performed as previously described using our custom-built pressurized hydrogenation apparatus.[7] Briefly, the appropriate amount of the metal precursor salt was weighed into a 1-dram glass vial (3.6 μmol in a Standard Conditions hydrogenation). Proton Sponge was added to the vial (1 equivalent for Ir^{I} and Rh^{I} and 2 equivalents for Pt^{II}, Pd^{II}, and Ru^{II}). When added ligand was employed, the appropriate amounts of ligand or ligand stock solution plus solvent were added to make a 2.5 mL homogeneous solution. The resultant solution was added to a new 22 × 175 mm Pyrex borosilicate culture tube containing a new 5/8 × 5/16 in Teflon-coated magnetic stir bar, and 0.5 mL of cyclohexene was added to the solution (resulting in a metal concentration of 1.2 mM in a Standard Conditions hydrogenation). The culture tube was placed in a Fischer–Porter (hereafter F-P) bottle, which was then sealed and brought out of the drybox. The bottle was placed in a mineral oil bath maintained at 22.0 ± 0.1 °C by a constant temperature recirculating water bath (VWR Scientific). The bottle was connected to the hydrogenation

apparatus via its TFE-sealed Swagelock quick connects. Stirring was started, and the bottle was purged 13 times with hydrogen (15 s per purge) and stirred for an additional 1 min 45 s (total time elapsed 5 min). The pressure in the bottle was set to 40.0 ± 0.1 psig of H_2, $t = 0$ was noted, and data collection was initiated using an Omega PX-621 pressure transducer interfaced with a PC running LabVIEW 6.1.[7] Correction for the initial increase in acetone vapor pressure (when acetone was used as the solvent) was performed as described elsewhere[16] by independently measuring a curve (i.e., the initial increase in pressure) of a mixture of 2.5 mL of acetone and 0.5 mL of cyclohexene and then subtracting point by point that vapor pressure increase contribution from the kinetic data at early times.[16]

Data analysis was performed using nonlinear least-squares curve fitting to the analytic equation for the two-step mechanism[8a] (Microcal Origin version 7) or, for the three- or four-step mechanisms,[2] numerical integration via MacKinetics version 0.9.1b.[17] A good fit using MacKinetics corresponded to residuals of ≤0.02 as well as a visually close fit; residuals were typically between 0.007 and 0.01. The details of the fitting procedure have been described previously in detail, along with a discussion of the larger error bars intrinsic to fits of the four-step mechanism.[2]

Reduction of the in situ generated platinum complex, [Pt(1,5-COD)Cl(acetone)]$^+$[BF_4]$^-$

In the drybox, 1.9 mg of Pt(1,5-COD)Cl_2 (5.08 μmol) was dissolved in 2.5 mL of acetone to make a clear, colorless solution. This solution was added to a vial containing 1.0 mg of $AgBF_4$ (5.14 μmol, 1.01 equivalents versus Pt); a white precipitate of AgCl immediately formed. The vial was capped and Parafilmed and

was brought out of the drybox. The vial was centrifuged for 20 min at ~1600 rpm to settle the white precipitate to the bottom of the vial. The vial was then returned to the drybox, and the clear colorless liquid was decanted into a new culture tube. The white solid (AgCl, 0.7 mg, 100%) was weighed to ensure that the reaction went to completion. Attempts to isolate the complex for characterization failed. Next, 0.5 mL of cyclohexene was added to the culture tube, and hydrogenation was performed as described above. The acetonitrile solvated complex $[Pt(1,5\text{-}COD)Cl(CH_3CN)]^+[BF_4]^-$ and its Pd analogue were prepared, isolated, and characterized (see Supporting Information); these results parallel well-known metal-solvate complex literature where the CH_3CN solvates are of greater stability than the acetone solvates.[18] However, the acetonitrile complex gives irreproducible results when hydrogenated.

GLC studies following the evolution of cyclooctane from the hydrogenation of [Ir(1,5-COD)Cl]$_2$

A Standard Conditions reaction (with the exception that all quantities were doubled) was started using $[Ir(1,5\text{-}COD)Cl]_2$ and 5 equivalents of pyridine. Samples for GLC analysis were taken using the following procedure: the gas-regulator valve between the F-P bottle and the hydrogen tank was opened. Next, the top valve of the F-P bottle was opened to allow a continuous stream of H_2 through the F-P bottle and out of the top valve. A ~0.1 mL aliquot of the reaction solution was removed with a gastight syringe equipped with a 30 cm long needle, and the aliquot was placed in a 1 mL screwcap vial. The top valve of the F-P bottle was immediately closed. After waiting 10 s for the F-P bottle to become repressurized to ~40 psig of H_2, the valve to the hydrogen tank was closed. The entire operation took less than 1 min. The sample

was immediately analyzed by GLC using a Hewlett-Packard HP-5890 equipped with a Supelco SPB-1 capillary column (30 m × 0.25 mm) and a flame ionization detector and interfaced to a PC running Galaxie software (Galaxie Chromatography Data System, version 1.7.403.22). The sampling parameters were as follows: initial temperature 50 °C, initial time 3 min, ramp rate 10 °C/min, final temperature 160 °C, final time 10 min, injector temperature 180 °C, detector temperature 200 °C. The results of the GLC experiment are described in the main text.

Higher temperature studies

These hydrogenations were performed as above, except the temperature of the recirculating water bath was raised to a higher temperature (from 30.0 °C to 80.0 °C; see Results and Discussion). The temperature of the solution in the F-P bottle was verified by placing a thermometer in a culture tube inside the F-P bottle that contained 3 mL of propylene carbonate. For these high-temperature reactions, the F-P bottle was kept in the oil bath for 3–5 min before purging with H_2 to allow the temperature of the solution to equilibrate with the temperature of the oil bath. At the highest temperature studied (80 °C), the cyclohexane formed during the reaction boiled (cyclohexane bp 80.7 °C) and recondensed at the top of the culture tube in the F-P bottle. This cyclohexane "distillation" resulted in a series of pressure spikes as measured by the pressure transducer. A representative example of this phenomenon is shown in the Supporting Information, Figure 3S.1. However, the rate constants were obtained by fitting only the first half of the data[8a] (i.e., before too much of the "distillation" occurs), so that this phenomenon is not expected to have a significant impact on the calculations of the rate constants. As a control to test the

reproducibility, the reactions were reproduced three times and resulted in the same observed rate constants (within error) each time.

Another way to judge the quality of the fit: The F test

In the data sets which follow, the residual given by the MacKinetics program has been used to judge how closely the fit matches the data, lower values of r (along with a visually close fit) indicating a better fit. To provide an independent and more universal measure of the fit quality, we also employed the statistical F test. Details of this statistical technique are given elsewhere,[19] but the essence for the purposes of this paper is that the variances of the fit to the data and the fit were compared to determine whether the two sets of data are statistically equal. The F value is the measure of the similarities of the variances of the fit to the data—the closer that value is to 1, the more likely the data and fits are equal. For example, for the data in Figure 3.1 which follows, the fit to the four-step mechanism gives an F value of 1.000(6) at the 95% confidence level, indicating an excellent fit. The F value associated with the two-step mechanism fit is 0.825 at the 95% confidence level, indicating an inferior fit (Figure 3.S2a in the Supporting Information shows the visually inferior fit of the two-step mechanism). The results of the F test for representative four-step fits in this study are tabulated in the Supporting Information, Table 3S.1.

Results and Discussion

The kinetic method employed

It is important to understand how the kinetics of the multistep, self-assembly nanocluster formation reaction (eq 3.1) are monitored. The kinetic data are obtained indirectly, but powerfully and in real time, by the method first developed in a series

of papers[7,8] dating back to 1994. This method employs the ability of the resulting metal^0 product, *the bulk-like metal (C) in the case of the four-step mechanism,*[1,2] to serve as a fast cyclohexene hydrogenation catalyst, eq 3.2—that is, the rate of the hydrogenation in eq 3.2 is fast relative to the rates of the reactions in eqs 3.1a-3.1d.

$$A \xrightarrow{k_1} B \tag{3.1a}$$

$$A+B \xrightarrow{k_2} 2B \tag{3.1b}$$

$$B+B \xrightarrow{k_3} C \tag{3.1c}$$

$$B+C \xrightarrow{k_4} 1.5C \tag{3.1d}$$

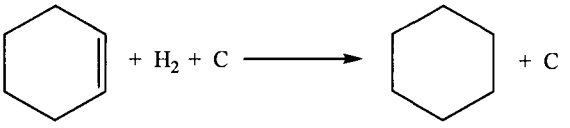

(3.2)

The fast cyclohexene hydrogenation reporter reaction can therefore be used to follow the loss of H_2 via a computer-interfaced, high-precision (±0.1 psig) pressure transducer. The H_2 loss is, for convenience, converted to the equivalent cyclohexene loss (by the known 1 H_2:1 cyclohexene stoichiometry in Scheme 3.1), and then the rate constants for the nanocluster nucleation, growth, and agglomeration steps, k_1-k_4 in Scheme 3.1, are obtained[1,2,8] using the now well-documented pseudoelementary step method (*vide infra*).[7] This method—the addition of the fast catalytic reporter reaction (eq 3.2) to the slow steps that produce C (eqs 3.1c and 3.1d)—allows one to write eq 3.3 to make the needed connection between cyclohexene loss and the formation of C (the pseudoelementary step in this system is eq 3.3d).[7] The rate constants k_1-k_4 are then found by numerical integration curve-fitting and grid-search

methods using MacKinetics.[17,20] Full details of the pseudoelementary step method,[7] the MacKinetics curve-fitting, and the grid-search methods employed are also documented in earlier papers.[2,7]

$$x\,[B + B \longrightarrow C] \tag{3.3a}$$

$$1\text{-}2x\,[B + C \longrightarrow 1.5C] \tag{3.3b}$$

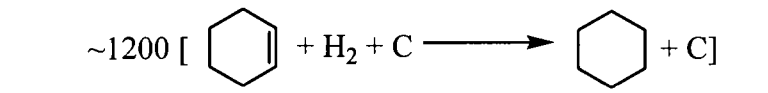

(3.3c)

(3.3d)

As briefly noted in the Introduction, the four-step, double-autocatalytic mechanism in Scheme 3.1 is a culmination of our studies investigating the mechanism of nanocluster formation from metal salts under reductive conditions such as H_2. For what follows, it will be important to be able to quickly and visually distinguish between the four-step mechanism (e.g., Figure 3.1, *vide supra*, or Figure 3.3, *vide infra*) from the two-step mechanism (Scheme 3.2 and Figure 3.2a) or three-step mechanism (Scheme 3.3 and Figure 3.2b).

Scheme 3.2

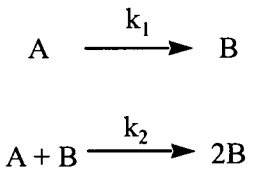

Scheme 3.3

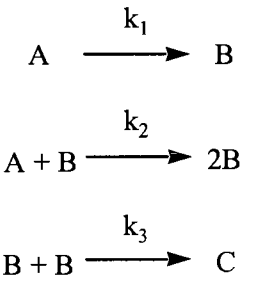

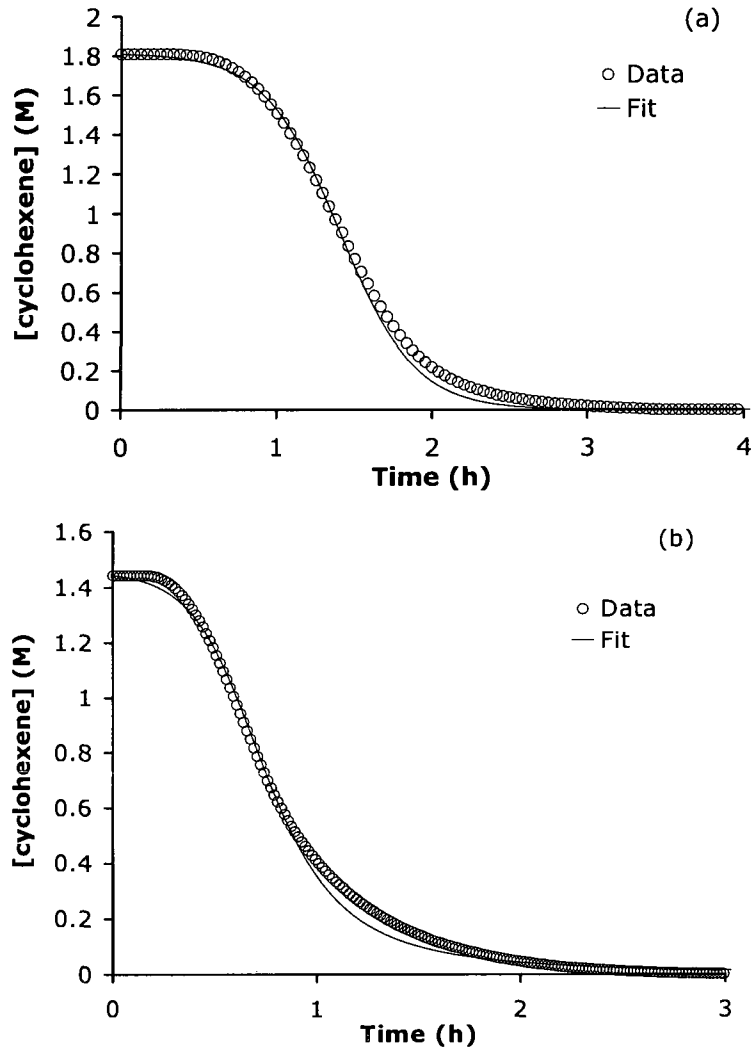

Figure 3.2. Kinetic curves for the reduction of $(Bu_4N)_5Na_3[(1,5\text{-}COD)Ir{\cdot}P_2W_{15}Nb_3O_{62}]$ (a) in the absence of added ligand and (b) in the presence of 2 equivalents of pyridine. The curve fit in (a) is to the two-step mechanism in Scheme 3.2 (with rate constants and indicated error bars $k_1 = 0.012(1)\ h^{-1}$ and $k_2 = 3.21(7) \times 10^3\ M^{-1}\ h^{-1}$), while the curve fit in (b) is to the three-step mechanism in Scheme 3.3 (with rate constants $k_1 = 0.063\ h^{-1}$, $k_2 = 5.4 \times 10^3\ M^{-1}\ h^{-1}$, and $k_3 = 1.8 \times 10^3\ M^{-1}\ h^{-1}$ and residual = 0.025). In (b), the fit misses some of the early and later parts of the curve, an indicator that the four-step mechanism is beginning to be a component (*vide infra*) of that particular reaction. Note the clear difference in the appearances of these curves to that shown in Figure 3.1. Error bars are reported for the two-step fit since the fit uses an analytic equation,[8a] while a residual is reported for the four-step fit since that fit is obtained using MacKinetics numerical integration.[1,2]

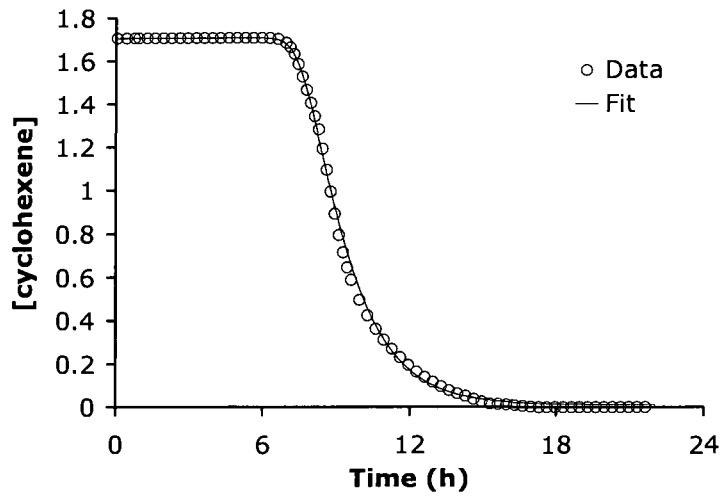

Figure 3.3. Kinetic curve for the reduction of 1.2 mM Pt(1,5-COD)Cl_2 with 2 equivalents of Proton Sponge and the concomitant cyclohexene hydrogenation reporter reaction. For clarity in visualizing the fit, only every fourth datum point is shown. The curve fit is to the four-step, double-autocatalytic mechanism: $k_1 \approx 1 \times 10^{-7}$ h^{-1}, $k_2 \approx 1.6 \times 10^3$ M^{-1} h^{-1}, $k_3 \approx 1.7 \times 10^2$ M^{-1} h^{-1}, $k_4 \approx 9.1 \times 10^2$ M^{-1} h^{-1} (residual = 0.010). For a discussion of the precision and error limits on k_1-k_4, see the discussion elsewhere.[2]

Two immediate visual properties of the kinetic curves serve to distinguish the four-step mechanism from the two- and three-step mechanisms: (i) the sharp loss of cyclohexene after the induction period (the sudden "turn-on" mentioned above and shown in Figure 3.1) and (ii) the absence of an inflection point in the curve. These two qualitative features (which can be seen in Figure 3.1, but are absent from both of the curves in Figure 3.2) are instant indicators that the four-step, double-autocatalytic mechanism should be considered.

Herein we will search primarily for conclusions that are based on (i) whether or not the diagnostic curves of the four-step mechanism are seen and can be closely curve fit (i.e., with residuals ≤ 0.02), and (ii) conclusions involving comparisons between rate constants with differences $\geq 10^4$ in k_1 and $\geq 10^2$ in k_2-k_4 and, therefore, which should be valid.[1,2] This approach is necessary since minimization of the

residual of the curve fit will in general be improved as one adds more parameters, so that, again, use of the *minimal* number of steps (i.e., the two- or three-step mechanism versus the four-step mechanism) is the "Ockham's Razor"[21] approach one must take.

Metal and ligand dependencies

The observed kinetic curves, and hence the resultant mechanism, proved to be *the most dependent on the metal being reduced and the added ligands/poisons.* Hence, the main results for the metal and ligand surveys are given first in what follows. These results are summarized in Table 3.1.

Platinum

Reduction of Pt(1,5-COD)Cl_2 in the presence of 2 equivalents of tributylamine was the first system for which the four-step mechanism was observed (Table 3.1, entry 1);[1,2] a typical kinetic curve is shown back in Figure 3.1.[2] As a control experiment, Pt(1,5-COD)Cl_2 was reduced in the absence of Bu_3N, with the expectation that the two-step mechanism would be observed. Interestingly, this latter reduction still follows the four-step mechanism, Figure 3.3, with an excellent fit to the observed data. Attempted curve fits to the two- and three-step mechanisms, and their associated rate constants, are given in the Supporting Information, Figure 3S.2; they are clearly inferior to the fit with the four-step, double-autocatalytic mechanism. In fact, the four-step mechanism is needed to fit the data for the reduction of Pt(1,5-COD)Cl_2 over a range of reaction temperatures and metal concentrations (*vide infra*). It appears, therefore, that the 2 equivalents of Cl^- from the precursor complex alone are sufficient to ligate/poison the Pt_n^0 nanoclusters to the point that the four-step mechanism is necessary to fit the data.

Table 3.1. Summary of metal and ligand dependence on reduction mechanism. All reactions are in acetone solvent at room temperature. The appropriate amount of Proton Sponge™ as noted in the Experimental section is also present.

Entry	Precursor complex	Added ligand (equiv)	Kinetic Fit
	Pt		
1	$Pt(1,5\text{-}COD)Cl_2$[a]	Bu_3N (2)	4-step
2	$Pt(1,5\text{-}COD)Cl_2$	None	4-step
3	$[Pt(1,5\text{-}COD)Cl(acetone)][BF_4]$	None	2-step
	Ru		
4	$Ru(1,5\text{-}COD)Cl_2$	None	4-step
	Ir		
5	$(Bu_4N)_5Na_3[(1,5\text{-}COD)Ir{\bullet}P_2W_{15}Nb_3O_{64}]$[b]	Pyridine (44)	4-step
6	$[Ir(1,5\text{-}COD)Cl]_2$	None	2-step
7	$[Ir(1,5\text{-}COD)Cl]_2$	Bu_4NCl (1)	4-step
8	$[Ir(1,5\text{-}COD)Cl]_2$	Pyridine (1)	2-step
9	$[Ir(1,5\text{-}COD)Cl]_2$	Pyridine (5)	4-step
10	$[Ir(1,5\text{-}COD)(CH_3CN)_2][BF_4]$	None	2-step
11	$[Ir(1,5\text{-}COD)(CH_3CN)_2][BF_4]$	Bu_4NCl (2)	4-step
12	$[Ir(1,5\text{-}COD)(CH_3CN)_2][BF_4]$	Pyridine (1)	4-step

Entry	Precursor complex	Added ligand (equiv)	Kinetic Fit
	Rh		
13	$[Rh(1,5\text{-COD})Cl]_2$	None	2-step
14	$[Rh(1,5\text{-COD})Cl]_2$	Bu_4NCl (1)	4-step
15	$[Rh(1,5\text{-COD})Cl]_2$	Pyridine (50)	2-step
16	$[Rh(1,5\text{-COD})Cl]_2$	4-dimethylaminopyridine (1)	2-step
17	$[Rh(1,5\text{-COD})Cl]_2$	4-dimethylaminopyridine (10)	4-step
18	$[Rh(1,5\text{-COD})(CH_3CN)_2][BF_4]$	None	2-step
19	$[Rh(1,5\text{-COD})(CH_3CN)_2][BF_4]$	Bu_4NCl (2)	4-step
20	$[Rh(1,5\text{-COD})(CH_3CN)_2][BF_4]$	Pyridine (80)	2-step
21	$[Rh(1,5\text{-COD})(CH_3CN)_2][BF_4]$	4-dimethylaminopyridine (10)	4-step
	Pd		
22	$Pd(1,5\text{-COD})Cl_2$	None	Exponential
23	$Pd(1,5\text{-COD})Cl_2$	4-dimethylaminopyridine (20)	Exponential
24	$Pd(1,5\text{-COD})Cl_2$	1,10-phenanthroline (1)	Exponential
25	$Pd(1,5\text{-COD})Cl_2$	Octanethiol (0.5)	Exponential
26	$Pd(1,5\text{-COD})Cl_2$	1,5-COD (20)	4-step

(a) From ref 8. (b) From ref 8c.

As a control to see whether both Cl^- ligands present in Pt(1,5-COD)Cl_2 are necessary to bring about the four-step mechanism in the Pt complex, the solvated complex $[Pt(1,5\text{-COD})Cl(acetone)]^+[BF_4]^-$ was prepared *in situ* in acetone and reduced under H_2 (Table 3.1, entry 2). The data, shown in Figure 3.4, are well fit by the two-step mechanism, not the four-step mechanism as seen for Pt(1,5-COD)Cl_2. Rather clearly, 1 equivalent of Cl^- is insufficient to force the four-step mechanism for Pt.

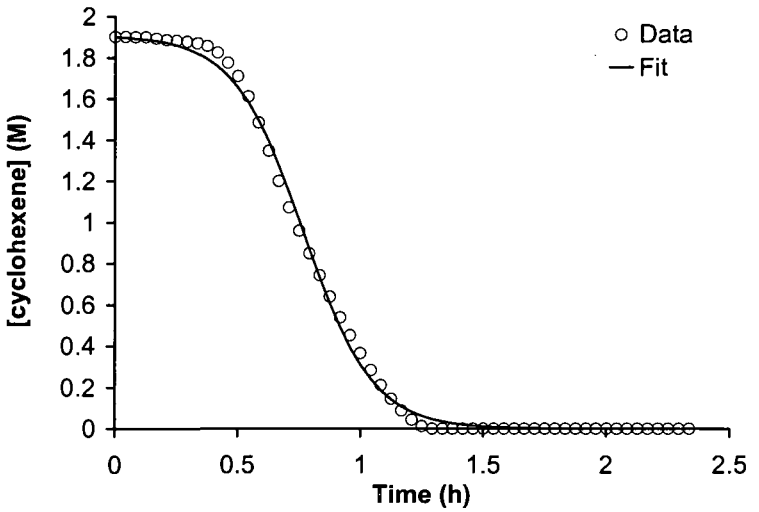

Figure 3.4. Kinetic curve for the reduction of *in situ* generated 1.2 mM $[Pt(1,5\text{-COD})Cl(acetone)]^+[BF_4]^-$ with 1 equivalent of Proton Sponge and the concomitant cyclohexene hydrogenation. The curve fit is to the two-step mechanism: $k_1 = 0.015(2)$ h^{-1}; $k_2 = 6.3(2) \times 10^3$ M^{-1} h^{-1}, meaning that removal of one Cl^- from Pt(1,5-COD)Cl_2 to give $[Pt(1,5\text{-COD})Cl(acetone)]^+[BF_4]^-$ has changed the mechanism from the four-step mechanism with C as the catalyst to primarily the two-step mechanism with B as the catalyst.

A very interesting point in comparing the Pt(1,5-COD)Cl_2 + 2 equivalents Proton Sponge system, Figure 3.3, versus the $[Pt(1,5\text{-COD})Cl(acetone)^+][BF_4]^-$ + 2 equivalents Proton Sponge system, Figure 3.4, is that it appears that the difference of just one additional Cl^- triggers a change from the two- to four-step mechanism (i.e., triggers agglomeration). Initially, one might have expected the opposite—that more Cl^- might lead to better stabilized nanoclusters. But, additional salt (i.e., the Proton

Sponge-H^+Cl^- reaction byproduct) can apparently compact the Debye double layer surrounding the clusters, allowing closer cluster–cluster contact and, ultimately, agglomeration.[22] A look at the rate constants for these two- versus four-step systems is actually more informative. In addition to turning on measurable k_3 and k_4 values (1.7×10^2 M^{-1} h^{-1} and 9.1×10^2 M^{-1} h^{-1}, respectively, versus ~0 for these in the two-step mechanism), the main difference is that the nucleation rate is slower in the four-step mechanism, even given the $10^{\pm 4}$ error bars associated with k_1 in the four-step mechanism, $k_1 \approx 10^{-7}$ h^{-1} versus $k_1 = 10^{-2}$ h^{-1} in the two-step system. Restated, it is really *fewer nuclei*, and the resultant larger nanoclusters from largely unchanged growth ($k_2 = 6.3 \times 10^3$ M^{-1} h^{-1} for the two-step system versus $k_2 \approx 1.6 \times 10^3$ M^{-1} h^{-1} for the four-step system) that, in turn, lead to more agglomeration. *That is, the nucleation step is largely controlling the subsequent agglomeration.* This example nicely illustrates how, without knowledge of the nucleation kinetics, erroneous interpretation of why greater agglomeration results would be hard to avoid.

Ruthenium

The ruthenium complex Ru(1,5-COD)Cl_2 was reduced under H_2 in the absence of poison in acetone at room temperature, Figure 3.5. Reduction of this complex showed the same kinetics as the platinum dichloride complex; that is, 2 equivalents of Cl^- is a sufficient amount of coordinating ligand to make the reduction follow the four-step mechanism. The significance of this result is that it provides immediate evidence that the four-step mechanism is applicable to metals other than platinum.

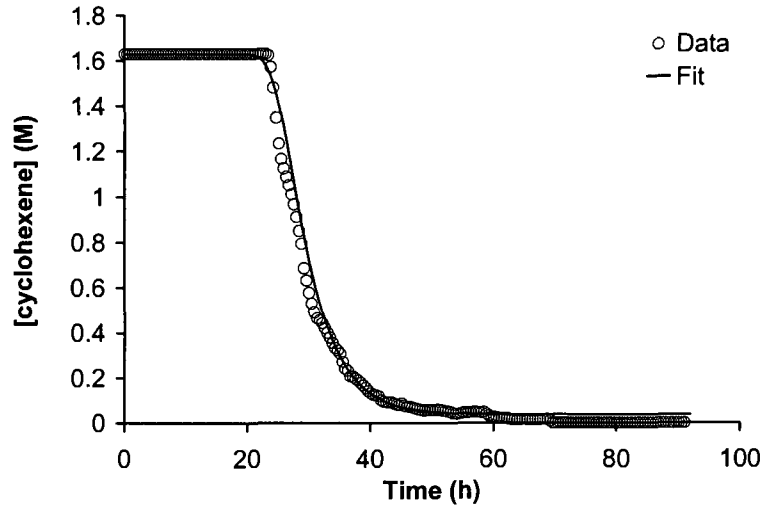

Figure 3.5. Kinetic curve for the reduction of 1.2 mM Ru(1,5-COD)Cl_2 with 2 equivalents of Proton Sponge in the absence of ligand. The curve fit is to the four-step mechanism: (a) $k_1 \approx 2 \times 10^{-7}$ h^{-1}, $k_2 \approx 470$ M^{-1} h^{-1}, $k_3 \approx 46$ M^{-1} h^{-1}, $k_4 \approx 340$ M^{-1} h^{-1} (residual = 0.030). For clarity, only 1 out of every 10 datum points is shown.

We tried to prepare the solvated ruthenium complex, [Ru(1,5-COD)Cl(CH_3CN)]$^+$[BF_4]$^-$, for study, but this was unsuccessful, as was the preparation of [Ru(1,5-COD)Cl(acetone)]$^+$[BF_4]$^-$. The difficulties inherent in the preparation of solvated Ru complexes have been previously documented.[23]

Iridium

Reduction of Ir^I to form nanoclusters has been extensively studied;[7,8] the B+B→C agglomeration step of the nanoclusters (B) when ligands such as pyridine are added, Scheme 3.3, has also been investigated.[8c] In the present work, [Ir(1,5-COD)Cl]$_2$ was reduced in acetone alone and in the presence of added ligands, namely chloride and the known nanocluster poison pyridine.[8c] Bulk Ir^0 metal proved to be the only product in both cases. In the absence of added ligands, the reduction followed the two-step mechanism, Figure 3.6, circles, as seen previously.[24] When 1 equivalent of chloride was added in the form of Bu_4NCl to make 2 equivalents of total Cl^-

present versus Ir, the four-step mechanism was needed to fit the data, Figure 3.6, squares. Five equivalents of pyridine was also enough ligand to "force" the reduction into the four-step, double-autocatalytic mechanism, Figure 3.6, triangles. One equivalent of pyridine, however, is not enough to change the mechanism; the two-step mechanism was sufficient to fit the data, Supporting Information, Figure 3S.3. In short, with either 2 total equivalents of Cl^- or 5 equivalents of added pyridine, the reduction of Ir^I is forced into the four-step mechanism. A small k_1 ($\approx 10^{-7}$ h^{-1}) is again apparent for the added pyridine system (albeit not for the added Cl^- system, $k_1 \approx 10$ h^{-1}, a result which may reflect the large error in the k_1 value[1,2]).

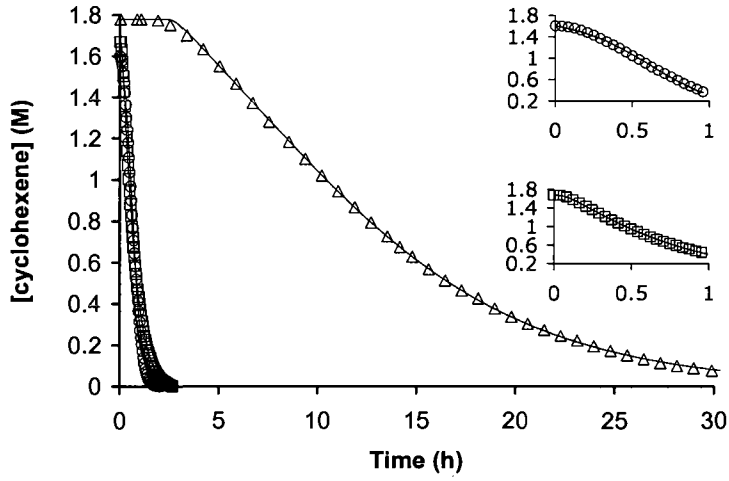

Figure 3.6. Kinetic curves for the reduction of 0.6 mM $[Ir(1,5\text{-COD})Cl]_2$ (1.2 mM Ir) in the absence of added ligand (circles), in the presence of 1 equivalent of Bu_4NCl (almost hidden squares), and in the presence of 5 equivalents of pyridine (triangles, the slow reaction that ends at ~30 h). One equivalent of Proton Sponge is present in each reaction. The insets show the induction periods for the reduction of $[Ir(COD)Cl]_2$ with no ligand (circles, top inset) and with 1 equivalent of Bu_4NCl (squares, bottom inset). The curve fits are to the two-step mechanism fit (no ligand), $k_1 = 0.28(2)$ h^{-1}, $k_2 = 3.6(1) \times 10^3$ M^{-1} h^{-1}, and to the four-step mechanism for the data with Bu_4NCl and pyridine—Bu_4NCl, $k_1 \approx 10$ h^{-1}, $k_2 \approx 8.5 \times 10^3$ M^{-1} h^{-1}, $k_3 \approx 4.1 \times 10^3$ M^{-1} h^{-1}, $k_4 \approx 3.0 \times 10^3$ M^{-1} h^{-1} (residual = 0.004), and pyridine, $k_1 \approx 2 \times 10^{-7}$ h^{-1}, $k_2 \approx 4.6 \times 10^3$ M^{-1} h^{-1}, $k_3 \approx 18$ M^{-1} h^{-1}, $k_4 \approx 200$ M^{-1} h^{-1} (residual = 0.005). For clarity, only 1 out of every 4 datum points is shown for the pyridine data. As before, error bars are reported for the two-step fit since the fit uses an analytic equation,[8a] while a residual is reported for the four-step mechanism fits obtained via MacKinetics numerical integration.[1,2]

The same result was seen with the solvated complex [Ir(1,5-COD)$(CH_3CN)_2]^+[BF_4]^-$: in the absence of added ligand/poison, the two-step mechanism was able to fit the data, but the addition of either 2 equivalents of Cl^- or 1 equivalent of pyridine was sufficient to change the mechanism so that the four-step mechanism was required to fit the data, Supporting Information, Figure 3S.4.

Recent results in our laboratory have suggested that the addition of pyridine may poison the cyclohexene hydrogenation reporter reaction to the point that it becomes ineffective in reporting the kinetics of nanocluster formation.[25] To see whether this is the case in the current system of $[Ir(1,5\text{-}COD)Cl]_2$ with 5 equivalents of pyridine, we performed two control experiments. In the first, the concentration of cyclohexene was changed from the standard 1.65 M to 0.825 and then 3.30 M, that is, to one-half and then twice the standard concentration. These changes in cyclohexene concentration did not change the kinetics of the reaction, indicating that the nanocluster formation reaction remains zero-order in cyclohexene over this concentration range. In the second control experiment, described in a later section, the evolution of cyclooctane from the $[Ir(1,5\text{-}COD)Cl]_2$ complex was measured using gas–liquid chromatography. The rate constants from that measurement were the same within experimental error as those determined from the cyclohexene hydrogenation reporter reaction, indicating that the reporter reaction is indeed accurately reporting the kinetics of nanocluster formation for this system.

Rhodium

It was expected that the behavior of rhodium would be similar to that of iridium, the two metals being in the second and third rows of the same group;[26] however, this proved to be the case only for the addition of chloride. When [Rh(1,5-

COD)Cl]$_2$ was reduced under H_2 in the absence of added ligands to form bulk Rh^0 metal as the final product, the two-step mechanism fit the data well, Figure 3.7, circles. Like the Ir system above, 1 equivalent of added chloride (i.e., 2 equivalents of total Cl^-) was sufficient so that the four-step mechanism was needed to fit the data, Figure 3.7, squares. However, unlike the Ir^I reduction case, the addition of pyridine did *not* change the mechanism to even the three-step mechanism; in fact, even 50 equivalents of pyridine did not change the two-step mechanism. The reaction was significantly slowed compared to the reduction of [Rh(1,5-COD)Cl]$_2$ alone, but the kinetics still followed the two-step mechanism, Figure 3.7, triangles.

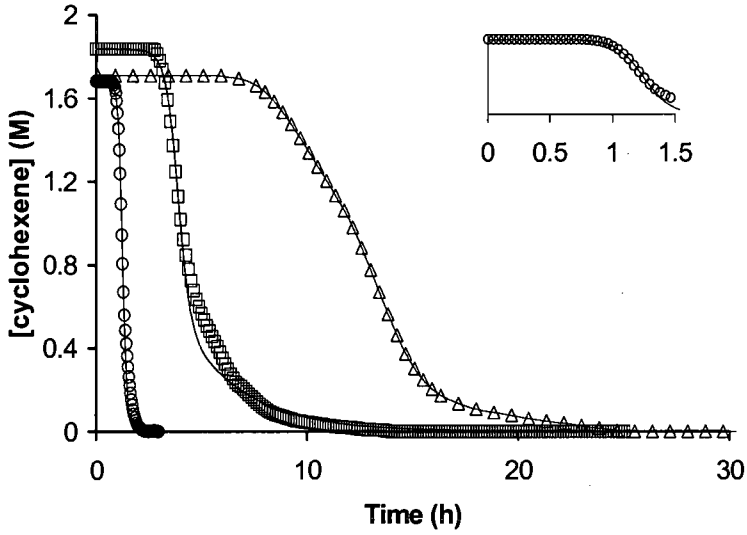

Figure 3.7. Kinetic curves for the reduction of 0.6 mM [Rh(1,5-COD)Cl]$_2$ (1.2 mM Rh) and 1 equivalent of Proton Sponge in the absence of ligands (circles, the faster reaction that ends at ~3 h), in the presence of 1 equivalent of Bu_4NCl (squares), and in the presence of 50 equivalents of pyridine (triangles, the slower reaction that ends at ~25 h). The inset shows the induction period and fit for the reduction of [Rh(1,5-COD)Cl]$_2$ with no ligand (circles). The fits in the curves with no added ligand and with pyridine are to the two-step mechanism; with no ligand: $k_1 = 7(3) \times 10^{-4}$ h^{-1}, $k_2 = 6.0(4) \times 10^3$ M^{-1} h^{-1}; with 50 equivalents of pyridine: $k_1 = 3.9(2) \times 10^{-4}$ h^{-1}, $k_2 = 4.8(5) \times 10^2$ M^{-1} h^{-1}. The fit to the curve with added Bu_4NCl is to the four-step mechanism: $k_1 \approx 6 \times 10^{-6}$ h^{-1}; $k_2 \approx 2.9 \times 10^3$ M^{-1} h^{-1}; $k_3 \approx 310 \times 10^3$ M^{-1} h^{-1}; $k_4 \approx 690 \times 10^3$ M^{-1} h^{-1} (residual = 0.010). Error bars, not a residual, are reported for the two-step fit since the fit uses an analytic equation,[8a] not MacKinetics numerical integration.[1,2] For clarity, only 1 out of 4 datum points is shown.

In light of the above results, pyridine was replaced with a stronger base, namely 4-(dimethylamino)pyridine (p*K*a of the conjugate acid = 9.7 versus 5.2 for pyridine), the prediction being that the stronger basicity (and hence stronger σ-donor ability) of this ligand would make it a more effective ligand for the second-row metal, Rh, with its weaker (than Ir) metal–ligand bond energy. Indeed, when 10 equivalents of 4-(dimethylamino)pyridine were added to the reaction solution, the four-step mechanism became necessary to fit the kinetic curve, Figure 3.8. However, with only 1 equivalent, the two-step mechanism was still sufficient to fit the data.

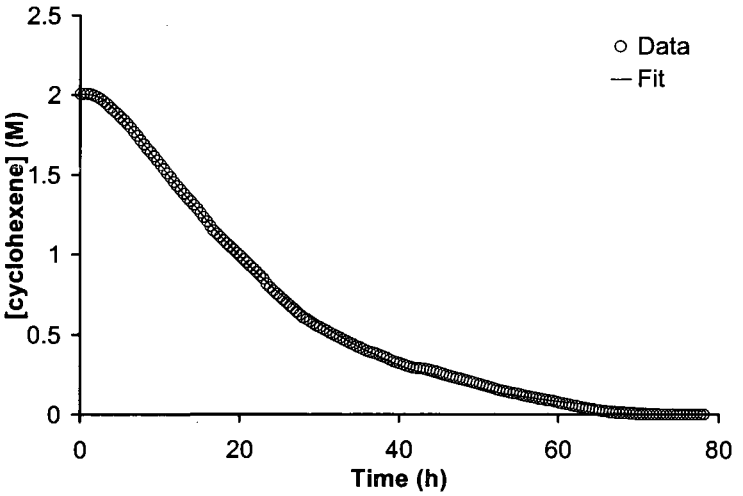

Figure 3.8. Kinetic curve for the reduction of 0.6 mM $[Rh(1,5\text{-}COD)Cl]_2$ (1.2 mM Rh) with 1 equivalent of Proton Sponge in the presence of 10 equivalents of 4-(dimethylamino)pyridine. The curve is best fit by the four-step mechanism: $k_1 \approx 0.3$ h^{-1}, $k_2 \approx 250$ M^{-1} h^{-1}, $k_3 \approx 9.7$ M^{-1} h^{-1}, $k_4 \approx 82$ M^{-1} h^{-1} (residual = 0.010). For clarity, only 1 out of every 10 datum points is shown.

Similar results were obtained using the solvated complex $[Rh(1,5\text{-}COD)(CH_3CN)_2]^+[BF_4]^-$, Supporting Information, Figures 3S.5 and 3S.6—the addition of 2 equivalents of Cl^- changed the mechanism from the two-step to the four-step mechanism, similar to the solvated Ir complex, but even 80 equivalents of pyridine were unable enforce the four-step mechanism. However, using 10

equivalents of the stronger base 4-(dimethylamino)pyridine did yield the four-step mechanism in the reduction of $[Rh(1,5\text{-}COD)(CH_3CN)_2]^+[BF_4]^-$ under H_2.

In short, the donor strength, as well as the concentration, of the added ligand and the nature of the metal (e.g., second row versus third row) are important in determining which mechanism the reduction will follow. More generally, it appears that high metal–ligand bond energies, plus sufficient concentrations of ligand to ensure bonding to the nanocluster, are crucial for enforcing the four-step mechanism. The resultant slowing of the k_1 nucleation step appears to be one key to inducing the formation of larger nanoclusters that agglomerate more readily, perhaps due to their weaker metal–ligand bond energies, as already discussed.[1,2]

Palladium

The reduction of $Pd(1,5\text{-}COD)Cl_2$ using our Standard Conditions began immediately without an induction period, Figure 3.9; the curve has the appearance of the four-step mechanism with the induction period removed. More specifically, the induction period was extremely short; the clear yellow $Pd(1,5\text{-}COD)Cl_2$ solution changed to black during the 5 min H_2 purge cycle of the Fischer–Porter bottle. Attempts to produce an induction period failed even on addition of the strongly coordinating ligands 4-(dimethylamino)pyridine (20 equivalents) and 1,10-phenanthroline (1.0 equivalent; this ligand has been implicated as a stabilizer in Moiseev's giant Pd clusters[27] and has recently been found by our group to be an effective nanocluster poison[28]). Even the common heterogeneous catalyst poison octanethiol failed to produce an induction period (0.5 equivalent; this ligand has also been shown to poison/stabilize Pd nanoclusters[29]). The effect of all three added ligands was the same: they each slowed the hydrogenation of cyclohexene but did not

introduce an induction period into the reduction; the general shape of the curve in Figure 3.9 was retained, Figure 3S.7 of the Supporting Information.

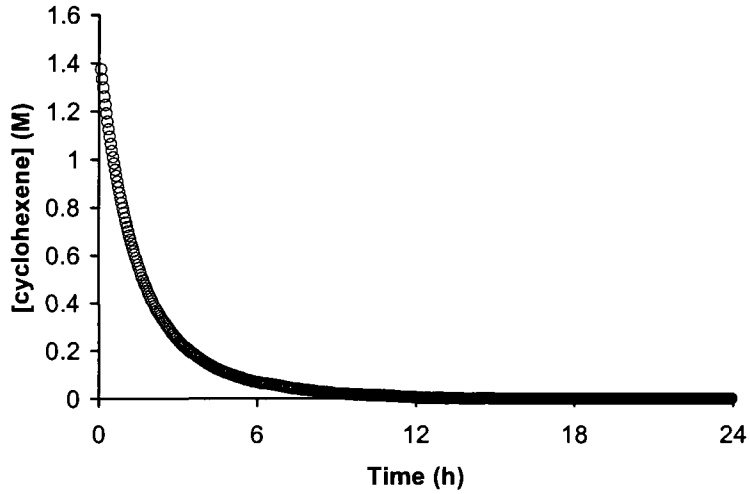

Figure 3.9. Kinetic curve for the reduction of 1.2 mM Pd(1,5-COD)Cl_2, and concomitant cyclohexene hydrogenation, in the presence of 2 equivalents of Proton Sponge in acetone at room temperature.

Because it is important to find conditions where a slower, more kinetically controlled nucleation and growth of Pd_n^0 occurs, other ligands were examined. The addition of 20 equivalents of 1,5-COD did provide an induction period of ~0.6 h to the reduction, Figure 3.10. Visual inspection reveals the sharp "turn-on" and lack of inflection point in this short portion of the curve; these qualities indicate that the reduction follows the four-step mechanism as did a fit to the four-step mechanism, Figure 3.10. Note that the nucleation rate is still relatively large, $k_1 \approx 0.3\ h^{-1}$.

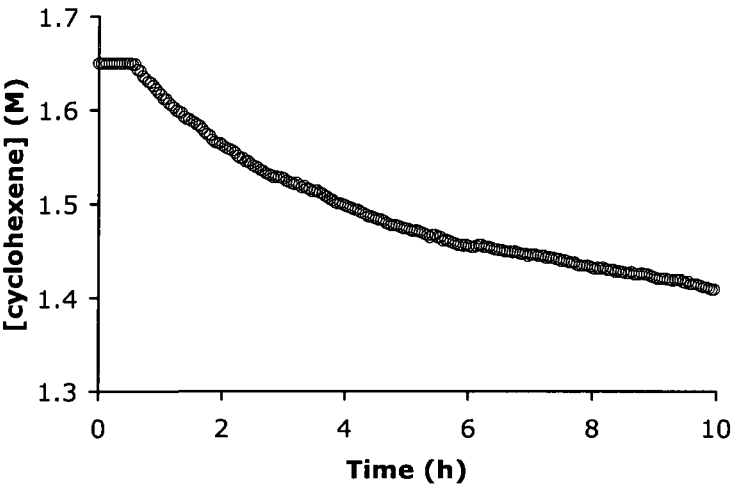

Figure 3.10. Kinetic curve for the reduction of Pd(1,5-COD)Cl_2 in the presence of 20 equivalents of 1,5-COD in acetone. The fit to the first 10 h is to the four-step mechanism: $k_1 \approx 0.3\ h^{-1}$; $k_2 \approx 8.1 \times 10^3\ M^{-1}\ h^{-1}$; $k_3 \approx 11\ M^{-1}\ h^{-1}$; $k_4 \approx 0.75\ M^{-1}\ h^{-1}$; the residual is 0.094.

The addition of 20 equivalents of 1,5-COD did not yield more stable nanoclusters, however. At the end of the induction period, the solution changed from clear and yellow to gray and then to clear and colorless with bulk metal present almost instantaneously. The change occurred so quickly that there was insufficient time to harvest a sample of the gray solution for TEM analysis.

Putting all of the observations up to this point together, some conclusions about the generality of the double autocatalytic mechanism are apparent. First, the four-step, double-autocatalytic mechanism appears general to the metals studied herein, Pt, Ru, Ir, Rh, and Pd, at least under the conditions examined. Second, sufficient amounts of a strongly coordinating ligand are crucial to "turning on" the four-step mechanism. Third, the nature of the metal is significant; for example, second row metals with weaker metal–ligand bonds require more basic ligands to enforce the four-step mechanism. Fourth, 2 equivalents of chloride ion is a sufficient

amount of coordinating ligand to turn on the four-step mechanism in all of the metals studied other than Pd, while 1 equivalent is not.

The behavior of ligands other than chloride is more complex, as seen in the experiments reducing Ir^I and Rh^I in the presence of pyridine. Pyridine binds tightly enough to Ir to poison it when present in 5 equivalents, but not even 50 equivalents of pyridine can ligate/poison Rh to the point that the four-step mechanism is needed to fit the data—the two-step mechanism is sufficient even when 50 equivalents of pyridine is present. However, the more basic 4-(dimethylamino)pyridine ligand does induce the four-step mechanism for Rh, although 10 equivalents of this more coordinating ligand are required. The effect of the ligands on the nucleation rate is relevant to these observations as are nanocluster size effects on the inherent metal–ligand bond energies; see the Supporting Information and data in Figure 3S.8.

In the case of $Pd(1,5\text{-COD})Cl_2$, the reduction takes place immediately upon exposure to H_2. Addition of excess 1,5-COD gives the reduction an observable induction period and shows that the four-step mechanism is operative in this case. A 1,5-COD dissociation equilibrium is implied, eq 3.4, but has not been unequivocally demonstrated. Note again that the four-step mechanism is followed.

$$Pd(1,5\text{-COD})Cl_2 + 2solvent \rightleftharpoons PdCl_2(solvent)_2 + 1,5\text{-COD} \quad (3.4a)$$

$$PdCl_2(solvent)_2 + H_2 \longrightarrow Pd^0 + 2H^+Cl^- \quad (3.4b)$$

In light of the finding that with excess 1,5-COD the Pd complex is reduced under the four-step mechanism, the original data obtained in the absence of excess 1,5-COD was fit to the four-step mechanism to quantitate the kinetics of that fast reduction. The fit for $Pd(1.5\text{-COD})Cl_2$, shown in the Supporting Information, Figure

3S.9, gives a k_1 value of 20, a factor of ~10^8 greater (with a $10^{\pm4}$ error[1,2]) than the k_1 value for the reduction of Pt(1,5-COD)Cl_2. It should be noted that while these values could conceivably be the same within the large, $10^{\pm4}$ experimental error for each k_1, visual inspection of the curves in Figure 3.3 (for the reduction of Pt(1,5-COD)Cl_2) and Figure 3.9 (for the reduction of Pd(1,5-COD)Cl_2) strongly suggests that these rate constants are *not* the same and that k_1 for Pd^{2+} is significantly greater than k_1 for Pt^{2+}.

Indeed, the fast, kinetically *un*controlled reduction of Pd(1,5-COD)Cl_2 greatly counters the ≥0.4 h induction period for the reduction of Pt(1,5-COD)Cl_2. The reaction conditions—precursor, temperature, concentration, stirring rate—are the same for both complexes; the only difference is the metal (Pd^{2+} versus Pt^{2+}). The *aqueous* solution reduction potentials of Pd^{2+} and Pt^{2+} are similar: 0.99 V for Pd^{2+} and ca. 1.2 V for Pt^{2+}.[30] Hence, the difference in Pd^{2+} and Pt^{2+} reductions would appear to be primarily kinetic as opposed to thermodynamic in origin. Marcus theory considerations imply to us that a larger Pt versus Pd intrinsic barrier (reflecting larger Pt-ligand versus Pd-ligand BDEs) is very likely involved. Overall, the bottom line here is that nucleation is, again, a key.

It is worth noting in this regard that the nucleation steps for nanocluster formation are not well understood, even for the best studied polyoxoanion-stabilized $Ir^0_{\sim300}$ nanocluster system.[8a] For example, metal hydrides[31] may be more important than the (controversial[32]) idea of metal^0 atoms as intermediates. The data above imply that the nucleation steps may be different when different conditions are used (e.g., when the metal or ligands are changed). Deeper investigation into nanocluster nucleation is needed and is in progress.[33]

Dependence on other variables for the prototype Pt(1,5-COD)Cl_2 and [Ir(1,5-COD)Cl]$_2$ reductions

Previously, we found that by changing reaction conditions (namely precursor concentration, reaction temperature, and solvent), we were able to tune the system to prepare either Pt_n^0 nanoclusters or bulk metal.[1,2] Two questions arise from this result: (i) Do these changes in reaction conditions induce mechanistic changes, that is, will variations in these conditions change the number of steps necessary to fit the data? (ii) What reaction conditions have the greatest influence over the product of the reaction (nanoclusters versus bulk metal)? To probe these questions, the reductions of Pt(1,5-COD)Cl_2 and [(Ir(1,5-COD)Cl]$_2$ were carried out several times while changing separately the reaction temperature, the initial metal concentration, the solvent, and the stirring rate, to determine what effect, if any, these variables have on the reduction of the metals.

Temperature effects

The effect of temperature on the reduction mechanism of Pt(1,5-COD)Cl_2 and [Ir(1,5-COD)Cl]$_2$ was studied using a reaction temperature range of 22–80 °C and an initial metal concentration of 1.2 mM (i.e., the Standard Conditions concentration). Because of the relatively low boiling point of acetone (56 °C), the higher boiling solvent propylene carbonate (bp 242 °C) was used for these studies. Control experiments verified that the change of solvent from acetone to propylene carbonate did not affect the number of steps in the mechanism needed to fit the data, Supporting Information, Figures 3S.10 and 3S.11, showing that the same mechanism results when either acetone or propylene carbonate is used as the solvent. The results, listed in Table 3.2 for Pt^{II} reduction and Table 3.3 for Ir^{I} reduction, show that in the wide

range of temperatures studied the temperature at which the reduction takes place has no effect on the number of steps in the mechanism—reduction of $Pt(1,5\text{-}COD)Cl_2$ requires all four steps to fit the kinetic curves, while reduction of $[Ir(1,5\text{-}COD)Cl]_2$ requires only the two-step mechanism. Although it is tempting to draw correlations between the calculated rate constants and the temperatures, the high experimental error that is inherent in the calculated rate constants for the four-step mechanism,[2] Table 3.2, makes such a comparison tenuous at best—the rate constants are well within the experimental errors of $\sim 10^{\pm 4}$ for k_1 and ≥5–7-fold for k_2-k_4.[2]

Table 3.2. Variation with temperature of the calculated rate constants (observed via MacKinetics) for the reduction of $Pt(1,5\text{-}COD)Cl_2$ via the 4-step mechanism of Scheme 3.1

Temperature (°C)	k_1 (h^{-1})	k_2 ($\times 10^3$ $M^{-1}h^{-1}$)	k_3 ($\times 10^3$ $M^{-1}h^{-1}$)	k_4 ($\times 10^3$ $M^{-1}h^{-1}$)
22.0	$\sim 10^{-5}$	2.7	0.040	0.32
30.0	$\sim 10^{-8}$	5.2	0.094	0.61
40.0	$\sim 10^{-6}$	8.1	0.32	2.1
50.0	$\sim 10^{-8}$	11	0.74	1.5
60.0	$\sim 10^{-11}$	16	1.4	3.2
70.0	$\sim 10^{-8}$	19	1.5	4.1
80.0	$\sim 10^{-7}$	28	2.0	4.1

Table 3.3. Variation with temperature of the calculated rate constants (using Microcal Origin) in the 2-step mechanism of Scheme 3.2 for the reduction of $[Ir(1,5\text{-COD})Cl]_2$

Temperature (°C)	k_1 (h^{-1})	k_2 ($\times 10^3$ $M^{-1}h^{-1}$)
22.0	0.38(2)	5.8(2)
30.0	0.30(4)	5.8(5)
40.0	0.57(2)	3.0(1)
50.0	1.25(7)	9.0(5)
60.0	0.49(6)	10.7(7)
70.0	1.4(1)	4.3(6)
80.0	4.1(2)	12.8(8)

The rate constants in Table 3.3 for the two-step reduction of Ir^I, however, are more reliable, and therefore, Eyring plots can be constructed for the nucleation and growth steps. The plots, Supporting Information, Figure 3S.12 give rare activation parameters for nucleation and growth, respectively, $\Delta H^{\ddagger}_1$ = 15(1) kcal/mol and $\Delta S^{\ddagger}_1$ = -14(1) eu, and $\Delta H^{\ddagger}_2$ = 10(2) kcal/mol and $\Delta S^{\ddagger}_2$ = -11(4) eu for $[Ir(1,5\text{-COD})Cl]_2$. The activation parameters are similar to those found for the formation of $Ir^0_{\sim 300}$ nanoclusters from $(Bu_4N)_5Na_3[(1,5\text{-COD})Ir{\cdot}P_2W_{15}Nb_3O_{62}]$,[8a] $\Delta H^{\ddagger}_1$ = 15(1) kcal/mol and $\Delta S^{\ddagger}_1$ = -36(3) eu; $\Delta H^{\ddagger}_2$ = 14(2) kcal/mol and $\Delta S^{\ddagger}_2$ = -13(6) eu. Significantly, $\Delta H_{nucleation}$ is *not* much greater than ΔH_{growth}, as previous literature has implied.[34] Note also that the negative entropy of the nucleation step, k_1, is evidence for its true higher-order $n\text{A} \rightarrow \text{A}_n$ (= B_n) nature at least for Ir and as detailed elsewhere.[35]

Concentration effects

These studies were carried out at 60 °C at concentrations of 0.3, 0.6, 0.9, 1.2, 2.4, and 12.0 mM $Pt^{II}(1,5\text{-COD})Cl_2$ and $[Ir^I(1,5\text{-COD})Cl]_2$ with no added ligands. As

can be seen from the data, Table 3.4 for Pt and Table 3.5 for Ir, the mechanism does not change over the range of concentrations studied. The reduction of Pt^{II} follows the four-step mechanism over the range of 0.3–12.0 mM, and the reduction of Ir^{I} follows the two-step mechanism over the same concentration range. The greater error[1,2] in determining the four rate constants for the four-step mechanism, versus the better determined two-step rate constants, is one point obvious from comparing the data in Tables 3.4 and 3.5. The interesting concentration dependence of the k_1 and k_2 rate "constants" in Table 3.5 is at least partially understood but requires a more detailed treatment than is possible here. Hence, the required analysis and discussion will be provided elsewhere.[35]

Table 3.4. Variation of the mechanism and rate constants versus initial concentration of Pt^{II} in the reduction of Pt(1,5-COD)Cl_2

$[Pt^{II}]$ (mM)	k_1 (h^{-1})	k_2 ($\times 10^3$ $M^{-1}h^{-1}$)[a]	k_3 ($\times 10^3$ $M^{-1}h^{-1}$)[a]	k_4 ($\times 10^3$ $M^{-1}h^{-1}$)[a]
0.3	$\sim 10^{-4}$	24	0.80	0.59
0.6	~0.2	13	5.0	32
0.9	$\sim 10^{-5}$	52	0.76	0.52
1.2	$\sim 10^{-7}$	45	1.1	9.6
2.4	$\sim 10^{-6}$	33	0.40	2.0
12.0	$\sim 10^{-2}$	1.4	0.46	0.15

a The values of k_2, k_3, and k_4 were each corrected by multiplying the observed rate constant by [cyclohexene]/[Ir], as described in a previous report.[8a]

Table 3.5. Variation of the mechanism and observed rate constants versus initial Ir^I concentration for the reduction of $[Ir(1,5\text{-COD})Cl]_2$

$[Ir^I]$ (mM)	k_1 (h^{-1})	k_2 ($\times 10^3$ $M^{-1}h^{-1}$)[a]
0.3	0.28(2)	11.0(6)
0.6	0.68(3)	6.5(4)
0.9	0.62(7)	9.3(8)
1.2	0.82(4)	5.1(2)
2.4	0.92(5)	4.7(2)
12.0	6.0(5)	1.1(2)

a The values of k_2 were each corrected by multiplying the observed rate constant by [cyclohexene]/[Ir], as described in a previous report.[8a]

Stirring effects

The effects of stirring on transition-metal nanocluster synthesis have been studied, specifically the need to avoid H_2 gas-to-solution mass-transfer limitations resulting from insufficient stirring which will otherwise ruin nanocluster syntheses if present.[36] Therefore, in examining the effects of stirring on the mechanism, care must be taken to maintain catalyst-dependent (i.e., chemical reaction rate-limiting) kinetics so that the kinetics of nanocluster formation are what is being measured, not the mass transfer of gaseous H_2 into solution.

The rate of stirring used throughout this study was ~640 rpm. Reduction of $(1,5\text{-COD})PtCl_2$ was carried out using a higher stirring rate, ~1500 rpm, to determine whether this faster rate would have an effect on the mechanism. Not only did the faster stirring rate *not* affect the mechanism, but the calculated rate constants themselves remained unchanged within experimental error, Table 3.6: the rate constants k_2-k_4 are nearly identical, and the k_1 values are within the known,[1,2] $10^{\pm4}$ experimental error of k_1.

Table 3.6. Control experiments probing any variation of the rate constants in the mechanism of Scheme 3.1 with stirring rate for the reduction of Pt(1,5-COD)Cl_2

Stirring rate (rpm)	k_1 (h^{-1})	k_2 (× 10^3 $M^{-1}h^{-1}$)	k_3 (× 10^3 $M^{-1}h^{-1}$)	k_4 (× 10^3 $M^{-1}h^{-1}$)
640	~10^{-11}	16	1.4	3.2
1500	~10^{-6}	16	1.4	4.1

The same result was seen for the reduction of [Ir(1,5-COD)Cl]$_2$—the reduction follows the two-step mechanism at both of the stirring rates studied. The calculated rate constants k_1 and k_2 at both stirring rates are also the same within experimental error, Table 3.7. We note that these stirring rate controls are not trivial—both as done herein and for literature systems where they remain to be done—due to the documented large effects of mass-transfer limitations on nanocluster syntheses and other reactions with autocatalytic steps.[15b]

Table 3.7. Control experiments probing any variation of the rate constants in the mechanism of Scheme 3.2 with stirring rate for the reduction of [Ir(1,5-COD)Cl]$_2$

Stirring rate (rpm)	k_1 (h^{-1})	k_2 (× 10^3 $M^{-1}h^{-1}$)
640	0.42(8)	3.6(1)
1500	0.52(4)	4.1(6)

Effects of changing precursor concentrations and reaction temperatures on the product of the reductions (nanoclusters versus bulk metal)

At this point we have shown that the reduction of Pt(1,5-COD)Cl_2 follows the four-step, double-autocatalytic mechanism over the concentration range of 0.3–12.0 mM (at a constant reaction temperature of 60.0 °C) and over the temperature range of 22.0–80.0 °C (using a constant Pt concentration of 0.6 mM). In previous reports[1,2] we showed that reduction of a 1.2 mM Pt(1,5-COD)Cl_2 solution in acetone at 22.0 °C

gave only bulk Pt^0 metal, while reduction of a 0.6 mM solution in propylene carbonate at 60.0 °C gave Pt_n^0 nanoclusters with no bulk metal present; both reductions followed the four-step mechanism. The question arises, then, of what factors (concentration, temperature, solvent) are significant in determining whether the major product is nanoclusters or bulk metal.

To answer this question, we considered to the products of the reductions under each set of conditions given in Tables 3.2-3.5. At every temperature studied using a 1.2 mM solution of $Pt(1,5\text{-}COD)Cl_2$ in propylene carbonate, bulk Pt^0 metal was the only observed product. This suggests that the reaction temperature has little or no effect on the reaction product (nanoclusters versus bulk metal) at a given metal concentration. The results of changing the concentration while keeping the temperature constant at 60 °C, however, are more complex. At concentrations of 0.3 and 0.6 mM in propylene carbonate, nanoclusters were the only observable product (i.e., no bulk metal was observed). At 0.9 and 1.2 mM, some bulk metal was observed in light gray solutions, indicating the presence of both nanoclusters and bulk metal in the reaction solution. At 2.4 mM, bulk metal was the only observed product. These results confirm that at a given temperature (e.g., 60 °C in the present case) the precursor concentration is one important variable in determining whether the final, observed product includes, or primarily is, bulk metal.

To further test the importance of the solvent (acetone versus propylene carbonate) on the observed products, a 0.6 mM solution of $[Ir(1,5\text{-}COD)Cl]_2$ (containing 1.2 mM Ir) was reduced at 30 °C separately in acetone and in propylene carbonate. The reduction followed the two-step mechanism in both solvents; however, in acetone, bulk Ir^0 metal was the only observed product, while in propylene

carbonate, a clear brown Ir_n^0 nanocluster solution resulted with *no* black precipitate (no Ir^0 bulk metal present). Additionally, the reduction of $[Ir(1,5\text{-COD})Cl]_2$ in the presence of 5 equivalents of pyridine was repeated in propylene carbonate. In acetone, a clear colorless solution with black precipitate resulted after cyclohexene hydrogenation was complete (see the kinetic curve in Figure 3.6). In propylene carbonate, however, a clear black solution was present along with some black precipitate. This black solution persisted for several hours after the reduction was complete, and TEM showed the presence of 5 ± 2 nm nanoclusters. We conclude, therefore, that the solvent (and in particular propylene carbonate) has a major influence on whether a nanocluster or bulk metal product is the final product of a reduction—presumably by effectively stabilizing and thus slowing the rate of agglomeration, even when the mechanism of agglomeration remains as the four-step mechanism. The effects can be subtle, and, again, nucleation is probably important since the solvent can also be a ligand. In addition, DLVO theory predicts that solvents with higher dielectric constants will be more stabilizing.[37] Finally, our previous, tentative conclusion that increasing temperature and decreasing concentration favors nanocluster formation[1,2] must be modified, therefore, to emphasize the role of the higher dielectric constant and, therefore, more stabilizing, solvents as the greater influence in favoring nanocluster preparations.

What is the nature of B versus C?

A second question that arises is: if a reduction that gives no bulk metal but large $Pt^0_{\sim 2200}$ nanoclusters[1,2] follows the four-step mechanism, then what is the nature of C? That is, is C larger bulk-like (but still soluble) metal particles? If so, at what point does B (nanoclusters) become C (larger, apparently more bulk-metal-like

particles)? To gain some insight into this question, we note that even when no visible bulk metal is present in the reduction of $Pt(1,5\text{-}COD)Cl_2$ (i.e., when a clear brown solution with no black precipitate is the product of the reaction), the four-step mechanism, with C as the active hydrogenation catalyst, is necessary to fit the kinetic data. Therefore, C must include larger, closer to bulk-metal-like, but still soluble Pt_n^0 particles. The Pt_n^0 nanoclusters formed using the modified conditions of 0.6 mM and 60 °C in propylene carbonate without added ligand are 7 ± 3 nm by TEM, Supporting Information, Figure 3S.13; this is consistent with the four-step mechanism's prediction of larger particles being formed as the final product. However, the point at which nanoclusters (B) change to C (i.e., how large B must get before they become C) remains an open question that will require further study. EXAFS, XANES, and SAXS experiments are in progress.[3]

Comment on the observation of two-step kinetics yet bulk metal as the observed product

Another important observation and associated question not yet addressed is "how can bulk metal be the (final) product when the two-step mechanism fits the kinetic data?" The primary answer here is apparent if one looks at the times at which bulk metal forms when two-step versus four-step mechanism fits to the kinetic data are seen, Table 3.1. When the two-step mechanism is followed, bulk metal is observed *after* the cyclohexene hydrogenation is complete. That is, meta-stabilized nanoclusters, B, are formed and are the main species present while the cyclohexene hydrogenation reporter reaction is operative. Agglomeration still occurs, undoubtedly via the k_3 and k_4 pathways, but after the kinetics are completed; hence, the k_3 and k_4 steps are not detected.

On the other hand, when the four-step mechanism is followed, bulk metal is observed to form at the end of the induction period (*vide supra*). Thus, the cyclohexene hydrogenation reaction reports both the formation of the nanoclusters, B, and their agglomeration to C. Overall, it is again apparent, however, that spectroscopic studies directly monitoring B, C, and bulk metal versus time would be valuable studies that need to be undertaken.[3]

Effect of the four-step mechanism on nanocluster size and size distribution and the relationship between the k_3 and k_4 steps and "Ostwald ripening"

When nanoclusters are formed via the four-step mechanism, the final sizes are larger and of broader dispersity than those seen for formed via the two-step mechanism. For example, the average size of the polyoxoanion-stabilized $Ir^0_{\sim 300}$ nanoclusters formed by the two-step mechanism is 22 ± 3 Å,[8] corresponding to ±≤15% (so-called "near-monodisperse" clusters[38]), while Ir^0_n nanoclusters formed from $[Ir(1,5\text{-COD})Cl]_2$ in the presence of pyridine and by the four-step mechanism average 5 ± 2 nm, or a polydisperse ± 40%. Other factors may be at play in the size and size distributions of the nanoclusters, including ligands or solvent, but on the basis of these results, the four-step mechanism provides a mechanism-based rationale for the "size refocusing" of nanoclusters that is mentioned in the literature,[39] in which agglomeration of clusters causes a widening ("defocusing") of the size distribution. Historically, size refocusing has generally been attributed to Ostwald ripening, in which larger particles grow at the expense of smaller particles. The difference between the mechanism presented herein and Ostwald ripening is that in the present mechanism no particle dissolution is assumed to take place; rather, two nanoclusters (B) agglomerate to form a larger cluster (C). Overall, it seems likely that our k_3 and k_4

steps are an intimate part of what has been loosely called "Ostwald ripening" in the literature.

Exclusion of three additional alternative mechanisms

Previously, 15 alternative mechanisms were experimentally excluded on the basis of alternative fits of the data for Pt(1,5-COD)Cl_2 reduction in the presence of Proton Sponge and Bu_3N.[2] We have tested three more alternative mechanisms: a mechanism that replaces the second step in Scheme 3.1 with A+B+B→3B; a mechanism that includes an equilibrium between A+B and a complexed [AB] species; and a mechanism that excludes the autocatalytic growth step A+B→2B from Scheme 3.1. None of these mechanisms fit the experimental data well. (The attempted fits are given in the Supporting Information, Figure 3S.14.) In short, we have been able to rule out a total of 18 other mechanisms en route to providing strong support for the four-step mechanism in Scheme 3.1.

Testing the alternative, A+C→1.5C double-autocatalytic mechanism

Previously, it was found that a different autocatalytic mechanism fit equally well the cyclohexene-loss curves for the reduction of Pt(1,5-COD)Cl_2 shown in Figure 3.1.[1,2] This second mechanism simply replaces the final B+C→1.5C step of the four-step mechanism, Scheme 3.1 with A+C→1.5C, Scheme 3.4 (i.e., this mechanism assumes that bulk metal, C, is the dominant catalyst for the reduction of the precursor, A, as well as for the hydrogenation of cyclohexene).[2]

Scheme 3.4

$$A \xrightarrow{k_1} B$$

$$A + B \xrightarrow{k_2} 2B$$

$$B + B \xrightarrow{k_3} C$$

$$A + C \xrightarrow{k_4} 1.5C$$

In order to distinguish the two mechanisms, the reaction was followed by GLC in our prior work[1,2] to gain more direct (albeit less precise) data by following the evolution of cyclooctane from reduction of the 1,5-COD in the $Pt(1,5\text{-COD})Cl_2$ precursor. The resultant rate constants calculated from the GLC data are within the range of those calculated from cyclohexene loss data when both data sets were fit by the four-step mechanism in Scheme 3.1, but *not* when both data sets were fit by the alternative mechanism with the conceivable A+C→1.5C step.[1,2] That is, the dominant mechanism for reduction of $Pt(1,5\text{-COD})Cl_2$ is that provided back in Scheme 3.1 with B+C→1.5C as the fourth, second autocatalytic step.

We also wondered whether Scheme 3.4, with its A+C→1.5C step, provides a better or worse fit to the data in Figure 3.5 for the reduction of $[Ir(1,5\text{-COD})Cl]_2$ with 5 equivalents of pyridine. The mechanism in Scheme 3.4 gave a fit that was visually as good as that for the mechanism in Scheme 3.1 with the B+C→1.5C step, Supporting Information, Figure 3S.15. Therefore, we performed the GLC study on this $[Ir(1,5\text{-COD})Cl]_2$ + 5 pyridine system as well—it is well-known that changing reaction conditions can (sometimes dramatically) change reaction mechanisms in transition-metal chemistry.[40] The rate constants derived from the cyclooctane data, Figure 3.11, fall within the range of those derived from the cyclohexene data when

both data sets were fit by the B+C→1.5C mechanism; this is not the case for the A+C→1.5C mechanism, Supporting Information, Figure 3S.16. Therefore, the dominant mechanism for the reduction of $[Ir(1,5\text{-COD})Cl]_2$ with 5 equivalents of pyridine is, again, the B+C→1.5C mechanism of Scheme 3.1. (As noted before,[2] we cannot exclude some contribution by the A+C→1.5C mechanism.)

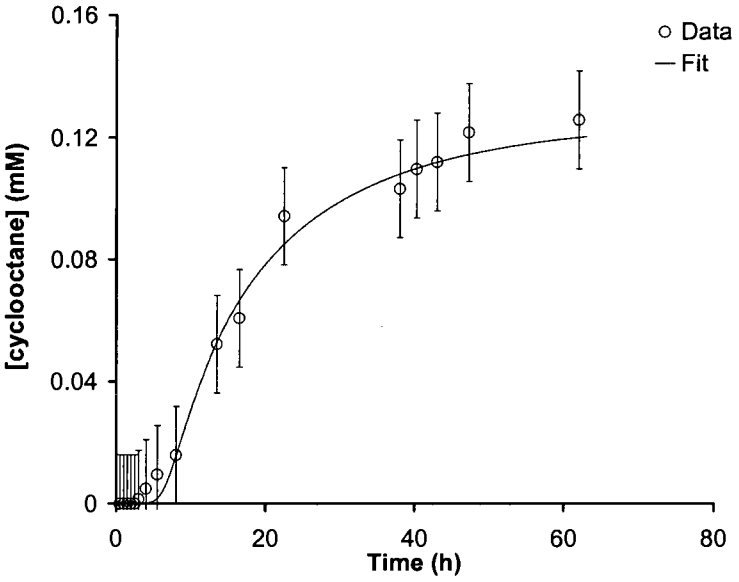

Figure 3.11. Direct measurement of cyclooctane evolution for the reduction of $[Ir(1,5\text{-COD})Cl]_2$ with 5 equivalents of pyridine. The data are well fit to the double-autocatalytic mechanism given in Scheme 3.1 with C as the catalyst and with B+C→1.5C as the fourth step of the mechanism. The calculated rated constants fall within the range of values obtained via the cyclohexene reporter reaction (see Figure 3.5), giving strong support to the hypothesis that the reduction indeed follows the four-step mechanism given in Scheme 3.1 (with B+C→1.5C and not A+C→1.5C, as the fourth step of the mechanism). $k_1 \approx 3 \times 10^{-3}$ h^{-1}; $k_2 \approx 830$ M^{-1} h^{-1}; $k_3 \approx 37$ M^{-1} h^{-1}; $k_4 \approx 69$ M^{-1} h^{-1}; residual = 0.024.

Three literature systems which follow the four- step mechanism: further evidence for the greater generality of the four-step mechanism

We have found three additional nanocluster preparations that follow the four-step, double-autocatalytic mechanism. The first was described previously[1]—it is the reduction of $H_2PtCl_6 \cdot 6H_2O$ in the presence of poly(vinlypyrrolidone) in methanol.

The step-function-like kinetics of that reduction were best fit by the four-step mechanism (although the formation of bulk Pt^0 metal in that system appears to compromise the fit somewhat).[41] Under different conditions, we have also seen a two-step mechanism for H_2PtCl_6 reduction.[41]

Looking back at our own literature revealed another example of the four-step mechanism. In 2002, a study in our laboratories ranked common anionic nanocluster stabilizers.[42] One of those stabilizers ranked was the citrate ion, $C_6H_5O_7^{3-}$. Reduction of the solvated iridium complex $[Ir(1,5\text{-}COD)(CH_3CN)_2]^+[BF_4]^-$ in the presence of 1 equivalent each of $[Bu_4N]_3[C_6H_5O_7]$ and Bu_4NOH gave a kinetic curve with a sudden "turn-on" and no inflection point, the two visual signs that the four-step mechanism is in operation (see Figure S8 of the Supporting Information in reference 42). Fitting the data originally in that figure demonstrates that the four-step mechanism fits the $Ir(1,5\text{-}COD)^+$/$citrate^{3-}$ system, Figure 3S.17 of the Supporting Information.

One more observation of the four-step mechanism comes from the work of Scheeren et al. using PtO_2 clusters to hydrogenate cyclohexene in ionic liquids.[43] The formation and catalysis of those clusters also follows the same four-step mechanism depending on reaction conditions as demonstrated by the fits provided elsewhere,[43] which employ the four-step mechanism.[1,2]

Conclusions

Herein we have shown the following:

• The four-step, double-autocatalytic mechanism discovered previously[1,2] for the reduction of the platinum salt $Pt(1,5\text{-}COD)Cl_2$ is more general to the reduction of the analogous salts of Ru^{II}, Ir^{I}, Rh^{I}, and Pd^{II} (and thus presumably other metals) in the presence of appropriate ligands and under the conditions examined.

• The features of the four-step mechanism are seen in three additional cases of transition-metal reduction from the literature, further evidence for the greater generality of the four-step mechanism.

• The main factors that decide what mechanism will be followed are the metal, the ligands that are present (in particular, the metal–ligand bond energy), and the amount of ligand.

• One main effect of added ligand appears to be the slowing of the k_1, nucleation step. This, in turn, leads to fewer, but larger, nanoclusters and thus more agglomeration. An underlying, controlling effect appears to be the change of M_n-ligand bond energy with nanocluster size (i.e., with changing n value): added ligands bond more tightly to small nanoclusters, decreasing k_1, while larger nanoclusters with weaker M_n-ligand bonds can still undergo agglomeration by either the k_3 and/or k_4 pathways.

• The number of steps in the mechanism seems to be unaffected by changes in metal concentration, temperature, stirring rate, and solvent, at least within the ranges studied.

• However, the solvent used does influence the final products of the reductions, higher dielectric solvents (such as propylene carbonate[37]) favoring the formation of nanoclusters over bulk metal.

• The activation parameters for nucleation and growth are rather similar to one another, as was found for polyoxoanion-stabilized Ir^0 nanoclusters, in contrast to implications of previous literature that nucleation should have a larger $\Delta H^{\ddagger}$.[34]

• Both the size and size distribution of the nanoclusters are larger when the four-step mechanism is followed, as the mechanism predicts.

• The alternative mechanism in which the metal product C catalyzes the reduction of precursor A is not a major contributor for the reduction of either Pt(1,5-COD)Cl_2 or $[Ir(1,5\text{-COD})Cl]_2$, the latter in the presence of pyridine.

• The true nature of products B and C need to be investigated in more detail by EXAFS, XANES, SAXS, and other appropriate methods in order to intimately characterize the products and to determine at what point B effectively becomes C.[3]

Overall, the present work demonstrates that the four-step mechanism should be considered any time a transition-metal salt is reduced to form nanoclusters and curves like those in Figures 3.1, 3.3, 3.5, 3.6, 3.7, 3.8, or 3.10 are seen. The present work also provides considerable additional insight into the four-step, double-autocatalytic mechanism. Since the four-step mechanism is, in the end analysis, the "Ockham's Razor" (i.e., minimalistic) mechanism of "just" nucleation (autocatalytic) growth, (bimolecular) agglomeration, and a second type of (autocatalytic) agglomeration, it seems likely that the four-step mechanism[1,2] may well prove to be much more general. Time will tell.

Acknowledgments

We thank Professors Irving R. Epstein at Brandeis University and James D. Martin at North Carolina State University for their suggested alternative mechanisms shown in Figure 3S.14 of the Supporting Information and Professor Thomas Meersman at CSU for his suggestion to use the *F* test in discerning data sets. Support from DOE Grant DE-FG02-03ER15453 is gratefully acknowledged.

Supporting Information Available:

Experimental procedure for the synthesis of the solvated metal complexes $[Ir(1,5\text{-COD})(CH_3CN)_2]^+[BF_4]^-$ and the previously unreported rhodium solvate

complex $[Rh(1,5\text{-}COD)(CH_3CH)_2]^+[BF_4]^-$; preparations of the solvated complexes $[Pt(1,5\text{-}COD)Cl(CH_3CN)]^+[BF_4]^-$ and $[Pd(1,5\text{-}COD)Cl(CH_3CN)]^+[BF_4]^-$; pressure oscillations in reductions carried out at 80 °C; two- and three-step mechanism fits to the data for the reduction of $Pt(1,5\text{-}COD)Cl_2$ in the absence of ligand; kinetic curve for the reduction of $[Ir(1,5\text{-}CODCl]_2$ in the presence of 1 equivalent of pyridine; kinetic curves for the reduction of $[Ir(1,5\text{-}COD(CH_3CN)_2]^+[BF_4]^-$ in the absence of ligand and in the presence of 1 equivalent of pyridine, 1 and 2 equivalents of Bu_4NCl; kinetic curves for the reduction of $[Rh(1,5\text{-}COD)(CH_3CN)_2]^+[BF_4]^-$ in the absence of ligand and in the presence of 80 equivalents of pyridine, 1 and 2 equivalents of Bu_4NCl, and 10 equivalents of 4-(dimethylamino)pyridine; reduction of $Pd(1,5\text{-}COD)Cl_2$ in the presence of 4-(dimethylamino)pyridine, 1,10-phenanthroline, and octanethiol; an alternate explanation for the difference between the reductions of $[Ir(1,5\text{-}COD)Cl]_2$ and $[Rh(1,5\text{-}COD)Cl]_2$ in the presence of pyridine, including TEM images of nanoclusters formed from the reductions of $[Ir(1,5\text{-}COD)Cl]_2$ and $[Rh(1,5\text{-}COD)Cl]_2$; four-step mechanism fit of the kinetic data for the reduction of $Pd(1,5\text{-}COD)Cl_2$ in the absence of ligand; control experiments showing that the change in solvent from acetone to propylene carbonate has no effect on the number of mechanistic steps; Eyring plots for the nucleation and growth of Pt and Ir nanoclusters; TEM of Pt_n^0 nanoclusters formed from the reduction of a 0.6 mM solution of $Pt(1,5\text{-}COD)Cl_2$ at 60.0 °C; attempted fits of three additional alternative mechanisms for the reduction of Pt(1,5-COD)Cl2; fitting the cyclooctane evolution data for the reduction of $[Ir(1,5\text{-}COD)Cl]_2$ with 5 equivalents of pyridine to the alternative A+C⟶1.5C mechanism (cyclohexene loss and cyclooctane evolution data); fit to the four-step mechanism of the reduction of [Ir(1,5-

COD)$(CH_3CN)_2]^+[BF_4]^-$ in the presence of 1 equivalent each of tetrabutylammonium hydroxide and tetrabutylammonium citrate; table comparing *F* values for the two- and four-step mechanisms for the reduction of Pt(1,5-COD)Cl_2, Ru(1,5-COD)Cl_2, and [Ir(1,5-COD)Cl]$_2$ in the presence of 1 equivalent of Bu_4NCl and 5 equivalents of pyridine, [Rh(1,5-COD)Cl]$_2$ in the presence of 1 equivalent of Bu_4NCl and 10 equivalents of 4-(dimethylamino)pyridine.

References

[1] Besson, C.; Finney, E. E.; Finke, R. G. *J. Am. Chem. Soc.* **2005**, *127*, 8179.

[2] Besson, C.; Finney, E. E.; Finke, R. G. *Chem. Mater.* **2005**, *17*, 4925.

[3] (a) Autrey, T.; Linehan, J. C.; Fulton, J. L.; Özkar, S.; Finke, R. G. Experiments in progress. (b) Menard, L.; Frenkel, A. I.; Nuzzo, Finney, E. E.; Graham, C.; Alley, W. M.; Finke, R. G. Experiments in progress.

[4] Izzo, B.; Harrell, C. L.; Klein, M. T. *AIChE J.* **1997**, *43*, 2048.

[5] Weissmüller, G.; Bisch, P. M. *Eur. Biophys. J.* **1993**, *22*, 63.

[6] (a) Epstein, I. R.; Pojman, J. A. *An Introduction to Nonlinear Chemical Dynamics. Oscillations, Waves, Patterns and Chaos*; Oxford University Press: Oxford, 1998; p 98. (b) Kondepudi, D. K.; Asakura, K. *Acc. Chem. Res.* **2001**, *34*, 946.

[7] Lin, Y.; Finke, R. G. *J. Am. Chem. Soc.* **1994**, *116*, 8335.

[8] (a) Watzky, M. A.; Finke, R. G. *J. Am. Chem. Soc.* **1997**, *119*, 10382. (b) Widegren, J. A.; Aiken, J. D., III; Özkar, S.; Finke, R. G. *Chem. Mater.* **2001**, *13*, 312. (c) Hornstein, B. J.; Finke, R. G. *Chem. Mater.* **2004**, *16*, 139 (see also the addition/correction published in *Chem. Mater.* **2004**, *16*, 3972).

[9] Özkar, S.; Finke, R. G. *Langmuir* **2002**, *18*, 7653.

[10] Leff, D. B.; Ohara, P. C.; Heath, J. R.; Gelbart, M. W. *J. Phys. Chem.* **1995**, *99*, 7036.

[11] Reboredo, F. A.; Galli, G. *J. Phys. Chem. B* **2006**, *110*, 7979.

[12] (a) Karmazyn, A. D.; Fiorin, V.; King, D. A. *J. Am. Chem. Soc.* **2004**, *126*, 14273. (b) Nørskov, J. K.; Bligaard, T.; Logadottir, A.; Bahn, S.; Hansen, L. B.; Bollinger, M.; Bengaard, H.; Hammer, B.; Sljivancanin, Z.; Mavrikakis, M.; Xu, Y.; Dahl, S.; Jacobsen, C. J. H. *J. Catal.* **2002**, *209*, 275.

[13] Schmid, G. *Chem. Re*V. **1992**, *92*, 1709.

[14] Parks, E. K.; Nieman, G. C.; Kerns, K. P.; Riley, S. J. *J. Chem. Phys.* **1998**, *108*, 3731.

[15] (a) Stirring effects are known from Epstein's seminal work[15b] to have a dramatic effect on the level of reproducibility of systems involving autocatalytic reactions, A+B→2B (i.e., where B is both a reactant and a product). The classic case in point is the chlorite-thiosulfate, ClO_2^-—$S_2O_3^{2-}$, "clock" reaction Epstein describes.[15b] He notes that: "Careful efforts to remove all the sources of variability among (repeat) experiments met with *total failure* (italics have been added). Despite elaborate

schemes to ensure that all experiments were the same with regard to temperature, initial concentrations, exposure to light, vessel surface, age of solutions and mixing procedure, the reaction times still varied over a wide range." (b) Epstein, I. R. *Nature (London)* **1995**, *374*, 321.

[16] Widegren, J. A.; Aiken, J. D., III; Ozkar, S.; Finke, R. G. *Chem. Mater.* **2001**, *13*, 312.

[17] Leipold, W. S., III. http://members.dca.net/leipold/mk/advert.html.

[18] Wendlandt, W. W.; Bear, J. L.; Horton, G. R. *J. Phys. Chem.* **1960**, *64*, 1289.

[19] Draper, N. R.; Smith, H. *Applied Regression Analysis*, 3rd ed.; Wiley: New York, 1998; Chapter 1.

[20] (a) Because of the difficult problem[20b] of searching a 5-dimensional space for five adjustable parameters (the four rate constants, k_1-k_4, plus the residual) for their global minimum, it is important to realize that the resultant k_2-k_4 rate constants are known only to within a factor of ca. 5–7-fold, while the k_1 is in what surface-mapping[2] shows is a very flat potential surface so that it is known to no better than ca. $10^{\pm 4}$ in some cases—even for the present state-of-the-art system[2] that may prove hard to better with its large amount of high precision ($\pm \leq 0.01$ psig of H_2 pressure; ($\pm \leq 0.025\%$ out of 40 psig of H_2) data (typically 500–1500 data points and, hence, 100–300 data points per parameter).[2] (b) The following book on numerical analysis methods notes on p 387, in their chapter on minimization or maximization of functions, the fact that "Finding a global extremum is, in general, a very difficult problem": Press, W. H.; Teukolosky, S. A.; Vetterling, W. T.; Flannery, B. P. *Numerical Recipes in Fortran: The Art of Scientific Computing*, 2nd ed.; Cambridge University Press: New York, 1992.

[21] Hoffmann, R.; Minkin, V. I.; Carpenter, B. K. *Int. J. Philos. Chem.* **1997**, *3*, 3.

[22] Evans, D. F.; Wennerström, H. *The Colloidal Domain*, 2nd ed.; Wiley-VCH: New York, 1999.

[23] Widegren, J. A.; Weiner, H.; Miller, S. M.; Finke, R. G. *J. Organomet. Chem.* **2000**, *610*, 112.

[24] Özkar, S.; Finke, R. G. *J. Am. Chem. Soc.* **2005**, *127*, 4800.

[25] Ott, L. S.; Finke, R. G. *Chem. Mater.* **2008**, *20*, 2592.

[26] The second- and third-row metals are well known to have properties that are similar to each other and different from the first-row metals; this is a consequence of the lanthanide contraction. See for example: Miessler, G. L.; Tarr, D. A. *Inorganic Chemistry*; 3rd ed.; Prentice Hall: Upper Saddle River, NJ, 2004, Chapter 2.

[27] (a) Vargaftik, M. N.; Kozitsyna, N. Y.; Cherkashina, N. V.; Rudyi, R. I.; Kochubei, D. I.; Novgorodov, B. N.; Moiseev, I. I. *Kinet. Catal.* **1998**, *39*, 806. (b) Starchevsky,

M. K.; Hladiy, S. L.; Pazdersky, Y. A.; Vargaftik, M. N.; Moiseev, I. I. *J. Mol. Catal. A: Chem.* **1999**, *146*, 229.

[28] Hagen, C. M.; Vieille-Petit, L.; Laurenczy, G.; Süss-Fink, G.; Finke, R. G. *Organometallics* **2005**, *24*, 1819.

[29] (a) Brust, M.; Walker, M.; Bethell, D.; Schiffrin, D. J.; Whyman, R. *J. Chem. Soc., Chem. Commun.* **1994**, 801. (b) Zelakiewicz, B. S.; Lica, G. C.; Deacon, M. L.; Tong, Y. *J. Am. Chem. Soc.* **2004**, *126*, 10053.

[30] Huheey, J. E. *Inorganic Chemistry*, 3rd ed.; Harper & Row: New York, 1983; p A-51.

[31] Widegren, J. A.; Aiken, J. D., III; Özkar, S.; Finke, R. G. *Chem. Mater.* **2001**, *13*, 312.

[32] (a) Henglein, A.; Giersig, M. *J. Phys Chem. B* **2000**, *104*, 6767. (b) See footnote 4e of ref 31.

[33] Finney, E. E.; Ott, L. S.; Watzky, M. A.; Finke, R. G. "Transition-metal Nanocluster Formation Kinetic and Mechanistic Studies en Route to Size Control." Manuscript in preparation.

[34] (a) Turkevich, J.; Stevenson, P. C.; Hillier, J. *Faraday Discuss. Chem. Soc.* **1951**, *11*, 55. (b) Bullen, C. R.; Mulvaney, P. *Nano Lett.* **2004**, *4*, 2303.

[35] Note that, during the induction period so that [A] is effectively constant for $n\mathrm{A} \rightarrow \mathrm{A}_n$, rate constant k_1', where $1/nk_1'[\mathrm{A}]_n = k_1$ (for $\mathrm{A} \rightarrow \mathrm{B}$, rate constant k_1). That is, to a good first approximation, we can still use the A f B mechanism in the curve fits and even if the underlying mechanism is the higher-order $n\mathrm{A} \rightarrow \mathrm{A}_n$ ($=\mathrm{B}_n$), at least for Ir. See ref 33.

[36] Aiken, J. D., III; Finke, R. G. *J. Am. Chem. Soc.* **1998**, *120*, 9545.

[37] Ott, L. S.; Finke, R. G. *Coord. Chem. Rev.* **2007**, *251*, 1075.

[38] Finke, R. G. In *Metal Nanoparticles: Synthesis, Characterization and Applications*; Feldheim, D. L.; Foss, C. A., Jr., Eds.; Marcel Dekker: New York, 2002; Chapter 2.

[39] (a) Peng, X.; Wickham, J.; Alivisatos, A. P. *J. Am. Chem. Soc.* **1998**, *120*, 5343. (b) Rogach, A. L.; Talapin, D. V.; Shevchenko, E. V.; Kornowski, A.; Haase, M.; Weller, H. *Adv. Funct. Mater.* **2002**, *12*, 653.

[40] See for example: Nappa, M. J.; Santi, R.; Halpern, J. *Organometallics* **1985**, *4*, 34. In this case, reactions of $\mathrm{RMn(CO)_4L}$ with $\mathrm{HMo(CO)_4L}$ proceed by different mechanisms depending on the solvent, concentration of CO, and identity of L. The present work also makes this point, but now in transition-metal nanocluster

chemistry, showing that addition of ligands changes the nanocluster formation and agglomeration mechanisms.

[41] Mondloch, J.; Finney, E. E.; Yan, X.; Finke, R. G. Manuscript in preparation.

[42] Özkar, S.; Finke, R. G. *J. Am. Chem. Soc.* **2002**, *124*, 5796.

[43] Scheeren, C. W.; Domingos, J. B.; Machado, G.; Dupont, J. *J. Phys. Chem. B* **2006**, *110*, 13011.

Supporting Information

Synthesis of the solvated metal complexes [Ir(1,5-COD)(CH_3CN)$_2$][BF_4] and [Rh(1,5-COD)(CH_3CN)$_2$][BF_4]

The crystalline [Ir(1,5-COD)(CH_3CN)$_2$][BF_4] solvate was prepared by a method analogous to that in the literature for the corresponding PF_6 salt,[1] and its purity was checked by ^{1}H NMR. The previously unreported, crystalline Rh solvate, [Rh(1,5-COD)(CH_3CN)$_2$][BF_4], was prepared in the same way[1] in 62.4 % yield (0.19 g). Anal. Calcd for $C_{12}H_{18}N_2BF_4Rh$: C, 37.93; H, 4.77; N, 7.37. Found: C, 37.93; H, 4.98; N, 7.46. ^{1}H NMR (300 MHz, CD_2Cl_2, 22 °C): δ 4.5 (s, 4H, =CH), 2.5 (M, 4H, *endo*-CH), 2.3 (s, 6H, CH_3), 1.9 (m, 4H, *exo*-CH).

Preparation of the solvated complex [Pt(1,5-COD)Cl(CH_3CN)][BF_4]

In the drybox, 30.6 mg Pt(1,5-COD)Cl_2 (81.8 μmol) was dissolved in 6 mL CH_3CN to make a clear, colorless solution. This solution was added to a vial containing 16.0 mg $AgBF_4$ (82.2 μmol, 1.005 equivalents versus Pt(1,5-COD)Cl_2). A white precipitate immediately formed (AgCl, 11.6 mg, 99.0%). The vial was capped and Parafilmed, and was brought out of the drybox. The vial was centrifuged for 20 min at ~1600 rpm to settle the white precipitate to the bottom of the vial. The vial was then returned to the drybox and the clear colorless liquid was decanted into a new vial. The solvent was removed under vacuum and the pale yellow solid was dried under vacuum overnight. Yield 0.023 g, 60.2 %. ^{1}H NMR (300 MHz, CD_2Cl_2, 22 °C): 5.8 (t, 4H, =C-H), 2.7 (m, 4H, C-H), 2.4 (m, 4H, C-H), 2.0 (s, 3H, CH_3CN).

Preparation of the solvated complex [Pd(1,5-COD)Cl(CH_3CN)][BF_4]

The Pd complex was prepared using the same procedure given above, using 23.6 mg Pd(1,5-COD)Cl_2 (82.7 μmol) and 16.1 mg $AgBF_4$ (82.7 μmol, 1.000 equivalents versus Pd(1,5-COD)Cl_2). Yield 0.019 g, 61.9 %. ^{1}H NMR (300 MHz, CD_2Cl_2, 22 °C): 6.5 (s, 4H, =C-H), 3.0 (m, 4H, C-H), 2.6 (m, 4H, C-H), 2.2 (s, 3H, CH_3CN). AgCl formed: 11.8 mg, 100%.

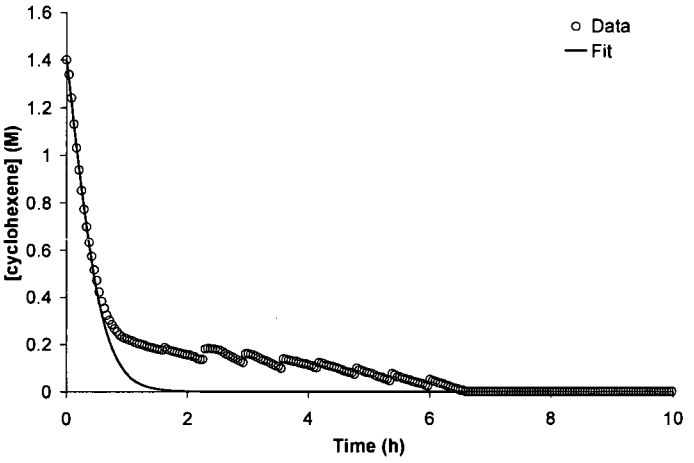

Figure 3S.1. Kinetic data for the reduction of [Ir(1,5-COD)Cl]$_2$ with one equivalent of Proton Sponge in propylene carbonate at 80.0 °C. The oscillations in pressure begin just after 2 h and are likely due to the "distillation" (boiling and recondensing) of cyclohexane (b.p. = 80.7 °C) at the 80.0 °C temperature of the experiment and in our apparatus.[2] The fit to the data is good for the first half of the data, suggesting that the pressure oscillations do not affect the kinetic data that results from fitting the first half of the data (i.e., until half of the cyclohexene has been lost).

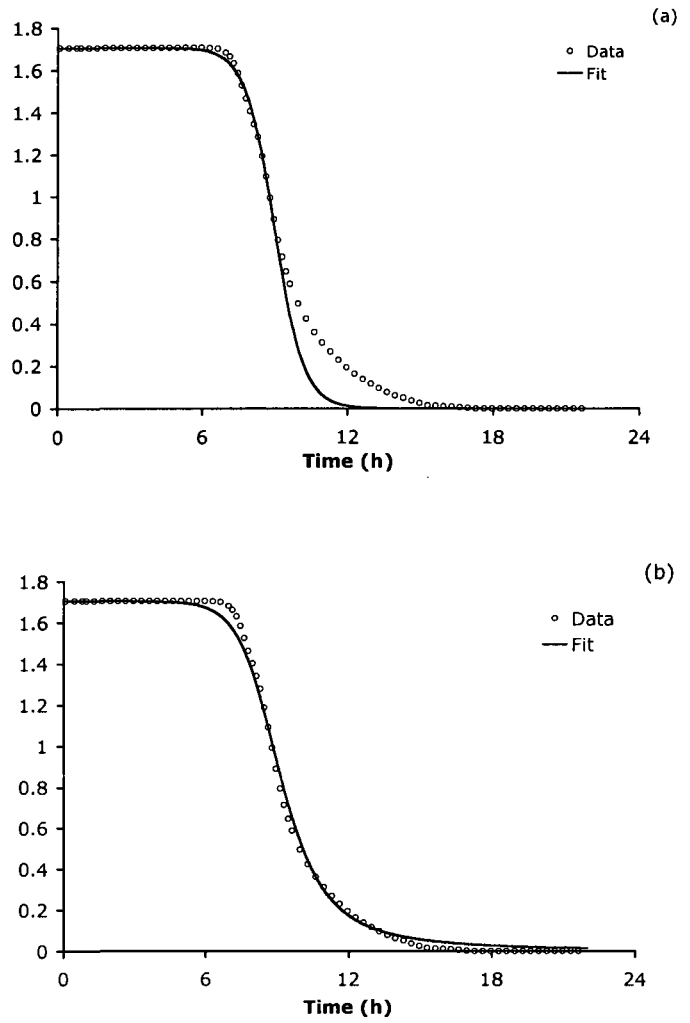

Figure 3S.2. Kinetic data for the reduction of (1,5-COD)$PtCl_2$ and two equivalents of Proton Sponge and concomitant cyclohexene hydrogenation showing curve fits to the 2-step (a) and 3-step (b) mechanisms, neither fit of which is as good as the fit to the 4-step mechanism (Figure 3.3 in the main text). (a): $k_1 = 6.7(9) \times 10^{-7}$, $k_2 = 1.35(1) \times 10^{3}$. (b): $k_1 \approx 9 \times 10^{-6}$, $k_2 \approx 9.4 \times 10^{2}$, $k_3 \approx 3.1 \times 10^{2}$; residual = 0.0258.

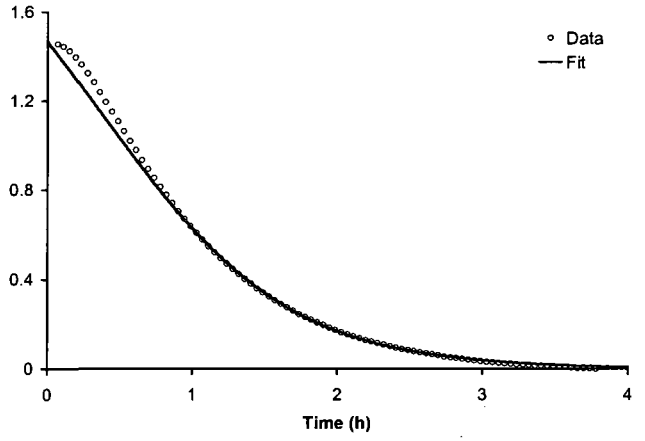

Figure 3S.3. Kinetic data for the reduction of $[Ir(1,5\text{-COD})Cl]_2$ and one equivalent of Proton Sponge in the presence of one equivalent of pyridine and concomitant cyclohexene hydrogenation showing a (poor) curve fit to the 2-step mechanism: $k_1 = 0.29(2)\ h^{-1}$; $k_2 = 2.4(2) \times 10^3\ M^{-1}\ h^{-1}$.

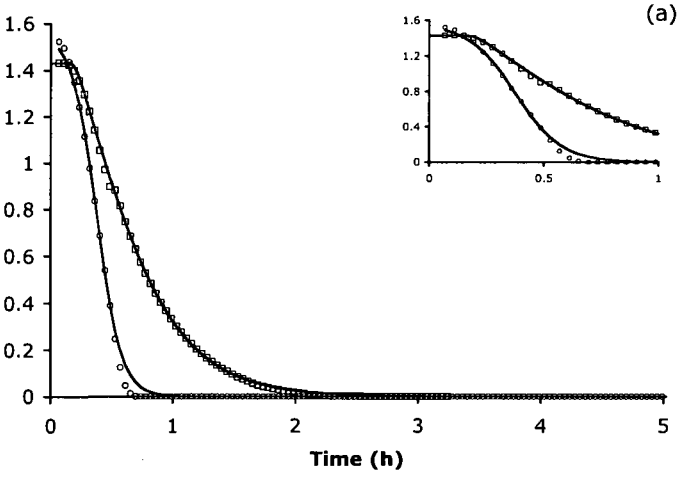

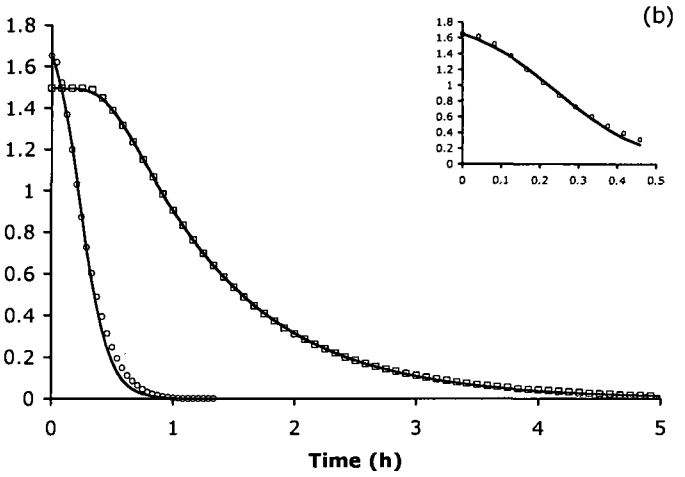

Figure 3S.4. Kinetic data for the reduction of $[Ir(1,5\text{-COD})(CH_3CN)_2][BF_4]$ with one equivalent of Proton Sponge and concomitant cyclohexene hydrogenation (a) in the absence of ligand (circles) and in the presence of one equivalent of pyridine (squares); and (b) in the presence of one equivalent (circles) and two equivalents (squares) of Bu_4NCl. In (a), the data in the absence of ligand is best fit by the 2-step mechanism: $k_1 = 0.23(3)\ h^{-1}$; $k_2 = 9.0(4) \times 10^3\ M^{-1}\ h^{-1}$; the data in the presence of one equivalent of pyridine is best fit by the 4-step mechanism: $k_1 \approx 0.02\ h^{-1}$; $k_2 \approx 3.6 \times 10^4\ M^{-1}\ h^{-1}$; $k_3 \approx 530\ M^{-1}\ h^{-1}$; $k_4 \approx 4.4 \times 10^3\ M^{-1}\ h^{-1}$ (residual = 0.007). In (b), the data in the presence of one equivalent is best fit by the 2-step mechanism: $k_1 = 0.88(9)\ h^{-1}$; $k_2 = 7.1(7) \times 10^3\ M^{-1}\ h^{-1}$; the data in the presence of two equivalents of pyridine is best fit by the 4-step mechanism: $k_1 \approx 0.5\ h^{-1}$; $k_2 \approx 5.9 \times 10^3\ M^{-1}\ h^{-1}$; $k_3 \approx 420\ M^{-1}\ h^{-1}$; $k_4 \approx 1.7 \times 10^3\ M^{-1}\ h^{-1}$ (residual = 0.002).

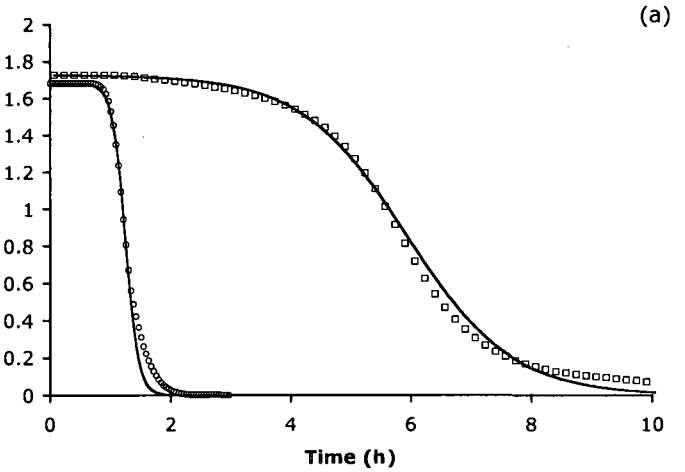

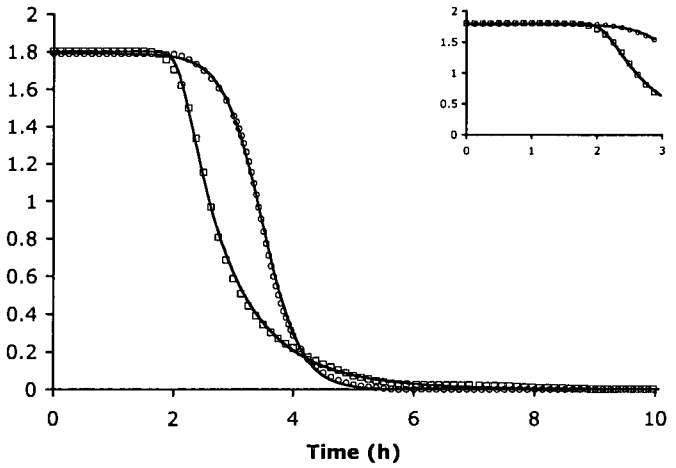

Figure 3S.5. Kinetic data for the reduction of $[Rh(1,5\text{-}COD)(CH_3CN)_2][BF_4]$ with one equivalent of Proton Sponge and concomitant cyclohexene hydrogenation (a) in the absence of ligand (circles) and in the presence of 80 equivalents of pyridine (squares); and (b) in the presence of one equivalent (circles) and two equivalents (squares) of Bu_4NCl. In (a), the data in both curves is best fit by the 2-step mechanism—no ligand (circles); $k_1 = 7.0(3) \times 10^{-4}\ h^{-1}$; $k_2 = 6.0(4) \times 10^{3}\ M^{-1}\ h^{-1}$; with 80 equivalents of pyridine (squares): $k_1 = 1.32(7) \times 10^{-3}\ h^{-1}$; $k_2 = 9.3(1) \times 10^{2}\ M^{-1}\ h^{-1}$. In (b), the data in the presence of one equivalent of Bu_4NCl is best fit by the 2-step mechanism: k_1 $7.0(5) \times 10^{-5}\ h^{-1}$; $k_2 = 2.40(1) \times 10^{3}\ M^{-1}\ h^{-1}$; the data in the presence of two equivalents of Bu_4NCl is best fit by the 4-step mechanism: $k_1 \approx 2 \times 10^{-6}\ h^{-1}$; $k_2 \approx 5.1 \times 10^{3}\ M^{-1}\ h^{-1}$; $k_3 \approx 570\ M^{-1}\ h^{-1}$; $k_4 \approx 1.3 \times 10^{3}\ M^{-1}\ h^{-1}$ (residual = 0.004).

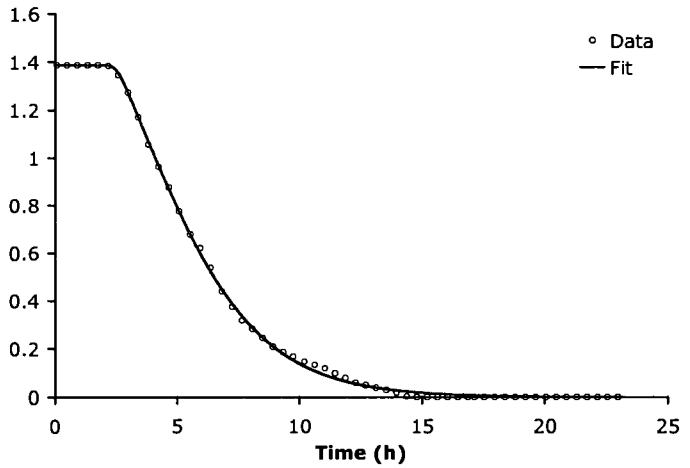

Figure 3S.6. Kinetic data for the reduction of $[Rh(1,5\text{-}COD)(CH_3CN)_2][BF_4]$ with one equivalent of Proton Sponge and concomitant cyclohexene hydrogenation in the presence of 10 equivalents of 4-dimethylaminopyridine. The data is best fit by the 4-step mechanism: $k_1 \approx 2 \times 10^{-5}\ h^{-1}$; $k_2 \approx 4.7 \times 10^{3}\ M^{-1}\ h^{-1}$; $k_3 \approx 75\ M^{-1}\ h^{-1}$; $k_4 \approx 720\ M^{-1}\ h^{-1}$ (residual = 0.009).

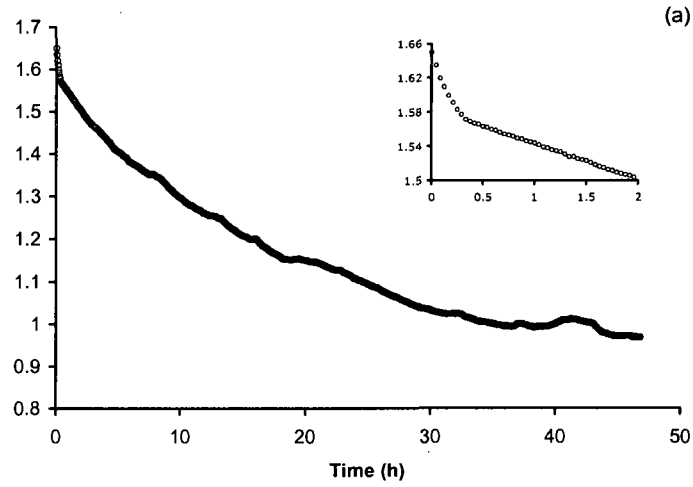
(a)
1.7
1.6
1.5
1.4
1.3
1.2
1.1
1
0.9
0.8
0
10
20
30
40
50
Time (h)
1.66
1.62
1.58
1.54
1.5
0
0.5
1
1.5
2

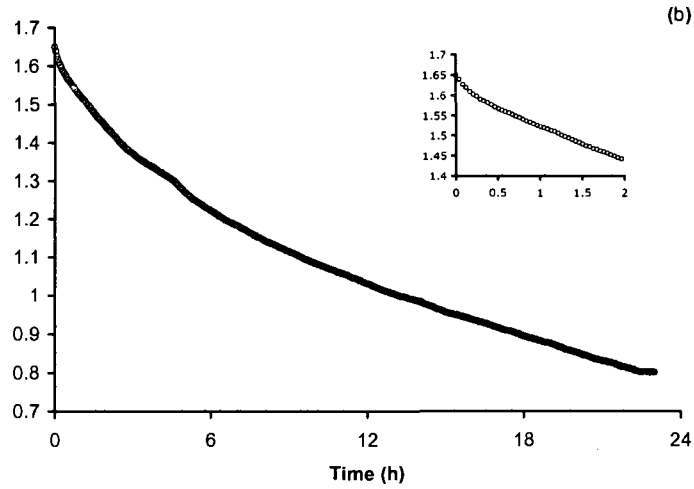
(b)
1.7
1.6
1.5
1.4
1.3
1.2
1.1
1
0.9
0.8
0.7
0
6
12
18
24
Time (h)
1.7
1.65
1.6
1.55
1.5
1.45
1.4
0
0.5
1
1.5
2

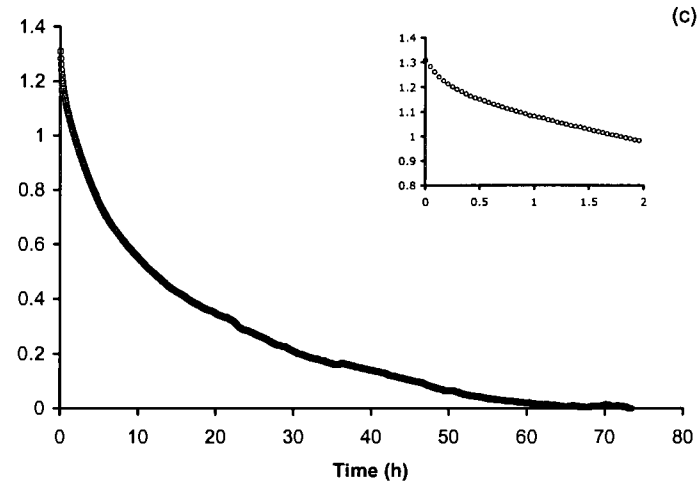

Figure 3S.7. Kinetic curves for the reduction of Pd(1,5-COD)Cl_2 with two equivalents of Proton Sponge in the presence of (a) 20 equivalents of 4-dimethylaminopyridine, (b) 0.3 equivalents of 1,10-phenanthroline, and (c) 0.5 equivalents of octanethiol. The insets of each curve give the first two hours of the respective reductions and show that in each case, an induction period is *not* seen.

Alternate explanation for the difference between Ir and Rh reduction in the presence of pyridine

In light of the size-dependent fractional coverage hypothesis that we described previously,[3,4] we can infer an explanation for the observations given in the main text, that is, why the reduction of Ir^I follows the 4-step mechanism with relatively little added pyridine while the reduction of Rh^I follows the 2-step mechanism even when 50 equivalents of pyridine are added. As described elsewhere,[3,4] the idea behind the size-dependent fractional coverage hypothesis is that smaller nanoclusters have a higher affinity for ligands than larger nanoclusters; this higher affinity results in more effective poisoning of the surface of smaller nanoclusters versus larger ones. This could be due to an inherent bond strength difference[5] expressed, along with a size-dependent steric/ligand packing effect, as a change in surface coverage between smaller versus larger nanoclusters.

To provide evidence for or against the hypothesis that the change in mechanism could be due to such size effects, samples were harvested for TEM analysis in the reductions of $[Ir(1,5\text{-COD})Cl]_2$ and $[Rh(1,5\text{-COD})Cl]_2$ in the absence of added ligands at the same reaction time (i.e., when an equal amount of H_2 was lost in each reduction), Figure 3S.8. This experiment was repeated at early reaction time (when ~3 psig H_2 was lost) and at later reaction time (when ~7 psig H_2 was lost). At the early reaction time, the sizes of the Ir^0 and Rh^0 nanoclusters are not distinguishable given the experimental error (1.6 ± 0.5 nm versus 2.8 ± 1.0 nm, respectively). However, at the later reaction time, the Rh^0 clusters are about *five times* larger than the Ir^0 clusters (2.2 ± 0.7 nm versus 10 ± 3 nm, respectively).[6] This result is consistent with nanocluster size effects as a *contributing* reason for the fact that Rh is more difficult to poison than Ir. The Ir_n^0 clusters formed in the process of reducing $[Ir(1,5\text{-COD})Cl]_2$ are small and therefore readily poisoned by pyridine, while the Rh_n^0 nanoclusters formed in the process of reducing $[Rh(1,5\text{-COD})Cl]_2$ are larger and therefore less effectively poisoned.[3,4] In addition, a direct size comparison can be made from our previous literature of *fully-formed*[7] Ir_n^0 and[8] Rh_n^0 nanoclusters from the precursor complexes $[Bu_4N]_5Na_3[M^I(1,5\text{-COD})P_2W_{15}Nb_3O_{64}]$ (M = Ir, Rh). The fully-formed, $P_2W_{15}Nb_3O_{62}^{9-}$-stabilized Ir_n^0 nanoclusters have an average size of 20 ± 3 Å,[7] while the fully-formed $P_2W_{15}Nb_3O_{62}^{9-}$-stabilized Rh_n^0 nanoclusters have an average size of 40 ± 6 Å,[8] about twice as large. These results are consistent with, and lend additional support to, the nanoparticle particle-size-dependent fractional coverage hypothesis discovered in 2005.[3,4]

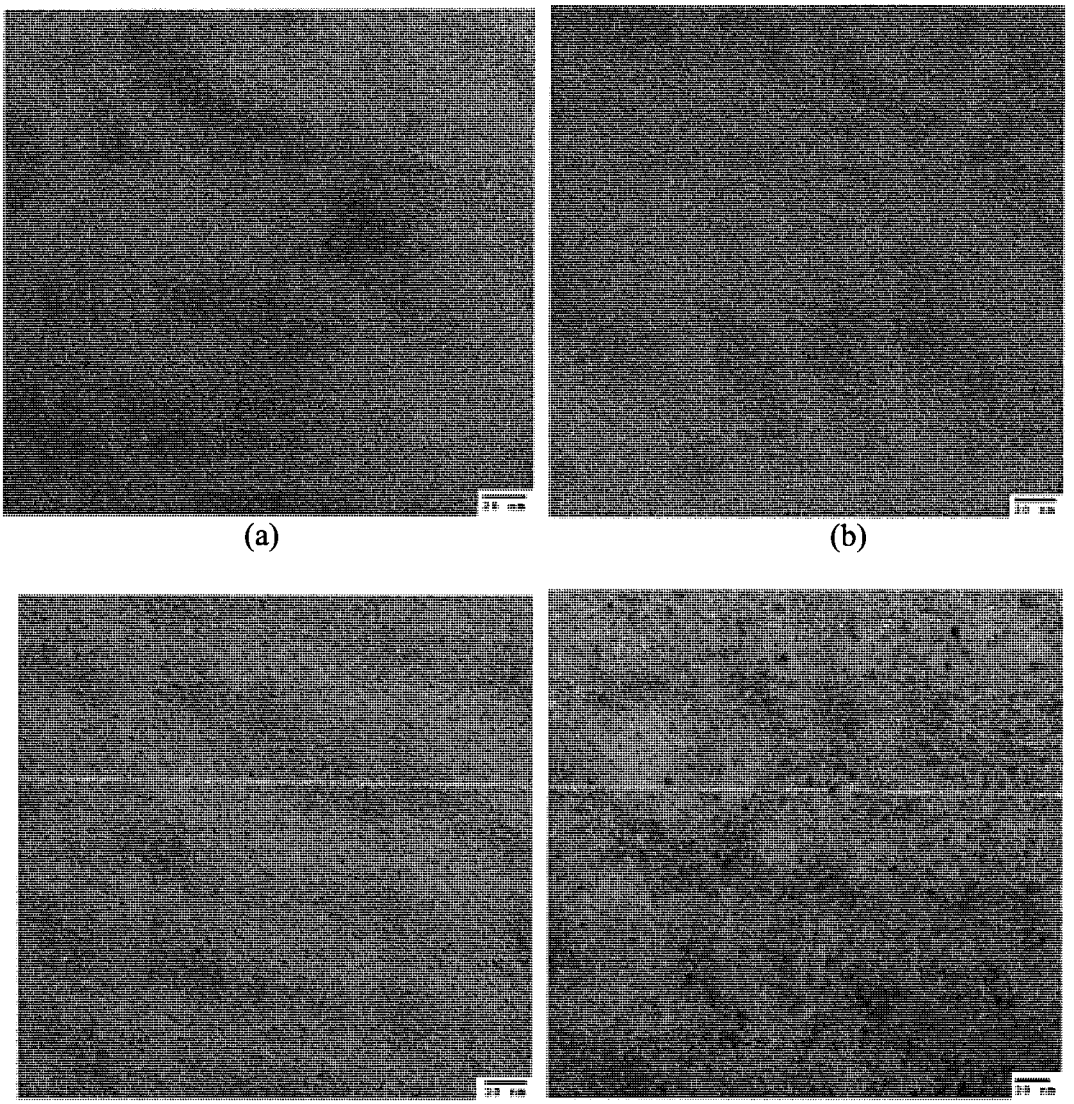

Figure 3S.8. TEM images of Ir ((a) and (c)) and Rh ((b) and (d)) nanoclusters formed in the reduction of $[Ir(1,5\text{-COD})Cl]_2$ and $[Rh(1,5\text{-COD})Cl]_2$ respectively. The nanoclusters in (a) and (b) were harvested after ~3 psig H_2 was lost in the reduction; the nanoclusters in (c) and (d) were harvested after ~7 psig $H_2$was lost. At early times, the Ir and Rh nanoclusters are the same size within experimental error (1.6 ± 0.5 nm and 2.8 ± 1.0, respectively). At later times, however, the Rh nanoclusters are ~5 times larger than the Ir nanoclusters (2.2 ± 0.7 nm and 10 ± 3 nm, respectively). As mentioned in the main text, the capability of TEM to form nanoclusters from $[Rh(1,5\text{-COD})Cl]_2$[9] requires that caution be taken when interpreting these images since we have shown elsewhere[6b] that TEM can cause the formation of Rh_n^0 nanoclusters from single-metal precursors. However, the large difference in the sizes at later reaction time gives us confidence that we are observing larger Rh_n^0 nanoclusters formed from the reduction of $[Rh(1,5\text{-COD})Cl]_2$ under H_2.

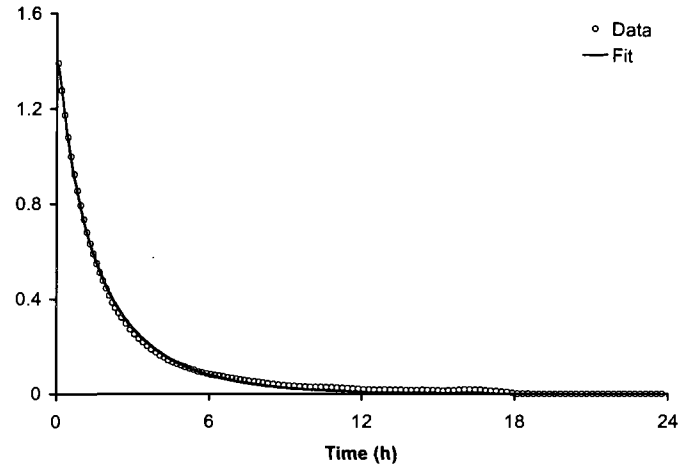

Figure 3S.9. Kinetic data for the reduction of $Pd(1,5\text{-}COD)Cl_2$ with two equivalents of Proton Sponge and concomitant cyclohexene hydrogenation. The reduction begins without an induction period but can still be fit to the 4-step mechanism: $k_1 \approx 20\,h^{-1}$; $k_2 \approx 1.1 \times 10^3\,M^{-1}\,h^{-1}$; $k_3 \approx 330\,M^{-1}\,h^{-1}$; $k_4 \approx 630\,M^{-1}\,h^{-1}$ (residual = 0.009).

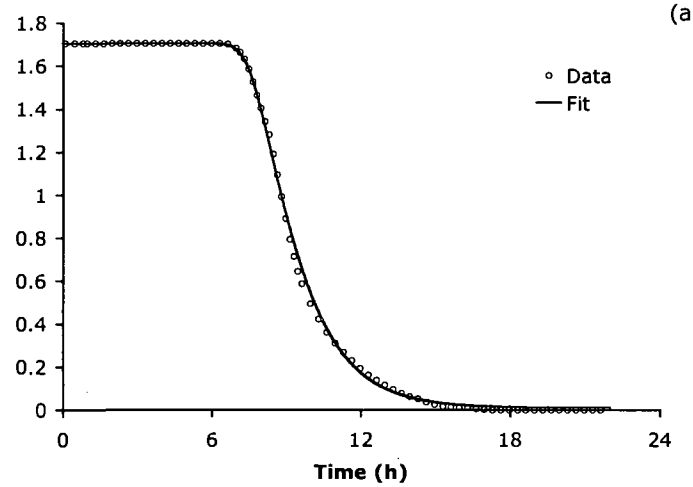

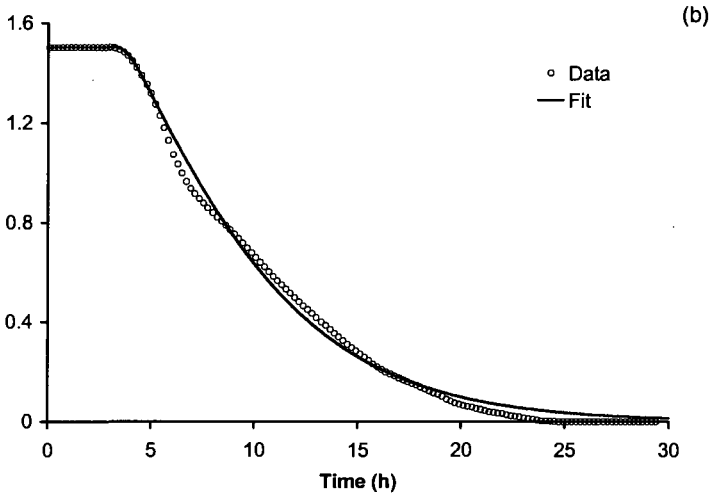

Figure 3S.10. Kinetic data for the reduction of Pt(1,5-COD)Cl_2 with two equivalents of Proton Sponge and concomitant cyclohexene hydrogenation in (a) acetone and (b) propylene carbonate. The reaction conditions other than solvent are the same in both reductions: 1.2 mM Pt(1,5-COD)Cl_2 at 22 °C. The fits to both curves are to the 4-step mechanism: (a) $k_1 \approx 1\ h^{-1}$; $k_2 \approx 1.6 \times 10^3\ M^{-1}\ h^{-1}$; $k_3 \approx 170\ M^{-1}\ h^{-1}$; $k_4 \approx 910\ M^{-1}\ h^{-1}$ (residual = 0.010) (this curve is identical to that shown in Figure 3.3 in the main text); (b) $k_1 \approx 8 \times 10^{-6}\ h^{-1}$; $k_2 \approx 2.9 \times 10^3\ M^{-1}\ h^{-1}$; $k_3 \approx 45\ M^{-1}\ h^{-1}$; $k_4 \approx 330\ M^{-1}\ h^{-1}$ (residual = 0.020). The reduction in propylene carbonate is slower than the reduction in acetone (reaction is complete in ~24 h in propylene carbonate versus ~15 h in acetone), but the rate constants are not distinguishable within experimental error.

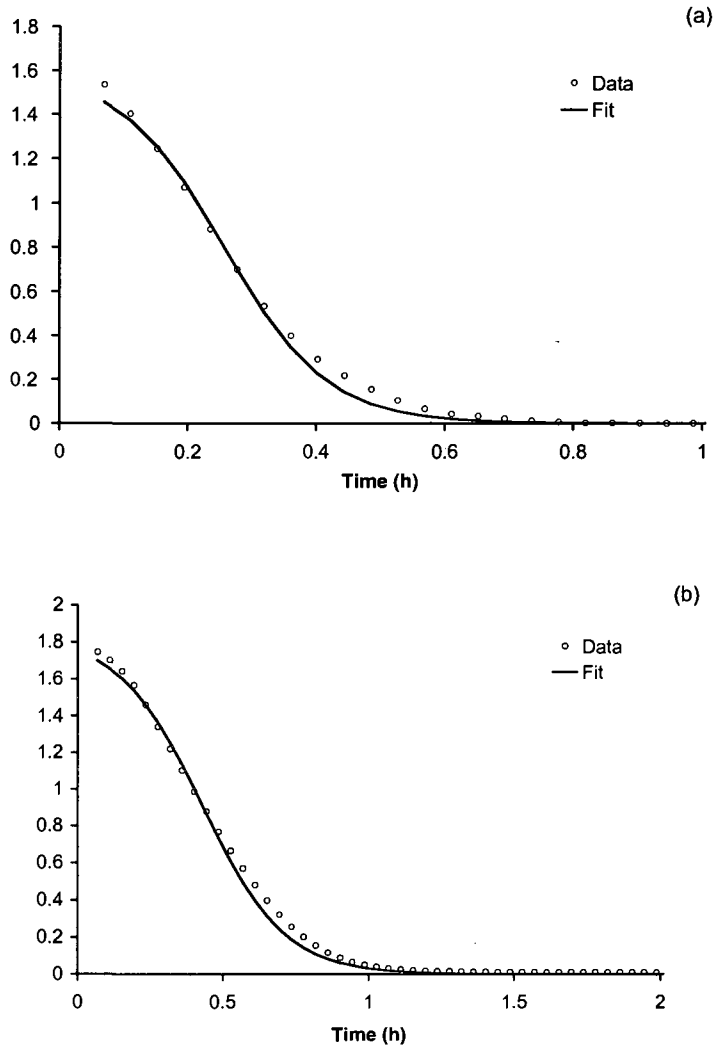

Figure 3S.11. Kinetic data for the reduction of $[Ir(1,5\text{-COD})Cl]_2$ with one equivalent of Proton Sponge and concomitant cyclohexene hydrogenation in (a) acetone and (b) propylene carbonate. The reaction conditions other than solvent are the same in both reductions: 0.6 mM $[Ir(1,5\text{-COD})Cl]_2$ (1.2 mM Ir) at 30 °C. The fits to both curves are to the 2-step mechanism: (a) $k_1 = 0.49(9)\ h^{-1}$; $k_2 = 1.1(1) \times 10^4\ M^{-1}\ h^{-1}$; (b) $k_1 = 0.33(4)\ h^{-1}$; $k_2 = 5.4(4) \times 10^3\ M^{-1}\ h^{-1}$.

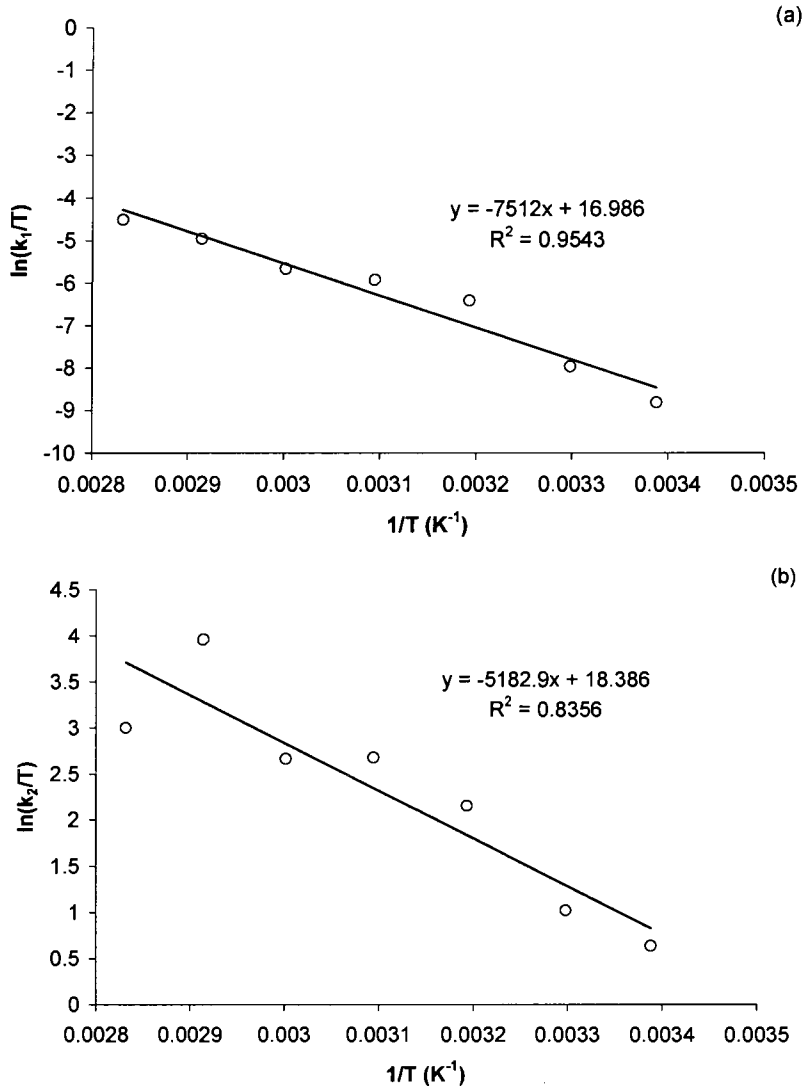

Figure 3S.12. Eyring plots for the nucleation (k_1, a) and growth (k_2, b) of Ir^0 nanoclusters from $[Ir(1,5\text{-COD})Cl]_2$ in the temperature range 22.0-80.0 °C. From these plots, $\Delta H^{\ddagger}_1$ = 15(1) kcal/mol and $\Delta S^{\ddagger}_1$ = -14(1) e.u., while $\Delta H^{\ddagger}_2$ = 10(2) kcal/mol and $\Delta S^{\ddagger}_2$ = -11(4) e.u.

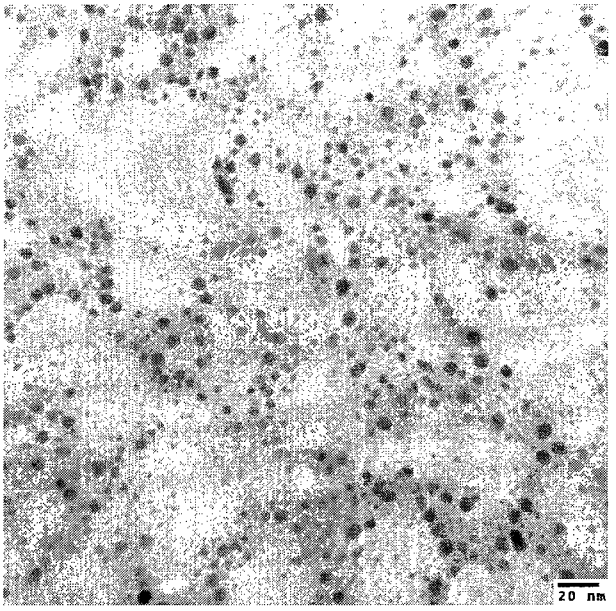

Figure 3S.13. TEM of nanoclusters prepared from the reduction of a 0.6 mM solution of $Pt(1,5\text{-}COD)Cl_2$ with two equivalents of Proton Sponge in propylene carbonate at 60 °C. The average size of the nanoclusters is 7 ± 3 nm (450 particles counted).

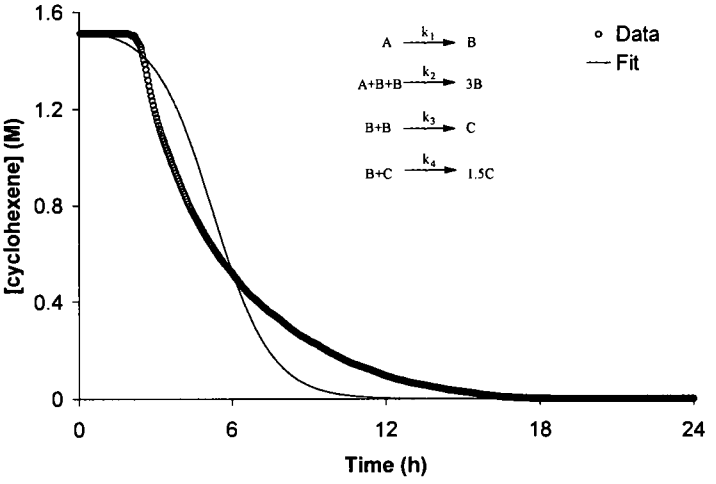

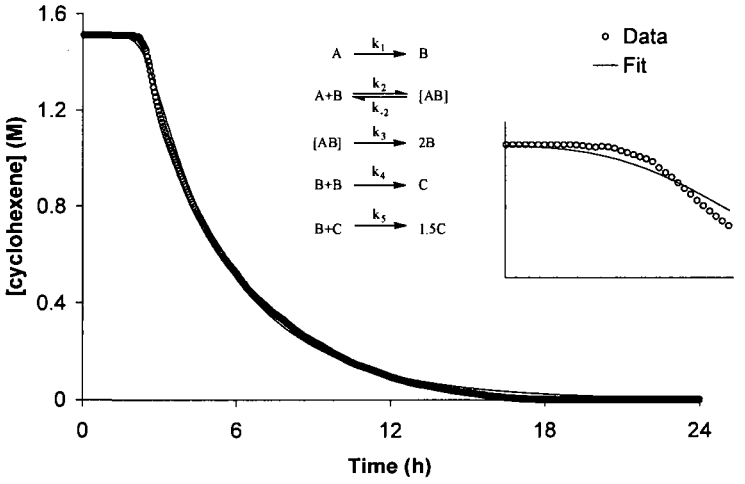

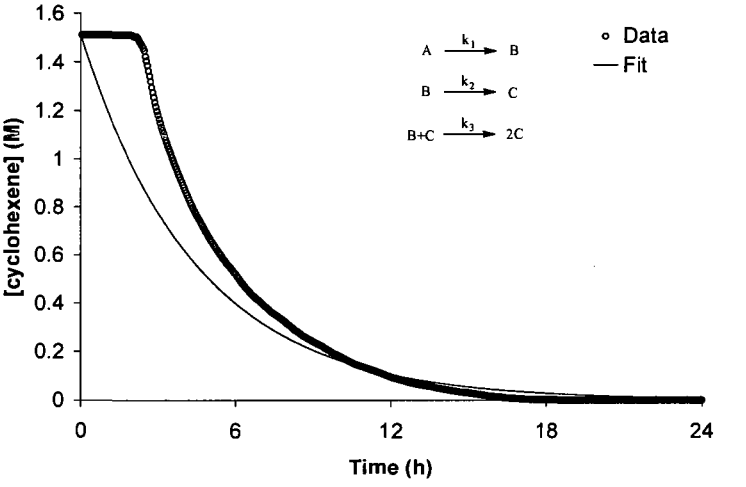

Figure 3S.14. Attempted curve-fits for three additional alternative mechanisms for the reduction of $Pt(1,5\text{-}COD)Cl_2$. The inset of the second curve shows that the mechanism tested does not fit the end of the induction period well. The fits of the other two mechanisms are obviously poor.

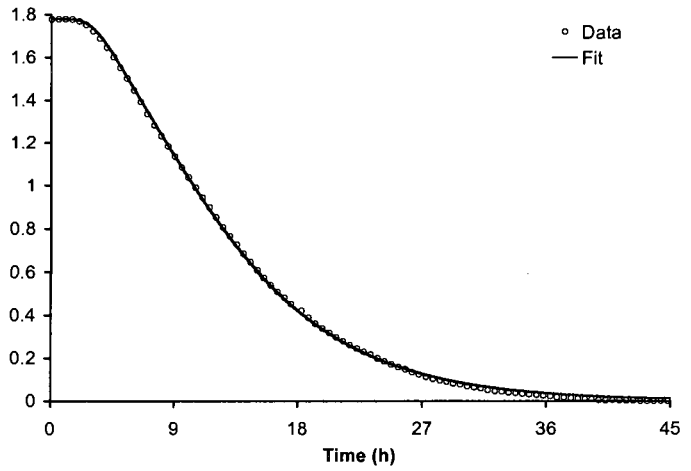

Figure 3S.15. Fit to the 4-step mechanism A→B, A+B→2B, B+B→C, A+C→1.5C (i.e., the mechanism in Scheme 3.4 of the main text) of the kinetic data for the reduction of 0.6 mM $[Ir(1,5\text{-COD})Cl]_2$ (1.2 mM Ir) in the presence of one equivalent of Proton Sponge and five equivalents of pyridine (the same data as is shown in Figure 3.5, squares, in the main text. The fit to the mechanism in Scheme 3.4 of the main text is excellent: $k_1 \approx 2 \times 10^{-3}$ h^{-1}; $k_2 \approx 920$ M^{-1} h^{-1}; $k_3 \approx 1.2 \times 10^4$ M^{-1} h^{-1}; $k_4 \approx 190$ M^{-1} h^{-1} (residual = 0.008).

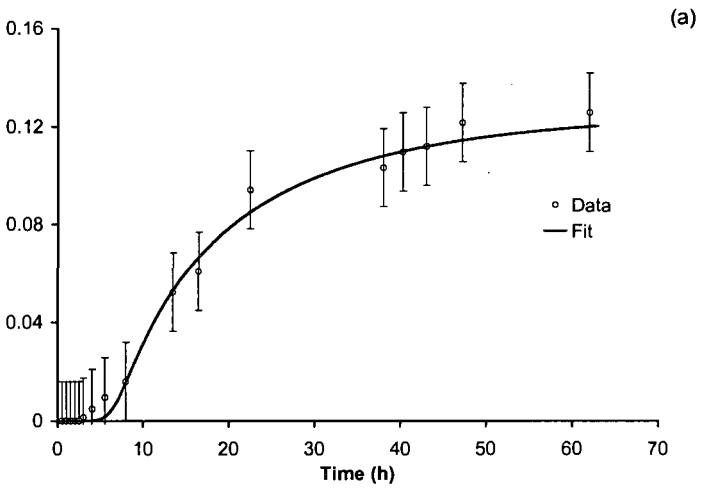

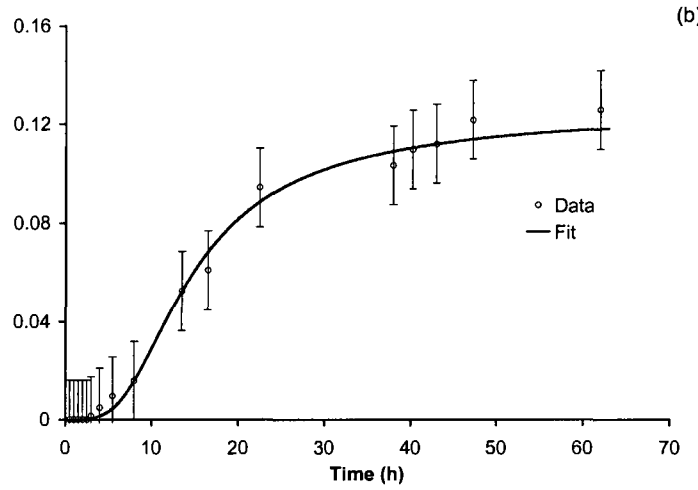

Figure 3.16. Cyclooctane evolution data for the reduction of 0.6 mM [Ir(1,5-COD)Cl]$_2$ (1.2 mM Ir) in the presence of one equivalent of Proton Sponge and five equivalents of pyridine as monitored by GLC. The fit in (a) is to the 4-step mechanism in Scheme 3.1 in the main text: $k_1 \approx 3 \times 10^{-3}$ h^{-1}; $k_2 \approx 830$ M^{-1} h^{-1}; $k_3 \approx 37$ M^{-1} h^{-1}; $k_4 \approx 69$ M^{-1} h^{-1} (residual = 0.024). The fit in (b) is to the 4-step mechanism with the fourth step replaced by A+C→1.5C: $k_1 \approx 2 \times 10^{-2}$ h^{-1}; $k_2 \approx 260$ M^{-1} h^{-1}; $k_3 \approx$ 190 M^{-1} h^{-1}; $k_4 \approx 22$ M^{-1} h^{-1} (residual = 0.024). The higher residual for this data is a result of the much lower precision of the GLC data in comparison to the pressure-transducer obtained H_2 (and equivalent cyclohexene) loss kinetic data. Comparing these rate constants to those found from the H_2/cyclohexene loss data, the rate constants are within the experimental error for the fits to the mechanism in Scheme 3.1 in the main text (compare the data in (a) here to that in Figure 3.5, squares, in the main text). However, they are not within experimental error for the fits to the alternative mechanism (compare the data in (b) here to that in Figure 3S.11; note especially the difference of 2 orders of magnitude for the calculated k_3 rate constants). This data allows us to exclude a significant contribution of the alternative mechanism using Ockham's Razor; however, some contribution of the A+C→1.5C step cannot be completely ruled out.

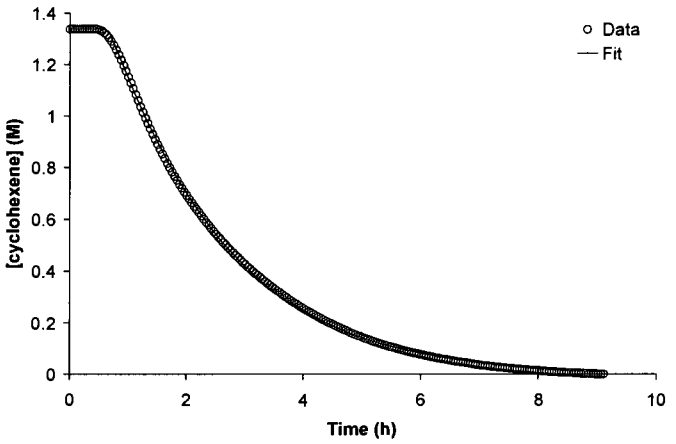

Figure 3S.17. Kinetic data for the reduction of [Ir(1,5-COD)(CH_3CN)][BF_4] in the presence of one equivalent each of tetrabutylammonium hydroxide and tetrabutylammonium citrate (adapted from Figure S8 elsewhere[10]). The fit is to the 4-step mechanism; $k_1 \approx 1 \times 10^{-5}$ h^{-1}; $k_2 \approx 2.1 \times 10^4$ $M^{-1}h^{-1}$; $k_3 \approx 210$ $M^{-1}h^{-1}$; $k_4 \approx 1.0 \times 10^3$ $M^{-1}h^{-1}$.

Table 3S.1. Comparison of the F-test values calculated for the 2-step and the 4-step mechanisms. In all cases, the *F* value for the 4-step mechanism is closer to 1, meaning that in all cases the 4-step mechanism provides a better fit.

System	*F* value	
	2-step mechanism	**4-step mechanism**
Pt(1,5-COD)Cl_2	0.937	1.012
Ru(1,5-COD)Cl_2	0.953	0.989
[Ir(1,5-COD)Cl]$_2$ + Bu_4NCl	0.395	0.991
[Ir(1,5-COD)Cl]$_2$ + 5 eq pyridine	0.946	1.002
[Rh(1,5-COD)Cl]$_2$ + Bu_4NCl	0.744	0.982
[Rh(1,5-COD)Cl]$_2$ + 10 eq 4-dimethylaminopyridine	0.922	1.005

References

[1] Day, V. W.; Klemperer, W. G.; Main, D. J. *Inorg. Chem.* **1990**, *29*, 2345.

[2] Lin, Y.; Finke, R. G. *J. Am. Chem. Soc.* **1994**, *116*, 8335.

[3] Besson, C.; Finney, E. E.; Finke, R. G. *J. Am. Chem. Soc.* **2005**, *127*, 8179.

[4] Besson, C.; Finney, E. E.; Finke, R. G. *Chem. Mater.* **2005**, *17*, 4925.

[5](a) Recent calculations of pyridine bonded to *single metal atoms*[5b] have shown that the Ir-pyridine bond is ~1.7 times stronger than the Rh-pyridine bond (44 versus 26 kcal/mol). If this trend for single metal atoms is assumed to hold for nanoclusters, then the stronger Ir_n^0-pyridine bond allows the Ir_n^0 nanoclusters to be poisoned by pyridine, while the weaker Rh_n^0-pyridine bond means that a more basic ligand is necessary to force a change in mechanism. (b) Wu, D.-Y.; Ren, B.; Xu, X.; Liu, G. K.; Yang, Z.-L.; Tian, Z.-Q. *J. Chem. Phys.* **2003**, *119*, 1701.

[6] These results must be interpreted with caution, due to the known ability of the TEM method to form nanoclusters from $[Rh(1,5\text{-}COD)Cl]_2$.[6b,c] Because there is some amount of $[Rh(1,5\text{-}COD)Cl]_2$ in the reaction solution at each of the times that a TEM sample is removed, we must assume that *some* of the nanoclusters observed were formed in the TEM beam. However, the large difference between the sizes of the Ir_n^0 and Rh_n^0 nanoclusters at later time relative to that at earlier time, as well as the difference in sizes of the polyoxoanion-stabilized Ir_n^0 versus Rh_n^0 nanoclusters allow us to reasonably conclude that the Rh_n^0 nanoclusters formed from $[Rh(1,5\text{-}COD)Cl]_2$ are indeed larger than the Ir_n^0 nanoclusters formed from $[Ir(1,5\text{-}COD)Cl]_2$. (b) Jaska, C. A.; Manners, I. *J. Am. Chem. Soc.* **2004**, *126*, 9776. (c) Hagen, C. M.; Widegren, J. A.; Maitlis, P. M.; Finke, R. G. *J. Am. Chem. Soc.* **2005**, *127*, 4423.

[7] Watzky, M. A.; Finke, R. G. *J. Am. Chem. Soc.* **1997**, *119*, 10382.

[8] Widegren, J. A.; Finke, R. G. *Inorg. Chem.* **2002**, *41*, 1558.

[9](a) Jaska, C. A.; Manners, I. *J. Am. Chem. Soc.* **2004**, *126*, 9776. (b) Hagen, C. M.; Widegren, J. A.; Maitlis, P. M.; Finke, R. G. *J. Am. Chem. Soc.* **2005**, *127*, 4423.

[10] Özkar, S.; Finke, R. G. *J. Am. Chem. Soc.* **2002**, *124*, 5796.

CHAPTER IV

IS IT HOMOGENEOUS Pt^{II} OR HETEROGENEOUS Pt^{0}_{n} CATALYSIS? EVIDENCE THAT Pt(1,5-COD)Cl_2 AND Pt(1,5-COD)$(CH_3)_2$ PLUS H_2 FORM HETEROGENEOUS, NANOCLUSTER PLUS BULK-METAL Pt^0 HYDROGENATION CATALYSTS

This dissertation chapter contains the manuscript of a paper published in *Inorganica Chimica Acta* (Finney, E. E.; Finke, R. G. *Inorg. Chim. Acta* **2006**, *359*, 2879). This chapter presents an investigation of whether catalysis of olefin hydrogenation by Pt(1,5-COD)Cl_2 and Pt(1,5-COD)$(CH_3)_2$ proceeds by a homogeneous Pt^{II} species or a heterogeneous Pt^{0}_{n} catalyst. Several lines of evidence are given that support the hypothesis that the above Pt^{II} complexes form Pt^0 nanocluster and bulk-metal catalysts for the hydrogenation of cyclohexene. Also provided in an Appendix is a brief overview of the literature of Pt-catalyzed hydrosilylation, focusing on the homogeneous-versus-heterogeneous question.

The experiments in this chapter were performed by E.E.F. The manuscript was prepared by E.E.F. with assistance and editing by R.G.F.

Abstract

An investigation of the question of "Is it homogeneous or heterogeneous catalysis?" is reported when using $Pt^{II}(1,5\text{-COD})X_2$ (X = halogen, alkyl) precatalysts for the hydrogenation of olefins. Using product studies, kinetic evidence, and Hg^0 poisoning experiments, it is shown that $Pt^{II}(1,5\text{-COD})Cl_2$ is a precatalyst and must be reduced to Pt^0 nanoclusters and bulk metal as the true hydrogenation catalyst. An investigation of the related complex $Pt^{II}(1,5\text{-COD})(CH_3)_2$ reveals that this complex does not form a hydrogenation catalyst by itself under H_2, in agreement with the literature. Kinetic and Hg^0 poisoning evidence confirms that $Pt^{II}(1,5\text{-COD})(CH_3)_2$, too, forms a Pt^0 heterogeneous catalyst if other metals (Ir^0, Pt^0) are used as seeds to initiate the reduction of Pt^{II}. A short review of the use of $Pt^{II}(1,5\text{-COD})Cl_2$ in hydrosilylation reactions is given, illustrating the continued controversy surrounding the nature of the true catalyst in that literature system.

Introduction

The question of "Is it homogeneous (e.g., discrete organometallic complex) or heterogeneous (e.g., nanocluster or bulk metal) catalysis?" is an important and challenging one.[1] This issue of the nature of the true catalyst when starting with reducible organometallic precursors has existed at least since Brian James' classic 1973 book on homogeneous hydrogenation.[2] A methodology developed in our labs in 1994[3] has permitted the identification of a heterogeneous, nanocluster catalyst in five cases where a discrete organometallic complex was originally believed to be the catalyst.[3–7] The essence of that methodology is shown in Figure 4.1. An expanded, 12-point version of the approach detailed in Figure 4.1 is available elsewhere.[3]

Is it Pt(II) homogeneous or Pt^0_n heterogeneous catalysis?

It is known that relatively stable, d^8 square planar Pt^{II} complexes are typically inactive for homogeneous hydrogenation; bulk Pt^0 metal formation is a common product in these reactions.[2] Consistent with this, many of the Pt complexes used as catalysts are olefin complexes of Pt^0; ready ligand dissociation, followed by Pt^0 atom nucleation into nanoclusters and/or bulk metal, can at least in principle provide precendented, active Pt^0_n as the true catalyst.[8] Indeed, one report observed that, upon removal of the styrene solvent from a solution of $Pt^0(PhCH{=}CH_2)_3$, the solution changed from yellow to brown (a characteristic color of Pt^0 and some other nanoclusters[9]), and bulk Pt^0 metal eventually precipitated.[10] Common among organometallic Pt precatalysts are complexes containing either strong ligands, such as phosphines (e.g., $PtCl_2(PPh_3)$[2,11]) or a tin cocatalyst (e.g., $Pt(SnCl_3)_5^{3-}$[2,12]) to stabilized the Pt against reduction to Pt^0 metal.[2,13] Hence, platinum complexes are

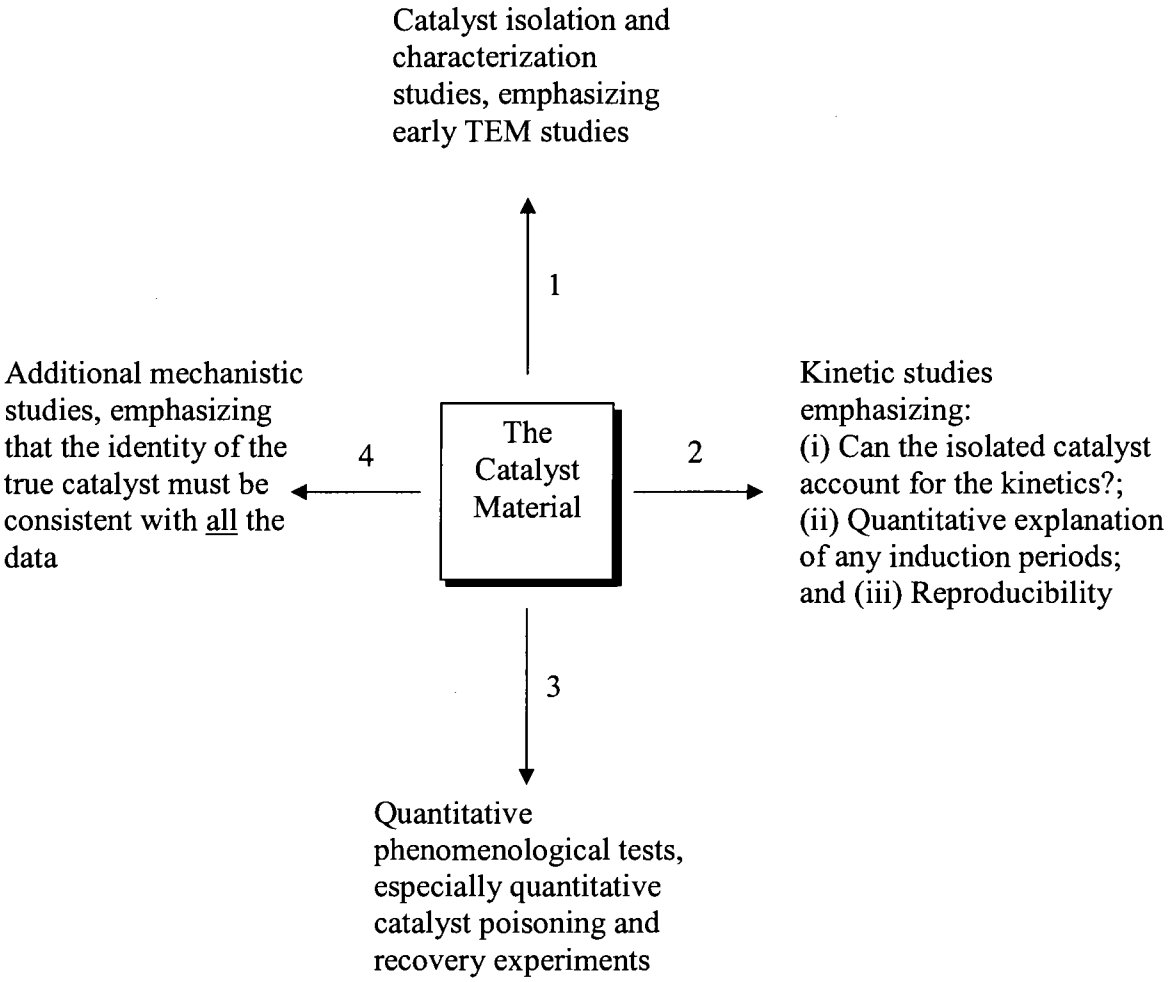

Figure 4.1. The most recent approach to distinguish a metal-particle heterogeneous from a metal-complex homogeneous catalyst.

among the systems where the nature of the true catalyst is unknown,[1] that is, where the "Is it homogeneous or heterogeneous catalysis?" question has not been examined in detail, but needs to be.

Hydrogenations with $Pt^{II}(1,5\text{-}COD)Cl_2$

Platinum(II) complexes are also used as hydrogenation precatalysts; among these the 1,5-cyclooctadiene complexes $Pt^{II}(1,5\text{-}COD)X_2$ are common where X = a halide or alkyl. In the case of $Pt^{II}(1,5\text{-}COD)X_2$ it is, therefore, highly plausible that

reduction to an active Pt_n^0 heterogeneous nanocluster and/or bulk metal hydrogenation catalyst is occurring. In fact, recent literature, as well as the evidence on Pt (and the related Pd) systems in a 2003 review (see Table A1 in reference 1), makes the alternative hypothesis that "heterogeneous Pt_n^0 is the true catalyst, not Pt^{II}" the crucial alternative hypothesis to be disproved[14] en route to providing reliable evidence for the true catalyst. It is just this crucial question for hydrogenation catalysis beginning with $Pt^{II}(1,5\text{-COD})Cl_2$[1] [15] that we examine herein, using the state-of-the-art, previously successful[3–7] methodology outlined in Figure 4.1.

Hydrogenations of $Pt^{II}(1,5\text{-COD})(CH_3)_2$

An interesting system related to $Pt^{II}(1,5\text{-COD})Cl_2$ is its dimethyl congener, $Pt^{II}(1,5\text{-COD})(CH_3)_2$: does it form a homogeneous Pt^{II} or heterogeneous Pt_n^0 hydrogenation catalyst? The extensive work done by Whitesides on the hydrogenation of $Pt^{II}(1,5\text{-COD})(CH_3)_2$ over a bulk Pt^0 catalyst, in which the olefin and methyl groups are hydrogenated and the Pt atom of the complex yields bulk metal, gives strong albeit not conclusive evidence for heterogeneous hydrogenation by Pt^0 versus homogeneous hydrogenation by Pt^{II}.[16] Perhaps the most suggestive evidence at present for heterogeneous hydrogenation in this system is the finding that

---

[1] A typical study that has led us to examine the question of "Is it homogeneous Pt^{II} or heterogeneous Pt_n^0 catalysis?" is Reetz et al.'s study of $Pt^{II}(1,5\text{-COD})Cl_2$ catalyzed hydrogenation of aromatic halo-nitro compounds.[15] The Pt complex, modified with β-cyclodextrin-modified diphosphines or tris(*m*-sulfonatophenyl)phosphine ligands, was shown to be a highly active and selective catalyst for the hydrogenation of aromatic halo-nitro compounds. The authors report no observations that would indicate either heterogeneous or homogeneous catalysis. However, the high H_2 pressure (20 atm) and temperature (80 °C), along with basic conditions that could promote heterolytic H_2 activation by the Pt^{II} ion, make the conditions favorable for the reduction of Pt^{II} to Pt_n^0 clusters stabilized by Cl^- and CO_3^{2-}.

$Pt^{II}(1,5\text{-COD})(CH_3)_2$ cannot be reduced by H_2 in the absence of Pt^0;[17] that is, the complex must be reduced heterogeneously. The $Pt^0+Pt^{II}\rightarrow 2Pt^0$ (under H_2) step involved is just the A+B→2B autocatalytic growth step of the nanocluster formation mechanism published elsewhere.[3–5]

Other $Pt^{II}(1,5\text{-COD})$ complexes are reduced only slowly under H_2 in the absence of Pt^0; these reactions were observed to be autocatalytic and formed colloidal, then bulk, Pt^0.[16] Determination of the rate law for hydrogenation of $Pt^{II}(1,5\text{-COD})(CH_3)_2$ provided kinetic evidence that the hydrogenation is heterogeneous;[17,18] no evidence for a homogeneous reaction between H_2 and $Pt^{II}(1,5\text{-COD})(CH_3)_2$ was observed. Addition of Hg^0 completely poisons the hydrogenation, further indicating that the reaction is heterogeneous Pt^0 rather than homogeneous Pt^{II}.[19] Hence, it will be important to briefly re-examine the reaction of $Pt^{II}(1,5\text{-COD})(CH_3)_2$ with H_2 by the methodology in Figure 4.1 in order to support or refute the above findings.

The present study

Two events triggered this study. The first was our recent review of the literature which raised the issue of Pt^{II} homogeneous versus Pt_n^0 heterogeneous catalysis;[1] the second was a referee of our recent mechanistic study of nanocluster formation from $Pt^{II}(1,5\text{-COD})Cl_2$ under H_2[20,21] who also raised the question: could we rule out a contribution to catalysis from Pt^{II}? Is the evidence compelling that the dominant catalyst is Pt_n^0? While we provided an initial list of arguments in the Supporting Information elsewhere,[20] we realized that the topic of Pt^{II} homogeneous versus Pt_n^0 heterogeneous hydrogenation catalysis is general and important enough to justify its own, more detailed examination. This is especially true when one considers

the related, still controversial Pt^{II} versus Pt_n^0 hydrosilylation reactions (see Appendix 5A), as well as the related topics of Pd^0 versus Pd^{II} versus Pd^{IV} catalyzed C–C bond coupling (e.g., Heck and Suzuki) reactions.[22]

Herein, we report the following evidence indicating that $Pt^{II}(1,5\text{-COD})Cl_2$ under 3.7 atm H_2 in acetone yields exclusively, to our experimental detection limits, a nanoparticle plus bulk-metal Pt_n^0 heterogeneous catalyst: (i) product studies, (ii) kinetic evidence, (iii) Hg^0 poisoning experiments, (iv) quantitative analysis of the data that allows us to rule out even $\leq$0.02% Pt^{II} catalysis, and (v) a brief examination of the $Pt^{II}(1,5\text{-COD})(CH_3)_2$ system which confirms the findings of Whitesides and co-workers.[16–19] We conclude in Appendix 5.A with a brief summary of the literature of the related problem of hydrosilylations also beginning with $Pt^{II}(1,5\text{-COD})Cl_2$ and its continuing controversy of Pt^{II} versus Pt_n^0 catalysis.

Experimental

General considerations

All manipulations were carried out under air-free conditions using a Vacuum Atmospheres N_2 drybox maintained at $\leq$5 ppm O_2 as continuously monitored by a Vacuum Atmospheres O_2-level monitor. Unless otherwise specified, all materials were used as received. Dichloro(1,5-cyclooctadiene) platinum (99%) was obtained from Strem and stored in the drybox. Hg^0 (99.9995%) and Proton Sponge (1,8-bis(dimethylamino)naphthalene, 99%) were obtained from Aldrich. Proton Sponge was stored in the drybox; Hg^0 was moved into the drybox just before it was needed, was used immediately, and was then removed as it is a poison of the drybox's O_2-scavenging catalyst. Cyclohexene (Aldrich, 99%) was purified by distillation over

sodium under argon to remove trace hydroperoxides, and was stored in the drybox. Acetone (Burdick and Jackson, water content <0.2%) was purged with argon for 20 min and stored in the drybox. Hydrogen gas (General Air, 99.5%) was purified by passing through a moisture trap, an O_2 cartridge, and an indicating O_2 trap (Trigon Technologies, Rancho Cordova, CA). Polyoxoanion ($P_2W_{15}Nb_3O_{62}^{9-}$)-stabilized $Ir^0_{\sim 300}$ nanoclusters used as seeds for studies reducing $Pt^{II}(1,5\text{-COD})(CH_3)_2$ were prepared as in the literature[3] and then transferred to the drybox, where the acetone solvent was removed under vacuum and the black solid was dissolved in 10 mL acetone to make an $Ir^0_{\sim 300}$ nanocluster solution that was 0.34 mM in Ir.

Standard Conditions hydrogenations with $Pt^{II}(1,5\text{-COD})Cl_2$

Hydrogenation reactions were performed as previously described using our custom-built pressurized hydrogenation apparatus.[3] Briefly, in the drybox, 1.4 mg $Pt^{II}(1,5\text{-COD})Cl_2$ (3.7 μmol) and 1.6 mg Proton Sponge (7.4 μmol, two equivalents versus Pt) were weighed into a 1-dram glass vial. The solids were dissolved in 2.5 mL acetone, yielding a clear and colorless solution. This solution was transferred to a new 22 × 175 mm Pyrex borosilicate culture tube containing a new 5/8 × 5/16 inch Teflon-coated magnetic stir bar, and 0.5 mL cyclohexene was added to the culture tube. The culture tube was placed in a 100-mL Fischer–Porter bottle, which was then sealed and brought out of the drybox. The bottle was placed in a reaction flask filled with mineral oil maintained at 22.0 °C by a constant temperature recirculating water bath (VWR Scientific). The bottle was connected to the hydrogenation apparatus via its TFE-sealed Swagelock quick-connects. Stirring was started (~800 rpm to avoid

mass-transfer limiting conditions[23]) and the bottle was purged 13 times with hydrogen (15 s per purge) and stirred for an additional 1 min 45 s (total time elapsed 5 min). The pressure in the bottle was set to 40.0 ± 0.1 psig H_2, $t = 0$ was noted, and data collection was initiated using an Omega PX-621 pressure transducer interfaced with a PC running LabVIEW 6.1. Correction of the H_2 versus time data for the initial increase in acetone vapor pressure was performed by independently measuring the acetone versus time vapor pressure curve and then correcting the data point-by-point, as described previously.[24] The H_2 pressure loss was converted to its equivalent cyclohexene loss by the known 1 H_2:1 cyclohexene reaction stoichiometry.

Data analysis

Curve fitting of the data was performed using Microcal Origin version 7.0, a linear regression subroutine (RLIN) using a modified Levenberg-Macquard algorithm, to fit curves to the two-step, autocatalytic A→B (rate constant k_1), A+B→2B (rate constant k_2) mechanism[24,25] using the analytic, integrated equation corresponding to this mechanism[24,25] and Microcal Origin's non-linear least-squares curve-fitting capabilities. MacKinetics version 0.9.1b[26] was used to curve-fit to the four-step, double autocatalytic A→B (rate constant k_1), A+B→2B (rate constant k_2), B+B→C (rate constant k_3), B+C→1.5C (rate constant k_4) mechanism.[20,21]

Gridsearches were performed to find initial guesses for the rate constants, and these initial guesses were iterated using the predictor-corrector program of MacKinetics. A curve-fit was judged good when the residual was ≤0.01 and the fit was visually good. The details of curve-fitting the double autocatalytic mechanism

with MacKinetics, as well as the problems of error bars and finding global minima in the overall five-dimensional space, have been discussed previously.[21]

Transmission electron microscopy (TEM)

A Standard Conditions hydrogenation was started with 1.2 mM Pt^{II}(1,5-COD)Cl_2 and two equivalents of Proton Sponge. At the end of the induction period, as the H_2 pressure just started to decrease, a sample for TEM was removed using the following procedure: the gas-regulator valve to the H_2 tank was opened, as was the top valve of the Fischer–Porter bottle, allowing H_2 to flow through the Fischer–Porter bottle. About 0.5 mL of the reaction solution was removed by a gastight syringe with a 30 cm needle and was transferred to a 5 mL glass vial capped with a rubber septum. The vial was immediately immersed in liquid N_2 to freeze the solution. The vial was transferred to the drybox, by which time (about 5 min more) the solution had melted. A drop of the solution was placed on a TEM grid (silicon monoxide type-A, Formvar backing, 300 mesh, copper grids from Ted Pella, Inc.). The solvent evaporated and the grid was sealed in a vial and sent to Clemson University for TEM analysis by Dr. JoAn Hudson and her staff.

It has been shown that some transition-metal precatalyst complexes form nanoclusters in the electron beam of the TEM.[7,27] Hence, a control experiment was performed in which a drop of an acetone solution of Pt^{II}(1,5-COD)Cl_2 and Proton Sponge was placed on a TEM grid and analyzed. No nanoclusters were observed, demonstrating that the nanoclusters seen in the above experiment are formed by the H_2 reduction of the Pt^{II} complex and not in the TEM beam.

X-ray photoelectron spectroscopy (XPS)

At the end of a Standard Conditions hydrogenation, the culture tube that contained the reaction solution was broken, and a ca. 1 × 1 piece of the glass that was coated with black solid was analyzed by XPS. The spectrum was collected using a Physical Electronics (PHI) Model 5800XPS system equipped with a monochromator (Al Kα source, $h\nu$ = 1486.8 eV; system pressure $\leq 5 \times 10^{-9}$ Torr = 6.7×10^{-7} Pa) and a hemispherical analyzer to detect the ejected photons. The binding energies were compared to the literature values[28] (given in parentheses) and confirmed that the solid is in fact Pt^0: 521 eV ($4p_{3/2}$, 520 eV), 332 eV ($4d_{3/2}$, 332 eV), 313 eV ($4d_{5/2}$, 315 eV), 74.2 eV ($4f_{5/2}$, 74 eV), 70.8 eV ($4f_{7/2}$, 71 eV).

Hg^0 poisoning experiment starting with Pt^{II}(1,5-COD)Cl_2

This experiment was performed with attention to the need for a large excess of Hg^0, and good stirring to ensure contact of the Hg^0 with the *preformed*, active catalyst, as described elsewhere.[1,5] A Standard Conditions hydrogenation was started with Pt^{II}(1,5-COD)Cl_2 and Proton Sponge; efficient stirring was achieved (~800 rpm). The reaction was stopped after the system lost ~8 psi H_2 (~30% completion of cyclohexene hydrogenation); the Fischer–Porter bottle was then vented, sealed and taken into the drybox. The culture tube was removed from the bottle and 0.272 g Hg^0 (1.4 mmol, ~340 equivalents versus Pt) was added to the reaction solution. The culture tube was returned to the Fischer–Porter bottle which was then sealed, brought out of the drybox, and reconnected to the hydrogenation apparatus. The bottle was purged with H_2 as before, and data acquisition was continued. The results are shown in Figure 4.4.

Hydrogenation of Pt^{II}(1,5-COD)$(CH_3)_2$ without, then with, $Ir^0_{\sim 300}$ seeds

Hydrogenation of Pt^{II}(1,5-COD)$(CH_3)_2$ in the absence of $Ir^0_{\sim 300}$ seeds was attempted as described above for Pt^{II}(1,5-COD)Cl_2, except 1.2 mg Pt^{II}(1,5-COD)$(CH_3)_2$ (3.6 μmol) was used instead of Pt^{II}(1,5-COD)Cl_2. The complex was inert to H_2 under 3.7 atm H_2 at 22.0 ± 0.01°C over 24 h.

To show that this was a problem of a lack of Pt^0 or other metal^0 catalyst, hydrogenation of Pt^{II}(1,5-COD)$(CH_3)_2$ in the presence of $Ir^0_{\sim 300}$ seeds was carried out in the same way, except 0.1 mL of the 0.34 mM $Ir^0_{\sim 300}$ solution was added. This corresponds to 1.0% Ir^0 versus Pt. The volume of acetone added was decreased to 2.4 mL to keep the total volume of the reaction solution at 3.0 mL. Ready hydrogenation was seen as described below.

Hg^0 poisoning experiment starting with $Ir^0_{\sim 300}$-seeded Pt^{II}(1,5-COD)$(CH_3)_2$

This experiment was performed as described above for the Hg^0 poisoning of the Pt^{II}(1,5-COD)Cl_2 system (*vide supra*), except that hydrogenation of Pt^{II}(1,5-COD)$(CH_3)_2$ was started in the presence of 1.0% $Ir^0_{\sim 300}$ nanoclusters. After the reaction reached ~30% completion (as judged by H_2 pressure loss), 0.246 g Hg^0 was added (1.2 mmol, ~340 equivalents versus Pt) with vigorous stirring using the same procedure as that described above.

Results and discussion

Reduction of $Pt^{II}(1,5\text{-COD})Cl_2$ by dihydrogen in the presence of base to give Pt^0 nanoclusters and then bulk Pt^0 metal—product studies

The reduction of $Pt^{II}(1,5\text{-COD})Cl_2$ under H_2 in the presence of two equivalents of Proton Sponge is shown in eq 4.1; the kinetic curve for the concomitant cyclohexene hydrogenation is shown in Figure 4.2. After a ~7 h induction period, Figure 4.2, the originally clear and colorless reaction solution turns grey and then black; within 5–10 min after that, a black solid precipitates out of the solution. Transmission electron microscopy of the solution just after the induction period (i.e., at ~7 h in Figure 4.2) showed the presence of 28 ± 9 Å nanoclusters (300 particles counted), along with nanocluster agglomerates measuring 340 ± 80 Å, Figure 4.3. At the end of the reaction (i.e., when H_2 loss stopped indicating that cyclohexene loss was completed), XPS analysis of the black solid verified that it was Pt^0. Bulk Pt^0 metal is, of course, known to be an active hydrogenation catalyst.[8,20,21] In separate experiments performed previously,[21] the loss of $Pt^{II}(1,5\text{-COD})Cl_2$ in the reaction solution was followed by ^1H NMR and the evolution of cyclooctane from the 1,5-COD ligand was followed by GLC methods and results which verify the stoichiometry given in eq 4.1a.

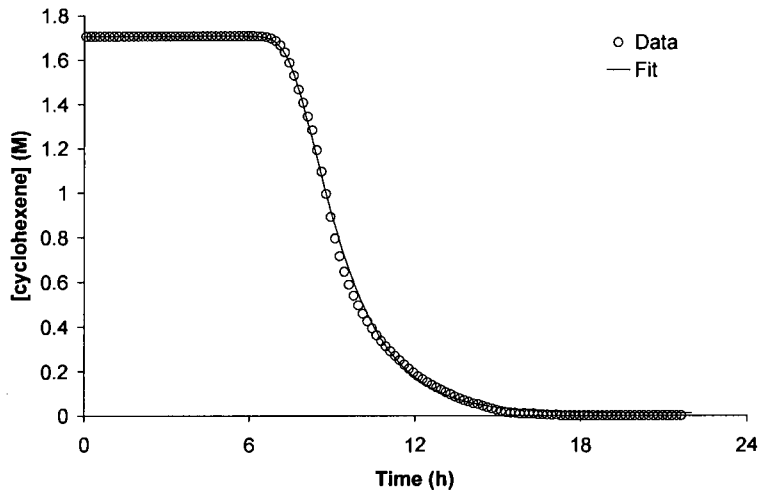

Figure 4.2. Kinetic curve for the reduction of $Pt^{II}(1,5\text{-COD})Cl_2$ and concomitant cyclohexene hydrogenation. The curve fit is to the four-step, double autocatalytic mechanism given in Scheme 4.1 (*vide infra*); the following rate constants result: $k_1 \approx 1 \times 10^{-7}\ h^{-1}$; $k_2 \approx 1.6 \times 10^{3}\ M^{-1}\ h^{-1}$; $k_3 \approx 1.7 \times 10^{2}\ M^{-1}\ h^{-1}$; $k_4 \approx 9.1 \times 10^{2}\ M^{-1}\ h^{-1}$; residual = 0.010.

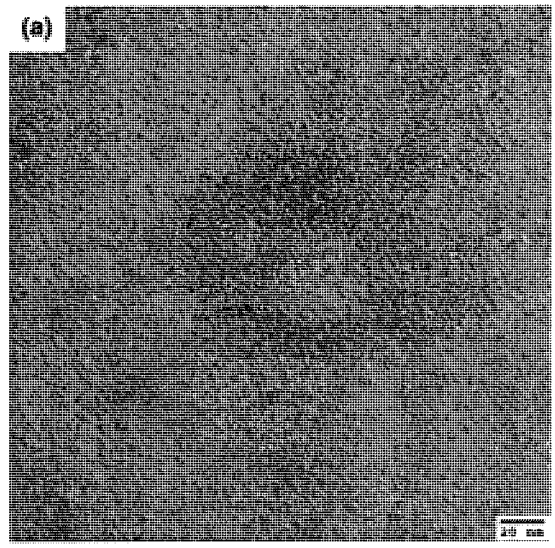

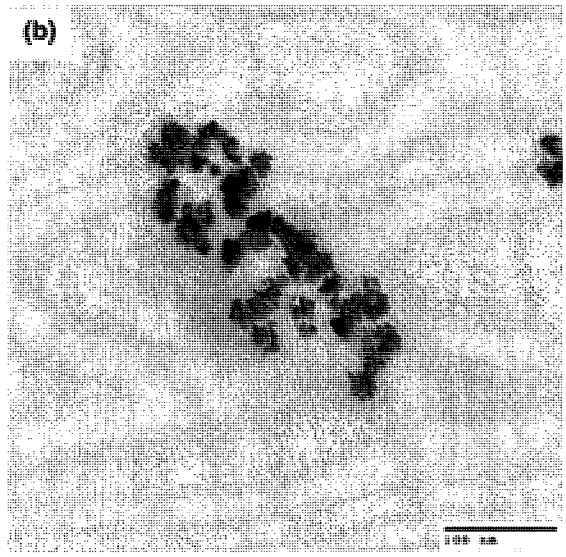

Figure 4.3. Typical TEM images of the same reaction solution taken just after the induction period showing both (a) 28 ± 9 Å nanoclusters and (b) 340 ± 80 Å agglomerates of the nanoclusters.

Kinetic evidence for heterogeneous Pt^0 catalysis

In two recent publications, the discovery was presented of the 4-step mechanism for the reduction of transition-metal salts under H_2, Scheme 4.1.[20,21] In Scheme 4.1, A is a precatalyst (in this case, $Pt^{II}(1,5\text{-COD})Cl_2$), B is a nanocluster ($Pt_n^0$ herein), and C is larger, bulk-metal-like Pt^0 particles, Pt_m^0 ($m >> n$).

Scheme 4.1.

$$A \xrightarrow{k_1} B$$

$$A+B \xrightarrow{k_2} 2B$$

$$B+B \xrightarrow{k_3} C$$

$$B+C \xrightarrow{k_4} 1.5C$$

The excellent curve-fit of the kinetic data in Figure 4.2 to the mechanism in Scheme 4.1 was only accomplished if C, *the bulk-metal-like Pt^0 particles*, are the catalyst for cyclohexene hydrogenation, not the smaller nanoclusters, B.[20,21] These kinetics, along with the product studies showing the formation of nanoclusters and bulk metal at the point that the catalyst becomes active, are as strong a single piece of evidence as is possible that heterogeneous Pt^0, not homogeneous Pt^{II}, is the true hydrogenation catalyst. Note that if $Pt^{II}(1,5\text{-COD})Cl_2$ was the true hydrogenation catalyst, then H_2 loss should have begun immediately, without an induction period. This is obviously not the case, as Figure 4.2 attests. In fact, ~7 h passed before hydrogenation began in Figure 4.2. This is additional strong evidence that $Pt^{II}(1,5\text{-COD})Cl_2$ (A in Scheme 4.1) is not the true hydrogenation catalyst; as the A→B, A+B→2B equations in Scheme 4.1 (and curve-fit to this scheme in Figure 4.2) show, A must react to form B and C, Scheme 4.1, before catalysis can ensue. The kinetics demand that A ($Pt^{II}(1,5\text{-COD})Cl_2$) is *not* the hydrogenation catalyst.

Hg^0 poisoning evidence for heterogeneous Pt^0 catalyst

A valuable test of metal^0 catalysis is the Hg^0 poisoning test.[1,29] Hg^0 poisons metal^0 catalysts by forming an amalgam with the metal and/or adsorbing onto the metal surface.[1,19] Keys to the reliable use of this test are: (i) a large excess of Hg^0, (ii) good stirring so the Hg^0 contacts the catalyst, and (iii) being sure that the Hg^0 is added to the *preformed*, active catalyst[1,5] so as to avoid artifacts due to not allowing the metal^0 catalyst to be formed prior to adding Hg^0.[7,29]

The Hg^0 poisoning experiment was started as a Standard Conditions hydrogenation experiment. When the reaction was approximately one-third complete

(as judged from H_2 pressure loss), ~340 equivalents of Hg^0 versus Pt was added with good stirring (~800 rpm). As shown above, Pt_n^0 nanoclusters are formed in this reaction immediately at the end of the induction period, and then agglomerate into bulk Pt^0 metal. The addition of Hg^0, Figure 4.4, completely halted all catalytic activities, consistent with (only) heterogeneous catalysis, results which also verify our preliminary Hg^0 poisoning experiment reported earlier.[20] This Hg^0 experiment therefore confirms that all of the active catalyst is heterogeneous Pt_n^0, rather than homogeneous Pt^{II}.

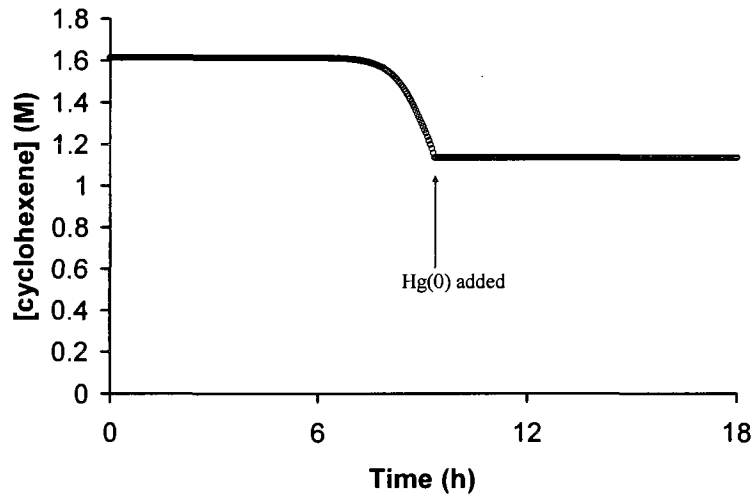

Figure 4.4. Plot of cyclohexene concentration versus time in a Hg^0 poisoning of the $Pt^{II}(1,5\text{-COD})Cl_2$ system. When ~340 equivalents of Hg^0 were added at ~9.5 h (~30% completion), no further cyclohexene hydrogenation ($\leq$0.01 psi over 15 h, or $\leq 7 \times 10^{-4}$ psi H_2/h) was observed.

Further evidence that >99.98% of the catalysis is heterogeneous Pt_n^0

Data from the Hg^0 poisoning experiment, Figure 4.4, allow us to estimate an upper limit to the extent of catalysis by Pt^{II}. Within the ±0.01 psig precision of our pressure transducer, *no* H_2 is lost over ~15 h after the Hg^0 is added, corresponding to

a *maximum* rate of hydrogenation of $\leq 7 \times 10^{-4}$ psi H_2/h after the Hg^0 was added versus a rate of ~3.2 psi H_2/h before. This means that $\leq (7 \times 10^{-4}/3.2 \times 100)$ or $\leq 0.02\%$ of the catalysis can be by Pt^{II}. Restated, $\geq 99.98\%$ of the catalysis is by Hg^0 poisonable Pt_n^0.

Emphasis that the true mechanism must account for all of the data

One of the key principles of mechanistic studies, as well as the methodology used herein as detailed in Figure 4.1, is that the correct description of the mechanism and the catalyst must be consistent with *all* of the data.[3] In the case of hydrogenation with $Pt^{II}(1,5\text{-COD})Cl_2$, we now have product, TEM, XPS, GLC,[21] NMR,[21] kinetic, and Hg^0 poisoning data that is all consistent with a heterogeneous, Pt^0 catalyst with a $\leq 0.02\%$ contribution by a homogeneous Pt^{II} catalyst. There is also the literature evidence, noted in the Introduction, that homogeneous Pt catalysis is rare and takes place only when strong ligands such as phosphines are coordinated to the platinum, or when a tin cocatalyst is used.[2,13] Indeed, even in those cases, the main alternative hypothesis—namely that the true catalyst is heterogeneous Pt_n^0—remains to be disproved. In short, all of the available data strongly supports Pt^0 metal as the true catalyst derived from $Pt^{II}(1,5\text{-COD})Cl_2$ under H_2.

The case of $Pt^{II}(1,5\text{-COD})(CH_3)_2$: does this methylated precursor also lead to heterogeneous catalysis?

Reduction of $Pt^{II}(1,5\text{-COD})(CH_3)_2$ under 40 psig of hydrogen under our Standard Conditions of 3.7 atm H_2 at 22.0 ± 0.1 °C was unsuccessful over 24 h, Figure 4.5, squares; this is, as expected, in full agreement with Whitesides' observations.[17] However, when preformed and isolated polyoxoanion-stabilized $Ir_{\sim 300}^0$

nanoclusters[3] were added to the reaction solution as nanocluster nucleation seeds, $Pt^{II}(1,5\text{-COD})(CH_3)_2$ was rapidly reduced to what should be $Ir^0_{\sim 300}$ core/ Pt^0_n shell nanoclusters which then agglomerated to nominally Pt^0 metal, Figure 4.5, circles. In addition, the kinetics are well-fit by the A→B, A+B→2B two-step mechanism of nanocluster formation as shown in Figure 4.5, now prima facie evidence[1] that M^0_n (Pt^0_n in this case) nanoclusters are the true catalysts.

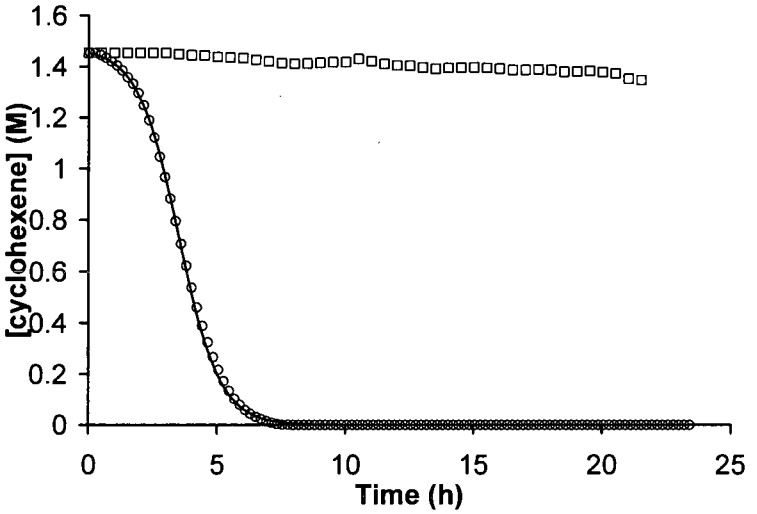

Figure 4.5. Kinetic curves for the hydrogenation of $Pt^{II}(1,5\text{-COD})(CH_3)_2$ with two equivalents of Proton Sponge (squares; the upper, flat curve) and then with two equivalents of Proton Sponge and 1.0% added $Ir^0_{\sim 300}$ seeds (circles; the lower, sigmoidal curve). The latter curve is fit to the autocatalytic A→B, A+B→2B mechanism with the following rate constants: $k_1 = 1.6(1) \times 10^{-2}\ h^{-1}$; $k_2 = 1.18(1) \times 10^3\ M^{-1}\ h^{-1}$.

In addition, a Hg^0 poisoning experiment on the $Ir^0_{\sim 300}$ seeded system showed the same behavior as the $Pt^{II}(1,5\text{-COD})Cl_2$ system: the addition of Hg^0 *completely halted* catalytic activity, Figure 4.6. These results (i) confirm the observation made by Whitesides, that $Pt^{II}(1,5\text{-COD})(CH_3)_2$ does not nucleate homogeneously, and also (ii) show that $Pt^{II}(1,5\text{-COD})(CH_3)_2$ alone is not a good hydrogenation catalyst nor even a

good catalyst precursor. The findings then: (iii) lend support to the more general finding that $Pt^{II}(1,5\text{-COD})X_2$ complexes (X = halogens, alkyls) are precatalysts to heterogeneous Pt^0_n catalysts.

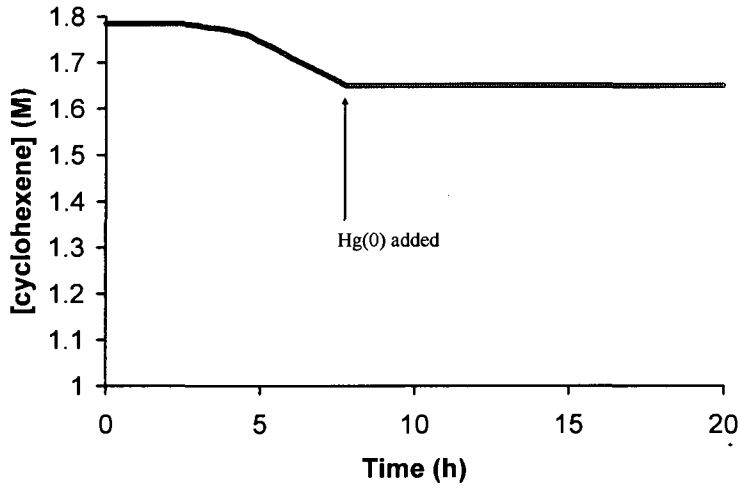

Figure 4.6. Plot of cyclohexene concentration versus time in a Hg^0 poisoning of the 1.0% $Ir^0_{\sim 300}$-seeded $Pt^{II}(1,5\text{-COD})(CH_3)_2$ system. When ~340 equivalents of Hg^0 were added at ~8 h (~30% completion), no further cyclohexene hydrogenation (≤0.01 psi over 15 h, or $\leq 7 \times 10^{-4}$ psi H_2/h) was observed, corresponding to ≥98% catalysis by heterogeneous Pt^0_n.

Conclusions

We have presented strong, we believe compelling evidence that hydrogenation reactions beginning with $Pt^{II}(1,5\text{-COD})Cl_2$ precatalysts are actually forming Pt^0_n under H_2 as the true catalyst. We have provided product, TEM and XPS spectroscopic, kinetic, and Hg^0 poisoning evidence that $Pt^{II}(1,5\text{-COD})Cl_2$ (A in Scheme 4.1) is not a hydrogenation catalyst; instead, this Pt^{II} precatalyst must be reduced to Pt^0 (B and C in Scheme 4.1) before hydrogenation can take place. A limit on the amount of Pt^{II} catalysis of ≤0.02% was provided; moreover, there is no positive evidence for any Pt^{II} hydrogenation catalytic activity. The present study has also confirmed that the

dimethyl complex $Pt^{II}(1,5\text{-COD})(CH_3)_2$ cannot be reduced in the absence of a heterogeneous catalyst; however, on the addition of a heterogeneous metal catalyst (bulk Pt^0 in Whitesides' work[16] or $Ir^0_{\sim 300}$ seeds in the present study), this precatalyst is readily hydrogenated to give bulk Pt^0 metal as the true catalyst.

These observations confirm the observation made over 30 years ago that homogeneous hydrogenations beginning with Pt^{II} often result in the formation of bulk Pt^0 metal.[2] These observations, along with the reducing conditions given in the literature for reactions that use $Pt^{II}(1,5\text{-COD})Cl_2$ as a catalyst, also strongly suggest that Pt^0 nanoclusters or bulk metal should be considered as the true catalyst whenever these systems are placed under H_2.

Acknowledgement

Financial support from DOE Grant DE-FG02-03ER15453 is gratefully acknowledged.

Appendix 4A

A look at the literature of $Pt^{II}(1,5\text{-COD})Cl_2$ and $Pt^{0}(1,5\text{-COD})_2$ hydrosilylation catalysis – Is it homogeneous or heterogeneous catalysis?

In 1986, Lewis et al. at General Electric proposed that the true hydrosilylation catalyst in systems using $Pt^{II}(1,5\text{-COD})Cl_2$ or $Pt^{0}(1,5\text{-COD})_2$ is actually Pt^0 colloids; that is, that the hydrosilylation is heterogeneous rather than homogeneous.[30] They concluded that the addition of silane to the Pt complexes causes colloid formation. Their evidence was: (i) that an induction period is observed before the reaction begins, indicating that the original complex is *not* the catalyst; (ii) that transmission electron microscopy and dynamic light scattering showed the presence of clusters; (iii) that the activity of the catalyst is "too high to be considered homogeneous"; (iv) that in the absence of conditions that caused colloid formation (i.e., silane addition), the precursor complexes are inactive for hydrosilylation; and (v) that addition of Hg^0 to the complexes *before* addition of silane prevents catalytic activity (this last experiment was done incorrectly, however, as the Hg^0 was added *before* the active catalyst was formed, not after, as it should have been[1,7]). Several subsequent reports have used $Pt^{II}(1,5\text{-COD})Cl_2$ as a hydrosilylation catalyst;[31] none of these reports makes any mention of the catalyst being heterogeneous (colloidal Pt^0).

Then in 1999, another study, also from General Electric, reported that the hydrosilylation reaction is actually *homogeneous*, that is, that the active catalyst is a mononuclear Pt complex.[32] However, this report studied a *different* Pt complex than $Pt^{II}(1,5\text{-COD})Cl_2$, namely Karstedt's complex. (In 1996, a report appeared describing colloids derived from Karstedt's complex in hydrosilylation reactions.[33])

Karstedt's complex

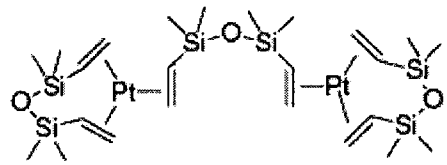

Their evidence for homogeneous catalysis was mainly speculative, specifically: (i) that the mononuclear Pt mechanism "is comprised of elementary steps well-known in organometallic chemistry"; this implies that the colloid mechanism does *not* include similar steps and, therefore, could be rejected; (ii) that studies of the reactivities of different silanes suggested that during the induction period, the silyl ligands of Karstedt's catalyst undergo hydrosilylation and/or ligand exchange (an analogous argument may or may not explain the induction periods seen with Pt^{II}(1,5-COD)Cl_2 and Pt^0(1,5-COD)$_2$); (iii) that the addition of Hg^0 did *not* inhibit catalytic activity (in this experiment, however, the Hg^0 was added and then removed *before* the hydrosilylation reaction was started, meaning that this experiment was performed incorrectly in that the Hg^0 not added the *preformed, active catalyst*; incorrectly performing this experiment continues to cause errors in the literature[6,29]); (iv) that EXAFS studies determined that "the bulk of the platinum exists as a mononuclear species during the hydrosilylation reaction" (such data have also been recently shown to often be misleading regarding the nature of the *true* catalyst, as a small amount of heterogeneous catalyst could be performing all of the chemistry[5,7]—"catalysis is a wholly kinetic phenomenon"[34] so that knowing both where the mass of the precatalyst, and the *kinetic contribution of each form*, is key); (v) that TEM of the

Karstedt's complex resulted in the formation of clusters (again, a different complex was used in this study, so the results cannot be extended to $Pt^{II}(1,5\text{-COD})Cl_2$ used in the original study); and (vi) that colloids were observed visually only at the end of the hydrosilylation reaction (no spectroscopic studies are reported, however, so this visual evidence is weak at best). Again and most importantly, *the key kinetic evidence required to identify the true catalyst[1] is lacking in both this study[32] and the original work.*[30]

The bottom line here is that given the compelling evidence in the present work that $Pt^{II}(1,5\text{-COD})Cl_2$ forms a heterogeneous, Pt^0_n catalyst for hydrogenation, the possibility that $Pt^{II}(1,5\text{-COD})Cl_2$ is a precatalyst to Pt^0_n nanoclusters and bulk metal in the hydrosilylation reaction must be reconsidered in depth and using the methodology given in Figure 4.1 which emphasizes full product studies and *kinetic evidence*; such studies remain to be done. However, the effects of trace O_2,[35] the differences due to the use of different silanes[36] (and the well-known result that changing reaction conditions can have a dramatic effect on the mechanisms of reactions involving transition metals[37]), as well as other variables of the Pt-based hydrosilylation catalysis promise to make the needed studies challenging and worth their own separate report.

References

[1] Widegren, J. A.; Finke, R. G. *J. Mol. Catal. A* **2003**, *198*, 317.

[2] James, B. R. *Homogeneous Hydrogenation*; Wiley–Interscience, New York, 1973.

[3] Lin, Y.; Finke, R. G. *Inorg. Chem.* **1994**, *33*, 4891.

[4] Weddle, K. S.; Aiken, J. D., III, Finke, R. G. *J. Am. Chem. Soc.* **1998**, *120*, 5653.

[5] Widegren, J. A.; Bennett, M. A.; Finke, R. G. *J. Am. Chem. Soc.* **2003**, *125*, 10301.

[6] Hagen, C. M.; Widegren, J. A.; Maitlis, P. M.; Finke, R. G. *J. Am. Chem. Soc.* **2005**, *127*, 4423.

[7] Hagen, C. M.; Vieille-Petit, L.; Laurenczy, G.; Süss-Fink, G.; Finke, R. G. *Organometallics* **2005**, *24*, 1819.

[8] Rylander, P. N. *Catalytic Hydrogenation Over Platinum Metals*; Academic Press: New York, 1967.

[9] Creighton, J. A.; Eadon, D. G. *J. Chem. Soc., Faraday Trans.* **1991**, *87*, 3881.

[10] Caseri, W.; Pregosin, P. S. *Organometallics* **1988**, *7*, 1373.

[11] Bailar, J. C., Jr.; Itatani, H. *J. Am. Chem. Soc.* **1967** *89*, 1592.

[12] Cramer, R. D.; Jenner, E. L.; Lindsey, R. V., Jr.; Stolberg, U. G. *J. Am. Chem. Soc.* **1963** *85*, 1691.

[13] Chaloner, P. A.; Esteruelas, M. A., Joó, F.; Oro, L. A. *Homogeneous Hydrogenation*; Kluwer Academic Publishers: Boston, 1994.

[14] Platt, J. R. *Science* **1964** *146*, 347.

[15] Reetz, M. T.; Frömbgen, C. *Synthesis* **1999**, *9*, 1555.

[16] Lee, T. R.; Whitesides, G. M. *Acc. Chem. Res.* **1992** *25*, 266, and references therein.

[17] Miller, T. M.; Izumi, A. N.; Shih, Y.-S.; Whitesides, G. M. *J. Am. Chem. Soc.* **1988**, *110*, 3146.

[18] McCarthy, T. J.; Shih, Y.-S.; Whitesides, G. M. *Proc. Natl. Acad. Sci. USA* **1981**, *78*, 4649.

[19] Whitesides, G. M.; Hackett, M.; Brainard, R. L.; Lavalleye, J.-P.; Sowinski, A. F.; Izumi, A. N.; Moore, S. S.; Brown, D. W.; Staudt, E. M. *Organometallics* **1985**, *4*, 1819.

[20] Besson, C.; Finney, E. E.; Finke, R. G. *J. Am. Chem. Soc.* **2005**, *127*, 8179.

[21] Besson, C.; Finney, E. E.; Finke, R. G. *Chem. Mater.* **2005**, *17*, 4925.

[22] (a) Moiseev, I. I.; Vargaftik, M. N. *New J. Chem.* **1998**, 1217. (b) Davies, I. W.; Matty, L.; Hughes, D. L.; Reider, P. J. *J. Am. Chem. Soc.* **2001** *123*, 10139. (c) Reetz, M. T.; Westermann, E. *Angew. Chem. Int. Ed.* **2000**, *39*, 165.

[23] Aiken, J. D., III; Finke, R. G. *J. Am. Chem. Soc.* **1998**, *120*, 9545.

[24] Widegren, J. A.; Aiken, J. D., III; Özkar, S.; Finke, R. G. *Chem. Mater.* **2001**, *13*, 312.

[25] Watzky, M. A.; Finke, R. G. *J. Am. Chem. Soc.* **1997**, *119*, 10382.

[26] Leipold, W. S., III. Available from: http://members.dca.net/leipold/mk/advert.html.

[27] Jaska, C. A.; Manners, I. *J. Am. Chem. Soc.* **2004**, *126*, 9776.

[28] Moulder, J. F.; Stickle, W. F.; Sobol, P. E.; Bomben, K. D. *Handbook of X-ray Photoelectron Spectroscopy*; Physical Electronics, Inc.: Eden Prairie, MN, 1995.

[29] Süss-Fink, G.; Faure, M.; Ward, T. R. *Angew. Chem., Int. Ed.* **2002**, *41*, 99.

[30] Lewis, L. N.; Lewis, N. *J. Am. Chem. Soc.* **1986**, *108*, 7228.

[31] (a) Heldmann, D. K.; Stohrer, J.; Zauner, R. *Synthesis* **2002**, *11*, 1919. (b) Effenberger, F.; Wezstein, M. *Synthesis* **2001**, *9*, 1368. (c) Sibi, M. P.; Christensen, J. W. *Tetrahedron Lett.* **1995**, *36*, 6213. (d) Roy, A. K. US Patent 5,567,848, 1996. (e) Kinting, A.; Kreuzfeld, H.-J. *J. Organomet. Chem.* **1989**, *370*, 343.

[32] Stein, J.; Lewis, L. N.; Gao, Y.; Scott, R. A. *J. Am. Chem. Soc.* **1999**, *121*, 3693.

[33] Ketelson, H. A.; Brook, M. A.; Pelton, R.; Heng, Y. M. *Chem. Mater.* **1996**, *8*, 2195.

[34] (a) Halpern, J. *Inorg. Chim. Acta* **1981**, *50*, 11. (b) Halpern, J.; Okamoto, T.; Zakhariev, A. *J. Mol. Catal.* **1977**, *2*, 65.

[35] Lewis, L. N. *J. Am. Chem. Soc.* **1990**, *112*, 5998.

[36] Amako, M.; Schinkel, J.; Freiburger, L.; Brook, M. A. *Dalton Trans.* **2005**, 74.

[37] Nappa, M. J.; Santi, R.; Halpern, J. *Organometallics* **1985**, *4*, 34.

CHAPTER V

IS THERE A MINIMAL CHEMICAL MECHANISM UNDERLYING CLASSICAL AVRAMI-EROFE'EV TREATMENTS OF PHASE TRANSFORMATION KINETIC DATA?

This dissertation chapter contains the manuscript of a paper submitted for publication which describes the discovery that the Finke-Watzky 2-step mechanism developed for the formation of transition-metal nanoclusters in solution can fit kinetic data for solid-state phase transitions that are classically fit using the Avrami-Erofe'ev equation. This chapter also shows that the Avrami-Erofe'ev equation can fit kinetic data for the formation of transition-metal nanoclusters. Fitting several literature solid-state phase transition data sets and mathematical analysis suggests that the two models describe the same underlying mechanism of nucleation and autocatalytic growth. The findings lend support to the hypothesis that the mechanism first used to describe nanocluster formation has a broader applicability and generality in nature.

Analysis of the data was performed by E.E.F. The manuscript was prepared by E.E.F. with assistance and multiple rounds of edits by R.G.F.

Abstract

We report herein our efforts to see if there is not a minimal chemical mechanism that can provide statistically equivalent fits to solid-state and other phase-transformation kinetic data classically treated by the Avrami-Erofe'ev (A-E) kinetic model or its derivatives. Doing so is an important, missing piece of attempts to fit and draw chemical insight from solid-state kinetics, as made apparent by citations and quotations from the literature which detail the presently confused state of solid-state kinetics and, especially, what those kinetics mean in terms of the underlying chemical mechanism(s). Specifically, we test herein if the one available, *minimalistic, chemical-mechanism-based* kinetic model, a model originally developed for transition-metal nanocluster nucleation and growth in solution, A→B (rate constant k_1) then A+B→2B (rate constant k_2). The 2-step model tested is able to fit solid-state phase transformation kinetic data equally well in comparison to fits obtained using the classic A-E equation from the 1940s. Statistically, it is found that while the A-E equation is statistically significantly superior for 4 of 12 literature data sets examine, the 2-step chemical mechanism-based model (known as the Finke-Watzky (F-W) model) is statistically significantly better for 2 of those 12 data sets, and the models give arguably indistinguishable fits within experimental error to the other 6 data sets. The results provide credence to the hypothesis that the two models can be viewed as different descriptions of the same underlying chemical and physical processes. Given the evidence that the chemical-mechanism-based 2-step model provides equivalent (to sometimes better) fits within experimental error in 8 of the 12 cases examined, the A-E and integrated F-W equations were then mathematically equated to see if this provides any insights into the long-standing question of the physical meaning of the A-E

parameters k and n. The math reveals that the A-E parameters k and n can be viewed as containing a complex convolution of the F-W chemical rate constants k_1 and k_2' (where $k_2' = k_2[A]_0$ of the F-W model)—at least under the experimentally supported assumption that the A-E and F-W equations are somehow equivalent. Simulated A-E data for selected values of A-E parameters k and n (that give representative sigmoidal kinetic curves), followed by fits of those simulated curves to the F-W model and then plotting the resultant F-W k_1 and k_2' rate constants as a function of the A-E k and n variables, provides additional interesting evidence that the A-E k and n and F-W k_1 and k_2' can be viewed as complex convolutions of one another. Specifically, k from this treatment appears as a convolution of k_1, k_2' and n (as well as time, t) and n as a convolution of k_1, k_2' and k (as well as t). A discussion of the advantages and limitations of each model is presented followed by a summary of the conclusions from the present studies. The significance of the results is two-fold: (i) there is now an experimentally supported way to deconvolute an average nucleation, k_1, from an average autocatalytic growth, k_2, rate constant from solid-state kinetic data and, importantly, (ii) there now are experimentally supported and rigorously defined words / concepts that can be used to support the discussion of those rate constants in terms of the underlying physical processes, namely "nucleation" and "autocatalytic growth". These are not trivial results in light of concepts such as "autocatalytic nucleation" that continue to be used without adequate experimental support and which, therefore, continue to cause confusion in the solid-state kinetics literature. A section listing important caveats to this work apparent from examining the solid-state kinetic literature, plus a look ahead to needed future work, are also briefly presented.

Introduction

We report herein our search to see if here is not a minimal chemical mechanism that can give equivalent fits to, and therefore by all appearances could be viewed to underlie, solid-state kinetic data traditionally fit by the Avrami-Erofe'ev (A-E) equation (see Table 5S.1 of the Supporting Information for a historical tabulation of the A-E equation, eq 5.1,[1] and its more than 13 variants).[2,3,4]

$$\ln(1-\alpha) = -(kt)^n \tag{5.1}$$

The chemical-mechanism-based, minimalistic kinetic model that we have examined is the Finke-Watzky (hereafter F-W) 2-step kinetic scheme consisting of nucleation followed by autocatalytic growth, Scheme 5.1.[5,6,7,8]

Scheme 5.1. The Finke-Watzky 2-step kinetic model of nucleation (k_1) and autocatalytic growth (k_2).[5]

$$A \xrightarrow{k_1} B$$

$$A+B \xrightarrow{k_2} 2B$$

We also look at the mathematical relationship between the A-E and F-W treatments to see if the A-E parameters k and n can be expressed and thus at least conceivably understood somewhat better (or at least differently) in terms of the F-W rate constants for nucleation (k_1) and autocatalytic growth (k_2), Scheme 5.1 (or actually $k_2'=k_2[A]_0$, *vide infra*). This is of some significance since A-E treatments often talk of "nucleation and growth", but *contain only a single rate parameter, k*, a practice that causes considerable confusion,[2,3,4] a confusion that originally drew us to this problem: *how is it possible to talk about 2 chemical processes with only 1 rate constant? Something must be amiss here!?* Simulations of kinetic data generated by the A-E equation for selected k and n

values that give sigmoidal curves, followed by fitting those simulated curves with the F-W model, are also employed to gain possible insight into the relationship between the A-E parameters k and n in terms of the F-W k_1 and k_2' rate constants. We also briefly discuss the plus/minus features of both the A-E and F-W treatments, and look ahead to possible new, future directions that the present findings might allow. Caveats in the present work that are apparent from examination of the complicated, sometimes confusing, and often controversial area solid-state kinetics[1c,9] are also provided and briefly discussed.

The potential significance of attempts such as the present work to bring more chemical mechanism to solid-state kinetics is presaged by Galweys' insightful comments[1c] illustrating the confusion that exists at present in the area of at least non-isothermal solid-state reaction kinetics. Notable are his points: that chemical reaction mechanisms are too often missing, that "the consideration of alternative possibilities (i.e., mechanisms) is frequently ignored...", or even that the term "mechanism" has lost its original and rigorous meaning in the area of solid-state thermal analysis kinetics.[1c] Galwey has also noted in a 2008 review (see p. 981) that it is important for kinetic investigations of solid-state reactions to be able to "distinguish... the roles of nucleation and growth"—again we see the problem of the A-E treatment providing only a single rate paratmeter, k. In another classic treatment, Galwey and Brown note that there is a "need for greater emphasis on chemical, rather than *mathematical*, representations"[4c] (i.e., of solid-state reaction kinetics). Brown's introduction in his 1997 paper "Steps in a Minefield. Some Kinetic Aspects of Thermal Analysis", reproduced in a footnote for the

interested reader, is also noteworthy—indeed, Brown's paper and its many insights and telling quotes are a must read for anyone interested in solid-state kinetics.[9]

The results presented herein provide, as their bottom lines and significance, (i) the ability to deconvolute a nucleation from an (autocatalytic) growth rate constant for solid-state kinetic data, and even more significantly (ii) experimental evidence for the use of the words/concepts of nucleation *and* autocatalytic growth in describing the results—both non-trivial accomplishments in the history of solid-state kinetics, so far as we can tell. The results presented herein are also of broader interest beyond solid-state kinetics since sigmoidal-type growth curves are ubiquitous throughout nature,[5,6,7,10,11,12,13] yet it has not proven possible until now to generally deconvolute even an average, *chemical-mechanism-based* nucleation rate constant from an average (autocatalytic, *vide infra*) growth rate constant. Cases where the "Ockham's Razor"-based 2-step F-W kinetic model employed herein has been able to quantitatively fit sigmoidal growth curves, while also deconvoluting (average) nucleation from (average) autocatalytic growth, include (originally) transition-metal nanocluster formation,[5,6,7,11] more recently protein aggregation involved in a wide variety of neurological diseases including Alzheimer's, Parkinson's, Huntington's and prion-based diseases,[10,11,12] and now in solid-state kinetic data.

Experimental

Selection of the Data to Be Fit

We selected several solid-state kinetic studies from the literature, in which the A-E equation or some variation of it was used to fit the data. We digitized the data from the literature using DigitizeIt version 1.5.8. We fit the data from those systems using the A-E

equation and the F-W model, and compared the two to see which, if either, gave a superior fit. Seven of these systems are given in the main text herein, and five additional systems are provided in the Supporting Information. We also fit kinetic data for the formation of $Ir^0_{\sim 300}$ nanoclusters[5] using both the F-W model and the A-E equation to show that both models can fit that data as well, *vide infra*.

Data analysis

The data from the solid-state reactions are typically given in terms of the amount of starting material transformed into product, α, which *increases* with time. In the Avrami equation, then, α also increases with time. The F-W model, in comparison, historically has fit data for the *loss* of concentration of nanocluster precursor, A in Scheme 5.1. The integrated rate equation for the loss of A over time is given in eq 5.2.[5]

$$[A]_t = \frac{\frac{k_1}{k_2} + [A]_0}{1 + \frac{k_1}{k_2[A]_0}\exp[(k_1 + k_2[A]_0)t]} \tag{5.2}$$

In order to compare fits between the F-W model and the A-E equation, eq 5.2 can be converted to a form that expresses α as a function of time, by recognizing that in the F-W model, $\alpha=([A]_0-[A]_t)/[A]_0$. To get eq 5.3, then, we simply set $[A]_t = [A]_0(1-\alpha)$ on the left-hand side of eq 5.2 and then solved the equation for α. Note that in eq 5.3 we have necessarily defined $k_2' = k_2[A]_0$; this removes the concentration dependences from the F-W model as is necessary since concentration is not a useful concept in the solid-state. The resulting eq 5.3 in turn allows the F-W and A-E models to be directly compared.

$$\alpha = 1 - \frac{k_1 + k_2'}{k_2' + k_1\exp[(k_1 + k_2')t]} \tag{5.3}$$

Note that in eq 5.3 the units of k_1 are time^{-1} while the units of $k_2'=k_2[A]_0$ are now also time^{-1} (versus the units in eq 5.2 of the rate constants for nucleation and growth of nanoclusters k_1 and k_2 of time^{-1} and M^{-1}time^{-1}, respectively). In the A-E equation, the parameter n is unitless, while the units of k are time^{-1}.

Non-linear least-squares curve fitting of the data was accomplished using Microcal Origin version 7.0. The data examined herein are fit using eq 5.1 for the A-E equation, and eq 5.3 for the F-W 2-step kinetic model.

Statistical judgment of the quality of the fits was performed for each system in two ways. First, values of R^2, the coefficient of determination, were calculated using eq 5.4.

$$R^2 = 1 - \frac{SS}{SS_{tot}} \tag{5.4}$$

The residual sum-of-squares, SS, is given by $SS = \sum_{i=1}^{N} (y_i - f_i)^2$, where y is the experimental value and f is the value predicted from the model. The total sum-of squares, SS_{tot}, is given by $SS_{tot} = \sum_{i=1}^{N} (y_i - \bar{y})^2$, where $\bar{y}$ is the average of all of the data values. Values of R^2 closer to 1 indicate a closer correlation, and therefore a better fit for the model employed. The other statistical method employed was Akaike's Information Criterion (AIC).[14] This method calculates the probability that one model should be used over another for a given data set. More specifically, we used Akaike's second-order method, eq 5.5, to calculate values of $AICc$ for each model.

$$AICc = N \ln\left(\frac{SS}{N}\right) + 2K + \frac{2K(K+1)}{N\text{-}K\text{-}1} \tag{5.5}$$

In eq 5.5, N is the number of data points, SS is the residual sum-of-squares as defined above, and K is the number of parameters in each model. Because lower SS values correspond to better fits, and because eq 5.5 imposes a positive penalty for a model with more parameters, the model with the lowest value of $AICc$ will be statistically favored. To make this determination more quantitative, one can convert the differences in $AICc$ values to Akaike weights, w (between 0 and 1), eq 5.6, which represents the likelihood (i.e., the relative probability) that a given model is favored.[14]

$$w = \frac{\exp(-\Delta AICc_i/2)}{\sum_{r=1}^{R} \exp(-\Delta AICc_r/2)} \tag{5.6}$$

Here, $\Delta AICc_i = AICc_i - AICc_{min}$, where $AICc_{min}$ is the lowest $AICc$ value. In effect, the Akaike weight is a relative probability that a given model is the best one of those considered by this established statistical approach for model comparisons. One can then construct "Evidence Ratios", ER, from the relative ratios of the w values, and in what follows we will give $ER_{(A\text{-}E/F\text{-}W)}$, the ratio of the A-E w value to the F-W w value.

Note that the use of the exponential in calculating w significantly magnifies any difference in $AICc$ values, making the w value enormously more sensitive to differences in fit quality than the (relatively insensitive) R^2 value. For example, we will see examples in what follows where small differences of *only* $\Delta R^2 = -0.0012$ correspond to a $ER_{(A\text{-}E/F\text{-}W)} \sim 10^{-16}$ in favor of the F-W model, while an *even smaller* $\Delta R^2 = +0.0005$ in another case corresponds to a $ER_{(A\text{-}E/F\text{-}W)} \sim 10^{15}$ in favor of the A-E model. In addition, five of the $ER_{(A\text{-}E/F\text{-}W)}$ values in what follows are between 0.37 and 52, one is 588 and one is 4554. Since we do not believe that w values smaller than $w = 10^{\pm 4}$ are different beyond the experimental error of the data and fits, we have called the seven values of w that are not

at least $w \geq 10^{\pm 4}$ as "equivalent within experimental error". Supporting this (admittedly somewhat arbitrary at present) treatment is our initial experience with *AICc ER* values elsewhere (a relatively rare use of *AICc* for such chemical systems) in which the *ER* values are 10^{-38} to 10^{-184}.[10] That said, much more experience with chemical systems and the *AICc* treatment will be needed before it is known if the above cutoff of "experimentally significantly different $ER_{(A\text{-}E/F\text{-}W)}$ values have $ER \geq 10^{\pm 4}$" is a good versus a poor assumption.

A-E curve simulations followed by fitting with the F-W model in search of the connections between the A-E parameters k and n and the F-W k_1 and k_2'

Kinetic data were simulated using the A-E equation, eq 5.1, in Microsoft Excel. A series of α versus time data were generated, starting with $k = 0.1$ and $n = 3$. The α versus time data were then imported into Origin and fit using the F-W model, eq 5.3, to obtain the corresponding values of k_1 and k_2'. Then, the parameters k and n were varied independently while keeping the other parameter constant to generate new α versus time data, with subsequent fits to the F-W model. Using the data obtained by this method, plots of k_1 and k_2' versus k at constant n, and plots of k_1 and k_2' versus n at constant k, were made. These plots are shown in Figure 5.9.

Results and Discussion

The seven literature systems examined below, along with the five additional systems examined in the Supporting Information, were examined by fitting the data to the A-E equation and also to the F-W model, and then looking at the resulting statistics of the fits as well as simply examining the fits visually to develop an intuition for the quality of the fits and the resultant statistics.

Phase transformation of Bi_3NbO_7

Lacorre et al. studied the transition between the meta-stable cubic and stable tetragonal phases of Bi_3NbO_7; the significance of the tetragonal phase is that it has a higher electronic conductivity than the cubic phase.[15] The transition was carried out at four different temperatures and the kinetics were analyzed by Lacorre et al. using the A-E equation. As is common in the solid-state literature, those authors linearized the fit in the following way: taking the ln of both sides of eq 5.1 gives eq 5.7, so that a plot of ln[-ln(1-α)] versus ln(t) is a straight line with slope n and intercept $n$ln(-k). The plot was approximately linear for $0.05 \leq \alpha \leq 0.90$. For the transformation at 840 °C, the A-E parameters obtained were $n = 2.60$ and $k = 5.66 \times 10^{-5}$ min^{-1}.

$$\ln[-\ln(1-\alpha)] = n\ln(k) + n\ln(t) \tag{5.7}$$

When we fit the entire sigmoidal data set, without linearization of it, we obtained the curve and the A-E parameters given in Figure 5.1, $n = 2.91(7)$ and $k = 0.00346(2)$ min^{-1}. Note the value that we obtained for n is close to that obtained from the linearized data, but the values of k are different by more than 10^2. This shows the significance of fitting the *entire* data set, and not just the data that can be linearized. (Of course, and since non-linear least squares is now readily available, one never wants to take a highly non-linear, sigmoidal curve and analyze it by a linearized function.) Fitting the same data using the F-W model gives the fit and rate constants also shown in Figure 5.1, $k_1 = 2.6(2) \times 10^{-4}$ min^{-1} and $k_2' = 0.0160(5)$ min^{-1}. The statistics of the fits, given in Table 5.1, shows that the A-E equation and the F-W model give essentially equal fits within experimental error (i.e., the A-E equation is "preferred" only by an almost surely truly insignificant

factor of 2.5). That is, the A-E and F-W models are equivalent for the purposes of fitting the data in Figure 5.1.

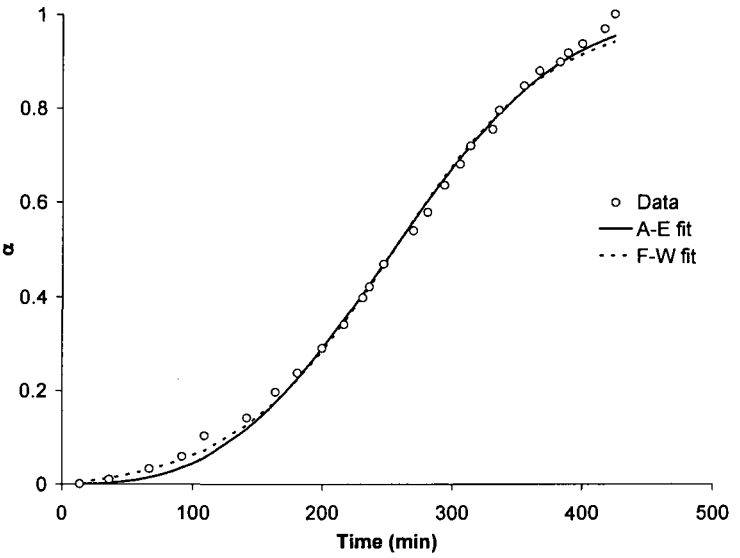

Figure 5.1. Kinetic data for the cubic and tetragonal phases of Bi_3NbO_7, with fits to the A-E equation (with $n = 2.91(7)$ and $k = 0.00346(2)$ min^{-1}) and to the F-W model (with $k_1 = 2.6(2) \times 10^{-4}$ min^{-1} and $k_2' = 0.0160(5)$ min^{-1}). The statistics of the fits are given in Table 5.1.

Crystallization of $Zr_{55}Cu_{30}Al_{10}Ni_5$

Liu et al. reported a study of the kinetics of the crystallization of bulk amorphous $Zr_{55}Cu_{30}Al_{10}Ni_5$, which follows sigmoidal-like kinetics.[16] For seven different temperatures between 466 °C and 480 °C, kinetic data were linearized and fit to the A-E equation. We chose the data taken at 470 °C for comparison between the linearized A-E fit, the full sigmoidal data A-E fit, and the F-W fit. For the linearized data, $n = 3.05$ and $k = 0.42$ min^{-1}.

When we fit the sigmoidal data to the A-E equation, we obtained the parameters $n = 6.57(7)$ and $k = 0.2223(3)$ min^{-1}, Figure 5.2, which are quite different from the parameters obtained from the linearized fit. We also fit the data to the F-W model, Figure

5.2, and obtained the rate constants k_1 = 1.54(9) × 10^{-4} $min^{-1}$and k_2' = 2.27(1) min^{-1}. For this system, the F-W model is statistically preferred over the A-E equation by what is interpreted as a significant factor of ~ 1 × 10^{16}, Table 5.1, and even though the ΔR^2 (= $R^2_{(E-R)} - R^2_{(F-W)}$) value in Table 5.1 is only ΔR^2 = -0.0012.

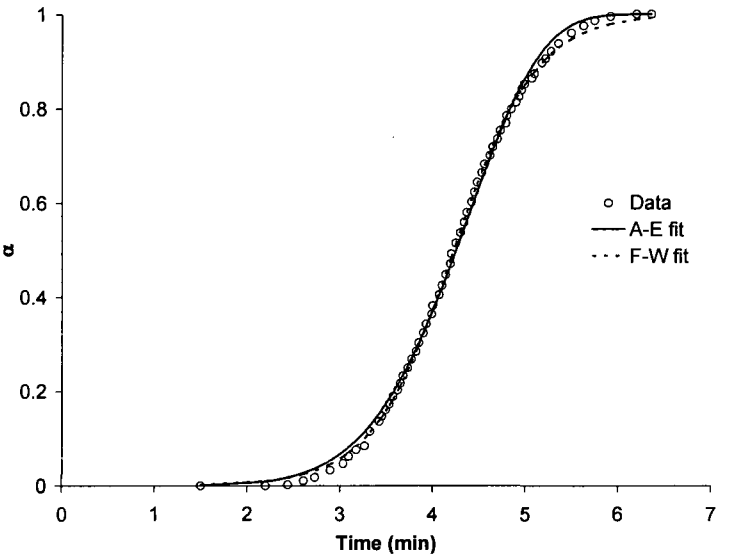

Figure 5.2. Kinetic data for the solid crystallization of bulk amorphous $Zr_{55}Cu_{30}Al_{10}Ni_5$, with fits to the A-E equation (with n = 6.57(7) and k = 0.2223(3) min^{-1}) and to the F-W model (with k_1 = 1.54(9) × 10^{-4} $min^{-1}$and k_2' = 2.27(1) min^{-1}). The statistics of the fits are given in Table 5.1.

Phase transition of $CuAlCl_4$

In a careful study, Martin et al. studied the transition between the β and α phases of $CuAlCl_4$ upon exposure to ethylene using X-ray diffraction and ^{63}Cu NMR.[17] The transition showed sigmoidal-like kinetics at various temperatures and Martin and co-workers fit the data in the usual way using the A-E equation. The data were linearized with a ln-ln plot between $0.15 \leq \alpha \leq 0.5$ and fit using linear regression. Only an average value was given for n (1.5), so we performed a linear regression analysis for one of the data sets (the transition at 125 °C measured using ^{63}Cu NMR) and obtained n = 1.7 and k

$= 3.3 \times 10^{-4}$ min^{-1} for this linearized data set. It should be noted that using the linearized form of the data removes the period from $\alpha = 0$ to $\alpha = 0.15$, effectively removing nucleation from the data.

Fitting all of the data to the A-E equation gives the curve shown in Figure 5.3, with $n = 1.46(3)$ and $k = 0.0185(2)$ min^{-1}. Fitting the data with the F-W model gives the curve also shown in Figure 5.3, with $k_1 = 0.0089(5)$ min^{-1} and $k_2' = 0.031(2)$ min^{-1}. The statistics of the fits, given in Table 5.1, show that the A-E equation has at best a slight statistical edge over the F-W model of ~4554, although both models provide good visual fits to the data.

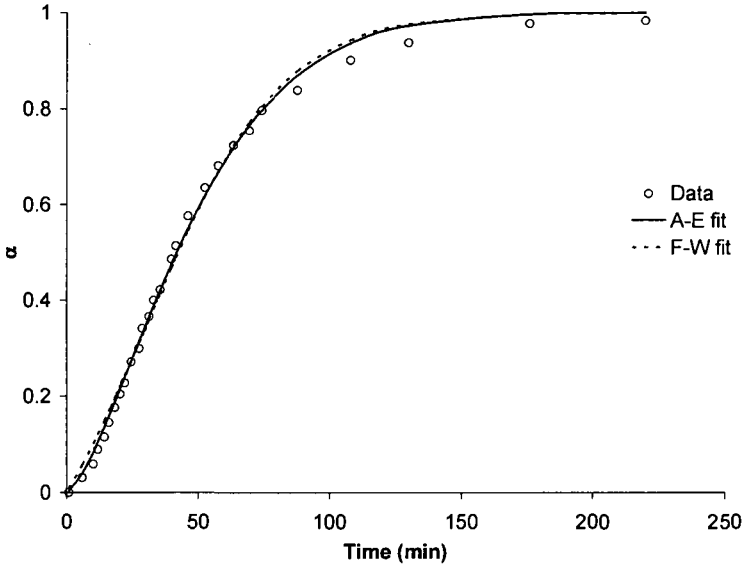

Figure 5.3. Kinetic data for the solid-state phase transition from β to α phases of $CuAlCl_4$, with fits to the A-E equation (with $n = 1.46(3)$ and $k = 0.0185(2)$ min^{-1}) and to the F-W model (with $k_1 = 0.0089(5)$ min^{-1} and $k_2' = 0.031(2)$ min^{-1}). The statistics of the fits are given in Table 5.1.

Lu and Hay's crystallization of poly(ethylene terephthalate)

The crystallization kinetics of poly(ethylene terephthalate) were studied using differential scanning calorimetry and were found to be sigmoidal-like at several different

temperatures.[18] The data were linearized and fit to the A-E equation; one data set, taken at 212 °C, gave $n = 2.7$ and $k = 0.00126\ s^{-1}$.

Fitting all of the sigmoidal data to the A-E equation gives the curve shown in Figure 5.4, with $n = 2.595(9)$ and $k = 0.00115(1)\ s^{-1}$; fitting the data with the F-W model gives the fit shown in Figure 5.4 with $k_1 = 1.24(3) \times 10^{-4}\ s^{-1}$ and $k_2' = 4.74(4) \times 10^{-3}\ s^{-1}$. For this system, the A-E fit is statistically significantly better than the F-W model by a factor of 10^{13}, Table 5.1.

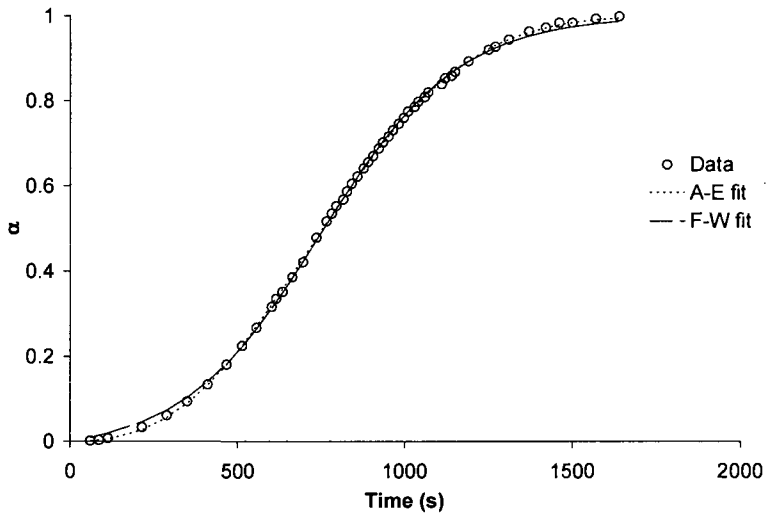

Figure 5.4. Kinetic data for the crystallization of poly(ethylene terephthalate), with fits to the A-E equation (with $n = 2.595(9)$ and $k = 0.00115(1)\ s^{-1}$) and to the F-W model (with $k_1 = 1.24(3) \times 10^{-4}\ s^{-1}$ and $k_2' = 4.74(4) \times 10^{-3}\ s^{-1}$). The statistics of the fits are given in Table 5.1.

Phase transition of $Al_{75}Cu_{15}V_{10}$

In 1991, Holzer and Kelton studied the transition from amorphous to icosahedral $Al_{75}Cu_{15}V_{10}$ at different temperatures using differential scanning calorimetry.[19] Transmission electron microscopy data suggested that the icosahedral nuclei were not distributed homogeneously; this counters the assumption in the A-E model that "germs" (nucleation sites) are randomly distributed. The authors recognized this, and stated that

"Any attempt to interpret isothermal transformation data according to [the Avrami model] is, therefore, fundamentally in error."[19] Nevertheless, the kinetics of transformation were sigmoidal and so the authors created a linearized ln-ln plot using data from $0.2 \leq \alpha \leq 0.8$. Over the range of temperatures studied, they obtained an average n of 2.3(2); values of k were not given.

We chose one dataset, for a phase transition measured at 442 °C, and fit the linearized data to see what n and k values resulted. We compared the resulting parameters, $n = 2.2$ and $k = 1.77$ min^{-1}, to those we obtained from fitting the entire data set to the A-E equation, $n = 1.74(2)$ and $k = 2.02(6)$ min^{-1}, Figure 5.5. We then fit the entire data set to the F-W model, obtaining rate constants $k_1 = 0.37(4)$ min^{-1} and $k_2' = 5.4(3)$ min^{-1}, Figure 5.5. The statistics of the fits, Table 5.1, show that the A-E and F-W fits are of essentially equal quality, with the A-E equation preferred by a small factor of just 41.

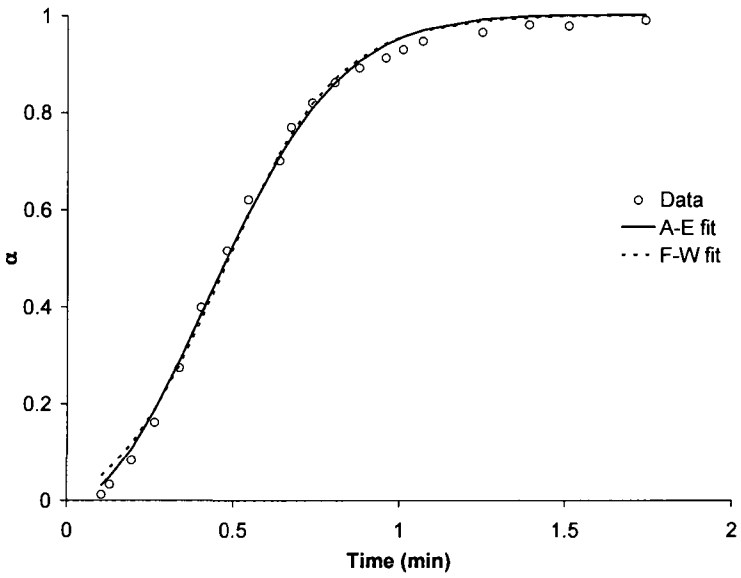

Figure 5.5. Kinetic data for the solid-state transition of amorphous to icosahedral $Al_{75}Cu_{15}V_{10}$ at 442 °C with fits to the A-E model (with $n = 1.74(2)$ and $k = 2.02(6)$ min^{-1}) and to the F-W model (with $k_1 = 0.37(4)$ min^{-1} and $k_2' = 5.4(3)$ min^{-1}). The statistics of the fits are given in Table 5.1.

Crystallization of glassy $Fe_{80}B_{20}$

The effects of crystallization on the magnetic properties of iron-based glasses were studied by Greer in 1982, in particular the glassy $Fe_{80}B_{20}$.[20] Using differential scanning calorimetry, Greer obtained the kinetic data shown in Figure 5.6. Using a linearized ln-ln plot of the data from ~0.2 ≤ α ≤ ~0.9, he obtained $n = 2.80(5)$. Again, the value of k was not reported, so we fit the same linear data and obtained $k = 0.057$ min^{-1}.

Fitting the entire data set to the A-E equation gave $n = 2.771(9)$ and $k = 0.05726(5)$ min^{-1}, Figure 5.6, in close agreement with the values from the linearized plot. Fitting the same data to the F-W model gave $k_1 = 4.8(1) \times 10^{-3}$ min^{-1} and $k_2' = 0.257(3)$ min^{-1}, Figure 5.6. Although the two models give very similar visual fits and R^2 values, the *AICc* statistics suggest that the A-E equation is favored by a factor of 10^{15}, Table 5.1.

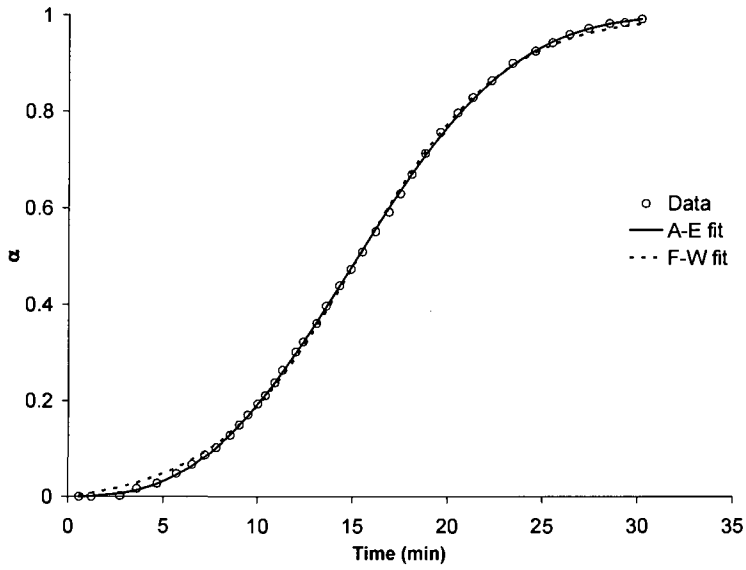

Figure 5.6. Kinetic data for the crystallization of $Fe_{80}B_{20}$ with fits to the A-E equation (with $n = 2.771(9)$ and $k = 0.05726(5)$ min^{-1}) and to the F-W model (with $k_1 = 4.8(1) \times 10^{-3}$ min^{-1} and $k_2' = 0.257(3)$ min^{-1}). The statistics of the fits are given in Table 5.1.

Crystallization of $Pd_{79}Cu_6Si_{10}P_5$ bulk metallic glass

Very recently, Liu et al. have studied the crystallization kinetics of $Pd_{79}Cu_6Si_{10}P_5$, which has a high glass-forming ability.[21] Using differential scanning calorimetry, the authors obtained kinetic curves for crystallizations at different temperatures; at each temperature studied, the kinetics were sigmoidal. The authors used a linearized ln-ln plot, taking data from $0.15 \leq \alpha \leq 0.85$ where the data are linear, to determine values for the A-E parameters. For one crystallization at 375 °C, they obtained $n = 2.52$ and $k = 0.06$ min^{-1}.

When we fit the entire data set to the A-E equation, we obtained the parameters $n = 4.68(4)$ and $k = 0.03573(5)$ min^{-1}, Figure 5.7. These values vary significantly from those obtained from the linearized data. Fitting the same entire data set to the F-W model gave the rate constants $k_1 = 2.7(2) \times 10^{-4}$ min^{-1} and $k_2' = 0.268(4)$ min^{-1}, Figure 5.7. The

statistics of the fits show a preference for the A-E equation by a factor of ~10^8, Table 5.1, although visually the fits are again very similar.

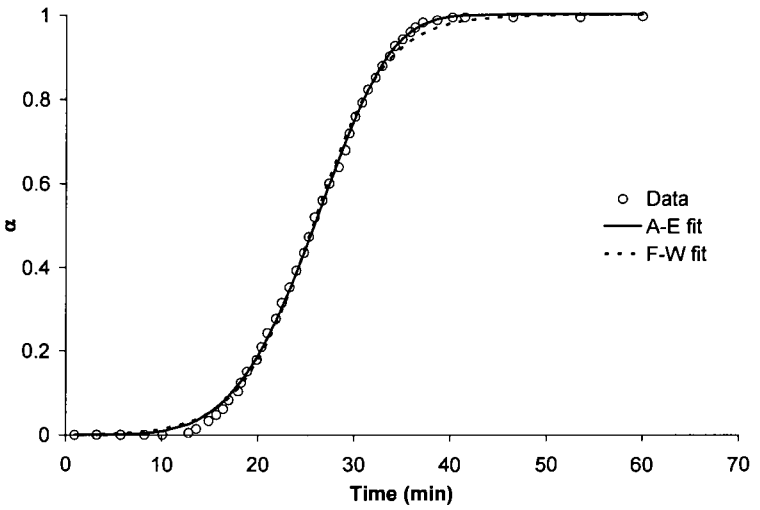

Figure 5.7. Kinetic data for the crystallization of $Pd_{79}Cu_6Si_{10}P_5$ at 375 °C with fits to the A-E equation (with $n = 4.68(4)$ and $k = 0.03573(5)$ min^{-1}) and to the F-W model (with $k_1 = 2.7(2) \times 10^{-4}$ min^{-1} and $k_2' = 0.268(4)$ min^{-1}). The statistics of the fits are given in Table 5.1

Table 5.1. Statistical data for the fits in the systems described herein to the A-E equation and the F-W model.

System (Figure)	R^2 (A-E)	R^2 (F-W)	*AICc* (A-E)	*AICc* (F-W)	*w* (A-E)	*w* (F-W)	$ER_{(A\text{-}E/F\text{-}W)}$
Bi_3 (5.1)	0.9967	0.9965	-210	-208	0.71	0.29	2.5
Zr (5.2)	0.9982	0.9994	-544	-617	1.1×10^{-16}	1	1.1×10^{-16}
$CuAlCl_4$ (5.3)	0.9969	0.9944	-223	-206	0.9997	0.0003	4554
Polymer (5.4)	0.9999	0.9995	-570	-508	1	4.1×10^{-14}	2.4×10^{13}
Al_{75} (5.5)	0.9968	0.9953	-152	-145	0.97	0.03	41
Fe_{80} (5.6)	0.9999	0.9994	-452	-380	1	3.4×10^{-16}	2.9×10^{15}
Pd_{79} (5.7)	0.9992	0.9985	-423	-385	1	5.6×10^{-9}	1.8×10^{8}

Summarizing the data in Table 5.1, we observe that the A-E equation is favored by a significant amount (as defined by an $ER_{(A\text{-}E/F\text{-}W)} \geq 10^{\pm 4}$) for two of the systems, the F-W model is strongly favored for one of the systems, and both models fit equally well (i.e., *ER* values under the for the$\geq 10^{\pm 4}$) for the remaining three systems. If one examines the statistics in Table 5S.2 in the Supporting Information for the other five data sets that were also randomly selected from the literature and fit, the overall results are as follows: the A-E equation is statistically preferred by a significant amount in three cases (with *ER* values ranging from 10^{8} to 10^{15}), the F-W model is statistically preferred in two cases (by *ER* values of 10^{-14} to 10^{-16}), and the fits are equivalent within experimental error (by the *ER* of $10^{\pm 4}$ criteria) in the other seven cases. The actual *ER* values for the fits deemed "equivalent within experimental error" are 0.37, 1.1, 2.5, 41, 52, 588, and 4554, values obviously small compared to the extremes of $10^{\pm 15}$ or more seen above, and especially small compared to the *ER* values of 10^{-38} to 10^{-184} seen elsewhere where a 4-step version of the F-W model that includes two type of agglomeration reactions provides much better fits in comparison to "dispersive kinetics" models.[10]

In short, the above data along with that in the Supporting Information suggest that it is not inappropriate to probe further the hypothesis the A-E and F-W models are somehow equivalent in at least 8 of the 12 cases examined for fitting solid-state kinetic data. Put another way, it would appear to be appropriate to probe further whether or not the chemical-mechanism-based concepts and words from the F-W 2-step mechanism, specifically nucleation and autocatalytic growth, are reasonable

concepts for describing solid-state processes where good fits to the observed kinetics can be obtained by the F-W model. The driving force for doing so—that is, the goal here—is to overcome the *disconnect currently between the observed kinetics versus the concepts*[10] *and words* employed in the highly complex area[22] of solid-state kinetics. Indeed, we have argued elsewhere that it is this disconnect between at least some of the mathematical-based models that hold little physical reality, versus the language that is then adopted from other areas (i.e., must be adopted since no other physical descriptors are available), that has contributed to much of the confusion in solid-state kinetics.[10] As a prime example witness the widespread use in the solid-state kinetics literature of the descriptors "nucleation" and "growth" alongside the A-E equation, *despite the A-E treatment having only one rate parameter, k,* incorrectly typically called a rate constant (which it rigorously is not, since rate constants are defined only via the balanced equations to which they refer). It is this specific disconnect (one "*k*" versus two words being used, nucleation and growth) that originally attracted us to try to fit solid-state kinetics via the chemical-mechanism-based F-W 2-step model. *This is not a trivial point.* This disconnect has led for example to concepts such as "autocatalytic nucleation", which is generally defined as the process by which nuclei appear within a matrix as the matrix ages or precipitates.[23] The autocatalytic nucleation mechanism is an assumption made in the solid-state literature; in light of the present comparison between the A-E and F-W models, a reasonable hypothesis (for example) is that the "autocatalytic nucleation" mechanism might be better thought of as continuous nucleation[24] followed by autocatalytic growth. Importantly, we will see in a moment that it is possible to view

the A-E parameters k and n as convolutions containing the chemical-reaction-based k_1 (nucleation) and k_2' (autocatalytic growth) of the F-W model.

Fitting Nanocluster Formation Kinetic Data by Both A-E and the F-W Models

We also hypothesized that data for the formation of $Ir^0_{\sim 300}$ nanoclusters prepared from the reduction of $(Bu_4N)_5Na_3[(1,5\text{-COD})Ir{\bullet}P_2W_{15}Nb_3O_{62}]$ that were well-fit originally by the F-W model[5] *could be equally well-fit by the A-E equation.* One such fit, which fully supports the above hypothesis, is also given in the Supporting Information, Figure 5S.6, the *AICc ER* values actually favoring the A-E model for the one kinetic curve examined. In short, both the A-E and F-W models are able to fit the variety of phase-transformation kinetic data examined herein, be it solid-state or solution nanocluster formation kinetic data.

Mathematically equating the A-E equation with the F-W mechanism: can the Avrami parameters k and n be viewed as convolutions of k_1 and k_2'?

Because the A-E and F-W models fit 8 of the 12 sigmoidal kinetic data tested similarly well, we looked at the A-E equation and the integrated rate equation for the F-W mechanism to see how the two models might be related mathematically. Restated, we explored the question of "can one learn anything of value by mathematically equating the two equations?"

In order to compare the two equations mathematically, we rearranged the F-W integrated rate equation into a form that is directly comparable to the A-E equation. Starting with the integrated rate equation in terms of α, eq 5.3:

$$\alpha = 1 - \frac{k_1 + k_2'}{k_2' + k_1 e^{(k_1 + k_2')t}} \tag{5.3}$$

Rearranging eq 5.3 gives eq 5.8:

$$1 - \alpha = \frac{k_1 + k_2'}{k_2' + k_1 e^{(k_1 + k_2')t}} \tag{5.8}$$

The A-E equation, eq 5.1, is reproduced below

$$\ln(1 - \alpha) = -(kt)^n \tag{5.1}$$

and can be rearranged to the form shown in eq 5.9.

$$1 - \alpha = \frac{1}{e^{(kt)^n}} \tag{5.9}$$

We then set eqs 5.8 and 5.9 equal to each other, thereby obtaining eq 5.10, again all in the spirit of a "mathematical experiment" just to see what resulted and if it is of use or not.[25] Initial inspection of the resultant eq 5.10 quickly reveals one (albeit not particularly interesting) case where the left (F-W) and right (A-E) sides of eq 5.10 become identical, namely that of $n = 1$ and $k_1 >> k_2'$; see eq 5S.8 of the Supporting Information for further details.[25]

$$\frac{k_1 + k_2'}{k_2' + k_1 e^{(k_1 + k_2')t}} \approx \frac{1}{e^{(kt)^n}} \tag{5.10}$$

More interestingly, eq 5.10 can be rearranged to isolate each of the parameters k and n (see the Supporting Information for the attempts to also isolated k_1, and k_2'). Isolation of k and n is straightforward, resulting in eqs 5.11a and 5.11b. Note that in each case a single parameter (i.e., k and n for eqs 5.11a and 5.11b, respectively and to start) is a function of the other *three* parameters, for example k is a f(k_1, k_2' and n) as

well as time, t, while n is a f(k_1, k_2' and k) as well as t as expected based on eq 5.10. More significantly and from a F-W perspective, eqs 5.11a and 5.11b reveal more clearly than eq 5.10 that *nucleation (k_1) and autocatalytic growth (k_2') rate constants are deeply convoluted into both of the A-E parameters n and k*, and if one accepts the premise behind the math of equating the two equations in the first place to see what one sees. To our knowledge, *this is the first time where an interpretation for the A-E parameters k and n has been offered in terms of a chemical-mechanism-based equation* and its associated integrated rate equation and rate constants and where experimental data for equivalent (to sometimes better) fits using the chemical model have also been demonstrated. As such, the above treatment suggests that *it may well be at best confusing, and at worst probably simply wrong—a highly misleading disconnect, to use the words "nucleation and growth" while discussing either of the k or n parameters of the A-E equation.*

$$k \approx \frac{\left\{\ln\left[\frac{k_2' + k_1 e^{(k_1+k_2')t}}{k_1 + k_2'}\right]\right\}^{\frac{1}{n}}}{t} \tag{5.11a}$$

$$n \approx \frac{\ln\left\{\ln\left[\frac{k_2' + k_1 e^{(k_1+k_2')t}}{k_1 + k_2'}\right]\right\}}{\ln(kt)} \tag{5.11b}$$

Attempts to do the opposite, that is to rearrange eq 5.10 to isolate k_1, and k_2' in terms of k and n, either by hand or using Mathematica, failed in the case of the attempted isolation of k_1 and gave a complicated formula in the case of k_2' as eq 5S.9 of the Supporting Information details.

A bottom line here is that equations 5.11a and 5.11b would appear to be of value primarily in suggesting an interpretation in which there is a convolution of one parameter in terms of the other three in each case for k, n, k_1, k_2 and time, t. Equations 5.11a and 5.11b give a specific hypothesis for how k or n may be dependent on k_1 and k_2' as well as the other A-E variable (i.e., n or k) as well as t—at least under the original postulate that the A-E and F-W could be equated in the first place and that doing so might reveal something useful. The reader will need to be the judge here of whether anything useful has resulted.

Simulations relating the A-E n and k to the F-W k_1 and k_2'

Our intuition was that we might be able to obtain a clearer, simpler insight in to the relationship between the A-E parameters and the F-W rate constants, so we approached this by simulating kinetic data using the A-E equation, eq 5.1, for selected values of k and n (selected to give "representative" sigmoidal curves as in Figure 5.8, for example), and we then fit those simulated data to the F-W kinetic model, eq 5.3, as described in the Experimental section to obtain resultant k_1 and k_2' rate constants. An example of this simulated data, for $n = 3$ and $k = 0.1$ is shown in Figure 5.8. An immediate conclusion from Figure 5.8 is that, again, the F-W equation is able to account rather well for A-E type (or in this case, A-E generated) sigmoidal kinetic curves such as the one in Figure 5.8.

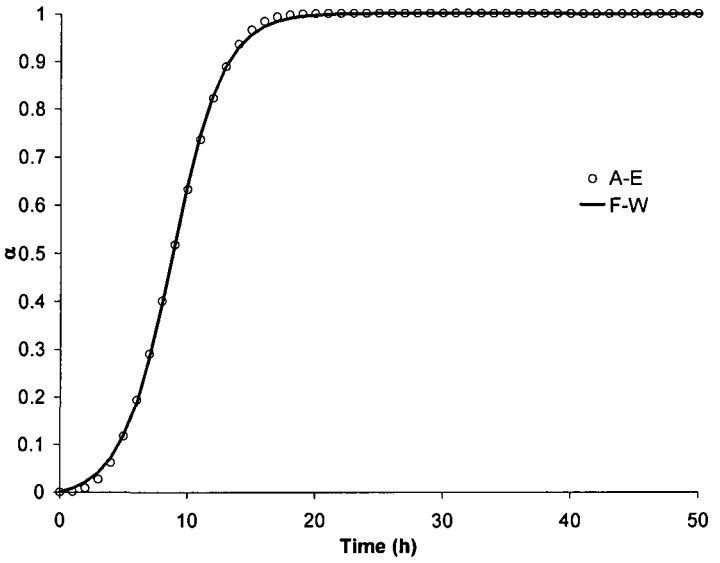

Figure 5.8. Simulated data using the A-E equation (circles) for the parameters $k = 0.1$ and $n = 3$, and the fit to the F-W mechanism, eq 5.3 (line) resulting in $k_1 = 6.1 \times 10^{-3}$ h^{-1} and $k_2' = 0.49$ h^{-1}.

Next, and en route to plots of k_1 and k_2' as function of k and n, we independently changed n and k (i.e., one variable at a time, while holding the other constant) and fit the resultant data to the F-W mechanism, eq 5.3, to see how those n and k changes affect k_1 and k_2'. The k_1 and k_2' versus k plots, and the k_1 and k_2' versus n plots, Figure 5.9, are quite interesting and proved surprisingly simple in light of the apparent complexity of eqs 5.11a and 5.11b.

As a check on the relatively simple results in Figure 5.9 versus the apparent complexity of eqs 5.11a and 5.11b, several of the data contained in Figure 5.9 were plugged back into the appropriate equation 5.11a or 5.11b for different values of time, t, and the resultant right and left hand sides of the equation used did in fact generally give the same numerical value within experimental error, showing, interestingly, that k and n are ca. constant functions of time (i.e., for the specific, limited range of k_1 and

k_2' values that were investigated, specifically those that provide sigmoidal kinetic curves). That is, the simple linear relationships in Figures 5.9a and 5.9b are actually contained within eqs 5.11a and 5.11b, a key here being *for the specific range of n and k values examined.* The interesting, more complete plots of n and k versus t which results from eqs 5.11a and 5.11b are provided in the Supporting Information as Figure 5S.7 and show that the values of n and k found from these plots are consistent with the values obtained from the simulations.

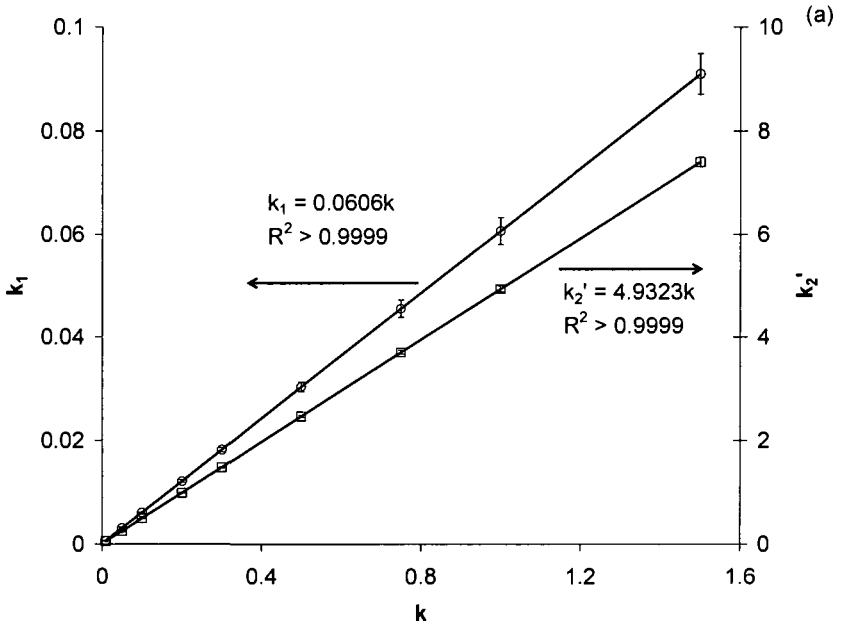

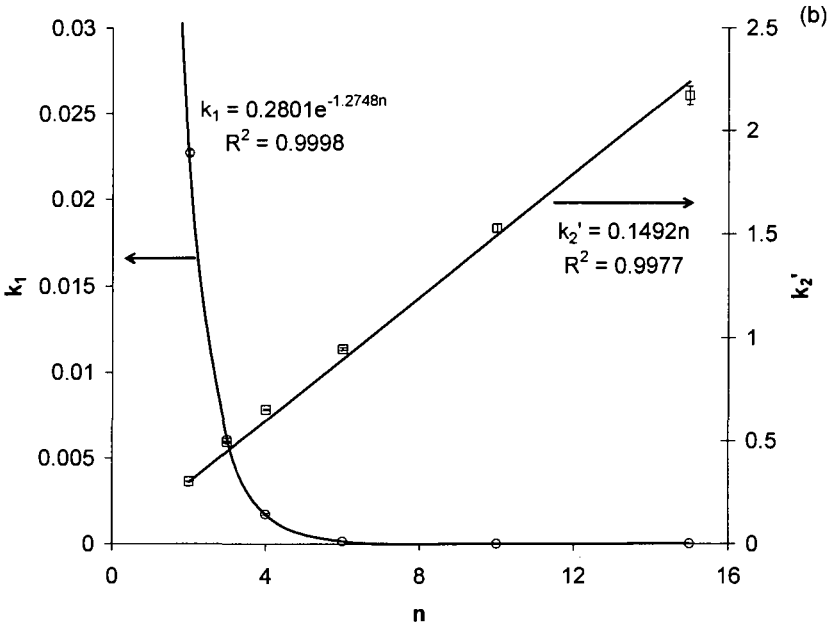

Figure 5.9. Dependence of the F-W rate constants k_1 and k_2', obtained from fitting simulated a versus t data for the A-E equation and varying the parameters k (with a constant $n = 3$, (a)) and n (with a constant $k = 0.1$, (b)). In (b), only n values of greater than 1 are plotted (results for $0 < n \leq 1$ are given in Figure 5S.8 of the Supporting Information).

Several observations from Figure 5.9 are worth noting. First, each of the F-W rate constants k_1 and k_2' appears to increase linearly with the Avrami rate constant k (and for this constant, $n = 3$, case). The value of k_1 has an inverse exponential dependence on n, at least for constant $k = 0.1$.[26] The dependence of k_2' on n is more complex. At $n > 1$ (which is almost always the case in the literature), k_2' has a linear dependence on n (at constant $k = 0.1$). When $n = 1$, $k_2' = 0$, since the result is a first-order reaction (with rate equation $\alpha = 1\text{-}e^{-kt}$), and $k = k_1$. When $n < 1$, k_2' is negative, and k_2' decreases rapidly as n approaches zero (see the Supporting Information, Figure 5S.8, for a plot of k_2' versus n for $0 < n \leq 1$). When $n = 0$, then the A-E equation becomes $\alpha = 1\text{-}e^{-1} = 0.632$; that is, α has a constant value for all t in this

nonsensical case. It is thought in the solid-state literature that changes in the Avrami exponent n are due to the change in mechanism during the course of the reaction;[27] *the present treatment suggests an alternative hypothesis: that the real change simply entails going from nucleation to growth, the k_1 versus k_2' (and t) contributions to n changing as the reaction progresses.*

Overall, this simulation-then-fit approach again makes it quite apparent—but now graphically—that there is a convolution of the F-W rate constants k_1 and k_2' into the A-E parameters n and k (or, if one likes, a convolution of the A-E k and n into the F-W k_1 and k_2), again at least to the extent that equating the two equations makes sense and is justified by the experimental observation of the equally competent fits by the two models in 8 of the 12 data sets examined. The present chemical-mechanism-based approach behind the F-W treatment provides evidence for the inherent physical/chemical disconnect between the A-E model and the underlying chemistry, specifically the F-W model suggests that discussing "nucleation" and/or "growth" from an A-E obtained rate parameter, k, is at best bound to generate confusion (witness the concept "autocatalytic nucleation", *vide supra*), and very possibly may be fundamentally flawed.

A caveat here is that the simulations leading to the above conclusion are just those we have done and found most interesting to date. Obviously, other simulations with a different range of n and k parameters is possible, although our intuition at present is that the initial, broad conclusions made above are not likely to be changed by additional simulations *if* sigmoidal-shaped curves are involved.[28]

Does Autocatalysis Make Sense for Such Solid-State Phase Transformations?

An important question, one we thank Prof. James Martin for emphasizing to us, is whether it makes physical sense to use the term autocatalysis for solid-state reactions? While certainly debatable, three points come to mind here to say that it does: (i) certainly the word "autocatalysis" has been often and widely used in the solid-state kinetics literature[3,4c] (see also the other reviews and references cited in the Supporting Information), albeit not always with the type of experimental support provided herein; and secondly (ii) at least phenomenologically, to the extent that the F-W model and its autocatalytic 2nd step fit the data, the use of the term "autocatalysis" in the growth step is, therefore experimentally supported (but *not* terms one can find in the solid-state literature such as "autocatalytic nucleation"). Thirdly, (iii) the idea of an advancing front or interface boundary in the growth of a solid after nucleation is intuitively autocatalytic to at least us in the sense of the rigorous definition of autocatalysis, where the product is also a reactant (i.e., A+B→2B being the rigorous chemical definition of autocatalysis). In short, at least in our view the term "autocatalysis" now has both experimental support as well as past history and usage in the solid-state kinetics literature.

Comments on the Strengths and Weaknesses of Each Model

What follows is a brief discussion of the strengths and weaknesses of both the A-E and the F-W models. A more detailed discussion of each, as well as more background information on both the A-E models and its variants as well as on the F-W model, are provided in the Supporting Information for the interested reader.

The main advantage of the A-E model for fitting solid-state data is that it is well-established in the literature, dating back to 1939 in its earliest version (see Table 5S.1 in the Supporting Information). In addition, as can be seen in Figures 5.1-5.7, as well as in the Supporting Information, the A-E model fits sigmoidally-shaped kinetic data quite well, be it data for solid-state reactions or solution nanocluster-formation reactions.

The main weakness of the A-E model is clear: *the difficulty in assigning physical meaning to the parameters k and n; note in this context that the original driving force for Khanna and Taylor's proposal of the modified Avrami equation used herein (eq 5.1) is a need to gain physical insight from the Avrami model and its derivatives.*[1] Another significant weakness is that although k is often called a rate constant, *it is not*, since it is not defined by a specific chemical equation. Instead, k is a (A-E) rate-related parameter, one that the findings herein suggest can be viewed as a convolution that includes the rate constants for chemically well-defined processes of nucleation and autocatalytic growth. Another issue is the A-E parameter n, a parameter generally believed to be related to the dimensionality of nucleation; however, exactly how it relates to dimensionality cannot be easily extracted and is indeed a subject of continuing debate as are non-physical values ("dimensions" in space) of $1 > n \geq 4$.[29,30] The present work provides the hypothesis that n might also be viewed as a convolution of nucleation and autocatalytic growth. Moreover, the visually good fits attained by the F-W model in all 12 cases, and the statistically equivalent within experimental error (or better) fits obtained in 8 of the 12 cases, do show that nothing that one would call a "dimensionality" is needed to obtain

equivalent fits to at least the sigmoidal solid-state kinetic data examined. This is not to say that one would not like to build the concept of dimensionality into more complex solid-state kinetic models (i.e., it is not our intention to turn back the clock 70 years on A-E theory and achievements); we also cannot rule out the argument that a F-W treatment of solid-state kinetic data is fundamentally flawed since it does not, at least presently, specifically take into account the dimensionality that physically it seems must be there. This discussion does, however, raise the interesting question for future work of whether a dimensionality can be extracted somehow from k_1 and/or k_2'?

Another fundamental weakness of the A-E and related equation-based solid-state literature is the large number of different models used to describe the kinetics of solid-state transformations, as Table 5S.1 of the Supporting Information makes very apparent and as Galwey and Brown's treatise emphasizes.[4c] An issue with the A-E and related models in Table 5S.1 of the Supporting Information is that some are quite complicated without compelling evidence being available that more complicated models are warranted. Indeed, we have shown in the Supporting Information that the A-E model can fit at least some of the data as well as or better than the more complex models used in the literature. Hence, it follows that: (i) the use of the simplest models where possible needs to be part of future approaches to solid-state kinetics (i.e., an Ockham's Razor based approach that is central tenant of rigorous mechanistic science and was a key to the discovery of the F-W model[5]), and (ii) the use of statistical methods, such as *AICc*, should be used to provide evidence for or against models with additional parameters. In addition, our results strongly suggest that (iii) linearization

of the inherently non-linear A-E and related equations (e.g., by ln-ln plots) should no longer be done since non-linear least squares routines are readily available. No matter what, these three insights would appear to be useful conclusions from the present studies.

Turning to the strengths and weaknesses of the F-W model, the F-W model is a simple, Ockham's-Razor-based mechanism which fits a wide variety of sigmoidal data in nature[5,10,11,12,13] closely using only two, chemically well-defined, rate constants. These rate constants have clear meaning from their chemical-equation basis (at least *in solution*) and can, therefore, be connected rigorously and without confusion to useful chemical concepts/words, notably nucleation (k_1) and (autocatalytic) growth (k_2'), and even if those words and concepts are oversimplifications that may have limitations for complex areas such as solid-state phase transitions.[1c,2,3,4,9,22,31] The F-W model has been able to provide physical insights into at least *solution* nanocluster synthesis and stabilization,[5,6,7,33] more than 9 insights that include: (i) understanding how to form routinely near-monodisperse (defined as $\leq \pm 15\%$ size distributions[6]) of typically "magic-number sized" (i.e., full shell) size distributions of supported nanoclusters by the separation of nucleation from growth in time;[6,32] (ii) *rational size control* via a recently developed nanocluster size versus time equation in terms of k_1, k_2 and the precatalyst concentration, $[A]_0$;[33] (iii) additional possible size control via olefin or other ligand dependence;[34] (iv) rational use of seeded-growth methods including the rational synthesis of all possible geometric isomers of multimetallic "nano-onions";[32a] (v) rational catalyst shape control via ligands capable of attaching to the growing nanocluster faces and thereby

preventing autocatalytic surface growth of that facet;[35] (vi) knowledge of the negative effects of, and insights into how to avoid, mass-transfer limitations in nanocluster syntheses;[32b] (vii) knowledge of what added nanocluster surface ligands can provide additional nanocluster stability if desired;[36] (viii) a ranking system for nanocluster stabilizers;[37] and (ix) the possibility of nanocluster size-dependent surface metal-to-ligand bond energies plus all that intriguing preliminary finding implies for catalysis.[32] This list itself would appear to significantly outpace the number of *chemical and physical insights* obtained from 70 years of application of A-E equations,[38] but with the significant caveat here being noted that solid-state kinetic processes are much more complex than are solution processes.[1c,2,3,4,9,22]

In addition, a more general 4-step mechanism of nanocluster formation and agglomeration was recently discovered that includes the two steps in Scheme 5.1, but adds two types of nanocluster agglomeration, bimolecular agglomeration B+B→C (rate constant k_3) and a novel autocatalytic agglomeration between smaller (B) and larger (C) nanoclusters, B+C→1.5C (rate constant k_4).[7] The latter, 4-step mechanism is fortified by the fact that 18 other conceivable mechanisms were ruled out en route to its elucidation.[7] An interesting question related to the present work is if either of the agglomeration steps could have anything to do with phase transformations leading to solid-state products—that is, are there (higher activation energy, slower) solid-state diffusion analogs of the above two steps in the solid state, *especially at higher temperature*? An even more fundamental question is whether greater application of the F-W model to the much more complex area[1c,2,3,4,9,22] of solid-state chemistry will help add badly needed physical and chemical insight to solid-state reactions—or will

the F-W model just prove to be just another model, in the worst scenario an inappropriate model that also commits the apparent sin[22b] of attempting to relate a reaction-order model to solid-state processes. Time will tell.

In terms of *drawbacks* of the F-W model back in Scheme 5.1, the biggest is surely that this arguably simplest possible, 2-step model hides the more intimate mechanistic steps of nucleation and growth in summed, pseudo-elementary steps of (average) nucleation and (average) autocatalytic growth.[39] As such the minimalistic F-W kinetic model necessarily conceals the more intimate—formulatable as "dispersive kinetic"[10]—details about the particle formation of phase transformation mechanism, a mechanism in the case of $Ir^0_{\sim 300}$ nanocluster formation that, logically, must involve >>300 steps for conversion of 300 equivalents of [(1,5-COD)Ir•$P_2W_{15}Nb_3O_{62}]^{8-}$ into one (on average) $Ir^0_{\sim 300}$ nanocluster according to the known, balanced stoichiometry in eq 5.12:[5]

$$300[(1,5\text{-COD})Ir{\cdot}P_2W_{15}Nb_3O_{62}]^{8-} + 750H_2 \longrightarrow$$

$$300 \text{ (cyclooctane)} + 1\ Ir^0_{\sim 300} + 300[P_2W_{15}Nb_3O_{62}]^{9-} + 150\ H^+ \qquad (5.12)$$

Hidden by the F-W model is the expectation that nucleation consists of multiple steps leading up to (one assumes) the classical critical nucleus, with dissolution of the cluster being more favorable than growth before the critical nucleus, at least if classical nucleation theory is correct (theory where, however, quantitative agreements between experiment and theory of 10^x, x = 1-6 or more, are common).[40] The nanoclusters grow essentially irreversibly post these initial, again classically

reversible steps leading up to the critical nucleus. The rate constants k_1 and k_2 are therefore *composite* rate constants, *averaged* over all of the nucleation and growth steps, rate constants that change with particle size so that a dispersion of (different) rate constants are really present so that a dispersive kinetic treatment is really needed fundamentally.[10] Those rate constants are, in the over-simplified F-W model, therefore effectively assumed to be independent of nanocluster size, which cannot physically be true at sufficiently high levels of precision. In short, the greatest *strength* of the F-W model, its simplicity and ability to deconvolute an average nucleation rate constant from an average growth rate constant for chemically and physically well-defined nucleation and autocatalytic growth, is also the source of its *greatest weakness*, that simplicity hiding important chemical details that one eventually wants. It follows that possible extensions of the F-W model in the solid state chemistry (or other areas[10,11,12,13]) should be carried out with both caution *and* the above limitations clearly in mind.[31]

Work is in progress attempting to elucidate the more intimate steps underlying the F-W model. In the mean time, application of the F-W model is proving to be valuable in deconvoluting an average nucleation rate constant from an average autocatalytic growth rate constant in areas where *this could not done previously*, be they nanocluster formation,[5,6,7,33,34,36,37] aggregation of proteins intimately involved in neurological diseases,[11,12,13] or, now, solid-state kinetic data previously treated by the A-E or related equations.

Conclusions

Herein we have shown:

- That the A-E equation derived for solid-state kinetics, and the F-W mechanism originally worked out for transition-metal nanocluster formation, each fit either solid-state reaction kinetic or solution nanocluster formation kinetic data equally well within experimental error for 8 of the 12 cases examined. This conclusion is fortified by statistical analysis of the fits in the form of R^2 and *AICc* (and also *AICc*-based w and *ER*) values as well as visual comparison of the fits.
- Hence, there is now an experimentally supported way to (i) deconvolute an average nucleation, k_1, from an average autocatalytic growth, k_2, rate constant from solid-state kinetic data and, importantly, (ii) experimentally supported and rigorously defined words / concepts that can be used to support the discussion of those rate constants, namely "nucleation" and "autocatalytic growth". These are not trivial results given the history and current confusion in solid-state kinetics,[Error! Bookmark not defined.,Error! Bookmark not defined.,Error! Bookmark not defined.,Error! Bookmark not defined.,Error! Bookmark not defined.,Error! Bookmark not defined.] and the resultant call for more chemical-mechanism-based approaches.[4c,4d,9]
- Mathematical analysis, as well as simulations of A-E curves for chosen k and n that yield representative sigmoidal curves, followed by F-W fits of those curves to yield k_1 and k_2', reveal that one alternative way to view the A-E parameters k and n are that they are convolutions

containing the F-W rate constants k_1 and k_2' (as well as t and the other A-E parameter, n or k).

- The A-E model has the advantage of its historical use in the literature, but the significant disadvantage that approaching 70 years of its use has not lead to a clear *physical interpretation* of even the two key n and k parameters,[38] at least so far as we can tell and so far as is discernable by an outsider to the field—as basic physical insights should be! Instead, much confusion and a proliferation of more complex models, Table 5S.1 of the Supporting Information, have resulted, all with less and less physical understanding, again that at least we as outsiders can discern.
- The F-W model has the advantage that it employs rigorously chemically defined, physically meaningful rate constants. Its use has allowed more than 9 chemical and physical insights into at least solution nanocluster formation and stabilization. The main limitation of the F-W model derives from its simplicity: it hides many kinetically important steps and size-dependent properties in average nucleation and average autocatalytic growth, pseudo-elementary steps and their associated rate constants. Other limitations of the F-W model are provided elsewhere that anyone planning to use the F-W model should consult.[33]
- Both the A-E and the F-W kinetic model can fit a variety of solid-state kinetic data from different literature systems, some of which use more

complex, yet less physically meaningful, equations. Moreover, the quality of the fits using the F-W mechanism and the A-E equation are in some cases better than the fits to more complex equations used in the specific literature system, and by the *AICc* criterion. *Greater use of AICc statistical methods in the solid-state kinetics area is warranted according to these result*s, especially for evaluating models with different number of parameters and thus of different complexity.

- Since A-E type analyses have been shown to generally fit sigmoidal-like kinetic curves for 13 other biological processes[41] ranging from various growth curves (e.g., bacterial growth, sunflower growth, or salamander leg re-growth), K^+ conductance in nerve axions or K^+ leakage from poisoned muscle, firefly flash light decay, to green leaf IR phosphorescence decay, and since it was shown herein that the F-W model gives equivalent fits to those using the A-E model in at least a number of cases, it follows that the F-W 2-step model should also fit the above-noted 13 biological processes. An example of the F-W and A-E models fitting biological data is given in the Supporting Information, Figure 5S.11.

Much remains to be done, however. Topics needing attention include: the fact that volumes of crystal growth that could range from 10 nm^3 to 10 μm^3 or more are obscured by the "fraction reaction" α in both the A-E and F-W treatments herein;[43] the need to analyze more literature data using the F-W model (as well as just the basic, A-E model) to probe for either the generality of the nucleation-plus-

autocatalytic-growth model *or its limitations*; the need for efforts aimed at breaking the F-W 2-step model into a greater number of its underlying, intimate steps; and the need to address the lack of important concepts from the solid-state literature that are missing in the present version of the basic F-W model, notably the dimensionality, n—is n somehow built into, and thus deconvolutable out of, k_1 and/or k_2'? Or, is the F-W model ultimately inappropriate for analyzing solid-state kinetic data solely based on the fact that it has no dimensionality component and if one cannot eventually be teased out of k_1 and/or k_2'?

Also unanswered at present is the central question of whether the present discovery will help reduce the confusion and lead to advances in the complex area of solid-state kinetics—or just add to that confusion?[1c,9,22] Overall, our hope is that the latter will not obtain but, rather, that the present contribution will stimulate the needed additional research en route to a better understanding of the kinetics and mechanisms of phase transitions, not just in solid-state chemistry, but instead throughout nature. Again, time will tell.

Acknowledgment: Multiple, valuable discussions with Professor James Martin about solid-state kinetics and the ideas presented herein are a pleasure to acknowledge, thanks that are not meant to imply that he agrees with (any of) the contents of the present paper. In addition, we thank Joe Mondloch and Aimee Morris for their generous critical reading, comments, and equation-checking assistance as we worked through multiple drafts of this paper over a 5 year period that began in 2003. Dr. Pete Skrdla is also thanked for pointing out reference 8c to us. Without their help, the present paper would not have been possible. This work was supported by the Chemical Sciences, Geosciences and Biosciences Division, Office of Basic Energy Sciences, Office of Science, U.S. Department of Energy, grant number DE-FFD02-03ER15453.

Supporting Information Available: A table of selected solid-state literature kinetics studies; fits to five additional literature solid-state kinetics systems to the A-E equation and the F-W model; fits of nanocluster formation data using the F-W and A-E models; an alternate way to relate mathematically the A-E equation and the F-W integrated rate equation; attempts to isolate eq 5.10 for k_1 and k_2'; simulations of the A-E parameters n and k as a function of time using eq 5.10; dependence of k_2' on n for $0 < n \leq 1$; background of the A-E and F-W models; one representative fit of protein agglomeration data to the F-W and A-E models.

References

[1] (a) Herein we use Khanna and Taylor's[1b] modified form of the Avrami equation which, after slight rearrangment of eq 5.5, is $\alpha = 1 - \exp\{-(kt)^n\}$. This form allows k to be in units of time^{-1}, and is recommeded by Khanna and Taylor[1b] as well as by Galwey[1c], although it is not preferred by others[1d] (albeit only for reasons that are a matter of preference in the final analysis[1d]). The original Avrami equation is $\alpha = 1 - \exp\{-k't^n\}$. These two equations are equivalent if $k' = k^n$, although the use of these two equations does cause confusion in the solid-state kinetics literature since the resultant k and k' have different values and units. Of interest and relevance to the present study is that Khanna and Taylor's modified Avrami equation was proposed in at attempt to make the resultant parameters one obtains closer *to being physically relevant / reasonable* for industrial polymer crystallization data.[1b] (b) Khanna, Y. P.; Taylor, T. J. *Polymer Engineering and Science* **1988**, *28*, 1042. (c) Galway, A. K. *Thermochemica Acta* **2004**, *413*, 139; see p. 160-161, sections 5.5.1 and 5.5.2. (d) Marangoni, A. G. *JAOCS* **1998**, *75*, 1465. Marangoni admits in his paper that "From a curve-fitting point of view, there are no differences between these two functions".

[2] (a) Avrami, M. *J. Chem. Phys.* **1939**, *7*, 1103. (b) Avrami, M. *J. Chem. Phys.* **1940**, *8*, 212. (c) Avrami, M. *J. Chem. Phys.* **1941**, *9*, 177.

[3] Fanfoni, M.; Tomellini, M. *Il Nuovo Cimento* **1998**, *20*, 1171.

[4] (a) Jun, S.; Zhang, H.; Bechhoefer, J. *Phys. Rev. E.* **2005**, *71*, 011908. (b) Brown, M. E. *Thermochim. Acta* **1997**, *300*, 93. (c) Galwey, A. K.; Brown, M. E. *Studies in Physical and Theoretical Chemistry, 86. Thermal Decomposition of Ionic Solids* Elsevier, 1999, Chapter 3, p. 75-115. (d) Galwey, A. K. *J. Thermal Anal. Calorimetry* **2008**, *92*, 967. (e) Khawam, A.; Flanagan, D. R. *J. Phys. Chem. B* **2006**, *110*, 17315.

[5] Watzky, M. A.; Finke, R. G. *J. Am. Chem. Soc.* **1997**, *119*, 10382.

[6] Finke, R. G. In *Metal Nanoparticles: Synthesis, Characterization, and Applications*, D. L. Feldheim, C. A. Foss, Jr., Eds.; Marcel Dekker, New York, 2001, Chapter 2.

[7] (a) Besson, C.; Finney, E. E.; Finke, R. G. *J. Am. Chem. Soc.* **2005**, *127*, 8179. (b) Besson, C.; Finney, E. E.; Finke, R. G. *Chem. Mater.* **2005**, *17*, 4925.

[8] (a) It has recently come to our attention[8f] that early work by Perez-Benito[8a-e] on MnO_4^- oxidations of, for example, Me_2NH, provide what can now be recognized as an early example of the 2-step "F-W mechanism" utilized herein. The Perez-Benito work seems to have been generally missed in the particle nucleation and growth literature for perhaps four reasons: (i) the early work fails to reference or tie into any prior particle formation literature of the time (e.g., LaMer's work); (ii) nucleation and growth are not mentioned in the early work, (iii) that work[8b,c] never recognized nor

wrote a generalized form of mechanism, that is the $A \rightarrow B$, $A + B \rightarrow 2B$ that was conceptualized in our 1997 paper[5] (instead it gives only a differential equation, "$r = k_1c + k_2(c(c_o-c)$",[8d] that one has to, and now can upon re-examination of that work, recognize as to correspond to the 2-step mechanism denoted the "F-W mechanism" herein); and perhaps most importantly (iv) that work does not investigate, nor therefore recognize, the broad applicability of the 2-step mechanism.[10,11,12,13] We even referenced one of Perez-Benito's papers[8b] in our early 1994 paper[34b] that had a non-generalized version of the 2-step mechanism in it, but cited that paper as reference 35a therein in regards to light scattering by the observed product, but not in any reference to their kinetics of mechanism which did not seem directly applicable at the time—in hindsight an error for which we apologize to Prof. Perez-Benito and his co-authors; the oversight was not intentional. We plan a badly needed review of the history leading up to the 2-step mechanism, in which we will be sure that Perez-Benito and co-workers receive proper credit for their early work. (b) Mata-Perez, F.; Perez-Benito, J. *Zeitschrift Physikalische Chemie* **1984**, *141*, 213. (c) Mata-Perez, F.; Perez-Benito, J. F. *J. Chem. Ed.* **1987**, *64*, 925. (d) Perez-Benito, J.; Arias, C. *Int. J. Chem. Kinetics* **1991**, *23*, 717. (e) There are several other papers in this series by Perez-Benito and co-authors; the latest is: Insausti, M. J.; Mata-Perez, F.; Alvarez-Macho, M. P. *Collection of Czechoslovak Chem. Comm.* **1996**, *61*, 232. (f) We thank Dr. Pete Skrdla for pointing out the *J. Chem. Ed.* Reference[8c] to us, and in turn thank Prof. Brown[9] who we understand first brought that reference to Dr. Skrdla's attention. There is truly an enormous, diffuse / largely unconnected, often conflicting or confusing literature of nucleation and growth phenomenon across Nature, a literature we are doing our best to comprehend, connect and distill[5,6,7,11,12,13,32,33,34,40] to its underlying essences, including the present contribution.

[9] (a) Brown notes, as the introduction to his paper,[9b] that " When one attempts to read the intimidating and rather indigestible literature of kinetics of solid-state processes and, in particular the papers on non-isothermal kinetics (NIK), one can not help noticing the similarities between Science and Religion. Those that believe that they have found the 'true way' promote their points-of-view with evangelistic fervor and often mention with contempt, or even attack, the practices of the "heathen". The field is full of dogma: 'Thou shall do this.....and thou shall not do the other'! An agnostic in the field (defined as a person who is uncertain or noncommittal) searches, perhaps in vain, for what is useful and what is not."
We agree; the above quote pretty much explains why we are only now publishing the present contribution despite starting it in 2003 when we first realized that A-E and F-W provided equivalent fits in at least a number of instances to both solution nanocluster and solid-state sigmoidal kinetic data. Hence, our approach to the present paper can be described using the above language as that of (hopefully) "non-evangelical agnostics". (b) Brown, M. E. *J. Thermal Anal.* **1997**, *49*, 17.

[10] For a list of lead references to sigmoidal curves in nature, see elsewhere[11,12,13,41] as well as references 1-11 summarized in: Finney, E. E.; Finke, R. G. Fitting and Interpreting Transition-Metal Nanocluster Formation and Other Sigmoidal-Like

Kinetic Data: A More Thorough Testing of Dispersive Kinetics versus Chemical-Mechanism-Based Equations and Treatments. *Chem. Mater.*, **2009**, in revision.

[11] Morris, A. M.; Watzky, M. A.; Agar, J. N.; Finke, R. G. *Biochem.* **2008**, *47*, 2413, and references therein.

[12] Watzky, M. A.; Morris, A. M. Ross, E. D.; Finke, R. G. *Biochem.* **2008**, *47*, 10790.

[13] Morris, A. M.; Watzky, M. A.; Finke, R. G. *Biophys. Biochem. Acta*, **2009**, 1794, 375.

[14] (a) Burnham, K. P.; Anderson, D. R. *Model Selection and Multimodel Inference: A Practical Information-Theoretic Approach*, 2nd Ed.; Springer-Verlag: New York; 2002. (b) Motulsky, H.; Christopoulos, A. *Fitting Models to Biological Data Using Linear and Nonlinear Regression*; Oxford: New York; 2004. (c) Bozdogan, H. *J. Math. Psych.* **2000**, *44*, 62. (d) A useful, readable introduction to both model building and testing, including the AIC method, is: Motulksy, H. J.; Christopoulos, A. "Fitting models to biological data using linear and nonlinear regression. A practical guide to curve fitting", 2003, GraphPad Software Inc., San Diego, CA, www.graphpad.com.; see p. 134-165.

[15] Wang, X. P.; Corbel, G.; Kodjikian, S.; Fang, Q. F.; Lacorre, P. *J. Solid State Chem.* **2006**, *179*, 3338.

[16] Liu, L.; Wu, Z. F.; Zhang, J. *J. Alloys Comp.* **2002**, *339*, 90.

[17] Liu, H.; Sullivan, R. M.; Hanson, J. C.; Grey, C. P.; Martin, J. D. *J. Am. Chem. Soc.* **2001**, *123*, 7564.

[18] Lu, X. F.; Hay, J. N. *Polymer* **2001**, *42*, 9423.

[19] Holzer, J. C.; Kelton, K. F. *Acta Metall. Mater.* **1991**, *39*, 1833.

[20] Greer, A. L. *Acta Metallurgica* **1982**, *30*, 171.

[21] Liu, L.; Zhao, X.; Ma, C.; Zhang, T. *Intermetallics* **2009,** in press.

[22] (a) We wish not to commit the much-discussed sin[9b,22b] of using a concentration, reaction-order based mechanistic model to infer possible insights into complex solid-state processes *without properly stating the caveats involved.* Specifically, one needs to recognize that solid-state kinetics has many complexities not present in typical solution reactions:[9b,22b] spatially constrained reactants, inhomogeneities in reactant distribution; surface area and particle size effects; geometric, preferred orientation, interfacial, and mass- and heat-transfer limitations and effects; as well as other documented complexities dependent on the history of the sample.[9b] In short, we have

no illusions that the observations and resultant hypotheses in the present paper will provide a panacea for all that ails solid-state kinetics. We do hope, however, that the present work will trigger new ideas and possibly new approaches by kinetics experts in the solid-state and thermal analysis communities. (b) Sesták, J. *J. Thermal. Anal.* **1979**, 16, 503. In particular, the "sin" we refer to is Sesták's (p. 516): "I do hope never to read again introductory sentences such as "solid-state process may be represented by a simplified kinetic relation defined by reaction order...". The point to be grasped here is that since concentration loses its meaning in solid-state kinetics, so does the concept of (concentration-change-determined) kinetic order in the starting material of the phase change (and at least in the absence of clever ways to change amount via, for example, fully mixed solid solution type systems (or change the surface area of very intimately mixed solids in some "homogeneous, continuous" way, etc). This, alone, tells one how different and more complex it is going to be to understand the kinetics and mechanism of solid-state processes.

[23] Somasundaran, P., Ed. *Encyclopedia of Surface and Colloid Science*, 2nd ed., CRC Press: New York, 2006; pp 4249. The confusion of "autocatalysis" with the "nucleation" step is apparent in Prout-Tompkins treatments as discussed in Flanagan's lucid review.[4e] Note that the equation defining the nucleation rate (eq. 32 elsewhere,[4e] $dN/dt = k_N N_0 + (k_B - k_T)N$) does not have a form consistent with the rigorous kinetic definition of autocatalysis (i.e., A + B $\rightarrow$ 2B; $-dA/dt = k[A][B]$), illustrating one example of an insidious disconnect between the kinetics and the words/concepts used to discuss those kinetics.

[24] Let us define what we mean by "continuous nucleation". By continuous we mean *average* nucleation, the process by which many single nucleation events occur over a period of time. This is the process measured by the composite (*vide infra*) nucleation rate constant k_1. The use of the term "continuous" nucleation historically served to distinguish the F-W model from LaMer's nucleation and growth mechanism,[24b] in which a hypothesized "burst nucleation" takes place with an essentially infinite nucleation rate. (b) LaMer, V. K.; Dinegar, R. H. *J. Am. Chem. Soc.* **1950**, *72*, 4847.

[25] As further detailed in the Supporting Information, one way to make eq 5.9 valid is by neglecting the growth step, that is, setting $k_2' = 0$, and by setting $n = 1$. Setting $n = 1$ is analogous to assuming a first-order kinetic process (or, in terms of the KJMA theory, having a one-dimensional phase transition). The resulting equation is then $(1-\alpha) = e^{-kt}$, where the Avrami k is then equal to the F-W k_1. (This case is also known as the Mampel first-order model as discussed by Flanagan on p. 17327 elsewhere.[4e]) The result is consistent with the nucleation step (only) of the F-W model being present. While mathematically these assumptions result in the equality between the F-W model and the A-E equation, this limiting case is of little value in treating higher-dimension phase transitions.

[26] For the simulations with changing n, it must be remembered that in general n is between 2 and 4 (although values of $n > 4$ are rare but not unheard of; e.g., see

Figures 5S.4 and 5S.5 of the Supporting Information). Hence, non-physical values of n up to 25 used in the simulations are of use only in establishing the general trends seen by going to such higher n values.

[27] Sun, N. X.; Liu, X. D.; Lu, K. *Scripta Mater.* **1996**, *34*, 1201.

[28] Since sigmoidal curves inherently include so-called "acceleratory" and "deceleratory" kinetic curves as labeled in solid-state kinetics, one might expect the present general results and conclusions to extend to those cases. That said, an important hypothesis that remains to be tested in future studies is the applicability (or not) of the F-W model to the 3 other of the 4 main classes of solid-state kinetics to date, "acceleratory, deceleratory, and order of reaction" models ("sigmoidal" curves as tested herein being the 4th class).[4c]

[29] Van Siclen, C. DeW. *Phys. Rev. B* **1996**, *54*, 11845.

[30] Tomellini, M.; Fanfoni, M. *Phys. Rev. B* **1997**, *55*, 14071.

[31] (a) One additional specific point here: Garn[31b] points out that the use of an Eyring analysis for temperature-dependent rate constants (e.g., such as would result from use of the F-W model) may prove inaccurate since this analysis relies on molecular vibrations which are suppressed in the solid state. Before anyone would try to extend the present treatment to non-isothermal kinetics (e.g, by the expression of k_1 and k_2 in terms of an Arrhenius treatment for each rate constant), one should read Galwey[1c] and Brown[9b] at a minimum. (b) Garn, P. D. *J. Thermal. Anal.* **1975**, *7*, 475.

[32] (a) Watzky, M. A.; Finke, R. G. *Chem. Mater.* **1997**, *12*, 3083. (b) Aiken III, J. D.; Finke, R. G. *J. Am. Chem. Soc.* **1998**, *120*, 9545. (c) Widegren, J. A.; Aiken III, J. D.; Ozkar, S.; Finke, R. G. *Chem. Mater.* **2001**, *13*, 312. (d) Hornstein, B. J.; Finke, R. G. *Chem. Mater.* **2004**, *16*, 139 (see also: *Chem. Mater.* **2004**, 16, 3972).

[33] Watzky, M. A.; Finney, E. E.; Finke, R. G. *J. Am. Chem. Soc.* **2008**, *130*, 11969.

[34] (a) Lin, Y.; Finke, R. G. *J. Am. Chem. Soc.* **1994**, *116*, 8335. (b) Lin, Y.; Finke, R. G. *Inorg. Chem.* **1994**, *33*, 4891.

[35] (a) Wang, T.; Lee, C.; Schmidt, L. D. *Surf. Sci.* **1985**, *163*, 181-197. (b) Ahmadi, T. S.; Wang, Z. L.; Green, T. C.; Henglein, A.; El-Sayed, M. A. *Science* **1996**, *272*, 1924-1926. (c) Tao, A. R.; Habas, S.; Yang, P. *Small* **2008**, *4*, 310-325.

[36] Ott, L. S.; Finke, R. G. *Coord. Chem. Rev.* **2007**, *251*, 1075-1110.

[37] (a) Özkar, S.; Finke, R. G. *J. Am. Chem. Soc.* **2002**, *124*, 5796. (b) Özkar, S.; Finke, R. G. *Langmuir* **2002**, *18*, 7653. (c) Ott, L. S.; Hornstein, B. J.; Finke, R. G. *Inorg. Chem.* **2006**, *45*, 8382.

[38] A telling testament to this claim is Galwey's and Brown's 1998 treatise:[4c] after being trained in solid-state reactions, then spending 38 years as an expert in the area before retiring in 1997 (see p. ix of the preface elsewhere[4c]), Galwey notes in the Preface (p. vii) of his and Brown's book[4c] the quote (cited in the main text herein) of "need for greater chemical, rather than mathematical, representations..." (of solid-stated reactions and their kinetics). Yet, Chapter 3 of that text presents the many (mathematical) models for solid-state reactions, but arguably *very few accepted chemical or physical insights*. His concluding statement, after his 38+ years in the area and the 60+ years at the time of application of A-E and related, typically theory-based equations, that: "In conclusion, a careful balance has to be maintained between the mathematical aspects of modeling and the molecular processes which the models are attempting to represent [99]. Progress in mathematical techniques and theory has far outstripped insights into the controls of reactivity and understanding of the bond redistribution processes involved in crystolysis [89] reactions".

[39] (a) The pseudoelementary step concept, first invented by Richard Noyes for use in treating complex oscillating reactions,[39b-d] involves summing one or more fast reactions with one (to a few) slower reaction(s), giving an overall reaction that can be treated as a (pseudo) elementary step, but which gives kinetic information about the slower reactions. For details about how this is used in nanocluster formation, see elsewhere.[5,7,32d] (b) Noyes, R. M.; Field, R. J. *Acc. Chem. Res.* **1977**, *10*, 214. (c) Noyes, R. M.; Field, R. J. *Acc. Chem. Res.* **1977**, *10*, 273. (d) Field, R. J.; Noyes, R. M. *Nature* **1972**, *237*, 390.

[40] Finney, E. E.; Finke, R. G. *J. Colloid and Interface Science* **2008**, *317(2)*, 351, and references cited therein.

[41] Cope, F. W. *Physiol. Chem. & Physics* **1977**, *9*, 443.

[42] We thank Prof. James Martin for this point. Analogous to what is done with the A-E model, one can set $\alpha = (V-V_o)/(V_m-V_o)$ where "V is the crystal volume, V_o is the initial crystal volume (usual zero), and V_m is the maximal crystal volume attained after crystallization is complete.[1d]

Supporting Information

A Brief Review of Solid-State Literature

Reactions in the solid state comprise a great deal of important chemical processes, including phase transitions,[1] decomposition,[2] pyrolysis of fossil fuels,[3] and dehydration of inorganic materials,[4] to mention a few. A common feature of kinetic data for many solid-state reactions is their sigmoidally-shaped kinetic curves like the ones shown in the main text. As will be seen in Table 5S.1 and the discussion that follows, such sigmoidally-shaped kinetic data have proven difficult for the solid-state literature to fit in an agreed-upon way. Especially lacking *are clear physical insights*, for example even into the basic steps of nucleation and growth, from previously employed fitting methods.

Good reviews of kinetic studies in the solid state exist.[5,6] Table 5S.1 provides a brief summary of the major developments in the study of solid-state kinetics; the systems and equations in Table 5S.1 represent the most common expressions used in the literature for fitting solid-state kinetic data. The A-E equation (entries 2 and 4) has been used to describe the decomposition of kaolinite, brucite, and $BaCO_3$.[7] Alternatively, the Prout-Thompkins equation (entry 3) has been used in pharmaceutical science to model the decomposition of organic solids.[8] In addition, the Šestàk-Berggren equation (entry 5) has been used in the analysis of thermal decomposition of malachite ($CuCO_3 \cdot Cu(OH)_2$) to extrapolate the temperature dependence of the kinetics,[9] and for the pyrolysis of kerogen, dehydration of $Ca(C_2O_4) \cdot H_2O$, and the decomposition of ammonium perchlorate.[4]

Table S1. History of kinetic models for solid-state reactions. A shorter version of this table first appeared in our review.[10]

Entry	Date	Author(s)	Reaction system	Rate equation(s)	Comments	Ref
1	1939	Johnson and Mehl	None, but the model was used to fit various existing experimental data	$f(t) = 1 - e^{-\frac{\pi}{3}N_v G^3 t^4}$ f(t)=fraction of reactant transformed to product N_v=nucleation rate G=growth rate t=time	Equation becomes more complex when nucleation and growth rates are allowed to change during the reaction. Good fits to experimental data.	11
2	1940	Avrami	None; based on general nucleation theory	$N' = N(1 - e^{-nt})$ N′=number of growth nuclei N=number of germ nuclei n=probability of growth nucleus formation	Lack of chemical equations has led to confusion about what the rate equation really describes physically.	12
3	1944	Prout and Tompkins	$2KMnO_4 \rightarrow MnO_2 + KMnO_4 + O_2$ Also decomposition of $AgMnO_4$	$\frac{p}{p_f - p} = e^{k(t - t_{max})}$ p=pressure p_f=final pressure k=rate constant (different for acceleratory vs deceleratory periods) t_{max}=time of maximum rate	Induction period is removed in order to get a good fit. Doesn't fit data for $AgMnO_4$ decomposition. Two different equations needed for "acceleratory" and "deceleratory" parts of the reaction before and after the inflection period of a sigmoidal plot	13
4	1946	Erofe'ev	None; derived from generalized nucleation theory	$\alpha = 1 - e^{-kt^n}$ α=fraction of reactant transformed to product n="dimensionality" of reaction	Uses empirically determined rate laws, Mott's nucleation theory for irreversible vs steady-state reaction.	14

Entry	Date	Author(s)	Reaction system	Rate equation(s)	Comments	Ref
5	1971	Šestàk and Berggren	None	General equation: $\frac{d\alpha}{dt} = k\alpha^m(1-\alpha)^n(-\ln(1-\alpha))^p$ m, n, and p are exponents that depend on the type of nucleation and growth	Begins to resemble autocatalysis (rate increases with amount of product). Used to describe various modes of nucleation and growth, with changing exponents (m, n, and p); the exponents are not given clear physical definitions. Later (in 1991)[15] found to not be general (i.e., does not agree with other, higher-order rate equations).[15]	16
6	1975	Ng	None	General equation: $\frac{d\alpha}{dt} = k\alpha^{1-p}(1-\alpha)^{1-q}$ p and q are exponents between 0 and 1, not clearly defined	Provides analysis of the general equation shown in relation to Avrami, Prout-Tompkins, Erofe'ev, and Roginskii-Shulz equations; asserts that these equations differ only in their values of p and q.	17
7	1981	Tamhankar et al.	Preparation of $SiCl_4$ from Si and CuCl	$\ln\frac{\alpha+k_1}{1-\alpha} = k_2(t-t_i)+\ln k_1$ t_i=induction period k_1 and k_2=rate constants	Explicitly includes autocatalysis and induction period. Reduces to Prout-Thompkins when k_1=0.	18

Entry	Date	Author(s)	Reaction system	Rate equation(s)	Comments	Ref
8	1984	Cardew et al.	None, but use their model to fit NH_4NO_3 decomposition data	$\alpha = \frac{t^4}{(\tau_N \tau_G^{\ 3})/2}$ τ_N=nucleation time τ_G=growth time	A more general model that reduces to the Avrami equation at early times. Introduces many complicating factors and reduced variables that obscure chemical meaning. Shows a dependence of particle size on ratio of growth to nucleation rates.	19
9	1996	Burnham et al.	Coal and kerogen pyrolysis and maturation	$\frac{d\alpha}{dt} = k\alpha(1-0.99\alpha)^m$	Similar to Avrami equation except for the use of the 0.99 term to account for nonzero initial rate.	20
10	1997	Jacobs	None, but uses model to fit Prout and Tompkins' $AgMnO_4$ data	$\ln\left[\frac{a}{1-\frac{a}{2a_i}}\right] - \ln\left[\frac{a_0}{1-\frac{a_0}{2a_i}}\right] = k(t-t_0)$ a=fraction of reactant transformed to product a_i=value of a at the inflection point a_0=value of a at the end of the induction period t_0=induction period	Called the "generalized Prout-Tompkins equation." Fits the $AgMnO_4$ data better than Prout-Tompkins reaction, in which the kinetic curve is not symmetric about the inflection point. States that the induction period is due to slow nucleus growth.	21

Entry	Date	Author(s)	Reaction system	Rate equation(s)	Comments	Ref
11	1997	Urbanovici et al.	Polymer crystallization	$\alpha = 1 - e^{-kt^n}$ (A-E equation) $k = k_0 \exp\left[U^* / R(T - T_\infty)\right] \exp\left[-K_g / T(\Delta T) f\right]$ k_0=pre-exponential factor U*=constant R=gas constant T=Vogel temperature f=2T/(T+T_m) T_m=melting temperature	Not specifically a solid-state reaction system, but uses the A-E equation. Focus is on analysis of the rate constant k and its dependence on temperature.	22
12	2004	Liu et al.	Crystallization of amorphous Mg-Ni alloys	$f = 1 - \exp\left[-K_0^n \alpha^n \exp\left(-\frac{nQ}{RT}\right)\right]$ K_0, n, α, Q are complex expressions that change depending on the type of nucleation: "mixed," Avrami, site saturation as well as isothermal vs icochronal (i.e., equal in time duration) processes	Quality of fit to different expressions of K_0, n, α, and Q determine the nucleation mechanism. Total of 5-6 fitting parameters depending on which expression is used.	23
13	2004	Skrdla	None, but uses model to fit Prout and Tompkins' $AgMnO_4$ data	$\frac{d\alpha}{dt} = k(1-\alpha) + k'(1-\alpha)\left(\frac{k}{k'} + \alpha\right)$ k=nucleation rate constant k'=growth ("nucleus branching") rate constant	Used to fit data from Prout and Tompkins. Still does not fit the induction period well.	24

Entry	Date	Author(s)	Reaction system	Rate equation(s)	Comments	Ref
14	2005	Skrdla and Robertson	None, but uses model to fit Prout and Tompkins' $AgMnO_4$ data	$\frac{dx}{dt} = e^{-\frac{\alpha}{t}e^{\beta t^2 - 1}}\left(-\frac{2\alpha\beta}{t}e^{\beta t^2-1} + \frac{\alpha}{t^2}e^{\beta t^2-1}\right)$ for "acceleratory kinetics"; $\frac{dx}{dt} = e^{\alpha' t e^{-\beta' t^2-1}}\left(-2\alpha'\beta' t e^{-\beta' t^2-1} + \alpha' e^{-\beta' t^2-1}\right)$ for "deceleratory kinetics" α, β, α', and β' are constants containing rate constant terms and various physical constants	Starts from ideal monatomic gas assumption, Maxwell-Boltzmann distribution of energies. Assumes so-called dispersive kinetics are key / necessary.	25
15	2006	Tsapatsis et al.	Formation of zeolites via nanocrystals	$\frac{dn_A}{dt} = -k_+ n_A + k_- n_{B_1}$ $\frac{dn_{B_M}}{dt} = k_+ n_{B_{m-1}} - k_- n_{B_m} - k_+ n_{B_m} - n_{B_m}\sum_{i=1}^{\infty} n_{C_i}\beta_{mi}$ $\frac{dn_{C_k}}{dt} = \sum_{j=1}^{m} n_{B_j}\left(n_{C_{(k-1)}}\beta_{j(k-1)} - n_{C_k}\beta_{jk}\right)$ n_A=number density of precursor ("A") particles n_{Bi}=number density of "B_i" particles n_{Ck}= number density of crystals of k particles β=rate constant for attachment of B to C k_+=rate constant for agglomeration of A to B k_-=rate constant for dissolution of B to A	Poor fit to data. Present a pictorial mechanism similar to the 1997 F-W 2-step mechanism (*vide infra*).	26

More literature data fit to the A-E equation and the F-W model

Phase transition of a pharmaceutical derivative

Li et al. studied the kinetics of the transition from the "dark red" to the "red" phases of the pharmaceutical model compound 5-methyl-2-[(4-methyl-2-nitrophenyl)amino]-3-thiophenecarbonitrile, including the effects of humidity on the kinetics of the transition.[27] After attempting to fit their sigmoidal data to ten different models, including the A-E equation with varying values of n, they found that the best fit (based on the value of R^2) was obtained with the A-E equation with $n = 3$ and $k = 0.0012$ h^{-1}.

When we fit the data using the A-E equation, the parameters we obtained were $n = 1.9(2)$ and $k = 0.076(3)$ h^{-1}, Figure 5S.1, values that are quite different from Li et al.'s $n = 3$ and $k = 0.0012$ h^{-1}. Also in Figure 5S.1 is the fit of the same data to the F-W model, with $k_1 = 0.015(5)$ h^{-1} and $k_2' = 0.26(5)$ h^{-1}. The statistics of the goodness of the fits, shown in Table 5S.2, show that while the R^2 values for the two fits are very similar, the AICc analysis shows that the F-W model is preferred for fitting the data (by a factor of ~ 10^{14}). Although the data for this system is not as good as for some of the other systems, it is important in that it is a representative pharmaceutical application of solid-state kinetic studies.

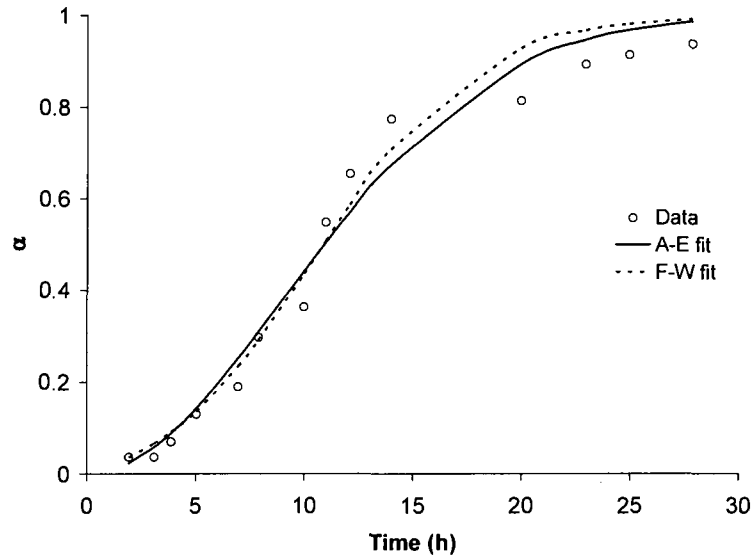

Figure 5S.1. Kinetic data for the solid-state phase transition from "dark red" to "red" phases of 5-methyl-2-[(4-methyl-2-nitrophenyl)amino]-3-thiophenecarbonitrile, with fits to the A-E equation (with $n = 1.9(2)$ and $k = 0.076(3)$ h^{-1}) and to the F-W model (with $k_1 = 0.015(5)$ h^{-1} and $k_2' = 0.26(5)$ h^{-1}). The statistics of the fits are given in Table 5S.2.

Phase transition of nanocrystalline titania

The calcination of a TiO_2 photocatalyst was studied by Yoshikawa et al.,[28] and it was noted that at 700 °C a solid-state phase transition from anatase to rutile takes place. The kinetics of this transition were studied and analyzed using the A-E equation. As is common in the literature, these authors linearized the data with a ln-ln plot. The A-E parameters obtained from their analysis were $n = 0.68$ and $k = 0.18$ min^{-1}. (Note that the value of n is less than one, a rare, but not unheard of, result.[29])

Since only the ln-ln plot was available in this paper, we converted this data back to α versus time, where α in this system is the fraction of rutile phase formed. Fitting this data with the A-E equation gave the curve and A-E parameters shown in Figure 5S.2; note that the value of n obtained herein is the same within error as that obtained from the ln-ln plot by Yoshikawa et al., while the value of k is quite different (0.09(1) min^{-1} herein

versus 0.18 min^{-1} in the original report[28]). The fit of the data to the F-W model is also given in Figure 5S.2, with k_1 = 0.19(3) min^{-1} and k_2' = -0.22(5) min^{-1}. The qualities of the fits are similar, as shown by the R^2 and AICc values given in Table 5S.2. Note that the less-than-one value of n and the corresponding non-physical, *negative* value of k_2' are consistent with the F-W fits to the simulated data derived from the A-E equation described in the main text (*vide infra*) (i.e., and which showed that values of n less than 1 correspond to negative k_2' values).

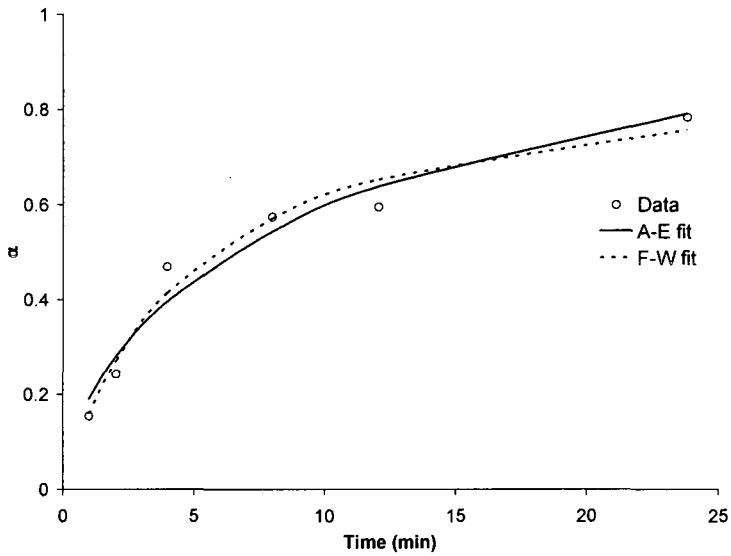

Figure 5S.2. Kinetic data for the solid-state phase transition from anatase to rutile titania, with fits to the A-E equation (with n = 0.63(8) and k = 0.09(1) min^{-1}) and to the F-W model (with k_1 = 0.19(3) min^{-1} and k_2' = -0.22(5) min^{-1}, note the *negative* value of k_2'). The statistics of the fits are given in Table 5S.2.

The Prout-Thompkins $KMnO_4$ system

A classic solid-state phase transition system is the decomposition of $KMnO_4$ studied by Prout and Thompkins in 1944.[13] The equation they used to fit that data is given in Table 5S.1, entry 3. Noticeably absent in this equation is a term for the induction period which is seen in the reaction. The fit to the data with the Prout-Thompkins

equation was close when the induction period was not taken into account. The fit was performed using a ln plot to linearize some of the data, Figure 5S.3a. However, in order for the data to be fit closely, two separate rate constants were necessary. The reaction was broken into two parts: a so-called "acceleratory" period (i.e., in general up to the inflection period of a sigmoidal curve), during which the rate of reaction is increasing, and a so-called "deceleratory" period (i.e., the part after the inflection period of a sigmoidal curve), during which the rate of reaction is decreasing. The same Prout-Thompkins equation was used for both parts of the reaction, but with different "acceleratory" and "deceleratory" rate constants, k and k'. In essence, two different equations were needed to fit all of the data, with the change occurring when the rate of reaction began to decrease.

Fitting *all* of the data to the A-E equation gives the fit shown in Figure 5S.3b and the parameters $n = 2.21(6)$ and $k = 7.24(8) \times 10^{-3}$ min^{-1}. It can be seen that this single equation can fit *all* of the data, including the induction period. However, only a single rate constant k results. Fitting the same data to the F-W model gives the curve shown in Figure 5S.3b and the rate constants $k_1 = 1.2(1) \times 10^{-3}$ min^{-1} and $k_2' = 0.026(1)$ min^{-1}. While the fit is not as close as we have seen with nanocluster formation, the F-W model fits the data well, and more significantly, it takes into account *all* of the data, *including the induction period*, and separates the nucleation and growth rate constants. Noteworthy here is that neither the A-E equation nor the F-W model fits the Prout-Thompkins data as well as the fits we saw for the data in Figures 5.1-5.7 of the main text. The suggested insight from the present work is that although the Prout-Thompkins $KMnO_4$ system and data are a classic in the solid-state literature, it is not clear how good the data really are,

especially in comparison to other literature data now available, *vide supra and vide infra*. The above fits and analysis suggest that this classic system might not be the best, or representative, system for developing new models which can treat solid-state kinetic data. The fact that the F-W model can fit this data is not surprising considering that the decomposition of $KMnO_4$ is autocatalytic, eq 5S.1. Linear regression tests for the fits of this data show that the A-E equation is probably again equivalent within experimental error to the F-W model in fitting this data—for the A-E equation, $R^2 = 0.9952$ and AICc = -230, and for the F-W model, $R^2 = 0.9927$ and AICc = -105. The visual quality of the fit to the A-E equation is very similar to the quality of the fit to the F-W model.

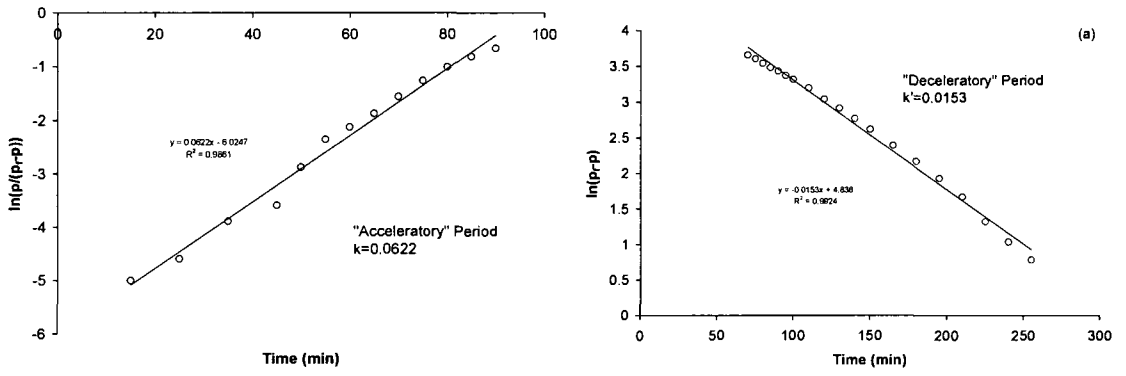

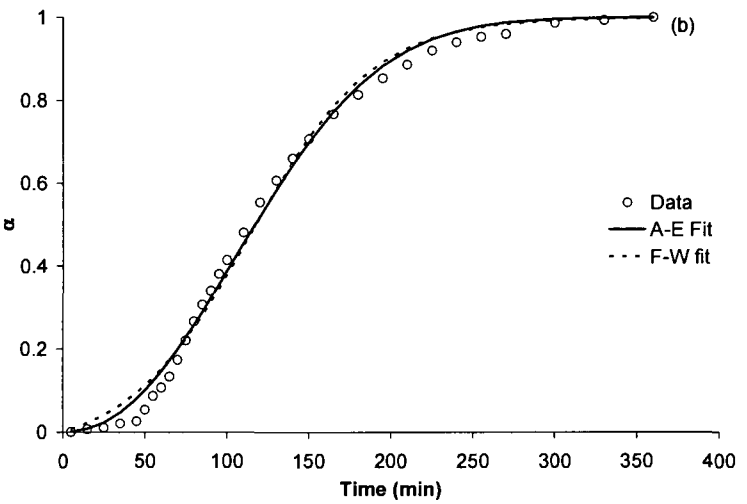

Figure 5S.3. Fits of the data obtained from Prout and Thompkins[13] for their classic system of the decomposition of $KMnO_4$ (eq 5S.1) using: (a) the Prout-Thompkins equation, and (b) the A-E equation ($n = 2.21(6)$ and $k = 7.24(8) \times 10^{-3}$ min^{-1}) and the F-W model ($k_1 = 1.2(1) \times 10^{-3}$ min^{-1} and $k_2' = 0.026(1)$ min^{-1}). The statistics of each fit are provided in Table 5S.2.

$$KMnO_4 \rightleftharpoons KMnO_3 + 1/2\ O_2 \qquad (5S.1a)$$

$$KMnO_4 + KMnO_3 \rightleftharpoons 2\ KMnO_3 + 1/2\ O_2 \qquad (5S.1b)$$

$$2\ KMnO_4 \rightleftharpoons 2\ KMnO_3 + O_2 \qquad (5S.1c)$$

Jacobs' simulated data

In 1997, Jacobs presented an analysis of the A-E equation for solid-state data.[21] In that report, Jacobs generated a sigmoidal curve of α versus time using eq 5S.2, which is an expansion of eq 5.1 and includes several additional variables.[21] Specifically, in eq 5S.2, g_1, g_2, and g_3 are the growth rates in three dimensions, $V(\infty)$ is the volume of all nuclei when growth is complete, n_0 is the number of "potential nucleus-forming sites", σ is a shape factor related to the shape if the nuclei (e.g., $\sigma = 4\pi/3$ for spherical nuclei), and k_0 is a rate constant. When the data generated by eq 5S.2 was fit to the A-E equation, *it was found that two different values of the exponent n were needed*—at early times, $n = 4$, and at later times, $n = 3$—a now understandable result since we now know that nucleation (k_1) and growth (k_2') are convoluted into n. Jacobs noted that using one value of n could fit all of the data, but stated that "it is doubtful if this result (the generalized equation using one value for n) would be of much practical use in a kinetic analysis."[21]

$$-[\ln(1-\alpha)] = \frac{6\sigma g_1 g_2 g_3 n_0}{V(\infty)k_0^3}\left[\exp(-k_0 t) - 1 + k_0 t - \frac{(k_0 t)^2}{2!} + \frac{(k_0 t)^3}{3!}\right] \qquad (5S.2)$$

When the data generated by Jacobs from eq 5S.2[21] is fit to the A-E equation, the curve in Figure 5S.4 results with n = 4.0(1) and k = 0.0025(1) min^{-1}. The fit is good, and it can be seen that only a single value of n (n = 4) is necessary for a close fit. Fitting the same generated data to the F-W model gives the rate constants k_1 = 5.0(3) × 10^{-5} min^{-1} and k_2' = 0.0132(3) min^{-1}, Figure 5S.4. The quality of the two fits are visually identical, and the statistical data agree with this—for the A-E fit, R^2 = 0.9994 and AICc = -258, while for the F-W fit R^2 = 0.9993 and AICc = -250, Table 5S.2. Moreover, the need for, or value of, a model with more than two variables is brought into question by the good fits shown in Figure 5S.4.

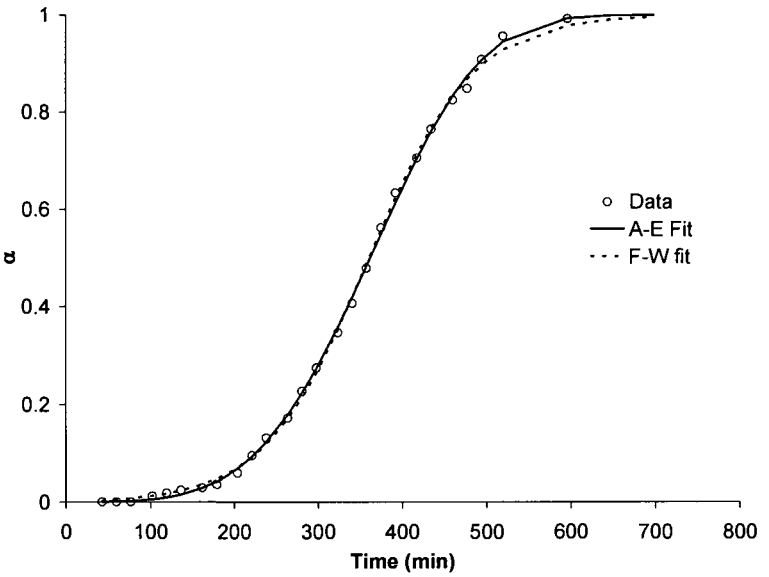

Figure 5S.4. Fits of the data generated by Jacobs[21] using A-E equation (with n = 4.0(1) and k = 0.0025(1) min^{-1}) and the F-W model (with k_1 = 5.0(3) × 10^{-5} min^{-1} and k_2' = 0.0132(3) min^{-1}). The statistics of each fit are given in Table 5S.2.

Tsapatsis' zeolite formation system

In 2006, a complex model for zeolite formation from agglomerating particles was presented by Tsapatsis et al. (entry 15 in Table 5S.1).[30] The basic mechanism that these authors propose (see entry 15 in Table 5S.1) is similar to the F-W model in Scheme 5.1. Following a zeolite formation over the course of more than a year gave the data and fit shown in Figure 5S.5, shown with the fits to the authors' model, the A-E equation (with n = 7.3(4) and k = 2.15(1) × 10^{-3} day^{-1}), and the F-W model (with k_1 = 1.3(5) × 10^{-6} day^{-1} and k_2' = 0.022(1) day^{-1}). The fits are *better* using the F-W model and the A-E equation (F-W: R^2=0.9985 and AICc = -40.0; A-E: R^2 = 0.9985 and AICc = -39.8) than the Tsapatsis fit (R^2 = 0.8322 and AICc = -16.2), *and use only 2 parameters*, as opposed to 4 parameters for the Tsapatsis model (k_+, k_-, β, and m). The fits of the data to the F-W and A-E models are very similar; statistically, based on the AICc values, the F-W model and the A-E equation are equivalent as well (the $ER_{A\text{-}E/F\text{-}W}$ is only 1.1, Table 5S.2).

The comparison of the three fits, as well as the fits shown above, demonstrate the issues in choosing a kinetic model that will both: (a) fit the data well, and (b) be able to describe the physical process in a meaningful way. Some quotes about models in science are relevant here, for example Hoffmann, et al's:[31b] "In the processing of models we must be especially cautious of the human weakness to think that models can be verified or validated. Especially one's own." Also noteworthy is their admonition that "Every model is, by definition, incomplete".[31b] Another useful quote is "All models are wrong, but some are useful" attributed to George E. P. Box (see p. 58 elsewhere[32]).

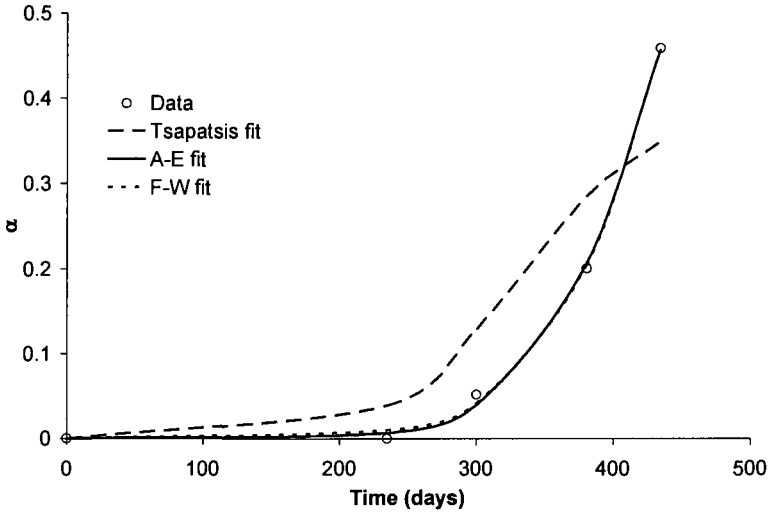

Figure 5S.5. Fits of Tsapatsis' data for zeolite formation to the set of equations given by Tsapatsis in Table 5S.1, entry 15 (with $k_+ = 9.01 \times 10^{-4}$ h^{-1}, $k_- = 2.55 \times 10^{-3}$ h^{-1}, $\beta = 2.12 \times 10^{-26}$ m^{-3}s^{-1}, and $m = 10$), the A-E equation (with $n = 7.3(4)$ and $k = 2.15(1) \times 10^{-3}$ day^{-1}), and the F-W model (with $k_1 = 1.3(5) \times 10^{-6}$ day^{-1} and $k_2' = 0.022(1)$ day^{-1}). The statistics for the A-E and F-W fits are given in Table 5S.2.

Table 5S.2. Statistical data for the fits in the systems described herein (Figures S1-S5) to the A-E equation and the F-W model.

System (Figure)	R^2 (A-E)	R^2 (F-W)	AICc (A-E)	AICc (F-W)	w (A-E)	w (F-W)	$ER_{(A\text{-}E/F\text{-}W)}$
ROY (S1)	0.9723	0.9721	-75	-139	1.7×10^{-14}	1	1.7×10^{-14}
TiO_2 (S2)	0.9595	0.9710	-30	-32	0.27	0.73	0.37
$KMnO_4$ (S3)	0.9949	0.9925	-230	-217	0.998	0.002	588
Jacobs (S4)	0.9994	0.9992	-258	-250	0.98	0.02	52
Zeolite (S5)	0.9985	0.9985	-39.8	-40.0	0.47	0.53	1.1

Fitting nanocluster formation data using the F-W and A-E models

To fit nanocluster formation data, which follows the loss of concentration of A, we had to change the fitting method somewhat. To fit the data with the F-W model, eq 5.2 was used as usual, since using a concentration-dependent expression makes sense for this data set. To fit the concentration data to the A-E equation, eq 5.1 was converted to a form that includes concentration, by noting that $\alpha = ([A]_0 - [A]_t)/[A]_0$. The resulting equation, eq 5S.2, was used to fit the nanocluster data to obtain values for the parameters k and n. This was done to show how the A-E equation can be modified to give the appearance of the nanocluster formation data, but doing so introduces a physically nonsensical concentration term into the solid-state equation. This equation was not used to fit any of the other data herein.

$$[A]_t = [A]_0 e^{-(kt)^n} \qquad (5S.2)$$

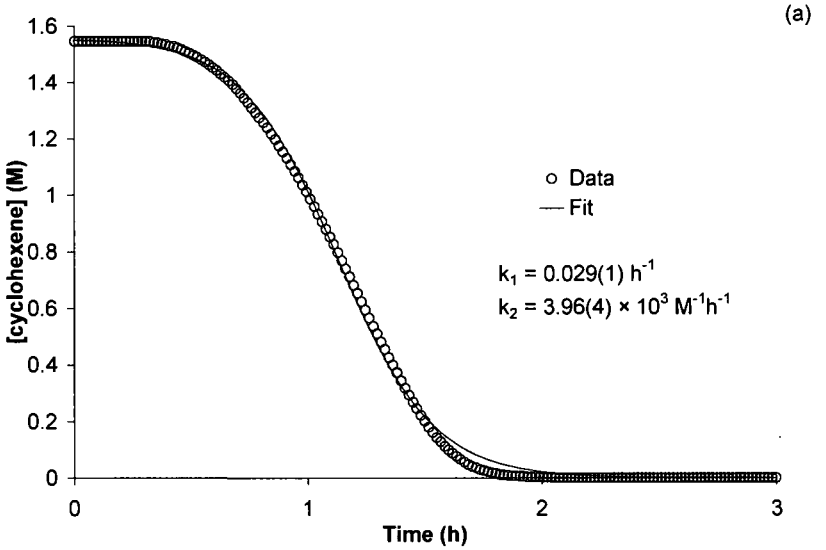

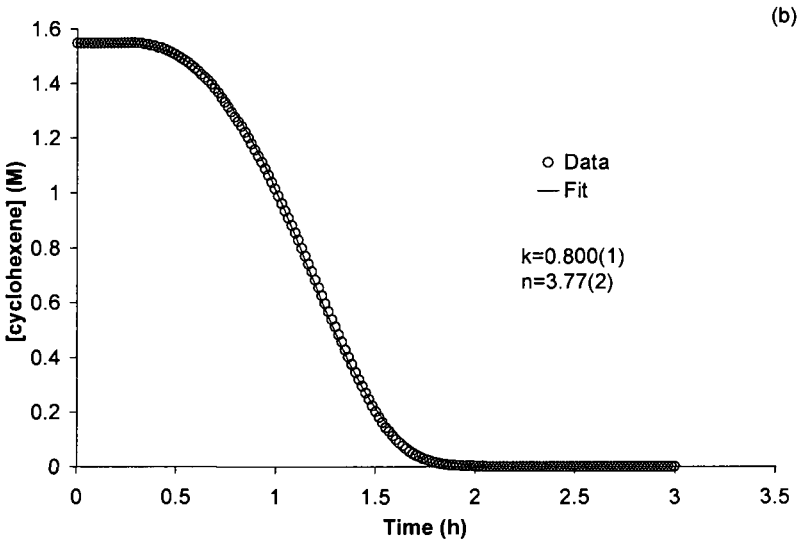

Figure 5S.6. Kinetic data for the formation of $Ir^0_{\sim 300}$ nanoclusters from the reduction of $[(Bu_4N)_5Na_3][(1,5\text{-COD})Ir{\bullet}P_2W_{15}Nb_3O_{62}]$ under H_2, as followed by the concomitant cyclohexene hydrogenation. The data are fit by (a) the F-W model and (b) the Avrami equation. The relevant parameters are shown within each curve. Note that the value of k_2 in the F-W fit is corrected for the [cyclohexene]:[Ir] ratio, as described elsewhere.[32] See the Experimental section of the main text for fitting details. Although the fit to the whole curve is shown above, at the end of the cyclohexene uptake the assumption that the cyclohexene is in a large excess, so that the reporter reaction is fast, is no longer true, so that the end of the curve is a region where the assumptions under which the kinetic data are obtained by the cyclohexene reporter reaction break down. Hence, the statistical parameters for the fits given below are for fits to the first half of the data: for the A-E model, $R^2 = 0.9995$ and AICc = -717 while for the F-W model, $R^2 = 0.9959$ and AICc = -574, corresponding to an ER of 1.5×10^{31}. In short, while both the A-E and F-W models fit the nanocluster formation data very closely visually, the AICc treatment gives the A-E model the statistical edge for the present set of data.

Of interest in the above is that, at least according to the AICc parameters and for this one set of data, A-E provides the better fit. We have long known that A-E would fit our nanocluster formation data, but rejected it as a valid treatment prior to even our 1997 paper[32] since (i) applying a sold-state kinetic model to our solution nanoclusters seemed inappropriate at the time (as one could argue the present application of the solution-derived F-W to solid-state problems may be inappropriate?!); (ii) there was no obvious "dimensionality", *n*, to our solution

nanocluster system as contained in the A-E equation; and therefore (iii) it was completely unclear—and still is—how to obtain any physically useful insights from the application of A-E to solution nanocluster formation kinetics. What do the parameters "*n*" and "*k*" from A-E tell one about the desired solution nanocluster formation mechanism?

An alternate way to relate the A-E equation and the F-W integrated rate equation

To mathematically compare the A-E equation, eq 5.1, and the F-W integrated rate equation, eq 5.2, in a way different than in the main text, we solve both equations for *t*, set them equal to each other (i.e., assume that the equations are the same), and see what results. Solving eq 1 for *t* gives eq 5S.3.

$$t = \frac{\left[-\ln(1-\alpha)\right]^{\frac{1}{n}}}{k} \tag{5S.3}$$

Solving the F-W integrated rate equation, eq 5.3, for *t* gives eq 5S.4,

$$t = \frac{\ln\left[\frac{k_2[\mathrm{A}]_0}{k_1[\mathrm{A}]_t}\left(\frac{k_1}{k_2} + [\mathrm{A}]_0 - [\mathrm{A}]_t\right)\right]}{k_1 + k_2[\mathrm{A}]_0} \tag{5S.4}$$

which when rearranged gives eq 5S.5.

$$t = \frac{\ln\left[\frac{[\mathrm{A}]_0}{[\mathrm{A}]_t}\left(\frac{k_1 + k_2[\mathrm{A}]_0 - k_2[\mathrm{A}]_t}{\mathrm{k}_1}\right)\right]}{k_1 + k_2[\mathrm{A}]_0} \tag{5S.5}$$

Since $[\mathrm{A}]_0/[\mathrm{A}]_t = 1/(1-\alpha)$ and $[\mathrm{A}]_t = [\mathrm{A}]_0(1-\alpha)$, we can rewrite the above equation as eq 5S.6,

$$t = \frac{\ln\left[\left(\frac{1}{1-\alpha}\right)\left(\frac{k_1 + k_2[\mathrm{A}]_0\alpha}{\mathrm{k}_1}\right)\right]}{k_1 + k_2[\mathrm{A}]_0} \tag{5S.6}$$

which can be rearranged to eq 5S.7, where we also make the substitution $k_2' = k_2[A]_0$.

$$t = \frac{-\ln\left[(1-\alpha)\left(\frac{k_1}{k_1 + k_2'\alpha}\right)\right]}{k_1 + k_2'} \tag{5S.7}$$

Making the assumption that the F-W and A-E models are the same, and therefore setting eqs 5S.3 and 5S.7 equal, gives eq 5S.8.

$$\frac{[-\ln(1-\alpha)]^{\frac{1}{n}}}{k} \approx \frac{-\ln\left[(1-\alpha)\left(\frac{k_1}{k_1 + k_2'\alpha}\right)\right]}{k_1 + k_2'} \tag{5S.8}$$

Like the treatment in the main text, we see that the equality is true if $k_1 >> k_2'$, so that the k_2' terms drop out of the right-hand side of eq 5S.8, and if $n = 1$. Again, this assumes both that growth is negligible and that the nucleation is a first-order process. While it is temping to set $k \approx k_1 + k_2'$ by looking at the denominators in eq 5S.8, the numerator shows that the true relationship is more complicated, a conclusion supported by the simulations given in the main text which show a more complex relationship between k, n and k_1 and k_2'.

Comparing eqs 5S.3 and 5S.7, it again seems clear that there is some convolution of the nucleation and growth rate constants k_1 and k_2' into the A-E rate constant k and parameter n. It is thought in the solid-state literature that changes in the Avrami exponent n are due to the change in mechanism during the course of the reaction;[33] *the present treatment suggests an alternative hypothesis: that the real change may simply entail going from nucleation to growth.* Looking at the A-E and F-W equations in the same general form supports this idea, and suggests that there is

some factor of the rate constants k_1 and k_2 ingrained into the Avrami exponent n, as well as in the Avrami rate constant k.

Atempted isolation of k_1 and k_2' from eq 5.9 in the main text

The solution of eq 5.9 for k_2' as given by Mathematica is given in eq 5S.9:

$$k_2' \approx -\frac{k_1}{e^{(kt)^n}-1} - k_1 - \frac{\text{ProductLog}\left[-\frac{k_1 t e^{k_1 t - \frac{t\left[k_1 + k_2'\left(e^{(kt)^n}-1\right)\right]}{e^{(kt)^n}-1}}}{e^{(kt)^n}-1}\right]}{t} \qquad (5S.9)$$

In this expression, the ProductLog function is defined as the solution to the equation $y = xe^x$. In other words, if $y = xe^x$, then ProductLog(y) = x.

As for our attempt to isolate eq 5.9 for k_1, Mathematica returned an error when asked to solve eq 5.9 for k_1. Since the attempt to isolate k_1 was unsuccessful, at least when using Mathematica, no attempt was undertaken to try to isolate k_1 classically, by hand.

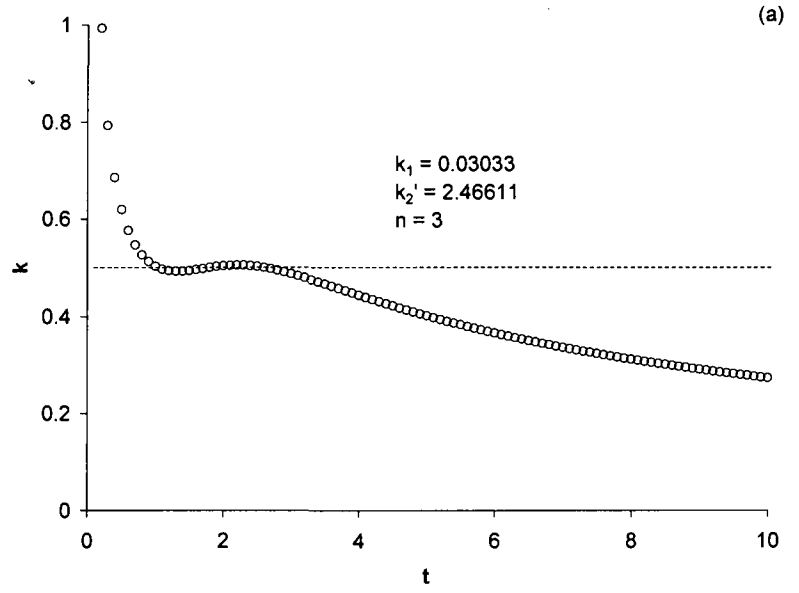
(a)
1
0.8
0.6
0.4
0.2
0
k
0
2
4
6
8
10
t
k_1 = 0.03033
k_2' = 2.46611
n = 3

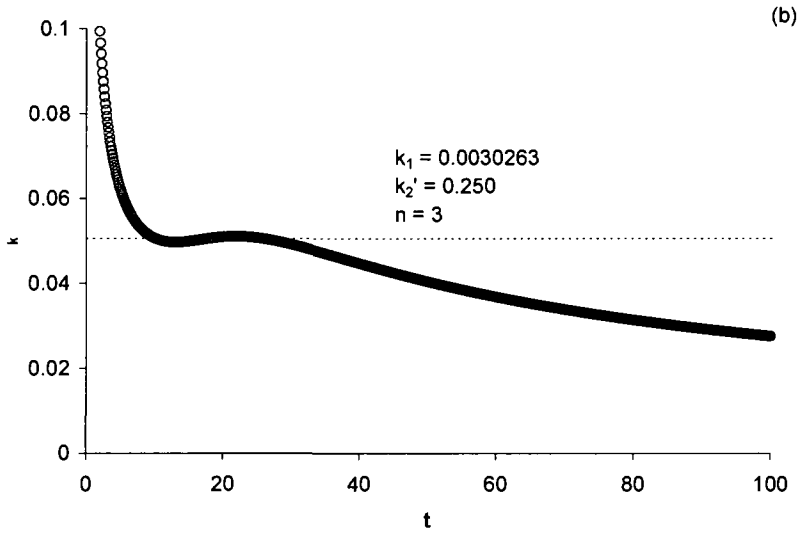
(b)
0.1
0.08
0.06
0.04
0.02
0
k
0
20
40
60
80
100
t
k_1 = 0.0030263
k_2' = 0.250
n = 3

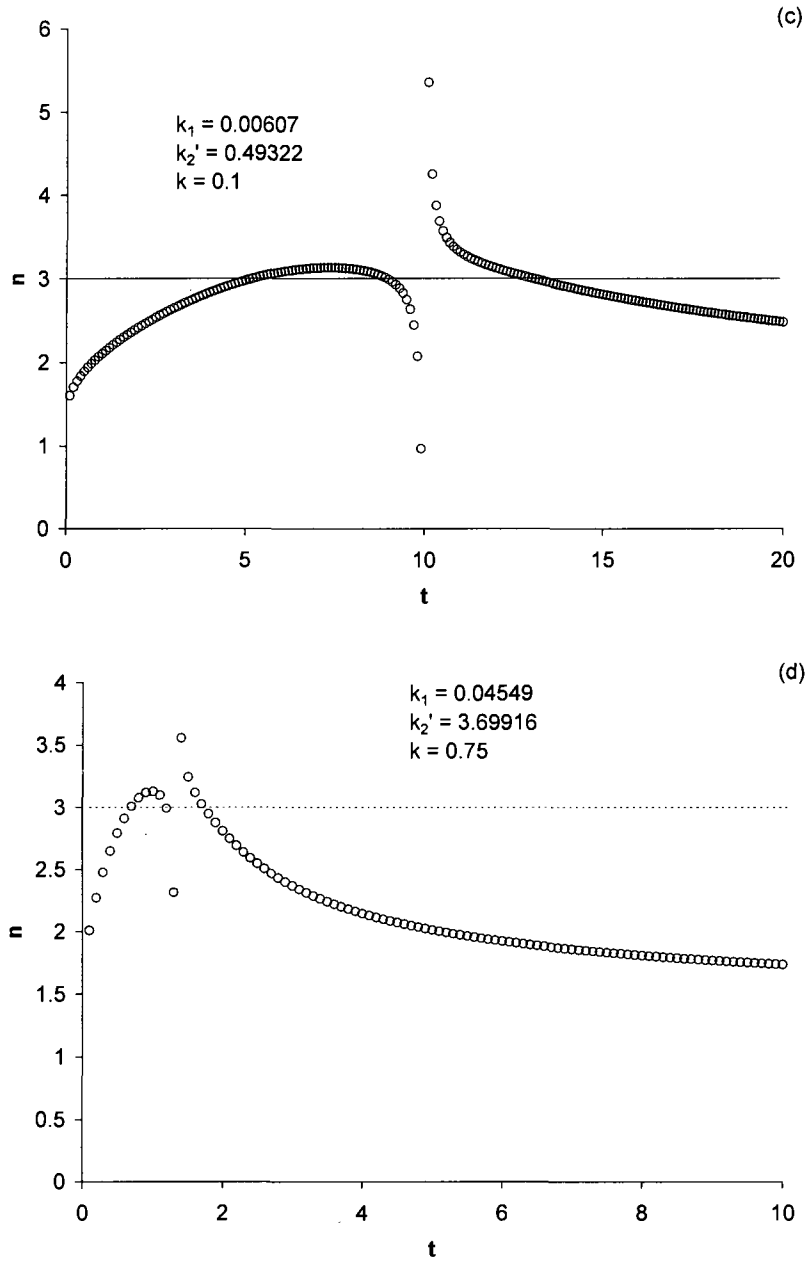

Figure 5S.7. Plots of k versus t (a and b) and n versus t (c and d) calculated from eqs 5.10a and 5.10b, respectively. The values of the parameters used for the calculations, shown within each curve, were taken from the simulated data described in the main text. The dotted lines in each plot show the constant value of k and n, respectively, that is expected (i.e., the value used in the original simulations: for a and b, $k = 0.5$, and for c and d, $n = 3$). The calculations come closest to the expected values at intermediate times, with some deviation at short and long times. Interesting is the observation in (a) and (b) that the curve has a local maximum at the expected value of k. The curves in (c) and (d) have discontinuities at times at which the denominator in eq 5.10b is zero; at these times, the value of n is closest to its expected value.

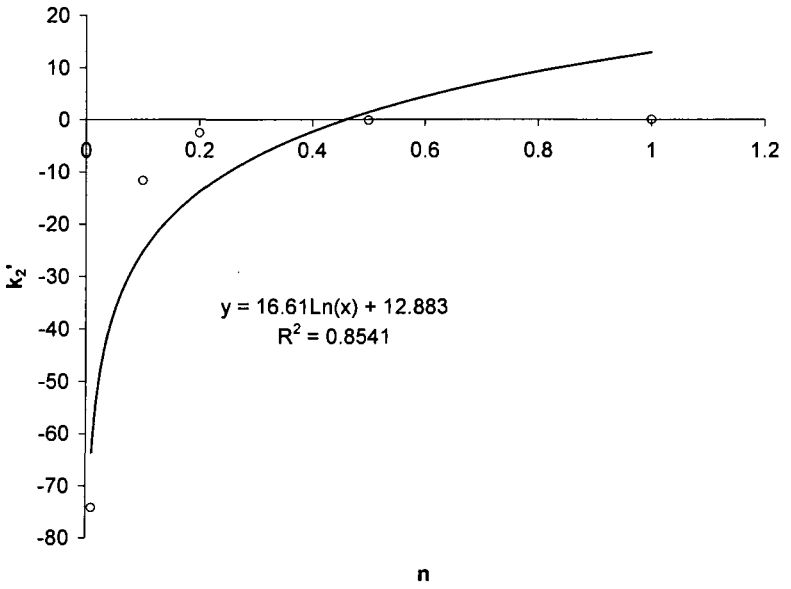

Figure 5S.8. Dependence of the F-W rate constant k_2' on the A-E parameter n for $0 < n \leq 1$. The decrease in k_2' as n approaches zero appears to be logarithmic, but is more drastic as the attempted fit to a logarithmic function shown demonstrates.

A more detailed look at the A-E model

The A-E equation is based on the model put forth by Kolmogorov,[34] Johnson and Mehl,[11] Avrami[12] (the KJMA theory), and Erofe'ev[14] (see entries 1, 2, and 4 in Table 5S.1). The basic KJMA theory consists of four main assumptions, summarized by Tomellini and Fanfoni.[5] They are: (i) that phase transformations occur via nucleation and growth; (ii) that "germs" (i.e., nucleation sites) are distributed randomly, that is, nucleation is homogeneous; (iii) that the critical nucleus size is zero, so that nucleation is completely spontaneous (this is counterintuitive, given that the theory for solid-state transformations is based on classical nucleation theory,[35] which requires a critical nucleus of at least 1 before growth occurs); and (iv) that the nucleation and growth laws are given *a priori*, meaning that the rate equations given are assumed and not based on experimental evidence or chemical or mechanistic insights or principles. This is a common problem in the solid-state literature, one that

leads to multiple, often increasingly complex equations (Table 5S.1, *vide supra*) to treat solid-state kinetic data. The enormous amount of literature that has evolved over the last several decades provides compelling evidence for Galwey and Brown's statement[36] as quoted on p. 136 elsewhere[37] that "formulating chemical mechanisms for reactions of solids has turned out to be far more difficult than was foreseen in early work."

One common way of fitting experimental data using the A-E equation is to linearize it by plotting $\ln[-\ln(1-\alpha)]$ versus $\ln(t)$, and extracting the values of k and n out of this plot. While this procedure makes the middle of the sigmoidal curve more linear, it still ignores the beginning and the end of the curve, and is unnecessary given modern computers and non-linear least squares curve fitting abilities and given that (as we show herein) the A-E equation can be used to fit all of the data without manipulating it by taking a ln-ln plot. Removing the initial nucleation part of the reaction data gives an incomplete analysis of the data. Early forms of the model do not even take the induction period into account, but rather set $t = 0$ to when growth begins (i.e., and after any induction period). Later models similarly treat the induction period by replacing t in the equations with $(t-t_0)$, with t_0 the induction time (e.g., entries 7 and 10 in Table 5S.1). Still other models "normalize" time, setting $t = 0$ when the reaction is halfway complete (i.e., when $\alpha = 0.5$). This results in negative time values, evidence of the lack of useful physical or chemical meaning as the result of such ad hoc analyses.

Analysis of the A-E equation (in the context of KJMA theory) sometimes involves the use of physically irrelevant (to nonsensical) entities. One such idea is the

"extended volume," which is defined as the total volume of all particles assuming that they grow unimpeded. In other words, the extended volume assumes that when two growing particles impinge on each other, growth does *not* stop. The extended volume, then, includes the volume of overlapping nuclei. Another problem with the KJMA analysis is that it uses a Poissonian function; this does not take into account the restriction of nucleation of the new phase to areas that have not already nucleated, therefore allowing nucleation to occur in the same places more than once.[38] This is obviously inaccurate, since once a nucleus of new phase in the solid state has formed it is impossible for nucleation to occur there. Related to this, the KJMA model requires the use of "phantom nuclei," nuclei that form in the areas where phase transition has already taken place. The ideas of phantom nuclei and extended volume are mathematical necessities in the KJMA model. In 1996, Van Siclen derived a modification that removed theses necessities by considering only the untransformed phase.[39] The mathematics of this derivation became even more complex.[39] Later, Tomellini and Fanfoni concluded that the phenomena of phantom nuclei and extended volume are "unavoidable accidents" of the KJMA theory.[40] Controversy and confusion remain to this day about the use of these non-physical concepts of "extended volume" or "phantom nuclei" that are inherent to the theory.

A more detailed look at the F-W model of transition-metal nanocluster nucleation and growth

In 1997, a mechanism was put forth to describe the nucleation and growth of transition-metal nanoclusters *in solution* under reducing conditions such as H_2.[32] The F-W model consisted of two steps: slow, continuous nucleation followed by fast,

autocatalytic growth, Scheme 5S.1. In Scheme 5S.1, A is the nanocluster precursor complex and B is the growing, typically metal^0 surface of the nanocluster. By design, the F-W model is a minimal, Ockham's Razor[30] approach to describing transition-metal nanocluster nucleation and growth.

Scheme 5S.1 gives the F-W model side-by-side with the A-E equation and shows that the F-W chemical starting material A can be related to the A-E (1-α) (more specifically, $[A]_t=[A]_0(1-\alpha)$, *vide infra*), while the F-W product B can be related to the A-E α (more specifically, $[B]=([A]_0-[A]_t)=[A]_0\alpha$).

Scheme 5S.1. The F-W model.[32] Note that the 2-step F-W model employs and thereby explicitly defines two rate constants, for nucleation (k_1) and growth (k_2), while the model derived from the A-E equation uses only one rate parameter (k) for the overall transformation.

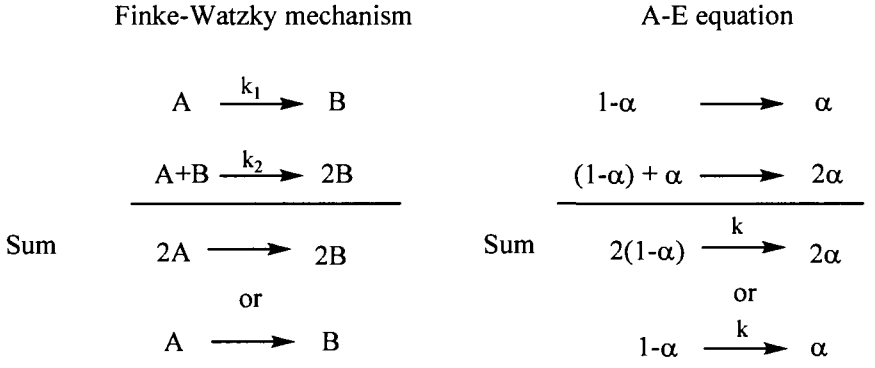

The F-W model was originally developed to describe the formation of $Ir^0_{\sim 300}$ nanoclusters from the reduction of the polyoxonaion-supported complex $(Bu_4N)_5Na_3[(1,5\text{-COD})Ir{\bullet}P_2W_{15}Nb_3O_{62}]$ under H_2;[32] a balanced stoichiometry for the overall reaction has been established and is given in eq 5S.10a. The kinetics of nanocluster formation are typically followed most conveniently, albeit indirectly, via the hydrogen of cyclohexene, eq 5S.10b (see elsewhere for details[32]). However, control experiments following the loss of A directly by ^{1}H NMR and the evolution of cyclooctane (see eq 5S.10a) by GLC quantitatively verify the indirect cyclohexene

hydrogenation reporter reaction kinetic method for following the nucleation and growth of the nanoclusters.[32,41] In the original report of the model, this 2-step, autocatalytic mechanism was found to be the only one that could closely fit the sigmoidally-shaped kinetic curves,[32] Figure 5S.9. Two significant parts of the kinetic curve in Figure 5S.9 are the induction period (the flat part at the beginning of the curve) and the linear part after the curve "turns on." It has been shown, *for this specific system and under the limited range of conditions examined*, that the nucleation rate constant k_1 is proportional to the inverse of the induction period (i.e., $k_1 \propto 1/t_{ind}$), and that the growth rate constant k_2 is directly proportional to the slope of the linear decrease in [cyclohexene] (and, due to the demonstrated 1:1 cyclohexene to H_2 stoichiometry, $k_2 \propto -d[H_2]/dt$ for that linear part of the curve). These relationships are shown graphically in Figure 5S.10. However, more generally the induction time is actually a function of *both* k_1 and k_2.[42]

$$300[(1,5\text{-COD})Ir{\cdot}P_2W_{15}Nb_3O_{62}]^{8-} + 750H_2 \longrightarrow$$

$$300 \text{ } \bigcirc + 1\ Ir^0_{\sim 300} + 300[P_2W_{15}Nb_3O_{62}]^{9-} + 150\ H^+$$

(5S.10a)

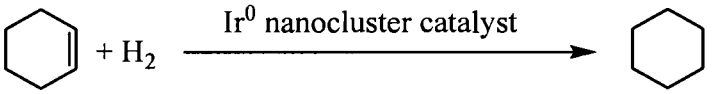

(5S.10b)

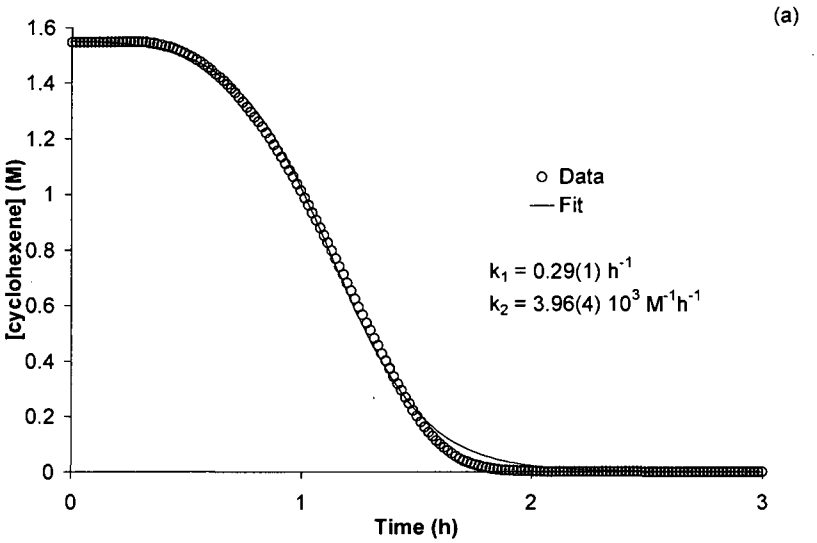

Figure 5S.9. Typical kinetic curve for the formation of $Ir^0_{\sim 300}$ nanoclusters from the reduction of $[Bu_4N]_5Na_3(1,5\text{-COD})Ir{\bullet}P_2W_{15}Nb_3O_{62}$ monitored by its cyclohexene hydrogenation catalysis, eq 5S.10b. Details of the fitting procedure are given in the main text.

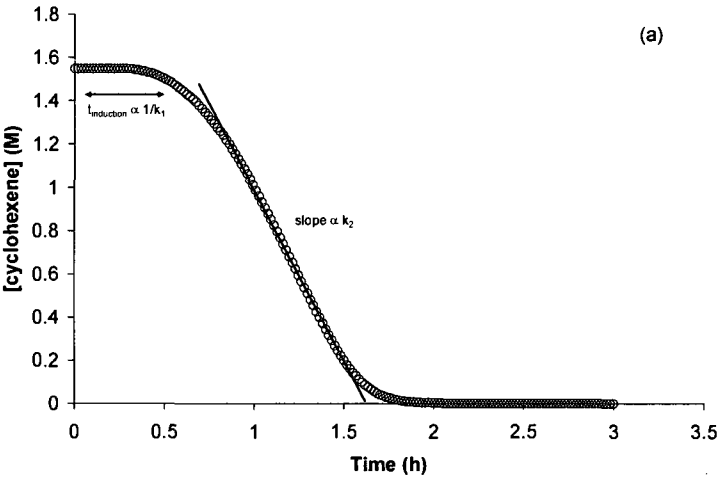

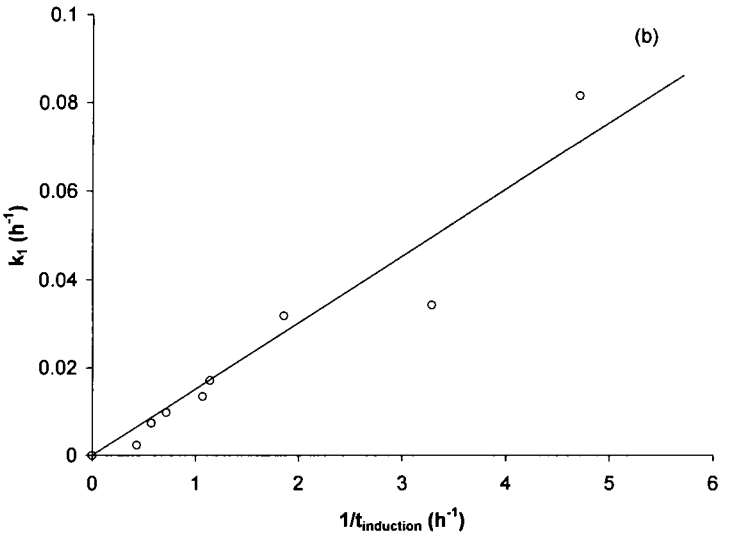

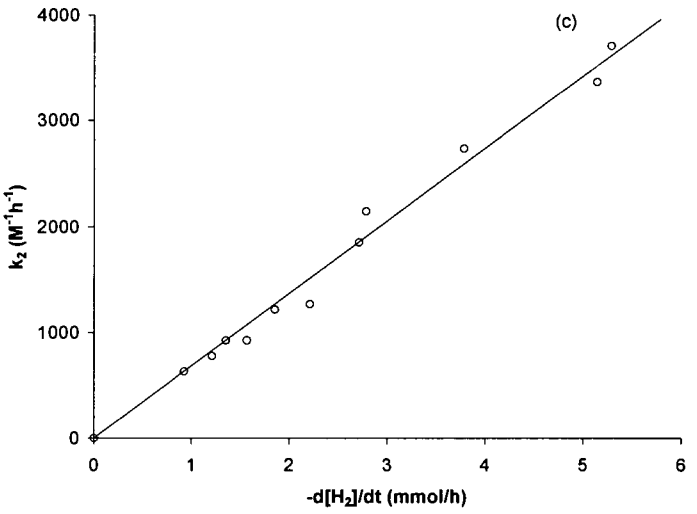

Figure 5S.10. (a) The relationship between k_1 and the induction period, and between k_2 and the slope, shown graphically on a typical kinetic curve. (b) The linear correlation between k_1 and the inverse of the induction period. (c) The linear correlation between k_2 and the slope of the linear part of hydrogen loss. Adapted from reference 32 with permission. The actual induction period definition (in (a) for example) is somewhat arbitrary, the induction period being defined previously as either the time after which a certain measurable extent of reaction has occurred,[32] or the intersection point (time) between the 2 lines drawn from the flat induction period and the ca. linear part of slope (e.g., as shown in (a)). It should be noted that, more generally, *both* k_1 and k_2 contribute to the induction time in other systems or under a broader set of conditions.[42]

The reduction of $[Bu_4N]_5Na_3[(1,5\text{-COD})Ir{\bullet}P_2W_{15}Nb_3O_{62}]$ to form $Ir^0_{\sim 300}$ nanoclusters has been performed as part of more than >700 kinetic experiments of nanocluster growth by several different researchers, and for a variety of metals and conditions, over the course of a more than 15 years.

The F-W model is an Ockham's-Razor based, simplest chemical mechanism, one which fits the sigmoidal data very closely using only two rate constants and no other variables. These rate constants have rigorous chemical and physical meaning defined by the balanced reaction equations in Scheme 5.1 of the main text: k_1 refers to nucleation and k_2 to autocatalytic growth. The F-W model has led to numerous insights about the formation of transition-metal nanoclusters, notably the >9 insights noted in the main text along with appropriate references.

The biggest drawback of the F-W model is that it hides the more intimate mechanistic steps of nucleation and growth in summed, pseudo-elementary steps;[43] as such it necessarily conceals the more intimate details about the nanocluster formation mechanism—a formation mechanism that must logically involve >>300 steps for conversion of 300 equiv of $[(1,5\text{-COD})Ir{\bullet}P_2W_{15}Nb_3O_{62}]^{8-}$ into one (on average) $Ir^0_{\sim 300}$ nanocluster according to eq 5S.1a. For example, nucleation is generally believed to consist of multiple steps leading up to the so-called critical nucleus, after which growth becomes favorable. At least according to classical nucleation theory, before the critical nucleus, dissolution of the cluster is more favorable than growth. Therefore, we can think of nucleation as a series of equilibria until the critical nucleus size is reached, at which point the nanoclusters grow essentially irreversibly. A general illustration of such a mechanism is given in Scheme 5S.2. Note that in

Scheme 5S.2, nucleation is presumed to occur by addition of a single metal atom at a time; combination of multiple "sub-critical" nuclei (e.g., $A_2+A_2 \rightleftharpoons A_4$, etc.) is ignored. Another weakness of the F-W model is that the true rate constants vary with nanocluster size to at least some extent, so that the true underlying problem is really one for the field of so-called "dispersive kinetics".

Scheme 5S.2. A more complete mechanism for transition-metal nanocluster nucleation leading up to the critical nucleus, A_n' (= B_n), followed by growth of the nanocluster via addition of more A onto B. For the system studied herein, A = $[Bu_4N]_5Na_3[(1,5\text{-COD})Ir{\bullet}P_2W_{15}Nb_3O_{62}]$ and B = Ir^0.

$$A + A \underset{k_{-1}}{\overset{k_1}{\rightleftharpoons}} A'_2$$

$$A'_2 + A \underset{k_{-2}}{\overset{k_2}{\rightleftharpoons}} A'_3$$

$$A'_3 + A \underset{k_{-3}}{\overset{k_3}{\rightleftharpoons}} A'_4$$

$$\vdots$$

$$A'_{n-1} + A \xrightarrow{k_{n-1}} A'_n$$

$$nA \xrightarrow{k_{1,sum}} A'_n$$

$$nA \xrightarrow{k_{1,sum}} B_n$$

$$A + B_n \xrightarrow{k_2} B_{n+1}$$

The critical nucleus in Scheme 5S.2 is composed of *n* atoms (*n* as used here should not be confused with the Avrami exponent, also designated *n*). Because the critical nucleus size itself depends on the kinetics of nanocluster formation (which in turn depend on a number of factors, such as solvent, reduction potential of the metal,[41,44] impurities in the solvent,[45] the presence of stabilizing ligands, olefins,[45] and polymers,[46] and the rate of H_2 gas-to-solution mass transfer[47]), the value of *n* is different for different systems. Therefore, the mechanism in Scheme 5S.2 changes so

that there are a total of n steps in the nucleation process. In other words, the quantitative result shown herein is an example of the mechanism, based on the value of n for this system, and is strictly true only for this exact system. Mechanisms similar to that shown in Scheme 5S.2 have been presented in the literature;[48] the main difference with the mechanism shown herein is the inclusion of the irreversible formation of the critical nucleus, A_n, in the last step. Computer simulations show that this step must be irreversible in order for the simulated curve to agree with experimental data.[49] Those simulations also provide good support for the ability of the F-W 2-step mechanism to account, at least via average k_1 and k_2 rate constants, for the system in Scheme 5S.2 with its "dispersion" of rate constants (using the word dispersion here in the sense it is used to describe "dispersive kinetics" systems). Comparing the specific, stepwise mechanism in Scheme 5S.2 (left) to the overall, general model (right), it can be seen that the k_1 that we measure is actually a *composite* nucleation rate constant—it is an average over all of the individual nucleation steps. The same is true for growth; therefore, in the F-W model k_1 and k_2 are assumed to be constant—to not change with size—for the growing nanoclusters, something that cannot physically be true at sufficiently high levels of precision. The growth rate constant, k_2, can be adjusted if desired by a "growth factor" as outlined elsewhere to accounts for the fact that only the surface atoms can be involved in nanocluster growth.[32,49] Similarly, a significant limitation of the F-W minimal kinetic model is that all the growing nanoclusters are lumped into "B", so that there is, again, an averaging and loss of information in the description of "B". In this sense, the rate constants of the F-W model are also somewhat convoluted, although nucleation and

growth are distinct in the F-W model. In addition, metal hydrides may be an important intermediate in nanocluster formation under H_2 reduction.[49] Also, prior equilibria involving the dissociation of ligands from the nanocluster precursor have been found to be important in nucleation.[50,51] Worth noting here, however, is that these added mechanistic complexities proved discernable by studying the effect on the k_1 value of concentration, additives and so on, showing the value of being able to deconvolute even an average nucleation k_1 value from its average k_2 growth counterpart.[32] Further investigations into the more intimate nucleation and growth steps are currently under investigation.[49]

Despite these limitations, the ability of the 2-step F-W kinetic model to fit a growing range of nucleation and growth kinetic data, thereby allowing a deconvolution of the (average) nucleation, k_1, from the (average) growth, k_2, rate constants, all with physically and kinetically well-defined meanings to those rate constants, is a very useful, state-of-the-art aspect of even the minimal F-W kinetic model. An application of the F-W model to deconvolute, for the first time, average k_1 from average k_2 values for α-synuclein, a protein involved in Parkinson's disease, is shown in Figure 5S.11.

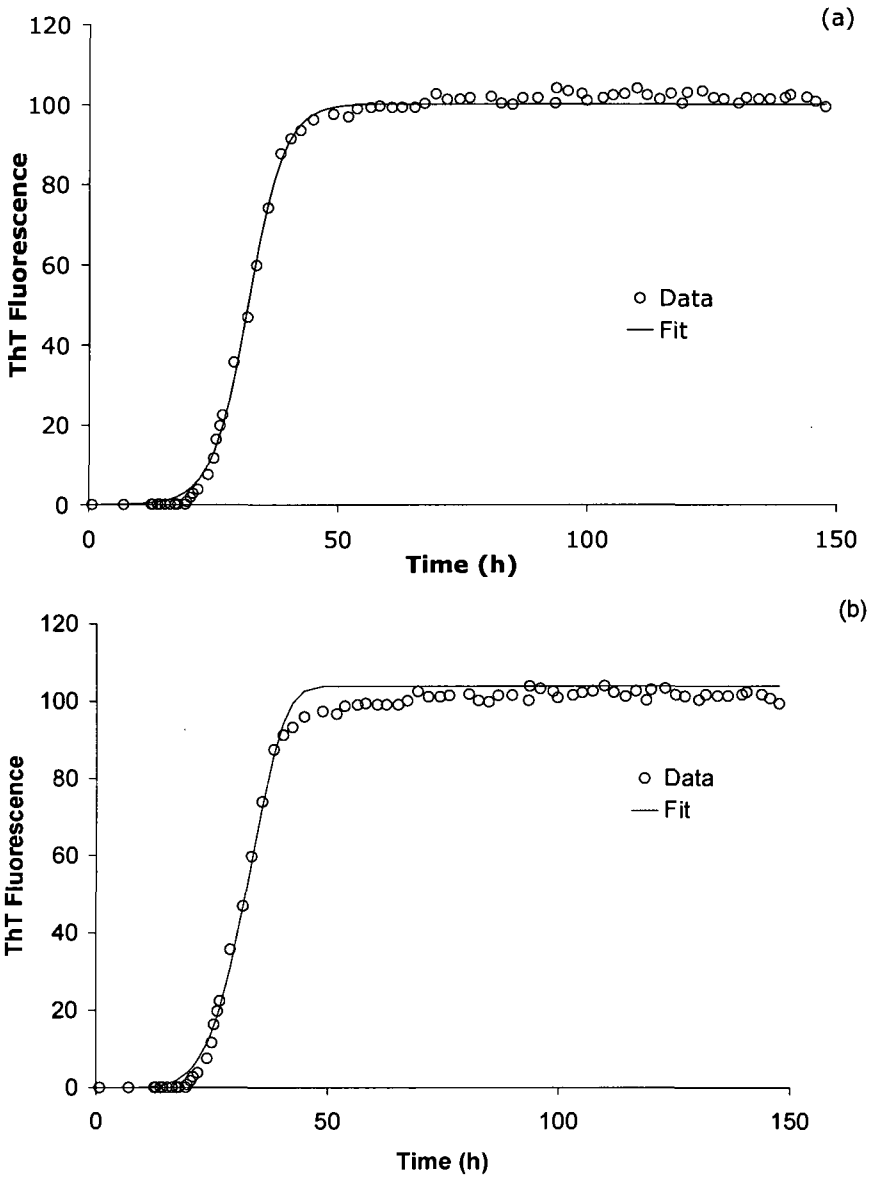

Figure 5S.11. Fit of α-synuclein aggregation data from Fink[52] to the F-W model (a)[42] and the A-E equation (b). α-Synuclein is a protein relevant to Parkinson's disease.

References

[1] Khachaturyan, A. G. *Theory of Structural Transformations in Solids*; Wiley: New York, 1983.

[2] Young, D. A. *Decomposition of Solids*; Pergamon Press: Oxford, 1966.

[3] Ungerer, P., Pelet, R. *Nature* **1987**, *327*, 53.

[4] Burnham, A. K. *J. Therm. Anal. Calor.* **2000**, *60*, 895.

[5] Fanfoni, M.; Tomellini, M. *Il Nuovo Cimento* **1998**, *20*, 1171.

[6] (a) Jun, S.; Zhang, H.; Bechhoefer, J. *Phys. Rev. E.* **2005**, *71*, 011908. (b) Brown, M. E. *Thermochim. Acta* **1997**, *300*, 93.

[7] Hancock, J. D.; Sharp, J. H. *J. Am. Ceram. Soc.* **1972**, *55*, 74.

[8] Brown, M. E.; Glass, B. D. *Inter. J. Pharm.* **1999**, *190*, 129.

[9] Koga, N. *Thermochim. Acta* **1995**, *258*, 145.

[10] Finney, E. E.; Finke, R. G. *J. Coll. Interface Sci.* **2008**,*317*, 351.

[11] Johnson, W. A.; Mehl, R. F. *Trans. AIME* **1939**, *135*, 416.

[12] (a) Avrami, M. *J. Chem. Phys.* **1939**, *7*, 1103. (b) Avrami, M. *J. Chem. Phys.* **1940**, *8*, 212. (c) Avrami, M. *J. Chem. Phys.* **1941**, *9*, 177.

[13] (a) Prout, E. G.; Tompkins, F. C. *Trans. Faraday Soc.* **1944**, *40*, 488. (b) Prout, E. G.; Tompkins, F. C. *Trans. Faraday Soc.* **1946**, *44*, 468.

[14] Erofe'ev, B. V. *Dokl. Akad. Nauk SSSR* **1946**, *52*, 511.

[15] Màlek, J.; Criado, J. M. *Thermochim. Acta* **1991**, *175*, 305.

[16] Šestàk, J.; Berggren, G. *Thermochim. Acta* **1971**, *3*, 1.

[17] Ng, W.-L. *Aust. J. Chem.* **1975**, *28*, 1169.

[18] Tamhankar, S. S.; Gokarn, A. N.; Doraiswamy, L. K. *Chem. Eng. Sci.* **1981**, *36*, 1365.

[19] Cardew, P. T.; Davey, R. J.; Ruddick, A. J. *J. Chem. Soc., Faraday Trans.* **1984**, *80*, 659.

[20] Burnham, A. K.; Braun, R. L.; Coburn, T. T.; Sandvik, E. I.; Curry, D. J.; Schmidt, B. J.; Noble, R. A. *Energy Fuels* **1996**, *10*, 49.

[21] Jacobs, P. W. M. *J. Phys. Chem. B* **1997**, *101*, 10086.

[22] Urbanovici, E.; Schneider, H. A.; Cantow, H. J. *J. Polymer Sci. B* **1997**, *35*, 359.

[23] Liu, F.; Sommer, F.; Mittemeijer, E. J. *J. Mater. Res.* **2004**, *19*, 2586.

[24] Skrdla, P. J. *J. Phys. Chem. A* **2004**, *108*, 6709.

[25] Skrdla, P. J.; Robertson, R. T. *J. Phys. Chem. B* **2005**, *109*, 10611.

[26] Davis, T. M.; Drews, T. O.; Ramanan, H.; He, C.; Dong, J.; Schnablegger, H.; Katsoulakis, M. A.; Kokkoli, E.; McCormick, A. V.; Penn, R. L.; Tsapatsis, M. *Nat. Mater.* **2006**, *5*, 400.

[27] Li, H.; Stowell, J. G.; He, X.; Morris, K. R.; Byrn, S. R. *J. Pharm. Sci.* **2007**, *96*, 1079.

[28] Sreethawong, T.; Suzuki, Y.; Yoshikawa, S. *J. Solid State Chem.* **2005**, *178*, 329.

[29] See for example: (a) Wright, A. J.; Hartel, R. W.; Narine, S. S.; Marangoni, A. G. *JAOCS* **2000**, *77*, 463. (b) Zhang, Z.; Wu, S.; Ren, M.; Xiao, C. *Polymer* **2004**, *45*, 4361.

[30] (a) Hoffmann, R.; Minkin, V. I.; Carpenter, B. K. *Bull. Chem. Soc. Fr.* **1996**, *133*, 117. (b) Hoffmann, R.; R.; Minkin, V.; Carpenter, B. K. *Int. J. Philosophy of Chemistry* **1997**, *3*, 3-28.

[31] A useful, readable introduction to both model-building and testing, including the AIC method, is: Motulksy, H. J.; Christopoulos, A. "Fitting models to biological data using linear and nonlinear regression. A practical guide to curve fitting", 2003, GraphPad Software Inc., San Diego, CA, www.graphpad.com.; see p. 134-165.

[32] Watzky, M. A.; Finke, R. G. *J. Am. Chem. Soc.* **1997**, *119*, 10382.

[33] Sun, N. X.; Liu, X. D.; Lu, K. *Scripta Mater.* **1996**, *34*, 1201.

[34] Kolmogorov, A. N. *Bull. Acad. Sci. USSR Phys. Ser.* **1937**, *3*, 555.

[35] Turnbull, D.; Fisher, J. C. *J. Chem. Phys.* **1949**, *17*, 71.

[36] Galwey, A. K.; Brown, M. E. *J. Therm. Anal. Calorim.* **2000**, *60*, 863.

[37] Plonka, A. *Annu. Rep. Prog. Chem. Sect. C* **2001**, *97*, 91.

[38] Fanfoni, M.; Tomellini, M.; Volpe, M. *Phys. Rev. B* **2002**, *65*, 172301.

[39] Van Siclen, C. DeW. *Phys. Rev. B* **1996**, *54*, 11845.

[40] Tomellini, M.; Fanfoni, M. *Phys. Rev. B* **1997**, *55*, 14071.

[41] (a) Besson, C.; Finney, E. E.; Finke, R. G. *J. Am. Chem. Soc.* **2005**, *127*, 8179. (b) Besson, C.; Finney, E. E.; Finke, R. G. *Chem. Mater.* **2005**, *17*, 4925.

[42] α-Synuclein Aggregation Variable Temperature and Variable pH Kinetic Data: A Reanalysis Using the Finke-Watzky 2-Step Model of Nucelation and Autocatalytic Growth, Morris, A. M. Finke, R. G. *Biophysical Journal*, **2008**, in press.

[43] (a) The pseudoelementary step concept, pioneered by Richard Noyes,[43b-d] involves summing one or more fast reactions with one (or more) slower reaction(s), giving an overall reaction that can be treated as an elementary step, but which provides kinetic information about the slower reactions. For details about how the pseudo-elementary step has been used in following nanocluster formation kinetics, see ref. 32. (b) Noyes, R. M.; Field, R. J. *Acc. Chem. Res.* **1977**, *10*, 214. (c) Noyes, R. M.; Field, R. J. *Acc. Chem. Res.* **1977**, *10*, 273. (d) Field, R. J.; Noyes, R. M. *Nature* **1972**, *237*, 390.

[44] Finney, E. E.; Finke, R. G. *Chem. Mater.* **2008**, *20*, 1956.

[45] Lin, Y.; Finke, R. G. *Inorg. Chem.* **1994**, *33*, 4891.

[46] Ott., L. S.; Hornstein, B. J.; Finke, R. G. *Langmuir* **2006**, *22*, 9357; see p. 9363-9364.

[47] Aiken, J. D., III; Finke, R. G. *J. Am. Chem. Soc.* **1998**, *120*, 9545.

[48] Many similar mechanisms exists in the biology literature: (a) Goldtein, R. F.; Stryer, L. *Biophys. J.* **1986**, *50*, 583. (b) Firestone, M. P.; de Levie, R.; Rangarajan, S. K. *J. Theor. Biol.* **1983**, *104*, 535. (c) Kamihira, M.; Naito, A.; Tuzi, S.; Nosaka, A. Y.; Saitô, H. *Protein Science* **2000**, *9*, 867.

[49] Finney, E. E.; Ott, L. S.; Watzky, M. A.; Finke, R. G., unpublished results and studies in progress.

[50] Lin, Y.; Finke, R. G. *J. Am. Chem. Soc.* **1994**, *116*, 8335.

[51] Ott, L. S.; Finke, R. G. *J. Nanosci. Nanotech.* **2007**, *7*, 2400.

[52] Fink, A. L. *Acc. Chem. Res.* **2006**, *39*, 628.

CHAPTER VI

SUMMARY

This dissertation has focused on the mechanisms of transition-metal nanocluster formation and agglomeration, along with its applications to solid-state reaction systems. A critical review of the relevant literature pointed out the progress made in studying the mechanisms of nanocluster formation, but then the areas in which more studies need to be done. Then, the recently discovered 4-step, double autocatalytic mechanism was shown to be general to the formation of nanoclusters of at least five metals (Pt, Ru, Ir, Rh, and Pd), and the experimental conditions that favored nanoclusters versus bulk metal were examined. The 4-step mechanism was used to help answer the question of "Is it homogeneous or heterogeneous catalysis?" for reactions using the complexes Pt(1,5-COD)X_2 (X = Cl, CH_3) under reducing conditions, specifically showing that the Pt^{II} complex must be reduced to Pt^0 nanoclusters or bulk metal before catalysis can take place. Finally, the relevance of the Finke-Watzky 2-step mechanism to the kinetics of solid-state reactions versus the

classic Avrami-Erofe'ev treatment was investigated, emphasizing the strengths and weaknesses of both approaches to the analysis of kinetic data.

There are several potential avenues for continued research based on the results described herein. They include: (i) the use of X-ray spectroscopies (e.g., EXAFS and XANES) to gain further insight into the more intimate steps of nanocluster nucleation, growth, and agglomeration (and under real-time, "operando" conditions; collaborative studies have already been started here); (ii) the study of platinum-catalyzed hydrosilylation reactions towards settling the question of "Is it homogeneous or heterogeneous catalysis?", as described herein in Chapter IV; (iii) further studies to possibly expand the generality of the 4-step mechanism beyond the five metals studied herein; and (iv) the extension of the generality of the Finke-Watzky mechanism to systems other than solid-state reactions (its application to protein agglomeration, for example, has been reported already[1,2,3,4]).

References

[1] "Fitting Neurological Protein Aggregation Kinetic Data via a 2-Step, Minimal / 'Ockham's Razor' Model: the Finke-Watzky Mechanism of Nucleation Followed by Autocatalytic Surface Growth", Morris, A. M.; Watzky, M. A.; Agar, J. N.; Finke, R. G. *Biochem.*, **2008**, *47*, 2413.

[2] "Fitting yeast and mammalian prion aggregation kinetic data with the Finke-Watzky Two-step model of nucleation and autocatalytic growth", Watzky, M. A.; Morris, A. M.; Ross, E. D.; Finke, R. G. *Biochem.*, **2008**, *47*, 10790.

[3] "α-Synuclein aggregation variable temperature and variable pH kinetic data: A re-analysis using the Finke–Watzky 2-step model of nucleation and autocatalytic growth", Morris, A. M.; Finke, R. G. *Biophysical Chemistry*, **2009**, *140*, 9.

[4] "Protein Aggregation Kinetics, Mechanism, and Curve-Fitting: A Review of the Literature", Morris, A. M.; Watzky, M. A.; Finke, R. G. *Biophys. Biochem. Acta*, **2009**, 1794, 375.

APPENDIX A

GENERAL STATEMENT ON "JOURNALS-FORMAT" THESES

(Written by Professor Richard G. Finke)

The Graduate School at Colorado State University allows, and the Finke Group in particular encourages, so-called journals-format theses. Journals-format theses, such as the present one, consist of a student written and lightly edited literature background section, chapters corresponding (in the limiting, ideal case) to final-form papers either accepted or at least submitted form publication, a summary or conclusions chapter, and short bridge or transition sections between chapters as needed to make the thesis cohesive and understandable to the reader. The "bridge" sections and summary are crucial so that the thesis fulfills the requirement that the thesis be an entity (an official requirement of most Graduate Schools). All chapters (manuscripts) in a journals-format thesis must of course be written initially by the student, with subsequent (ideally light) editing by the Professor, the student's committee, and even the student's colleagues where appropriate and productive.

The advantages for doing a journals-format thesis are several-fold and compelling. Specifically, some of the major advantages are: the level of science (i.e. of refereed, accepted publications) is at the highest level; the student and Professor

must interact closely and vigorously (i.e. to bring both the science and the writing to their highest level), hence the student is getting the best education possible and is being at least exposed to (if not held to) the highest standards; the needed clean-up or control experiments that invariably come up have all been identified and completed before the student leaves; there are no further time demands once the student has left the University (since all the publications are at least submitted; it is terribly inefficient to try to complete either writing or often specialized experiments once the student has left); and the American taxpayers, who ultimately pay the bill for the research, are getting their money's worth since all the research is published and thus widely disseminated in the highest form, as refereed science. Professorial experience teaches that a student who has achieved a journals-format thesis has indeed received a better education and has learned critical thinking and clear writing skills that will serve them well for a lifetime.

Experience also teaches, however, that much more than light editing is often needed in at least some student theses; it follows, then, that considerable professorial writing and editing might be needed for at least the initial chapters of most journals-format theses. Indeed, a journals-format thesis is not recommended (and may not even be possible) for less strong students. Hence, the issue arises of exactly how much of the science and the writing, in the final (or submittable) chapters, is due to the student versus the Professor and whether or not this level of contribution constitutes that acceptable of a new Ph.D. and independent investigator. An additional potential problem is that the journals-format thesis does not include unpublished/unpublishable experimental results (i.e., unless they are in footnotes or

the Supporting Information), which may have significant value for future members of the research group.

To deal with these issues, several recommendations are made; the recommendations below have been discussed with the committee signing Eric Finney's dissertation (Mr. Finney's dissertation is the fifteenth such thesis from the Finke Group following Dr. C. Garr's, Dr. Y. Lin's, Dr. M. Pohl's, Dr. J. Sirovatka's, Dr. J. Aiken's, Dr. R. Suto's, Dr. J. Widegren's, Dr. K. Doll's, Dr. C.-X. Yin's, and Dr. L. S. Ott's dissertations, and Ms. K. Weddle's, Mr. W. White's, Mr. C. Hagen's, and Mr. C. Graham's Master's theses). The recommendations are:

(i) That the present pages be enclosed in the thesis until such a time that it is no longer needed;

(ii) That for each chapter it is detailed, and to the satisfaction of the committed and the advisor, who made what contributions, both of intellectual substance and writing. [Substantial contributions of other students or Professors should of course also be acknowledged. In the case of disagreements, the various drafts (i.e., as their electronic files) can be examined by the committee (in light of a knowledge of who wrote which draft) to easily determine who contributed what. In possible borderline or controversial cases it may even be advisable to keep all (electronic) drafts of the papers as a record];

(iii) That it be specifically stated whether or not all the experimental work is the Ph.D. candidate's;

(iv) Furthermore, it is recommended that allowances be made for the expectation that a greater degree of involvement of the professorial advisor is likely in a journals-format thesis than in a traditional thesis. [That this is reasonable follows from the fact that some Professors wrote 100% of all their papers; this unfortunately, robs the student of the valuable experience of participating in the science and the end product as practiced at the highest levels.];

(v) Notwithstanding (iv), there needs to be ideally no more than ca. 40% Professorial writing contribution in a given early chapter in the thesis, and there should be a clear evolution in the thesis of a decreasing professorial involvement to, say, a 10-20% direct contribution in the last chapter or two;

(vi) As a further aid towards separating out the candidate's and the professorial (and other) contributions, it is recommended that the Introductory (usually literature background) chapter(s) and at least the final chapter be lightly edited only, so that authentic examples of the student's contributions are documented in an unambiguous form.

(vii) In order to avoid the loss of useful, but unpublished/unpublishable, experimental work by the student writing a journals-format thesis, the Finke Group requires the following: (1) carefully kept laboratory notebooks; (2) mandatory research reports detailing the results of any unpublished work; and (3) the extensive use of Supporting Information and textual footnotes, where appropriate, in all published work.

APPENDIX B

RESEARCH PROPOSAL

Synthetic Analogs of the Molybdenum Cofactor in Aldehyde Oxidoreductase: Synthesis and Mechanistic Studies

Abstract/Specific Aims

While the molybdenum-containing oxotransferase enzymes have been extensively characterized, the exact mechanism of the enzymes, in particular aldehyde oxidoreductase (AOR), is not clear. Therefore, a model complex for the molybdenum cofactor in AOR will be synthesized, using methods in the literature to obtain the closest possible match between the model and the enzyme. The model complex will then be subjected to kinetic and mechanistic studies to examine several hypotheses about the mechanism of AOR action. The model complex will also be examined with respect to catalytic activity, yields, and functional group tolerance, and the model will be compared in these respects to common laboratory methods used to oxidize aldehydes.

The overall goals of this research are to synthesize an accurate model of the enzyme aldehyde oxidoreductase, to learn as much as possible about how the enzyme works to catalyze the transfer of oxygen atoms to substrates, and to determine whether the model complex is a superior aldehyde oxidation catalyst.

The specific hypotheses of this research are:

1. The molybdenum cofactor of AOR, or a suitable model complex for the cofactor, can be synthesized.
2. A series of kinetic and mechanistic studies performed on the model complex will help to rule out one or more of the current hypotheses about how AOR works in living organisms.
3. The model complex will show greater catalytic activity (i.e., have faster rates and higher turnover numbers) and have better functional group tolerance than commonly used Cr^{VI} and MnO_4^- oxidation agents.

The specific aims of this project include:

1. We will synthesize the pterin ligand of the AOR enzyme or, in the event that this is not possible, a suitable protected analog.
2. We will coordinate the pterin ligand or its analog to molybdenum so that an accurate model of AOR can be prepared.
3. We will perform commonly used kinetic and mechanistic studies on the model complex, including rate studies and ligand replacement studies, to elucidate the mechanism of action of AOR.

4. We will study the catalytic activity of the model complex for simple aldehydes and compare this to the activity of Cr^{VI} and MnO_4^- oxidizing agents.
5. We will test the activity of the model complex for the *reduction* of sulfoxide with an eye toward sulfa drug chemistry.
6. We will prepare tungsten analogs of the Mo complexes and compare these to the Mo complexes in terms of activity and selectivity.

Background and Significance

Molybdenum-containing enzymes are ubiquitous in all life forms, where they catalyze metabolic reactions of carbon, sulfur, and nitrogen. Mo exists in two distinct forms among the at least 50 enzymes that contain it:[1] mixed Fe-Mo-S metallic clusters, which are found in the nitrogenases, and mononuclear complexes. The non-nitrogenase Mo enzymes are involved in so-called "oxotransferase" reactions, which transfer an oxygen atom to the substrate; the oxygen atom generally comes from water, eq B1, but other oxygen sources are common.

$$X + H_2O \longrightarrow XO + 2H^+ + 2e^- \qquad (1)$$

Representative of the mononuclear Mo enzymes is the xanthine oxidase (XO) family of enzymes. These enzymes catalyze the hydroxylation of C-H bonds in aldehydes and various heterocycles. The XO enzyme family has been found to have antimicrobial and antioxidant properties.[2] The enzyme aldehyde oxidoreductase (AOR) belongs to the XO enzyme family; its function is to convert an aldehyde to a carboxylic acid through the incorporation of an oxygen atom from water or some other source, eq B2. The crystal structure of the Mo cofactor of the enzyme (*1*) has

been attained at a resolution of 1.28 Å.[3] The R group is a nucleotide group in bacteria; that group is absent in eukaryotes.[4,5] The 2-aminopteridin-4-one ligand is commonly referred to as the "pterin" ligand.

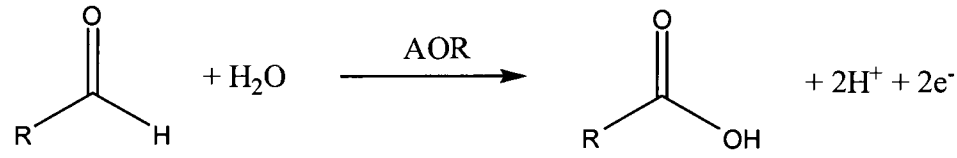

(2)

The Mo enzymes have been extensively studied, and many reviews of oxotransfer reactions with Mo enzymes, including AOR, exist.[1,5-8] However, the mechanism of AOR is still not clear.

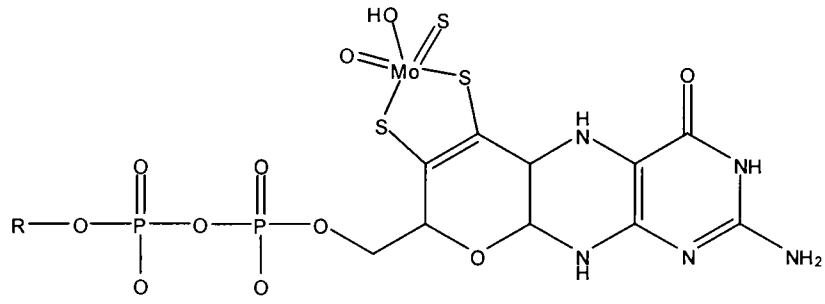

1

In fact, at present several hypotheses remain for what steps occur during oxygen transfer:

1. Transfer of a proton from the substrate to the sulfido of the enzyme, followed by nucleophilic attack of the carbanion on Mo
2. Coordination of water to Mo, followed by nucleophilic attack of the oxygen atom from water on the substrate
3. Addition of the C-H bond across the Mo=S bond

4. 2 + 2 cycloaddition of the C-H bond across the Mo=O bond
5. Addition of the C-H bond across the Mo=S bond followed by reaction of a bound O atom to form a Mo-O-C three-membered ring

Currently, the only experimental evidence for the mechanism of AOR activity comes from crystal structure data from purified xanthine oxidoreductase in the presence of a "slow substrate".[9] The finding of a Mo-SH group[9] in what was previously thought was a Mo=O group[10] led to the hypothesis that sulfido protonation by the substrate is an integral step in the mechanism. This finding is consistent with hypotheses 1 and 5 above.

In order model the structure of the XO family of enzymes, many Mo complexes have been prepared and characterized.[7] These models have used multidentate sulfur or nitrogen ligands on Mo, including mercaptoquinoline,[11] oxobisdithiolene,[4] cyclic triamine,[12] tetradentate N_2O_2,[13] tris(pyrazolyl)borate,[14] 1,10-phenanthroline,[15] and tetradentate N_2S_2[16] ligands. Of these model complexes, only the 1,10-phenanthroline ligated complex contains the oxo and sulfido groups that are both thought to be necessary for catalysis. Its straightforward preparation begins with the $[MoO_4]^{2-}$ ion and ends with complex ***2***,[15] with the oxo and sulfido group next to each other as in the enzyme.

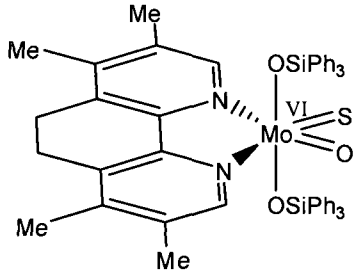

2

The absence of the pterin group in all of the above-mentioned model complexes is significant, because the ligand itself may be involved in the catalytic cycle of Mo oxotransferases.[17] Specifically, the reduction potential of (dithiolene)MoO complexes was found to change by over 0.3 V on changing the substituents on the dithiolene ligand.[18] The oxidizing ability of the Mo complexes is therefore highly sensitive to the dithiolene ligand on Mo. As a result, a model complex that more closely resembles the actual Mo cofactor is needed.

The synthesis of the pterin group itself has also been the subject of study in recent years. Joule et al. have been most active in the preparation of the pterin group of the Mo cofactor. In 2001, they reported the synthesis of a protected form of the pterin group (*3*) starting from pterin 8-oxide.[19] In another report, they hydrolyzed a similar compound and coordinated it to Co, *4*.[20] No form of the pterin compound has

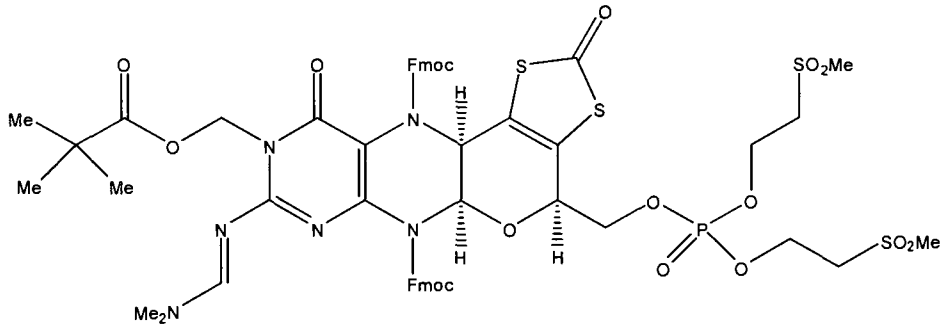

3

been coordinated to a Mo ion, however. In addition, although the authors remarked that "it is not envisioned that free MPT (molybdopterin), with an unprotected dithiolene group, will be sufficiently stable to be isolated and characterized"[19] (presumably due to its oxygen sensitivity—the authors did not report any air-sensitive techniques used in the preparation), no attempts to prepare the MPT with the unprotected pterin group have been reported.

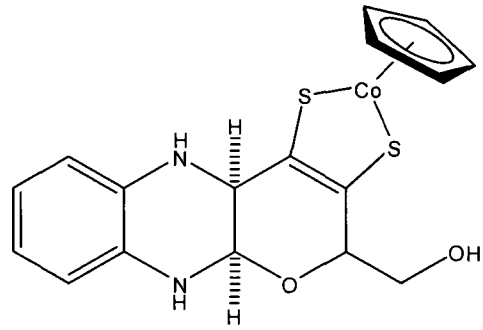

4

A similar dithiolene ligand has been prepared by Schulzke from flavanone and then coordinated to a molybdenum center, Scheme B1.[4] The similarities between the dithiolene ligand used therein and the pterin ligand in the cofactor are evident; the possibility therefore exists to prepare a model similar to the pterin ligand using this methodology.

Scheme B1

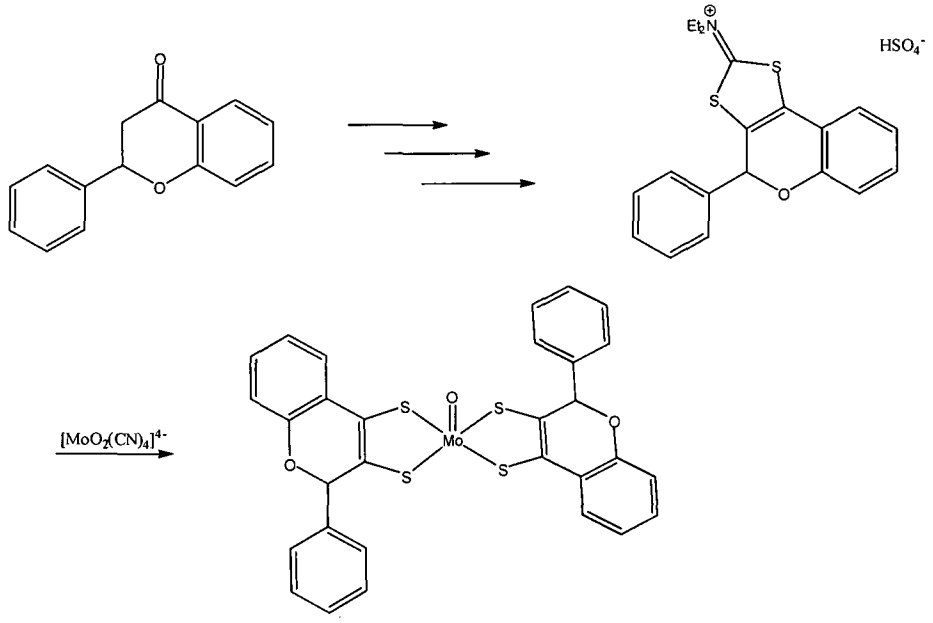

While the model complexes in the extant literature have been extensively characterized, kinetic and mechanistic studies of the complexes do not currently exist. Such studies, performed on a satisfactory model complex, should provide much new information about the mechanism of activity of AOR, in conjunction with the crystal structure data that currently exists.[9] Given the existing methods of preparing a Mo center with both an oxo and a sulfido ligand (both of which are thought to be needed for catalysis), ***2***, and, separately, the cofactor pterin group (albeit in protected form, ***3***), the combination of the two methods to yield a molybdopterin that also contains the oxo and sulfido ligands would be straightforward but significant, giving the first such model complex in the literature.

The ability of Mo complexes to oxidize aldehydes in the presence of other functional groups deserves study as well. Currently, the most commonly used methods for oxidizing aldehydes to carboxylic acids involve the use of Cr^{VI}, which is

a known carcinogen, and potassium permanganate. Both of these methods, however, also oxidize alcohols to carboxylic acids, and potassium permanganate oxidizes alkyl chains off of aromatic rings as well. In addition, these oxidizing agents are used in stoichiometric amounts, resulting in large amounts of Cr^{VI} and MnO_2 waste. The question arises, then, of whether a Mo-based aldehyde oxidation catalyst could be a viable alternative to these oxidation methods. Specifically, two questions are: (i) can the Mo complexes oxidize aldehydes in catalytic amounts? (ii) Will the Mo complexes show greater functional group tolerance than the MnO_4^- oxidizing agent, so that protecting groups are not needed when oxidizing aldehydes in the presence of other functional groups, such as amines? These questions will be addressed in the present proposal.

Research Design and Methods

This proposal is divided into two parts. First, the preparation of suitable AOR model complexes, or ideally the Mo cofactor itself, is proposed. Second, the obtained complexes are subjected to kinetic and mechanistic studies in an attempt to elucidate the mechanism of AOR's catalytic activity, and the activity of the model complexes are compared to Cr^{VI} and MnO_4^- oxidizing agents. For clarity, the specific questions to be answered will be given, followed by the methods that will be used to answer those questions.

Model Mo complexes for AOR

Can the unprotected pterin ligand be prepared and coordinated to Mo to give the most accurate model compound?

As mentioned above, a protected form of the pterin ligand has been synthesized, with the comment that "it is not envisioned that free MPT (molybdopterin), with an unprotected dithiolene group, will be sufficiently stable to be isolated and characterized."[19] However, the synthesis of the free molybdopterin has not been attempted to the best of our knowledge. In addition, the preparation of the unprotected pterin group represents a significant synthetic challenge, making its accomplishment worthwhile in its own right. Therefore, following a reproduction of Joule's synthesis of the protected ligand ***3***,[19] we will attempt to synthesize the unprotected pterin using a similar methodology, Scheme B2, under air-free conditions.

After the pterin ligand has been synthesized, it will be coordinated to Mo using the method of Thapper et al. for complex ***3*** along with hydrolysis of the dithiolene of the pterin, Scheme B3, also under air-free conditions. It should be noted that coordination of even the reported protected pterin group to Mo would be novel, given that the only similar compound to be ligated to a metal is ***4***, which is several functional groups away from the pterin group and is coordinated to cobalt, not molybdenum.[20] Therefore, in the event that the unprotected pterin ligand cannot be synthesized or coordinated to Mo in the way that is presently proposed, the protected pterin group will be coordinated to Mo in order to give a suitable model complex.

Scheme B2

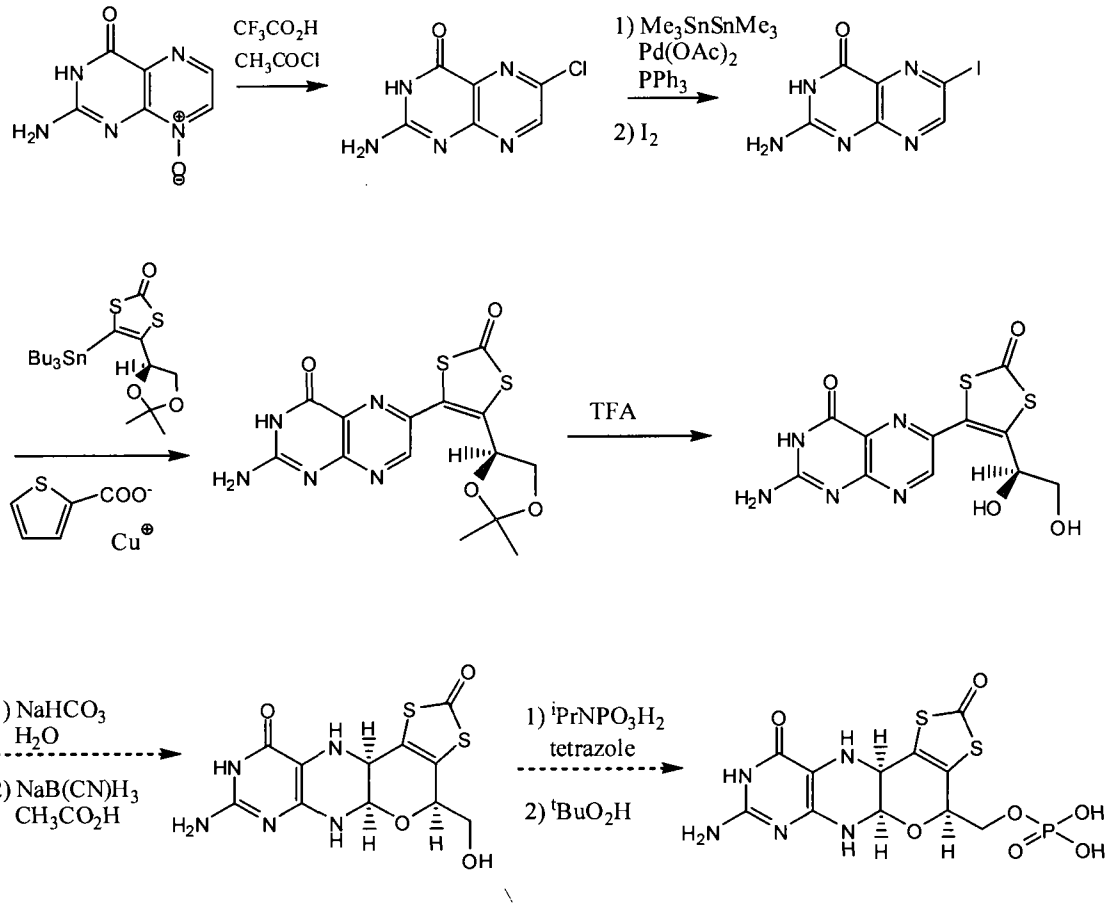

Scheme B3

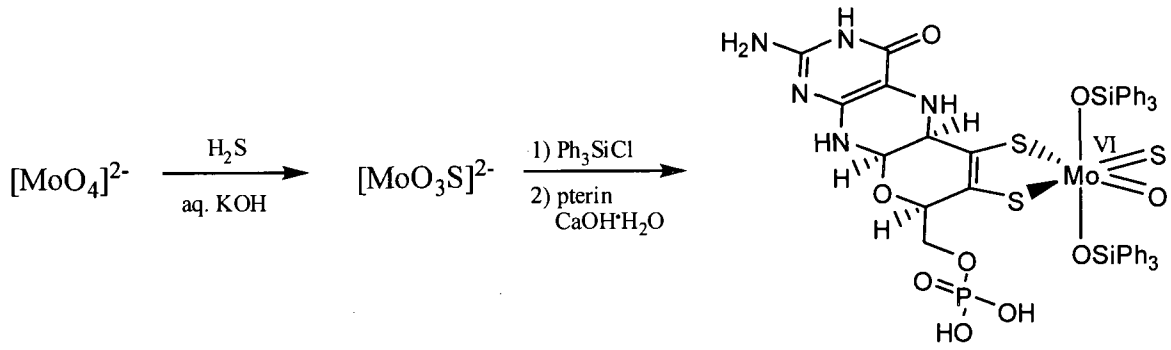

Characterization of the products will be performed using several physical methods. These will include ^{1}H and ^{13}C nuclear magnetic resonance (NMR) spectroscopy, infrared (IR) spectroscopy, mass spectrometry (MS), as well was electron paramagnetic resonance (EPR) spectroscopy and extended X-ray absorption fine structure (EXAFS) spectroscopy for the Mo complex. The wide variety of characterization methods available for the model complexes will give us a great deal of confidence that we have synthesized the model complexes that we desire.

Kinetic and mechanistic studies

The following studies will be performed on the AOR model complex obtained in the previous section. The specific questions to be answered are:

What can be learned from the model complexes about the action of aldehyde oxidoreductase (and possibly by extension, of xanthine oxidoreductase)?

Although the mechanism of AOR has been hypothesized based on enzyme crystal structures,[9] the well-established and widely used kinetic methods of elucidating mechanisms have not been used for the enzyme nor for the model complexes that have been prepared to date. Questions that remain unanswered include: (i) what is the reaction order with respect to enzyme and substrate? (ii) What rate constants are associated with the reaction? (iii) What is the dependence of the reaction on temperature? (iv) What are the activation parameters of the reaction? (v) Where does the incorporated oxygen atom come from—water[21] (or another oxygen source) or from the cofactor Mo=O, which has been shown to be a labile bond in coordination complexes?[8] There is currently confusion in the literature as to where the O atom comes from. Labeling experiments have shown that ^{18}O-labeled oxygen

source incorporates some ^{18}O into the substrate in reactions with XO; however, the reactions of XO and AOR have been shown to be quite different in several respects.[5]

Once a model compound is in hand, a few relatively simple kinetic experiments can be performed that will provide significant insight into the reaction mechanism. Early reactions will use acetaldehyde and benzaldehyde as substrates for the reaction, with more complex aldehydes planned for future studies. For example, to answer (i) above, a series of reactions will be carried out with varying Mo complex concentrations, and separately with varying aldehyde concentrations, and the reaction rate will be measured to determine the reaction order with respect to each species. The reaction rate can be measured by following the reaction quantitatively using ^{1}H NMR; the aldehyde and carboxylic acid handles of the substrate and product, respectively, will be useful in the NMR experiments for rate determination. It is assumed that the reaction is first order with respect to both species; however, since no explicit determination of this has been done, the results of this easily accomplished series of experiments are important and worthwhile, in that it will make possible the determination of the rate constant(s) for the reaction, thereby answering question (ii) above. To answer (iii), simply carrying out the reaction over a range of temperatures will give the dependence of the reaction on temperature. Since the reaction is expected to show Arrhenius behavior, obtaining the rate constants at each temperature will allow the activation parameters to be calculated, thereby answering (iv) above. To answer (v), reactions will be carried out using ^{18}O-labeled water and/or separately, ^{18}O-labled synthetic cofactor and the products of the reaction will be analyzed using mass spectrometry to determine where the transferred oxygen comes from.

Are both the oxo and sulfido ligands necessary for catalysis? Is there a "spectator oxo" or "spectator sulfido" effect?

After these straightforward but important experiments are complete, the model compounds and substrates can be altered to examine the mechanistic hypotheses given earlier. For example, three of the hypotheses assume direct involvement of the Mo=S bond of the cofactor (one involving protonation of the sulfido group and two involving addition of the substrate C-H bond to the catalyst Mo=S bond). Reaction of a model compound without the sulfido group (e.g., a dioxo Mo complex) and measurements of the model's reactivity with aldehydes will reveal whether the sulfido group is indeed necessary for the activity observed in the enzyme. Similarly, reaction of a Mo complex without the Mo=O bond (e.g., a disulfido Mo complex) will reveal whether the oxo group is needed in the oxidation. The hypothesis in which a three-membered Mo-O-C ring is formed is suggestive of a "spectator oxo effect," in which the presence of the Mo=O bond may facilitate catalysis.[22] A similar "spectator sulfido effect" is possible if the M=S bond is found to be necessary for activity. These effects will be given appropriate consideration. Since water is an important factor in one of the hypotheses (attack of water on the substrate), reactions in various protic (e.g., methanol, acetic acid, formamide) and aprotic (e.g., acetone, dimethylsulfoxide) organic solvents will give the significance of the presence or absence of water in the reaction.

All of the above-mentioned studies should prove to be useful in elucidating the mechanism of the cofactor. We must, of course, keep in mind that in studying a

model, one really learns about only the model. However, this is the best way to learn as much as possible about the mechanism of the Mo cofactor.

Can the model complex(es) be used to obtain a very active catalyst for aldehyde (and/or other functional group) oxidation under mild conditions? How does the model complex compare to the methods currently in use for such transformations?

As mentioned in the Introduction, a relevant hypothesis is that the Mo complexes prepared herein have better functional group tolerance than the Cr^{VI} and MnO_4^- oxidizing agents that are commonly used, and can be used in catalytic amounts. In order to test this hypothesis, substituted aldehydes will be oxidized with the Mo complexes and the products will be studied to determine the selectivity of the Mo complexes toward oxidizing aldehydes versus other functional groups. For example, aromatic aldehydes containing alkyl groups will be oxidized using the Mo complexes and $KMnO_4$ to see what products result, Scheme B4. Catalytic activity of the complexes will be quantitated by determining the yield, turnover frequency, and total turnover number of the Mo complexes.

Scheme B4

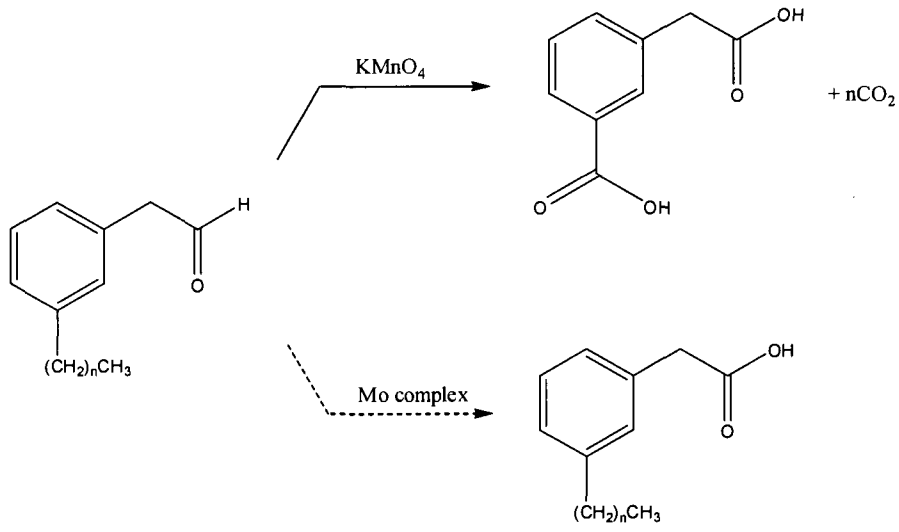

Can the model complex catalyze the reduction of sulfoxides, possibly leading to pharmaceutical applications?

It is also known that AOR, unlike other members of the general hydroxylase family, can catalyze the *reduction* of sulfoxides.[23] This implies that the reduction potentials of the model complexes are sensitive to substrates was well as the ligands on Mo[18] and further suggests that reactions with the model complexes with substituted aldehydes should yield interesting results. Scheme B5 shows the reduction of dimethyl sulfoxide; in addition, AOR is known to reduce sulfoxide groups in sulfa drugs. This reaction will also be studied with an eye toward possible pharmaceutical applications of the model complexes. This is a long-term goal of the research. Also interesting would be the reaction of the Mo complex with a substrate that contains both aldehyde and sulfoxide groups, to see what products result.

Scheme B5

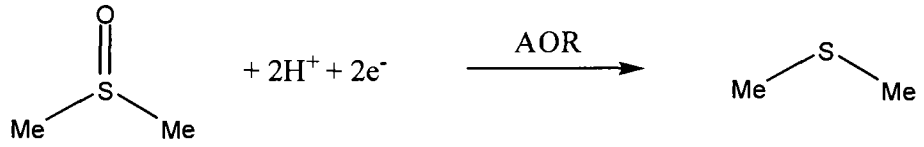

What results when the Mo in the model complexes is replaced with the chemically and biologically related W?

The hypothesis here is that complexes containing tungsten instead of molybdenum will be more active. To test this hypothesis, W analogs of the Mo complexes will be synthesized using the methods described above, and these complexes will be subjected to the same reactions as the Mo complexes. These

studies will take place after all of the Mo studies, so this represents another long-term research goal.

Conclusion

The chemistry of Mo-containing enzymes in general, and of AOR in particular, has been studied for decades, but many fundamental questions remain to be answered. The experiments described in the present proposal use established kinetic methods and literature bases for synthesis to answer these questions. The proposed experiments are straightforward to accomplish, but will almost certainly yield many important results and insight into the mechanism of aldehyde oxidoreductase. A list of potential publications from this study is as follows:

1. Preparation of a model for aldehyde oxidoreductase with a protected pterin ligand (Or, alternatively, 1a. Preparation of the unprotected pterin group of aldehyde oxidoreductase; 1b. Preparation of the molybdopterin cofactor of aldehyde oxidoreductase
2. Kinetic and mechanistic studies of a model for aldehyde oxidoreductase for the oxidation of aldehydes
3. Comparison of an aldehyde oxidoreductase model to commonly used Cr^{VI} and MnO_4^- oxidation agents: is the model complex a superior aldehyde oxidizing agent?
4. Reduction of sulfoxides with model complexes of aldehyde oxidoreductase
5. Preparation of tungsten analogs to aldehyde oxidoreductase models and comparison to the Mo complexes.

The proposed research will lead to long-term fruitful research in the areas of bioinorganic chemistry, organic synthesis, spectroscopic methods, and catalysis.

References

[1] Enemark, J. H.; Cooney, J. J. A.; Wang, J.-J.; Holm, R. H. *Chem. Rev.* **2004**, *104*, 1175.

[2] Berry, C. E.; Hare, J. M. *J. Physiol.* **2004**, *555*, 589.

[3] Rebelo, J. M.; Dias, J. M.; Huber, R.; Moura, J. J. G.; Romão, M. J. *J. Biol. Inorg. Chem.* **2001**, *6*, 791.

[4] Schulzke, C. *Dalton Trans.* **2005**, 713.

[5] Hille, R. *Chem. Rev.* **1996**, *96*, 2757.

[6] Holm, R. H.; Kennepohl, P.; Solomon, E. I. *Chem. Rev.* **1996**, *96*, 2239.

[7] Holm, R. H. *Coord. Chem. Rev.* **1990**, *100*, 183.

[8] Holm, R. H. *Chem. Rev.* **1987**, *87*, 1401.

[9] Okamoto, K.; Matsumoto, K.; Hille, R.; Eger, B. T.; Pai, E. F.; Nishino, T. *Proc. Natl. Acad. Sci.* **2004**, *101*, 7931.

[10] Rebelo, J.; Macieira, S.; Dias, J. M.; Huber, R.; Ascenso, C. S.; Rusnak, F.; Moura, J. J. G.; Moura, I.; Romão, M. J. *J. Mol. Biol.* **2000**, *297*, 135.

[11](a) Farchione, F.; Hanson, G. R.; Rodrigues, C. G.; Bailey, T. D.; Bagchi, R. N.; Bond, A. M.; Pilbrow, J. R.; Wedd, A. G. *J. Am. Chem. Soc.* **1986**, *108*, 831. (b) Wilson, G. L.; Kony, M.; Tiekink, E. R. T.; Pilbrow, J. R.; Spence, J. T.; Wedd, A. G. *J. Am. Chem. Soc.* **1988**, *110*, 6923. (c) Wilson, G. L.; Greenwood, R. J.; Pilbrow, J. R.; Spence, J. T.; Wedd, A. G. *J. Am. Chem. Soc.* **1991**, *113*, 6803.

[12] Herrmann, W.; Wieghardt, K. *Polyhedron* **1986**, *5*, 513.

[13] Hinshaw, C. J.; Peng, G.; Singh, R.; Spence, J. T.; Enemark, J. H.; Bruck, M.; Kristofzski, J.; Merbs, S. L.; Ortega, R. B.; Wexler, P. A. *Inorg. Chem.* **1989**, *28*, 4483.

[14] Cleland, W. E., Jr.; Barnhart, K. M.; Tamanouchi, K.; Collison, D.; Mabbs, F. E.; Ortega, R. B.; Enemark, J. H. *Inorg. Chem.* **1987**, *26*, 1017.

[15] Thapper, A.; Donahue, J. P.; Musgrave, K. B.; Willer, M. W.; Nordlander, E.; Hedman, B.; Hodgson, K. O.; Holm, R. H. *Inorg. Chem.* **1999**, *38*, 4104.

[16](a) Dowerah, D.; Spence, J. T.; Singh, R.; Wedd, A. G.; Wilson, G. L.; Farchione, F.; Enemark, J. H.; Kristofzski, J.; Bruck, M. *J. Am. Chem. Soc.* **1987**, *109*, 5655. (b)

Peng, G.; Nichols, J.; McCullough, E. A., Jr.; Spence, J. T. *Inorg. Chem.* **1994**, *33*, 2857.

[17] McNamera, J. P.; Joule, J. A.; Hillier, I. H.; Garner, C. D. *Chem. Commun.* **2005**, 177.

[18] Helton, M. E.; Gruhn, N. E.; McNaughton, R. L.; Kirk, M. L. *Inorg. Chem.* **2000**, *39*, 2273.

[19] Bradshaw, B.; Dinsmore, A.; Ajana, W.; Collison, D.; Garner, C. D.; Joule, J. A. *J. Chem. Soc., Perkin Trans. 1* **2001**, 3239.

[20] Bradshaw, B.; Dinsmore, A.; Collison, D.; Garner, C. D.; Joule, J. A. *J. Chem. Soc., Perkin Trans. 1* **2001**, 3232.

[21] Huber, R.; Hof, P.; Duarte, R. O.; Moura, J. J. G.; Moura, I.; Liu, M.-Y.; LeGall, J.; Hille, R.; Archer, M.; Romão, M. J. *Proc. Natl. Acad. Sci.* **1996**, *93*, 8846.

[22](a) Rappé, A. K.; Goddard, W. A., III. *Nature* **1980**, *285*, 311. (b) Rappé, A. K.; Goddard, W. A., III. *J. Am. Chem. Soc.* **1982**, *104*, 448.

[23] Tatsumi, K.; Kitamura, S.; Yamada, H. *Biochim. Biophys. Acta* **1983**, *747*, 86.